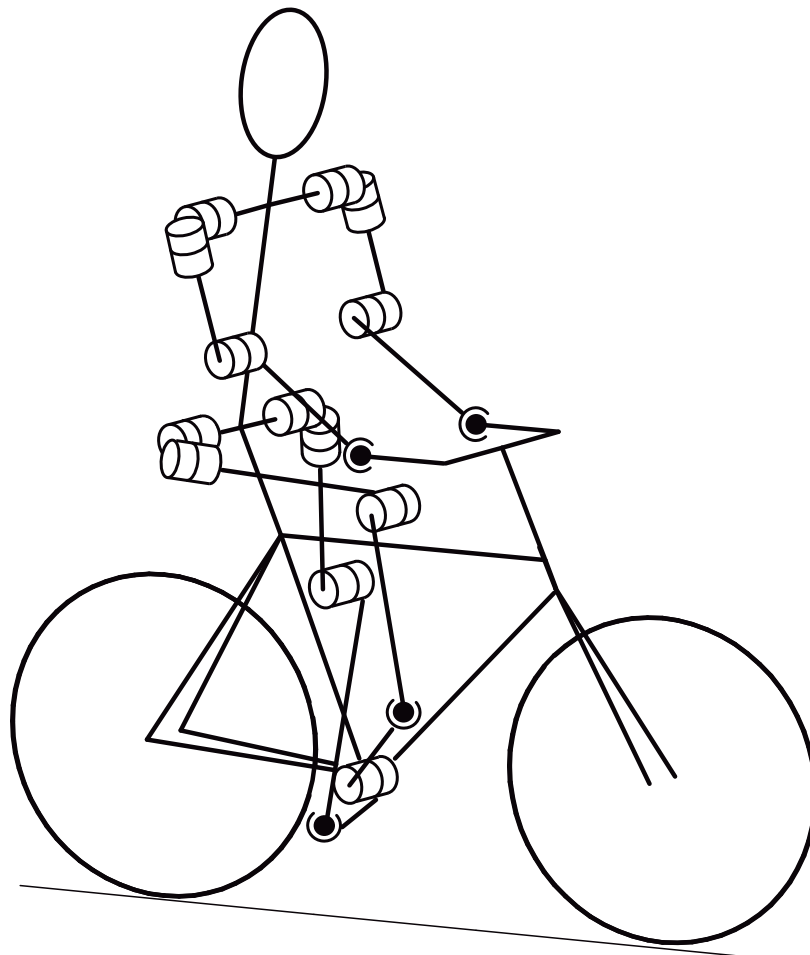


The influence of pedalling on the lateral dynamics of cycling;
a modelling approach

Patricia M. Baines



The influence of pedalling on the lateral dynamics of cycling; a modelling approach

by

Patricia M. Baines

to obtain the degree of Master of Science
at the Delft University of Technology,
to be defended publicly on Friday April 29, 2016 at 10.30

Student number: 1343653
Project duration: December 1, 2014 – June 15, 2015;
January 15, 2016 – April 29, 2016
Thesis committee: Dr. ir. A. L. Schwab, BMechE, TU Delft, supervisor
Dr. A. J. van Soest, VU Amsterdam, supervisor
Dr. ir. H. Vallery, BMechE, TU Delft
Ir. G. Wisse, PME, TU Delft
Dr. ir. J.P. Meijaard, Olton Engineering Consultancy

An electronic version of this thesis is available at <http://repository.tudelft.nl/>.



Abstract

There are still important knowledge gaps regarding stability and safety of bicycle riding. Every year around 60,000 people need hospital treatment for single sided accidents in the Netherlands alone. Supporting the need for understanding lateral bicycle dynamics.

One of the prominent disturbances on lateral bicycle and rider behaviour is pedalling. However, although there is a good understanding of the determinants effecting the forward or propulsive behaviour of the bicycle associated with pedalling, the effect on the lateral bicycle and rider behaviour is still poorly understood. This study focusses on determining what the effect of pedalling is on the lateral behaviour of the bicycle-rider system.

This determination is three fold. First the nature of the pedalling disturbance and parameters influencing it is ascertained. This is used to develop a pedalling disturbance model which can be easily applied to any dynamical bicycle-rider model, by applying harmonic external torques on the steering and roll of the bicycle.

Secondly the direct response of this pedalling disturbance of the bicycle-rider system is ascertained for a variety of models and cycling conditions. This is achieved by applying the pedalling disturbance to multiple bicycle-rider models for multiple cycling conditions. Methods, with various model complexity and solution approaches, are evaluated. Based on this evaluation we propose a simple and effective method of analytically obtaining a periodic solution based on a linearised time-invariant bicycle-rider system. This periodic solution represents the open loop lateral bicycle response corresponding to the periodic pedalling disturbance.

Thirdly the overall effect of pedalling, the closed loop response, is ascertained using experimental data. Specific cycling conditions are chosen to validate the open loop response of the model, since these cycling conditions should be only minimally effected by control. The experimental data corresponding to other cycling conditions are explored for parameter dependence and influence of control and upper body motions.

The nature of the pedalling disturbance is now understood. The pedalling disturbance is determined by vertical and the forward acceleration of the left and right leg centre of mass, the leg mass, the hip width and the cadence. This motion of mass promotes roll and yaw disturbances, where the yaw disturbance can be translated to a steering disturbance by bicycle parameters defining yaw-steering coupling.

The direct lateral response and the overall lateral bicycle-rider behaviour due to pedalling are explored. This uncovered parameter dependencies of the bicycle-rider system, differences due to rider upper body movements, rider control and cycling conditions such as forward speed and cadence.

We developed and validated a simple method of ascertaining the direct effect of a pedalling disturbance on the lateral behaviour of a bicycle-rider system. This is done by applying harmonic steering and roll toques to an easily obtained time-invariant linearised bicycle model. Some bicycle-rider combinations exhibit resonance behaviour due to pedalling within the normal cycling range, this model could be used to slightly change bicycle design parameters such that this dangerous behaviour is avoided.

Acknowledgements

Before I started working with Arend and Knoek I was convinced that my graduation project would be a thing of terror. When I had a look at other student's master thesis I was assured that I could never do it and certainly not produce something of more than 20 pages! Reading and writing was something other people did, words were just not for me. And I would certainly hate every moment of it! How wrong was I...

I got to know Arend through the multibody dynamics B course, this was one of my the first master courses. He didn't really know me then, but he did make a big impact on me and my friends, Sjarifa and Galya. That semester we lived and breathed and actually dreamt of the motion of the double pendulum. Besides developing intense friendships, dynamics really came alive for me.

The next year Arend gave me the opportunity to become a teaching assistant for this same course. I got the privilege of sharing my enthusiasm for the subject with co-students and developing my own knowledge and skills. During this time I got to know my colleague Maryam, who became a dear friend. I later found out we were known in the department as the 'dynamic duo', which I think was quite funny and fitting.

During this time I also got to know Arend. I really enjoyed our collaboration and I discovered he is enthusiastic, patient, positive, friendly and has a large willingness to share his broad knowledge and experience. When I saw the proposal for this project; a topic in dynamics modelling, in combination with human biomechanical modelling, with Arend; it was truly an easy choice.

As an expert on human biomechanical modelling, Arend introduced me to Knoek, my other supervisor for this project. I quickly understood why Knoek and Arend are friends. They obviously share enthusiasm and all the other positive character traits I see in Arend. It was a real pleasure to see them work together and join in the fun. I greatly respect Knoek for his critical approach to research. He gave me the opportunity to do an internship at the human movement sciences faculty at the VU in Amsterdam. During this time I learned what it is to do research and develop an enthusiasm for it myself.

During my thesis project Arend and Knoek really complemented each other in their mentoring styles. Typically I saw Arend frequently for short updates, where usually his response was 'maybe try this' or 'good work, keep going', this really helped me keep motivated and kept the project going when I got stuck. Knoek I saw much less frequent, but when I saw him, he really made time for me. We discussed my approach and results and usually the main message was 'why?' I learned a lot during these sessions and enjoyed them a lot too. I also quickly learnt that if I had an appointment with Knoek I should clear the entire afternoon and part of the evening, since usually we only brought these discussions to an end after his wife phoned him with the question when he was planning to come home.

They helped me develop a true passion for science and education, not only by their guidance and example, but also by the opportunities they gave me during my master period. With a lot of Knoek's help with the message and Maryam's help in the design I made my first conference poster, which Knoek presented for me at a World of Biomechanics conference. Arend and Knoek also proposed we should write an article out of our work during my internship at the VU. These experiences gave me a small taste of a possible future career in research and the confidence that maybe, just maybe, I too could learn to write.

Arend also supported me in the unique opportunity of tutoring a bachelor final project group. Elsbeth, Gijs-Jan, Laura and Nard set up an interesting experimental research project with a lot of enthusiasm and a remarkable self-critical view. It was a pleasure to work with them and an experience I learnt a lot from as well. Arend further supported me in my development as teaching assistant, not only by entrusting me with more and more responsibilities for the multibody dynamics course, but also by putting my name forward as teaching assistant for the bachelor course advanced dynamics. I already got to work with Martijn, Wouter and Heike earlier for multibody, which was a really nice, so I jumped at the opportunity. For advanced dynamics I got to work closely with Heike and Wouter, which could be described as intense in all possible ways. I learnt a lot, really a lot, in a short time span, not in the least the importance of consistency and how to use the psfrag package in latex.

Heike, I really look forward to working with you! I also hope, Arend and Knoek, we can keep collaborating with each other in future projects.

For my thesis project I also got a lot of support from other people. Riender Happee helped me during my literature search phase, to see the importance of directing research with the use of a research question. Dominic helped me by asking some critical questions during my project. Inge and Pier were always available for some discussions about bicycle behaviour. Maryam was always willing to look at my drawings and schematics for some good advise on the design. Jason Moore is absolutely great for making his experimental data so easily obtainable. He was always quick to reply my email when I found some weird behaviour in the data and helped me find an error in the code which was used to calculate the steering angle. Alfred Schouten helped me organise my thoughts in order to understand the possible control behaviour seen in the measurements. Hanneke, Nancy, Ingeborg and Sabrina without you the department would simply not work and your helpful and friendly approach just makes me happy.

I would like to thank all my friends at the university that helped my student life to be so much fun! Before I came to study in Delft I worked as a carer for several years. I lived in Leiden in an all female student house, together with 8 other girls. We had the most fun, you girls are like sisters to me. In a way, my student life began with you, before I ever set foot in a university. From the start I shared de fusie with the Marren and the Elines. I will never forget how we drank baileys and squished mice together. Long after I left, I was still sharing the same fusie, but now also with Sanne K, Chi, Maaïke, Kim and Caro. Somehow we all became oud huisgenoten, without ever living in the same house together.

From this all female house and all female work, it had been quite a transition to 3mE. It was an 'experience' as they say. My first real friend at the uni, was Fransien. We shared a first year project as the two females of the group, working together with 7 adolescent boys. Fransien made it a whole lot easier for me to be a woman at 3mE. With her very enthusiastic and good 'whispering' voice, she introduced me to practically all the friends I made during the bachelor: Elwin, Ewout, Sjarifa, Valerie, Robert, Marijke, Thomas, Leo, Maarten, Peter and Rik! I hope we will keep in touch and keep going on those great weekends you guys! Next year lustrum week!

Sanne L. darling, I think you are a wonderful person, I am happy that I knew you in Leiden and I am happy you came to Delft as well.

During my masters, some of you stayed at 3mE, some of you went funny in the head and went to TB. So I made some new friends. I moved into a new student house at the EduP, with Rik, Ewout and Adolfo. Thank you for taking me in Rik! I really had a good time and remember the yellow beam fondly. I already mentioned Galya and Sjarifa, our road trips were awesome! '*Onde supermercado?*' Maryam, I couldn't have done it without you! Thank you for all the support during the last few years! You literally (and later on figuratively) picked me up, when I was too tired to come to Delft. As a TA I also worked together with Kimberly, Arnoud, Sep, Ferry, Robert, Bram, Maaïke, Denise, etc. I really enjoyed working with you. We had a lot of fun, didn't we? Last, but certainly not least, the 🚲lab people Inge, Pier, Tim, George and Oliver. I know I sometimes talk too much, but I really enjoyed our discussions on 🚲 dynamics, our 🍷s and our 🚲 symbols. The people is what makes fun stuff great fun in my opinion.

On a personal level I got a lot of support from my family and friends. Here I would like to begin with thanking my mum and dad. I know you are always proud of me, will support and love me, whatever I do. You are a real example that a chronic illness does not have to stand in the way of contributing to society. You taught me that as long as you have each other, the rest will go off a slate roof. Everything is half left, because it cannot possibly be all right, it is physically impossible. If you don't agree, too bad peanut butter, it will be a sausage to me. Bedankt mam, diolch yn fawr tad.

My big sisters, Zwanneke and Rebecca, you both inspire me every day. I cannot begin to explain what you two mean to me. I have the up most respect for you two, your dedication in everything you do, how you treat me and the world around you. Your little Sies might have grown up, but I still strive to be like you.

My big brothers, Rene and Bram, I have also felt your support and confidence in me. I think we share a special bond and I love you for the support you give my sisters.

My very dear and old friends, Willemijn, Jessica, Benjamin and Dominic. You know me from before, you know what I feel and think before I do, I can share anything and everything with you, you know how crazy I really am.

Dominic, as a friend you helped me to start at the university by believing I could do it. You tutored me for my colloquium doctum. During the bachelor you helped me to study for calculus, dynamics and differential equations exams when I still believed I couldn't possibly do this difficult stuff myself. Afterwards we always had a lot of fun celebrating when I passed the exam or even if I failed, because then we could have some more fun and study for the exam again. You helped me to see, that maybe I could do more than I thought.

When I moved to Delft six years ago, I was lucky enough to make a partner out of my best friend. You would really love and support me, any possible version of me, in everything I do. Zelfs al word ik buschauffeur. I was smitten 15 years ago, I am smitten still and I hope to be smitten for the rest of our lives together. I love our nerdy irritations, our nerdy laughs, our nerdy floppy-drives, our nerdy talks and our nerdy walks. I really look forward to our house by the harbour and our long walks by the beach. Thank you love, for all your love and patience, especially the last few months and when I think about it, any month before that.

Domowomobomo, even though you would accept me in any shape or form, you truly inspire me to be the best version of myself I can be.

Contents

Abstract	I
Acknowledgements	III
1 Introduction	1
2 Pedalling Disturbance	4
2.1 Method	4
2.1.1 Leg Kinematics	4
2.1.2 d'Alembert Inertial Forces	6
2.1.3 Transformation to Generalised Coordinates: Virtual Power Principle	7
2.2 Results and Discussion	8
2.2.1 Leg Kinematics	8
2.2.2 Inertial Forces and Generalised Torques	11
2.3 Conclusion	14
3 Open Loop Response:	
Lateral Bicycle Behaviour due to Pedalling Disturbance	15
3.1 Method	15
3.1.1 Bicycle-Rider Models	16
3.1.1.1 Whipple Bicycle Model	16
3.1.1.2 Passive Upper Body Rider Model	18
3.1.1.3 Implementation of a new Multibody Dynamics Bicycle-Rider Model	18
3.1.2 Solution Methods	21
3.1.2.1 Numerical Method: Solving a non-linear Multibody Dynamics Model	21
3.1.2.1.1 Periodic Solution: Fourier Analysis	22
3.1.2.2 Analytic Method: Solving a System of Linearised Differential Equations	25
3.1.2.2.1 Periodic Solution: the Particular Solution	25
3.1.2.2.2 Transient Solution: the Homogeneous Solution	27
3.1.2.3 Simple Method: Conservation of Angular Momentum	27
3.1.3 Data analysis: Parameter Dependence and Method Evaluation	28
3.1.3.1 Model and Solution Method Evaluation	31
3.1.3.2 Cycling Condition and Parameter Dependent Response	31
3.2 Results and Discussion	32
3.2.1 Particular Solutions and Time Domain	33
3.2.2 Periodic Solutions and Frequency Domain	46
3.2.3 Conservation of Angular Momentum	57
3.2.3.1 Neglected Momenta	57
3.2.4 Evaluation of Model Simplifications and Solution Methods	59
3.2.5 Normal Cycling: Variation due to Parameters and Conditions	66
3.3 Conclusion	72
4 Closed Loop Response and Model Validation	73
4.1 Method	73
4.1.1 Model Validation	75
4.1.2 Open Loop Compared to Closed Loop Response	75
4.2 Results and Discussion	75
4.3 Conclusion	88
5 Conclusions and Recommendations	89
5.1 Future Work	90
References	92

List of Symbols **95**

A Research questions **96**

B Model details **99**

 B.1 Extra derivations: Leg Kinematics 104

 B.2 Extra derivations: 'd Alembert Forces 104

C Measurement details **106**

D Extra Results: Leg Motion **107**

E Extra Results: Eigenvalues Original Parameters Model CF **108**

F Extra Results: Neglected Momenta using Conservation of Angular Momentum Method**109**

G Extra Results: Time Solutions **113**

H Extra Results: Model Simplifications and Solution Method Evaluation **121**

1 Introduction

With the uncontrolled bicycle 'Whipple' model well established (Meijaard et al., 2007; Kooijman and Schwab, 2009), it is now interesting to see how humans interact with and control the lateral dynamics of the bicycle. Where we define the lateral dynamics in general terms as the roll (also known as lean) and steering motions and the associated torques of the bicycle. Aside from satisfying a natural scientific curiosity, where could the exploration of this interest lead us?

It would possibly lead us to better understand the important issues regarding stability and safety which are present in for example slow cycling speeds or regarding high accident rates for the elderly population. Within this area it is of special interest to understand why cyclists lose their balance, since one-sided bicycle accidents (with no other traffic involved) are the major cause of bicycle injury. These single-sided accidents account for around 60% of the total of 140,000 bicycle accidents occurring every year in the Netherlands of which around 65% requires hospital treatment. Especially for the elderly population the long-lasting health effects as a result of a fall can be detrimental and the percentage of single-sided accidents increase up to 85%. (CBS; Kingma et al. (1997); Schepers et al. (2014); VeiligheidNL (2014); Scaramuzza et al. (2015))

It would also possibly lead us to the ability to personalize bikes to the proportions and capabilities of the rider in order to increase sprint performance, efficiency or comfort. These have obvious interested parties in the professional sports sector, but a personalized bike could also be tempting for the general cycling enthusiast.

The research directions discussed above should be seen as so-called ultimate goals, which are very enticing, motivating and useful to keep in mind as a target on the horizon, but are not within reasonable reach for 1 person within a half year of research (which is the natural constraint for defining a master graduation research). Therefore it is necessary to identify small steps towards the possible ultimate goals.

There are already some steps taken towards understanding the human bicycle control. The energetics and muscle coordination of pedalling have been extensively explored. The muscle excitation patterns (usually as function of pedal angle) are investigated in previous research using an experimental (Neptune et al., 1997; Ting et al., 1999) and/or a musculoskeletal modelling approach (Raasch et al., 1997; Neptune and Hull, 1998; Raasch and Zajac, 1999; Neptune et al., 2000; van Soest and Casius, 2000). These mostly involve submaximal performance (Neptune et al., 1997; Neptune and Hull, 1998; Ting et al., 1999; Raasch and Zajac, 1999; Neptune et al., 2000), also maximal start-up cycling (Raasch et al., 1997) and maximal sprint cycling (van Soest and Casius, 2000) are investigated.

Experimental research identified the general behaviour and main bicycle rider control actions for laterally stabilizing the bicycle (Kooijman et al., 2009; Moore et al., 2011). The bicycle rider applies a steering action to the handlebars of the bicycle, which will influence the steering angle and thus the yaw of the front wheel. The change in steering angle will promote a lateral movement of the bicycle, whereby the support point of the bicycle is shifted towards the direction of the fall. This is the main method of controlling the lateral stability of the bicycle and is usually called steering into the fall (Schwab and Meijaard, 2013). Moore et al. (2011) were the first to establish significant lateral knee movement in low speed riding using a principle component analysis on motion capture experiments. They determined an increase of lateral knee movement with a decrease of forward speed seen for speeds of 5 km/h and below and proposed that it could be used as a low speed bicycle stabilization action. Moore et al. (2011) also found four dominant upper body motions during normal cycling; lean, bend, twist and bounce, which are dominantly present at a frequency coupled to the cadence. These upper body and lateral knee motions are not observed or observed less when the pedalling motion is not present.

A modelling approach is used to investigate dynamic behaviour, where steering and body lean control actions are modelled and applied using various control strategies (Sharp and Limebeer, 2004; Schwab et al., 2012, 2013). It is not clear if the rider controls the steering angle or the steering torque, although most rider models apply steer torque control (Popov et al., 2010; Schwab and Meijaard, 2013). Body lean as a rider control action has typically been modelled, mostly for motorcycles as well as bicycles, as a torque control over a body lean hinge joint (Popov et al., 2010; Schwab and Meijaard, 2013). These models typically use the Whipple model as a basis, which has a rigid rider attached to the bicycle frame.

The influence of a passive rider on the lateral dynamics is also investigated. Schwab et al. (2012) show that rider posture can dramatically change the dynamical properties of the bicycle-rider system, by evalu-

ating two different passive riding postures. They also show that the bicycle with a passive rider model is fully controllable by either steer torque or by upper body lean torque, even though steer torque seems more effective.

From this previous research it would seem that the most important parts of the dynamic stability, control and energetics of the bicycle are now understood. But in fact there is an important knowledge gap, that could greatly influence all these factors. Extensive research has been done to understand the control and energetics of the propulsive pedalling action of the lower body, but this has been primarily done in the sagittal plane on a stationary bicycle. The lateral stability of the bicycle-rider system has been thoroughly investigated using a rigid rider and also using control and passive dynamics of the upper body. It is safe to assume however, as experimental research also indicates, that the rider also influences the dynamics of the bicycle-rider system by the propulsive pedalling action. The moving masses of the legs will perturb the system, which in turn will likely increase the (steering) control effort and therefore the energetics of cycling. This perturbation could also directly impact the riders safety, if the control of this perturbation is difficult.

Now the next step is therefore to investigate the dynamic behaviour of a total bicycle-rider system that includes the propulsive pedalling action. This leads to the following comprehensive research question: *'What is the influence of the rider's propulsive pedalling action on the dynamic behaviour and control of the total bicycle-rider system?'* This main research question is divided into smaller subquestions in order to be able to further define the focus of this research. The subquestions are discussed with attention to what kind of approach would suit the question best in Appendix A. The focus of this master graduation research lies with the first subquestion:

'What is the effect of pedalling on the lateral behaviour of the bicycle-rider system?'

Here we are focussed on ascertaining the direct open loop response, where there is no control or lateral upper body movements added to the system, and setting this in relation with normal closed loop cycling, where there is control and a wide range of upper body movements. Answering this question is an important first step, since understanding the influence of pedalling on the rider-bicycle behaviour in general can only be done when we understand what system the rider needs to control. Herein the influence of the pedalling action on the lateral dynamics of the bicycle is still poorly understood.

Moore et al. (2011) found a significant influence of pedalling on rider behaviour and lateral bicycle behaviour using motion capture experiments on a large treadmill. It is, however, very difficult to explain this influence due to complexities in rider and bicycle behaviour due to for instance bicycle dynamics, rider's posture control, rider's bicycle-control and possible upper and lower body movement coupling.

Connors (2009) was the first to investigate the effect of pedalling using a modelling approach, specifically for recumbent cycling, which is a special type of bicycle where the rider is in a horizontal (lying) position. They used the benchmarked Whipple bicycle model (Meijaard et al., 2007) as basis for their own model by adjusting the parameters to fit a recumbent bicycle. They added five rigid bodies, two for each leg and a crank, and assumed that the movement of the legs was directly coupled to the movement of the rear wheel through a gear ratio. They implemented a steering torque control that minimizes the steering torque, steering angle, lean angle and the rate of change of these angles. It is not clear however if the human controller would minimize these angles or would actually allow some oscillation around its neutral point when a oscillatory disturbance is applied. (Connors and Hubbard, 2008; Connors, 2009) It is therefore difficult to ascertain the value of the result of this study. Since the behaviour of a disturbance is not investigated without a controller, it is difficult to separate the influence of the disturbance to the influence of the choice of the controller.

Therefore we are interested in what the influence is of this pedalling disturbance when there is no control present (open loop dynamics). Since the exclusion of control would pose a great challenge in implementation and safety using an experimental approach, a dynamic modelling approach is better suited to investigate what the influence is of the pedalling disturbance assuming an uncontrolled bicycle.

A modelling approach means we need to model the disturbance caused by pedalling and apply this disturbance to a dynamic bicycle-rider model. Herein it is important to realise that bicycle dynamics can vary significantly with bicycle riding conditions such as forward speed, bicycle-rider parameters and posture (Schwab and Meijaard, 2013). It is therefore unlikely that we can give a definitive answer on what the effect

of pedalling is on the lateral dynamic bicycle behaviour which holds for all possible cases and conditions. This study therefore focusses as it's primary goal on developing a simple and effective method of applying a pedalling disturbance to dynamic bicycle-rider models, which can be used to investigate specific cases and conditions. This could also be used in future research for instance to investigate the pedalling disturbance in a controlled system or investigate the coupling between pedalling and other rider movements. As secondary goal, this study also explores the general direct influence of pedalling for normal cycling conditions and parameters for the civil cyclist and relates this to the overall influence of pedalling on bicycle-rider behaviour.

First the pedalling disturbance is modelled and investigated in Section 2. By doing so, we can effectively answer the subquestion 1.(a) defined in Appendix A: *'What is the disturbance associated with pedalling?'* Here we will not only identify the nature of the disturbance, but also quantify it in such a way it can be used as a simple method for applying pedalling disturbance to a bicycle-rider system.

Second the subquestion 1.(b) is addressed in Section 3: *'What is the direct effect of the pedalling disturbance on the lateral dynamics of a bicycle-rider system?'* Here the pedalling disturbance is applied to dynamic bicycle-rider models, where different analytical and numerical approaches are evaluated, to find a simple and effective method of applying a pedalling disturbance. Here we also investigate the variation in the open loop response of the disturbance for a normal range of cycling conditions and parameters.

Thirdly the subquestion 1.(c) is explored in Section 4: *'What is the nature of the coupling between steering and pedalling?'* Here we will use available experimental data by Moore et al. (2011). They performed motion capture experiments during a wide range of cycling conditions on a large treadmill. Some of these cycling conditions are expected to have a reasonable agreement with an open loop response, these are therefore used as a general validation of the open loop model behaviour proposed in the previous sections. Mainly, the experimental data is used to relate the direct pedalling disturbance response found in Section 3 to the overall response including upper body movements and control. With this we can explore the contribution of these effects to the general behaviour.

In Section 5 we will present the overall conclusions corresponding to this study's research question *'What is the effect of pedalling on the lateral behaviour of the bicycle-rider system?'* Here we will also present some recommendation based on the findings of this study. This can be seen as some general ideas and methods that could possibly lead to answering the main research question: *'What is the influence of the riders propulsive pedalling action on the dynamic behaviour and control of the total bicycle-rider system?'* Taking us a step forward in the understand important issues regarding stability and safety.

2 Pedalling Disturbance

The bicycle rider propels the bicycle by transmitting power from the muscle joint system of the legs to the bicycle system. The associated joint torque is transmitted through the crank, the chain system and the rear wheel as a propulsive force acting at the contact point between the ground and the rear wheel. In order to generate this force the bicycle rider generates a force on the pedal, which is mainly directed vertically down together with a smaller forward (anterior-posterior) element and even smaller lateral component, quantified by Ruby et al. (1992). These pedal forces, together with the handle bar and saddle forces are the action-reaction forces between between the bicycle and rider. These internal forces add work to the system and influence the forward and lateral motions. In order to investigate the precise influence of these internal forces, the dynamic behaviour can be investigated by determining and solving the equations of motion of the entire bicycle-rider system. This approach is used in Section 3. In this section however, we are interested in understanding the disturbance itself. Using d'Alembert's principle we are able to determine and quantify the pedalling disturbance and answer the subquestion 1(a): '*What is the disturbance associated with pedalling?*' Here we will not only identify the nature of the disturbance, but also quantify it in such a way it can be used as a simple method for applying pedalling disturbance to a bicycle-rider system.

We can use d'Alembert's principle (Fowles and Cassiday, 1999) by defining the d'Alembert inertial forces to be in equilibrium with the external forces. Using this method we can view the inertia times the acceleration of inertia as an external inertial force. In order to be able to determine the d'Alembert forces associated with pedalling, we first need to model the leg kinematics in order to get the acceleration of the leg masses. Also using the virtual power principle the Cartesian d'Alembert forces can be transformed to generalised coordinates, used to define bicycle dynamics, the steering and the roll angle of the bicycle, in order to ascertain the disturbance of the leg mass acceleration on the bicycle dynamics.

2.1 Method

As explained above, we want to know what the disturbance due to pedalling is. This means we are interested in the leg kinematics (Section 2.1.1) and their associated inertial d'Alembert forces (Section 2.1.2). We need to transform the Cartesian d'Alembert inertial forces to d'Alembert inertial torques about the generalised coordinates, steering and roll, of the bicycle. This is done by using the virtual power principle. (Section 2.1.3).

2.1.1 Leg Kinematics

In order to estimate the influence of the pedalling action on the behaviour of the bicycle-rider system we need the leg kinematics. The simplest way to model the leg kinematics, if we regard the main aspect of the disturbance to be on the bicycle roll, is a sinusoidal up and down motion of the leg COM. However, to investigate if other possible components of the pedalling disturbance need to be taken into account a more realistic approach would be advised. Therefore a choice has been made to model the kinematics of the legs as a dual 3D four bar mechanism, which consists of both the legs together with the cranks and the bicycle frame part between crank axis and the saddle (shown in Figure 2.1). The lower leg is taken as a rigid segment, since the range of motion of the ankle is low (Bini et al., 2014). Also the lower and upper leg are constrained to move in a plane parallel to the bicycle frame, since the lateral knee movement during pedalling is small (Ruby et al., 1992), making the system fully determined as a function of cadence ($\omega = -\dot{\theta}_A$) if we assume isokinetic cycling.

The four bars are the crank (cr), the lower leg (ll), the upper leg (ul) and the axis (A) to saddle (C)

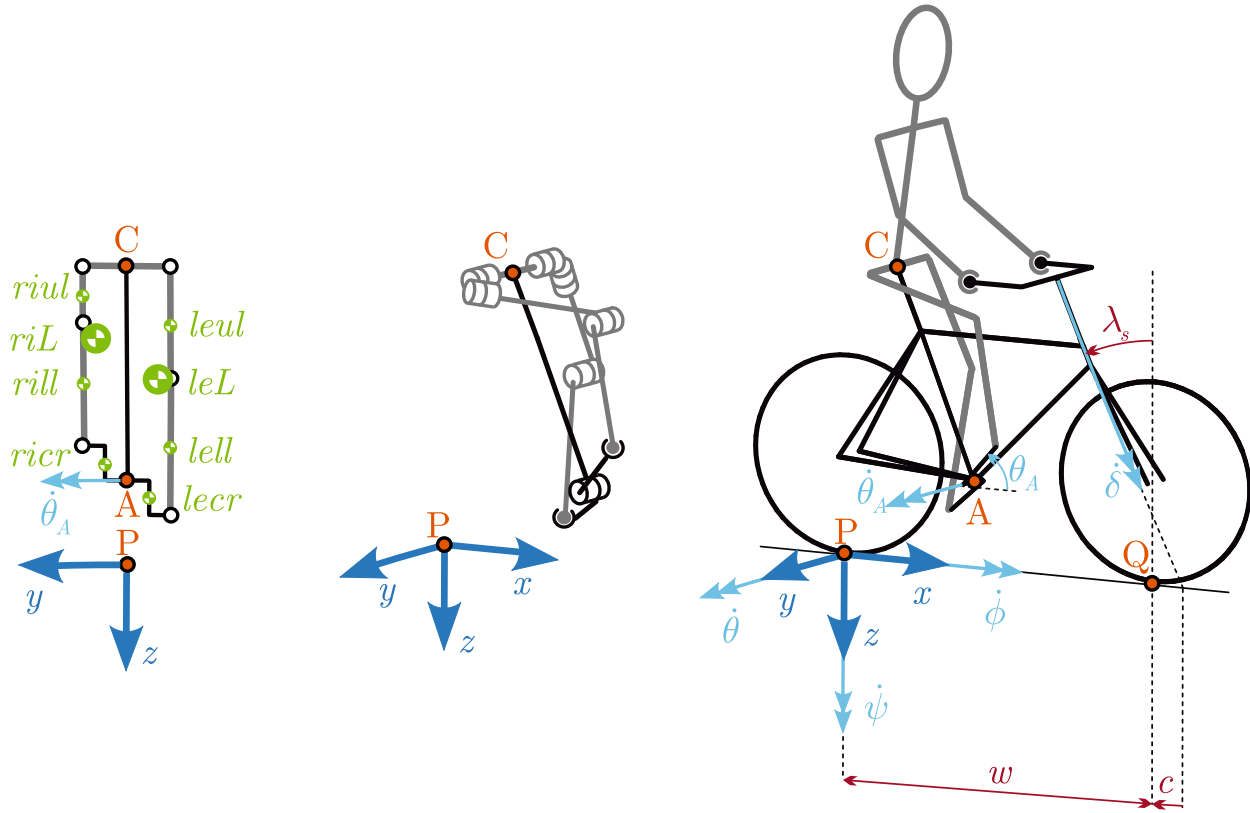


Figure 2.1: Schematic of the leg kinematic and bicycle model. Left the centre of mass (COM) locations are shown of the leg model segments in a frontal view. The middle schematic shows the connectivity of the leg segments in 3D view using a cans representation. The right schematic shows the total bicycle-rider system including bicycle variables roll ϕ , pitch θ , yaw ψ and steering δ and bicycle parameters wheelbase w , trail c and steering angle λ_s . The left leg (leL) and right leg (riL) COM move in two parallel sagittal planes fixed parallel to the bicycle frame. The leg kinematics are modelled as a dual 3D four bar mechanism: the crank (cr), the lower leg (ll), the upper leg (ul) and the axis (A) to saddle (C) length as the base. The crank angle $\theta_A(t)$ has a prescribed motion of $\theta_A t$, where $\dot{\theta}_A$ is the constant negative of the cadence ($\dot{\theta}_A = -\omega$) and $\theta_A = 0$ is defined as the position where the right foot is in it's most forward position. Also, the knee cannot be extended beyond 180 degrees ($\theta_{ul} \geq \theta_{ll}$), meaning the system kinematics are fully defined without adding any degree of freedom to the system.

length as the base, where the motion is prescribed by the following constraint equations:

$$\mathbf{x}_A + \begin{bmatrix} l_{cr} \cos(\dot{\theta}_A t) \\ \frac{1}{2} l_{hh} \\ -l_{cr} \sin(\dot{\theta}_A t) \end{bmatrix} + \begin{bmatrix} l_{ll} \cos(\theta_{rill}) \\ 0 \\ -l_{ll} \sin(\theta_{rill}) \end{bmatrix} + \begin{bmatrix} l_{ul} \cos(\theta_{riul}) \\ -\frac{1}{2} l_{hh} \\ -l_{ul} \sin(\theta_{riul}) \end{bmatrix} - \mathbf{x}_C = \mathbf{0} \quad (2.1)$$

$$\mathbf{x}_A + \begin{bmatrix} l_{cr} \cos(\dot{\theta}_A t + \pi) \\ -\frac{1}{2} l_{hh} \\ -l_{cr} \sin(\dot{\theta}_A t + \pi) \end{bmatrix} + \begin{bmatrix} l_{ll} \cos(\theta_{lell}) \\ 0 \\ -l_{ll} \sin(\theta_{lell}) \end{bmatrix} + \begin{bmatrix} l_{ul} \cos(\theta_{leul}) \\ \frac{1}{2} l_{hh} \\ l_{ul} \sin(\theta_{leul}) \end{bmatrix} - \mathbf{x}_C = \mathbf{0} \quad (2.2)$$

Where l is the segment length and θ is the segment pitch angle. These sets of equations have 2 unknowns (θ_{ll} and θ_{ul}) and 2 non-trivial equations. These can be solved when also the extra condition is added that the knee cannot be extended past a straight leg ($\theta_{ul} \geq \theta_{ll}$), otherwise the system has two possible configuration solutions.

The COM positions of the leg segments can be easily defined as a function of the now defined pitch angles (for full derivation see Appendix B.1). The COM position of an entire leg (+ crank) \mathbf{x}_L can be formulated

as the weighted average of the parts as follows (Winter, 1990):

$$\mathbf{x}_L = \frac{m_{cr}\mathbf{x}_{cr} + m_{ul}\mathbf{x}_{ul} + m_{ul}\mathbf{x}_{ul}}{m_{cr} + m_{ul} + m_{ul}} \quad (2.3)$$

The bicycle (\mathbf{x}_A & \mathbf{x}_C) and rider parameters (l & m) are consistent with parameters used for the passive rider models (Moore et al., 2009; Schwab et al., 2012), which are based on the bicycles and anthropomorphic data of the rider used in the experimental motion capture research (Moore et al., 2011) used in Section 4. A standard crank length and mass of 0.17 m and 2 kg was taken respectively and the seat post length of the Batavus Browser bicycle needed to be decreased to 0.19 m, since the value given in Moore et al. (2009); Schwab et al. (2012) did not accommodate for a full crank rotation. These parameters are based on common parameters for crank and seat height (van Soest and Casius, 2000; Wilson, 2004).

In general a standard value of 60 rpm ($\omega = 2\pi$ rad/s) is chosen as example for the cadence. This cadence is chosen, since it is a reasonably common cadence for recreational cycling (Wilson, 2004). However other cadences are also used to generate results to check if behaviour is consistent with expectations. Cadence dependent behaviour is either captured in figures or formulas.

The leg motion corresponding to the leg kinematic model can be applied directly to a full non-linear multibody dynamics bicycle-rider model, by adding elements that move as a function of cadence as discussed in Section 3.1.2.1. However in this study we want to investigate the possibility to develop a simple method of investigating the pedalling disturbance response. If the disturbance can be simplified in such a way that it is compatible with a linearised bicycle model and analytic solution approaches it would greatly increase the usability of the disturbance model. In order to investigate the dynamics and solve the system easily in an analytic manner, the leg motion can also be modelled as a sinusoidal motion with the pedalling frequency and an amplitude of the centre of mass (COM) corresponding to the leg model. Therefore we investigate a possible simplification, a simplified COM path that follows a skew-elliptical motion which is a function of the cadence frequency ω only.

$$\mathbf{x}_{L\text{simple}} = \begin{bmatrix} \bar{x}_L \\ \bar{y}_L \\ \bar{z}_L \end{bmatrix} + \begin{bmatrix} |X_L(\omega)| \cos(\omega t + \varphi_{X_L(\omega)}) \\ 0 \\ |Z_L(\omega)| \cos(\omega t + \varphi_{Z_L(\omega)}) \end{bmatrix} \quad (2.4)$$

where the leg motion amplitude $|X_L|$ and phase φ_{X_L} can be obtained by transforming the leg motion \mathbf{x}_L to frequency domain by applying a Fourier transform (for details on Fourier transform see Section 3.1.2.1.1) and consequently picking the amplitude and phase information for the frequency corresponding to cadence ω ($= -\dot{\theta}_A$). Here the difference for the right leg and the left leg is π rad phase angle difference ($\varphi_{\mathbf{x}_{leL}} = \varphi_{\mathbf{x}_{riL}} + \pi$ rad). The error of this simplification is illustrated by calculating the normalised root mean squared deviation NRMSD as an error percentage:

$$\text{NRMSD} = \frac{\sqrt{\frac{1}{N} \sum_{n=1}^N (\mathbf{x}_L(n) - \mathbf{x}_{L\text{simple}}(n))^2}}{\max(\mathbf{x}_L(n)) - \min(\mathbf{x}_L(n))} 100\% \quad (2.5)$$

This is the standard expression for root mean squared deviation, however normalised with the range of the signal and expressed as a percentage.

2.1.2 d'Alembert Inertial Forces

d'Alembert's principle implicates that a dynamic system can be viewed as a system in equilibrium similar to a static system by interpreting the acceleration of inertia as an inertial force which is a negative external force. These d'Alembert inertial forces $\mathbf{F}_{in} = -M\ddot{\mathbf{x}}$ together with the (other) external forces \mathbf{f} are then in equilibrium. (Fowles and Cassiday, 1999; Greenwood, 2006)

$$\sum \mathbf{f} - M\ddot{\mathbf{x}} = \mathbf{0} \quad (2.6)$$

$$\sum \mathbf{f} + \mathbf{F}_{in} = \mathbf{0} \quad (2.7)$$

Applying this same principle to our model we can investigate the d'Alembert inertial forces $\mathbf{F}_{\mathbf{x}_L}(t)$ and inertial torques $\mathbf{T}_{\mathbf{x}_L}(t)$ associated with the leg movement in all directions:

$$\mathbf{F}_{\mathbf{x}_L}(t) = - [\mathbf{M}_L \ddot{\mathbf{x}}_{riL}(t) + \mathbf{M}_L \ddot{\mathbf{x}}_{leL}(t)] \quad (2.8)$$

$$\mathbf{T}_{\mathbf{x}_L}(t) = - \left[\begin{array}{c} \mathbf{x}_{riL}(t) \times [\mathbf{M}_L \ddot{\mathbf{x}}_{riL}(t)] + \mathbf{x}_{leL}(t) \times [\mathbf{M}_L \ddot{\mathbf{x}}_{leL}(t)] + \dots \\ \mathbf{I}_{ul} \dot{\boldsymbol{\omega}}_{riul}(t) + \mathbf{I}_{ul} \dot{\boldsymbol{\omega}}_{leul}(t) + \mathbf{I}_{ll} \dot{\boldsymbol{\omega}}_{rill}(t) + \mathbf{I}_{ll} \dot{\boldsymbol{\omega}}_{lell}(t) + \mathbf{I}_{cr} \dot{\boldsymbol{\omega}}_{ricr}(t) + \mathbf{I}_{cr} \dot{\boldsymbol{\omega}}_{lecr}(t) \end{array} \right] \quad (2.9)$$

Where \mathbf{M}_L is a 3 by 3 mass matrix with the leg mass m_L on the diagonal, $\ddot{\mathbf{x}}_{riL}(t)$ and $\ddot{\mathbf{x}}_{leL}(t)$ is the acceleration vector of the right and left leg COM respectively and $\mathbf{x}_{riL}(t)$ and $\mathbf{x}_{leL}(t)$ are their corresponding position vectors, \mathbf{I}_{ul} , \mathbf{I}_{ll} and \mathbf{I}_{cr} are the moment of inertia tensors of the upper leg, the lower leg and crank respectively and $\dot{\boldsymbol{\omega}}_{riul}$, $\dot{\boldsymbol{\omega}}_{leul}$, $\dot{\boldsymbol{\omega}}_{rill}$, $\dot{\boldsymbol{\omega}}_{lell}$, $\dot{\boldsymbol{\omega}}_{ricr}$ and $\dot{\boldsymbol{\omega}}_{lecr}$ are rotational acceleration vectors of the right and left upper leg, lower leg and crank respectively (see Figure 2.1 and Section 2.1.1 for leg kinematic model). In the general case the inertial torques would also have $\boldsymbol{\omega} \times \mathbf{I}\boldsymbol{\omega}$ components, but because the leg segments only have a pitch rotational velocity ($\omega_y(t)$; $\omega_x = 0$, $\omega_z = 0$), these terms disappear.

Using this approach the d'Alembert inertial forces calculated here are purely the disturbance caused by the relative motion of the legs to the bicycle frame. Meaning that the d'Alembert inertial forces represent the disturbance applied to the **local** Cartesian reference frame of the bicycle. The implications of this property in bicycle model application are discussed in Section 3.1.2.2

2.1.3 Transformation to Generalised Coordinates: Virtual Power Principle

Since we are interested in the influence of the pedalling disturbance on the lateral dynamics of the bicycle, it would be insightful to represent the Cartesian inertial forces and torques in terms of the generalised coordinates used to describe the lateral dynamics of the bicycle. The established Whipple bicycle model, benchmarked by Meijaard et al. (2007), is discussed in more detail in Section 3.1.1.1. According to this validated model, if we assume constant forward speed the forward and lateral dynamics can be decoupled and the lateral dynamics can be fully described by the generalised coordinates roll ϕ and steering δ (see Figure 2.1).

The virtual power corresponding to the pedalling disturbance δP_L is the same expressed in generalised coordinates as Cartesian coordinates (Greenwood, 2006). Therefore we can uncover the generalised inertial forces \mathbf{f}_L by transforming the virtual power from Cartesian to generalised coordinates. We start by deriving the virtual power of the Cartesian inertial torques $\mathbf{T}_{\mathbf{x}_L}$ by linking the Cartesian coordinates to the corresponding angular velocities as depicted in Figure 2.1. This expression is equal to the virtual power expressed in generalised coordinates.

$$\delta P_L = T_{x_L} \delta \dot{\phi} + T_{y_L} \delta \dot{\theta} + T_{z_L} \delta \dot{\psi} \quad (2.10)$$

$$= T_{\phi_L} \delta \dot{\phi} + T_{\delta_L} \delta \dot{\delta} \quad (2.11)$$

Note that the notation for the virtual variation δ an upright Greek delta symbol is used, where the only slightly different notation for steering angle δ an italic Greek delta symbol is used. The generalised inertial roll torque T_{ϕ_L} can be directly found as the inertial torque about the local x axis T_{x_L} . The generalised inertial steering torque T_{δ_L} can be found by using kinematic relations between the bicycle coordinates $\dot{\theta}$, $\dot{\psi}$ and $\dot{\delta}$ (Meijaard et al., 2007):

$$\dot{\theta} = 0 \quad (2.12)$$

$$\dot{\psi} = \frac{\cos(\lambda_s)}{w} (v\dot{\delta} + c\dot{\delta}) \quad (2.13)$$

which is determined by the bicycle geometry corresponding to the yaw-steering coupling, c the trail, w the wheel base and λ_s the steering angle. These relationships can be understood as defining the vertical and lateral velocity of the front wheel contact point Q as a function of pitch velocity $\dot{z}_Q(\dot{\theta}) = w\dot{\theta} = 0$, yaw velocity $\dot{y}_Q(\dot{\psi}) = -w\dot{\psi}$, steering velocity $\dot{y}_Q(\dot{\delta}) = -c\cos(\lambda_s)\dot{\delta}$ and forward speed and steering angle $\dot{y}_Q(v) = -\delta\cos(\lambda_s)v$. Equations 2.12 and 2.13 can be used to transform 2.10 to generalised coordinates

$$\delta P_L = T_{x_L} \delta \dot{\phi} + T_{z_L} \frac{\cos(\lambda_s)}{w} c \delta \dot{\delta} \quad (2.14)$$

Comparing equations 2.11 and 2.14 a generalized inertial force vector \mathbf{f}_L can be defined to include the roll and steering torque.

$$\mathbf{f}_L = \begin{bmatrix} T_{\phi_L} \\ T_{\delta_L} \end{bmatrix} = \begin{bmatrix} T_{x_L} \\ \frac{1}{w} c \cos(\lambda_s) T_{z_L} \end{bmatrix} \quad (2.15)$$

2.2 Results and Discussion

The results and corresponding discussion is split into two main topics. First we cover the leg kinematics and secondly the inertial torques and forces associated with pedalling.

2.2.1 Leg Kinematics

The modelled leg kinematics are visualized in Figure 2.2 and 2.3. The leg centre of mass (COM) trajectory is followed very well by the skew-elliptical simplified motion, since the position is dominated by the cadence frequency ω . The error (NRMSD) of this simplified skew-elliptical motion compared to the leg model is 2% in forward direction and 3.6% in vertical direction. However looking at the speed and acceleration of the simplified motion, a higher discrepancy is seen (Figure 2.3). It is interesting to understand why this occurs, since the speed and acceleration determine the disturbance as momentum or inertial forces respectively. In Figure 2.4 it is seen that higher frequencies have a larger relative amplitude for the speed and acceleration. This increase of amplitude can be understood by looking at the signal as a superposition of multiple cosines and taking the second derivative with respect to time:

$$\mathbf{x}_L(t) = \mathbf{X}_L(0) + |\mathbf{X}_L(\omega)| \cos(\omega t + \varphi_{\mathbf{X}_L(\omega)}) + |\mathbf{X}_L(2\omega)| \cos(2\omega t + \varphi_{\mathbf{X}_L(2\omega)}) \dots \quad (2.16)$$

$$\ddot{\mathbf{x}}_L(t) = -|\mathbf{X}_L(\omega)| (\omega)^2 \cos(\omega t + \varphi_{\mathbf{X}_L(\omega)}) - |\mathbf{X}_L(2\omega)| (2\omega)^2 \cos(2\omega t + \varphi_{\mathbf{X}_L(2\omega)}) \dots \quad (2.17)$$

This explains why there is a relative change of amplitudes of n^2 for a frequency of $n\omega$ and why higher frequency content is more visible in the acceleration signal. Precise numerical frequency information of the leg movement $\mathbf{X}_L(n\omega)$ can be found in Appendix D (Table D.1 corresponding to hybrid bicycle and Table ?? corresponding to city bicycle).

The dual four bar mechanism is off course a simplification of the true pedalling motion. The motion of this model does not incorporate possible ankle angle, hip position and lateral knee motions. These assumptions are deemed reasonable, since the influence of these motions in general are relatively small due to the small deviations. Ruby et al. (1992) found a range of lateral knee motion of around 23 mm (SD 7 mm, 11 subjects, 22 cycles per subject), which would add to a lateral motion of around 11 mm to the centre of mass, which is an order of magnitude lower than the vertical or forward range of motion of the centre of mass. This small lateral component will add to the roll and yaw disturbance. The range of motion of the ankle is dependent on seat height and individual differences ($\pm 15^\circ$ Brown et al. (1996); $10^\circ - 25^\circ$ Bini et al. (2014)). Small ankle extensions are usually present in the downward part of the pedal stroke, this would slightly decrease the vertical range of motion of the centre of mass, slightly decreasing the roll disturbance. Also small vertical movements of the hip position are likely, due to the upper body bending seen during pedalling (Moore et al., 2011). The hip goes slightly up and down in sync with the pedal motion, meaning that the vertical centre of mass motion will slightly increase due to the hip motion. It could be that for individual cases or clinical applications these numbers are larger. In that case these influences should be taken into account, possibly by first identifying the leg motion using motion capture experiments.

Not only the motion of the four bar mechanism is a simplification, but also the mass distribution of the segments is simplified. The length and inertia parameters for our leg kinematic model are based on bicycle and rider parameters defined by Moore et al. (2009). For clarity and consistency, the same mass distribution is used proposed by Moore et al. (2009), where the leg segments are modelled as cylinders with homogeneous mass distribution. This is clearly a simplification on true human leg mass distribution. We could use anthropomorphic parameters based on cadaveric studies in order to reduce this simplification (Winter, 1990). This would mean that the upper leg COM is located closer to the hip (at distance $0.433 l_{ul}$

instead of $0.5 l_{ul}$) and the lower leg COM is located further away from the knee (at distance $0.606 l_{ll}$ instead of $0.5 l_{ll}$). For reference the numerical frequency information of the leg movement $\mathbf{X}_L(n\omega)$ corresponding to these anthropomorphic parameters are also found in Appendix D for both bicycles. Comparing the original consistent model, to the model using more accurate COM locations, an error of around 2% is found corresponding to this homogeneous mass distribution assumption, where this assumption leads to an overestimation of the amplitudes.

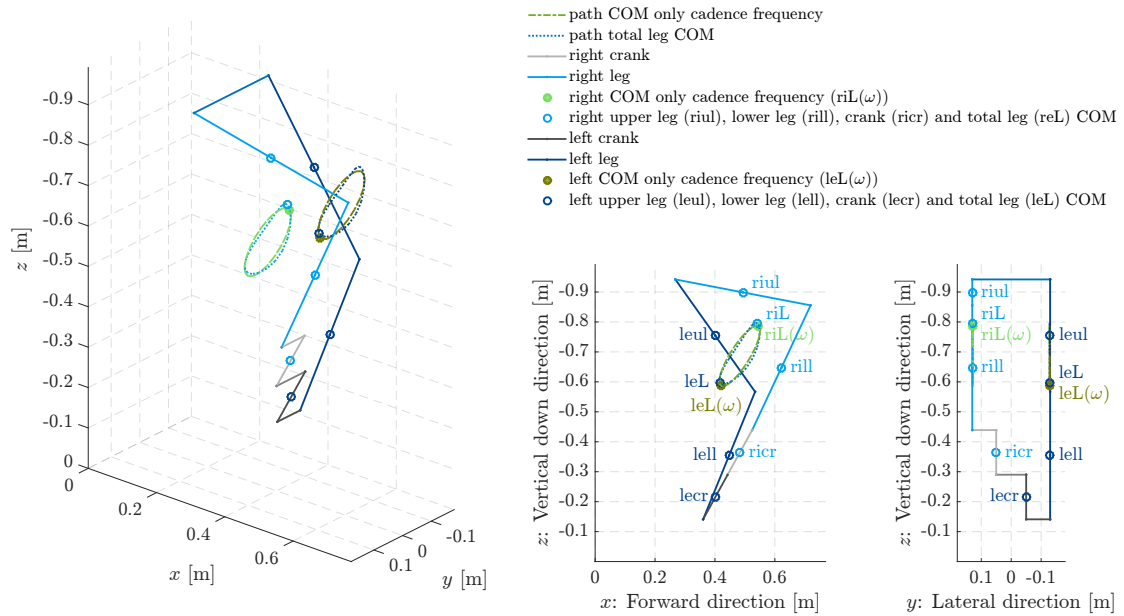


Figure 2.2: The leg motion is modelled as a dual 3D four bar mechanism and as a simple skew-elliptical COM path (COM only cadence frequency), shown in 3D view (left), side view (middle: sagittal plane) and front view (right: frontal plane). The COM locations of the leg model segments and total system are indicated. The simplified and dual four bar mechanism centre of mass (COM) paths are shown for comparison.

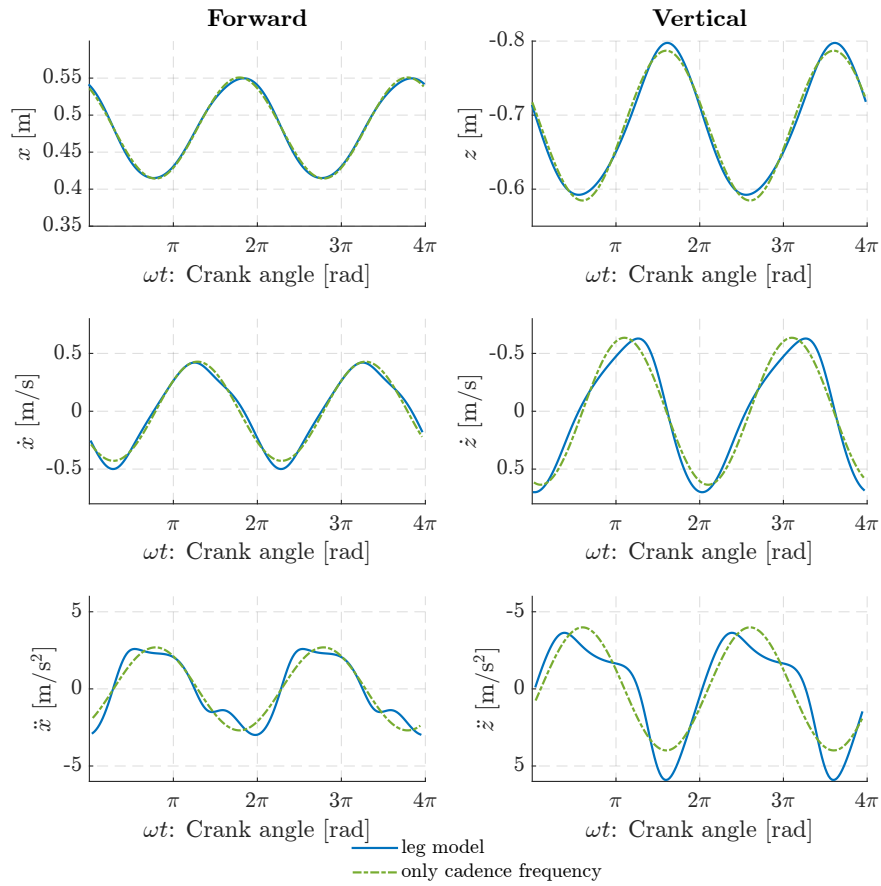


Figure 2.3: The right leg position (top), speed (middle) and acceleration (bottom) in forward direction (left) and vertical direction (right) as a function of crank angle, for cadence is 60 rpm ($= 2\pi$ rad/s). Crank angle is also a measure of time since we assume isokinetic cycling ($\omega t = -\theta_A$). The centre of mass of the four bar mechanism ('leg model') and the simple motion using only the cadence frequency are shown for comparison. The axes for vertical direction are inverted, since the positive direction of the z -axis is vertical downwards.

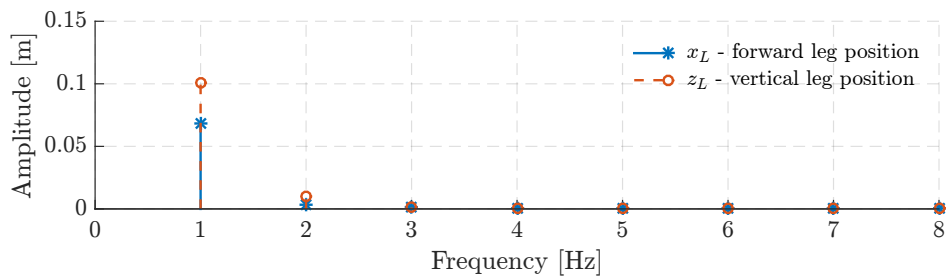


Figure 2.4: The amplitude of the position of the right leg COM as a function of frequency. For cadence is 60 rpm ($= 2\pi$ rad/s $= 1$ Hz), bicycle parameters corresponding to the hybrid bicycle (Batavus Stratos).

2.2.2 Inertial Forces and Generalised Torques

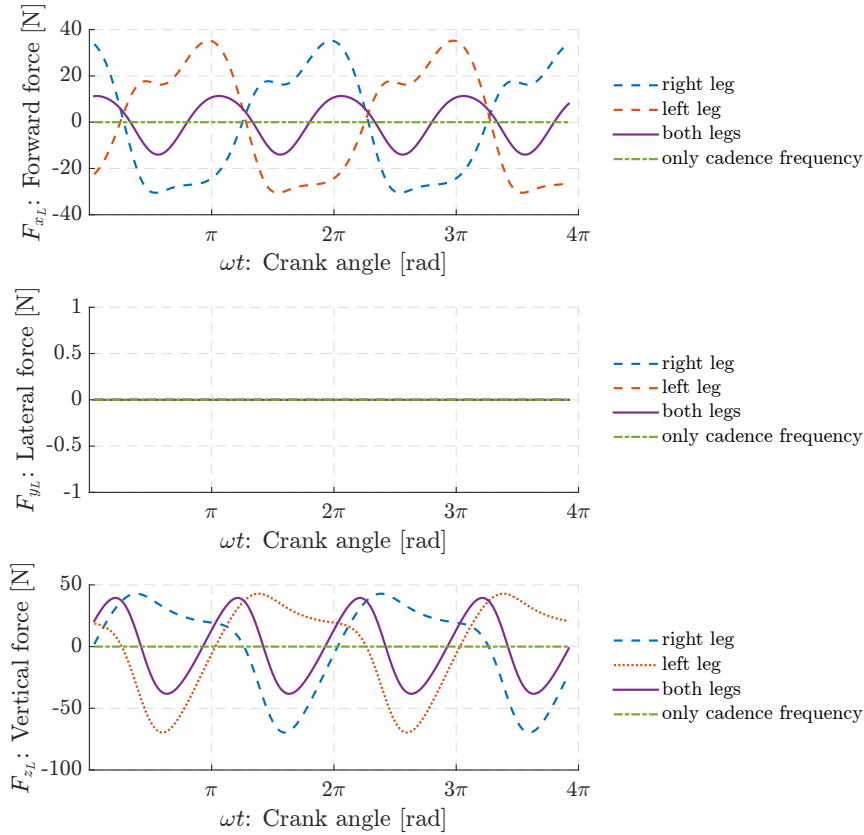


Figure 2.5: d'Alembert forces, the so called inertial forces associated with the acceleration of inertia, for the leg model and the simplified skew-elliptical COM motion as a function of crank angle, for cadence is 60 rpm ($= 2\pi \text{ rad/s} = 1 \text{ Hz}$). Crank angle is also a measure of time since we assume isokinetic cycling ($\omega t = -\theta_A$).

In order to understand what the effective disturbance is, the d'Alembert inertial forces (Figure 2.5) corresponding to these legs and simplified COM movements are investigated. The forward and vertical forces of both the legs are dominated by the first even multiple of the cadence frequency (2ω), since the odd multiples of the cadence frequency ($1\omega, 3\omega, \dots$) cancel each other out since these are associated with an odd number of π rad shifts:

$$\mathbf{F}_{x_L} = \sum_{n=1}^{\infty} m_L |X_L(n\omega)| (n\omega)^2 \left(\cos(n\omega t + \varphi_{X_L(n\omega)}) + \cos(n\omega(t + \pi/\omega) + \varphi_{X_L(n\omega)}) \right) \quad (2.18)$$

$$= \sum_{n=2,4,6,\dots}^{\infty} m_L |X_L(n\omega)| (n\omega)^2 2 \cos(n\omega t + \varphi_{X_L(n\omega)}) \quad (2.19)$$

$$\mathbf{F}_{z_L} = \sum_{n=2,4,6,\dots}^{\infty} m_L |Z_L(n\omega)| (n\omega)^2 2 \cos(n\omega t + \varphi_{Z_L(n\omega)}) \quad (2.20)$$

for full derivation see Appendix B.2. The physical interpretation of this algebraic derivation is that the even frequencies are effected by constructive interference and the odd frequencies are effected by destructive interference due to the phase difference of the right and left leg motion.

Since the modelled movement of the simplified motion does not consist of any even multiples of the cadence frequency, the d'Alembert forces of the right and left slider cancel each other out completely. This should not present a large problem, since the leg movement forces should not have a large effect on the overall lateral behaviour of the bicycle. The forces in forward direction will influence the forward speed by introducing a small periodic component (total mass of around 90kg and peak force of around 12N makes a peak acceleration of around $12/90=0.13\text{m/s}^2$). The forces in vertical direction will influence the ground reaction forces by introducing a small periodic component (around 39N amplitude on 900N total weight).

Similarly the d'Alembert pitch torque will influence the ground reaction forces. However the roll and yaw torques (Figure 2.6) will have a greater effect on the overall bicycle behaviour, since it will influence the roll and steering, defining the lateral dynamic bicycle behaviour. Here the cadence frequency is dominant again, since now not the odd multiples but the even multiples of the cadence frequency cancel each other out due to the difference in minus sign between left and right:

$$T_{\phi_L} = \sum_{n=1}^{\infty} m_L l_{hh}/2 |Z_L(n\omega)| (n\omega)^2 (\cos(n\omega t + \varphi_{Z(n\omega)}) - \cos(n\omega(t + \pi/\omega) + \varphi_{Z(n\omega)})) \quad (2.21)$$

$$T_{\phi_L} = \sum_{n=1,3,5,\dots}^{\infty} m_L l_{hh} |Z_L(n\omega)| (n\omega)^2 \cos(n\omega t + \varphi_{Z(n\omega)}) \quad (2.22)$$

$$T_{\psi_L} = \sum_{n=1,3,5,\dots}^{\infty} -m_L l_{hh} |X_L(n\omega)| (n\omega)^2 \cos(n\omega t + \varphi_{X(n\omega)}) \quad (2.23)$$

where l_{hh} is the hip to hip distance and the only difference in defining the yaw torque T_{ψ_L} to the roll torque T_{ϕ_L} is it uses the forward leg amplitude $|X_L(n\omega)|$ instead of the vertical leg amplitude $|Z_L(n\omega)|$ and has a minus sign due to positive direction definitions. The pitch torque T_{θ_L} cannot be easily simplified compared to the general definition given in Section 2.1.2, since there is synchronous movement in x and z direction, changing the lever arms for the torques corresponding to the inertial forces in x and z direction, also there are rotational accelerations of the lower limb pitch angles ($\ddot{\theta}_{ul}$ & $\ddot{\theta}_{ll}$) contributing to the pitch torque. However when expressing this pitch torque T_{θ_L} as a superposition of multiples of the cadence frequency (Appendix B.2) it is clear that the odd multiples of the right and left leg cancel each other out similar to the forward and vertical leg force.

It is clear that the yaw torque cannot be simply ignored, since it is in the same order of magnitude as the roll torque (see Figure 2.6). Therefore, in order to understand the main disturbance on the lateral dynamics caused by pedalling, we need to include the generalised inertial steering torque caused by the inertial yaw torque:

$$T_{\delta_L} = \frac{1}{w} c \cos(\lambda_s) \sum_{n=1,3,5,\dots}^{\infty} -m_L l_{hh} |X_L(n\omega)| (n\omega)^2 \cos(n\omega t + \varphi_{X(n\omega)}) \quad (2.24)$$

Because the second multiple of the cadence frequency is cancelled out in the roll and yaw torque, the simplified skew-elliptical motion gives a reasonably good fit by using only the cadence frequency. The error (NRMSD) corresponding to this simplification is 3.4% for the roll torque and 8.2% for the steering torque for a cadence of 60 rpm. This error is dependent on cadence and is determined by the amplitudes of the higher cadence multiples.

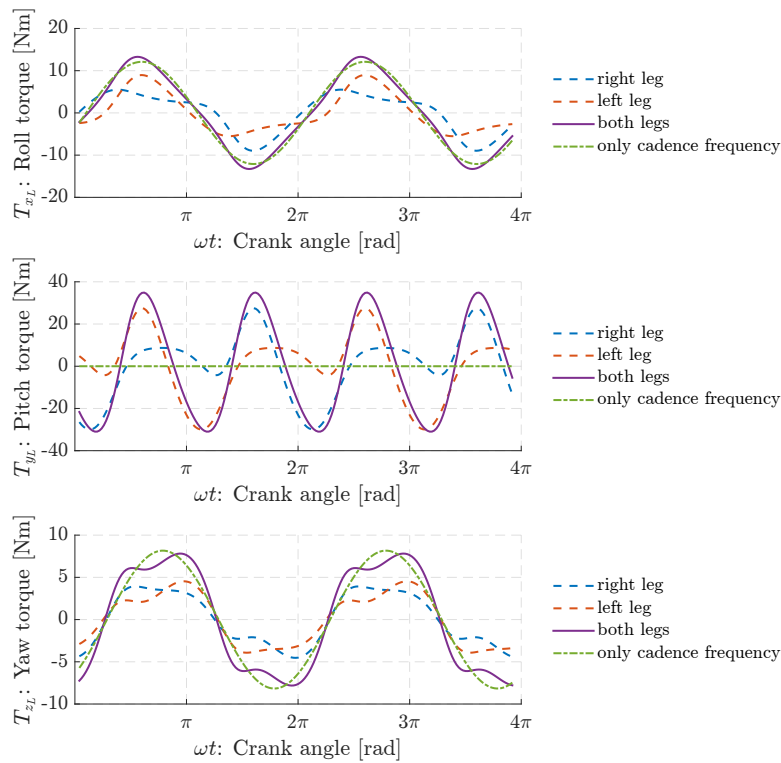


Figure 2.6: Cartesian d'Alembert torques, the so called inertial torques associated with the angular acceleration of inertia, for the leg model and the simplified skew-elliptical motion as a function of crank angle, for cadence is 60 rpm ($= 2\pi$ rad/s). Crank angle is also a measure of time since we assume isokinetic cycling ($\omega t = -\theta_A$).

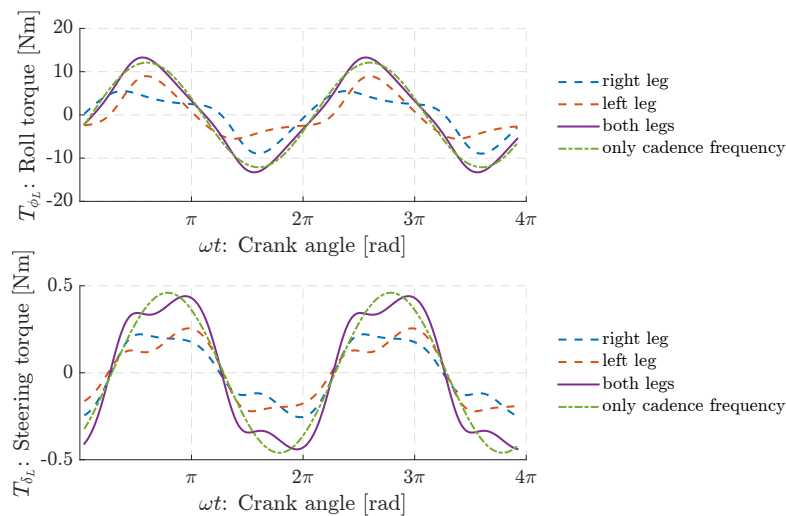


Figure 2.7: Generalised d'Alembert torques, the so called inertial torques associated with the generalised angular acceleration of inertia, for the leg model and the simplified skew-elliptical motion as a function of crank angle, for cadence is 60 rpm ($= 2\pi$ rad/s). Crank angle is also a measure of time since we assume isokinetic cycling ($\omega t = -\theta_A$).

The inertial torques developed here correspond to parameter sets for a specific rider and two specific bicycles. However these can be easily modified to be used for other riders, by changing the hip to hip width and the leg mass in the inertial torques equations. If the leg length is different, the COM trajectory will change. This could possibly be solved by scaling the amplitudes, or more accurately by solving the leg motion defined by the derived constraint equations in Section 2.1.1. The inertial torques can also be modified to be consistent with a wide range of other bicycles, by changing the orientation of the leg COM trajectory defined by \mathbf{X}_L (values and model parameters given in Appendix D). As an example, for recumbent cycling the same pedalling motion can be used, only the axis to saddle distance is orientated differently. To give a general indication; if we would assume that the orientation is around 90° tilted, we could then swap the yaw and roll torque contribution to the disturbance. This shows that in recumbent cycling the disturbance to the yaw (and dependent on the kinematic coupling possibly also the steering) is greater than in normal cycling and the disturbance to the roll is lower.

2.3 Conclusion

The disturbance on the lateral dynamics due to pedalling is caused by the vertical and the forward acceleration of the left and right leg centre of mass. The vertical acceleration promotes an inertial torque disturbance about the bicycle roll and the forward acceleration promotes an inertial torque disturbance about the steering of the bicycle. These generalised inertial torques only contain odd multiples of the cadence frequency. Both torques are proportional to the leg mass, the hip width and the cadence squared. The steering torque is also proportional to the mechanical trail ($c \cos(\lambda_s)$) and inverse proportional to the wheelbase ($\frac{1}{w}$), which are the parameters associated with yaw-steering coupling. The rest of the amplitude and phase behaviour is dependent on the geometry of the lower limbs and the saddle to crank axis distance and orientation defining the forward and vertical motion of the leg centre of masses.

The modelled forward and vertical motion of the leg centre of masses are based on a leg kinematic model represented by the motion of a dual 4-bar mechanism, consisting the saddle to crank axis frame part as the base, the cranks, upper and lower legs. The motion of the leg centre of mass can be represented by sinusoidal motions containing the cadence frequency and it's multiples. This can be approximated by using only the cadence frequency, with an error in the times series of 2% in forward direction and 3.4% in vertical direction. These simplified motions result in a simple representation of the disturbance as sinusoidal torques containing only the cadence frequency, which can be easily applied on the steering and roll of a bicycle model.

3 Open Loop Response: Lateral Bicycle Behaviour due to Pedalling Disturbance

This section addresses the research question: 'What is the direct effect of the pedalling disturbance on the lateral dynamics of a bicycle-rider system?' It has been established that pedalling has a significant influence on bicycle and rider behaviour. This influence was quantified by Moore et al. (2011) using experiments by capturing the motion of cyclists and their bicycle on a large treadmill under a wide range of test conditions. They tested 'normal cycling', where the rider propelled the bicycle by pedalling and a condition where the bicycle was towed and the rider only had to control the balance of the bicycle. They found that several types of upper body movements are somehow coupled to the pedalling action. They also found that a lot of steering actions taking place around the pedalling frequency. However it is not clear to what extent these movements are directly coupled to the rider motion, directly coupled to the disturbance and/or a result of the rider controlling the disturbance.

In order to begin to understand the mechanisms behind this coupling between pedalling and lateral bicycle and upper body motions, we can investigate the uncontrolled system where the upper body motions are not biomechanically coupled to the pedalling motion and determine the influence on the lateral bicycle dynamics. This influence of the disturbance on the uncontrolled bicycle behaviour is called open loop response and is used to investigate the direct dynamical coupling. Using this method we can identify the system the bicycle rider has to control, and take a step in better understanding bicycle riding behaviour.

In order to understand what the effect is of the pedalling disturbance (determined in Section 2) on the dynamic bicycle behaviour, we need to apply this disturbance to an appropriate model. The benchmarked Whipple bicycle model (Meijaard et al., 2007) is an obvious choice, since it is widely used and extensively validated (Sharp, 2008; Popov et al., 2010; Schwab and Meijaard, 2013). This bicycle model is dependent on the 25 bicycle design parameters and captures the dependence of forward speed. However this model has a rigid rider attached to the bicycle frame simply by adding inertia to it. Schwab et al. (2012) has shown that a more realistic passive rider, modelled as 9 rigid segments where the arms are attached to the handlebars, can drastically change the stability behaviour. Therefore it would be interesting to investigate if the behaviour due to the pedalling disturbance also changes depending on rider posture together with bicycle design, forward speed and cadence. For specific cases and future research we would like to investigate the possibility of a simple and effective disturbance application and solution method.

The dynamic bicycle-rider models and their implementation are discussed first. Then several methods for solving responses to the pedalling disturbance are explained. The obtained lateral motions and their amplitudes are investigated in time and frequency domain. These results are evaluated for different solution methods and the dependence of model design and cycling conditions is discussed.

3.1 Method

In this method section we first cover the bicycle-rider models. The lower extremity part of the rider model is based on the leg kinematic model proposed in Section 2. Here we cover the bicycle model part, the upper body part of the rider model and the total model implementation.

Secondly we cover solution methods for the response of these bicycle-rider models to the pedalling disturbance. Here we cover a numerical method for the comprehensive non-linear system, a simple analytic method for the linearised system and a very simple conservation of angular momentum principle based solution method.

Finally we cover the evaluation of the resulting lateral motions, their amplitudes, their time domain behaviour and their frequency domain behaviour are compared for the different conditions, approaches, models and simplifications thereof. The amplitude results are used to perform an error (or relative difference) analysis for the model and solution methods and the effect of cycling conditions, posture and bicycle design parameters.

3.1.1 Bicycle-Rider Models

The Whipple bicycle model benchmarked by Meijaard et al. (2007) is used as the basis for the bicycle model. The upper body of the bicycle rider is based on the passive upper body rider model by Schwab et al. (2012). The lower body of the bicycle rider is based on the model defined in Section 2, which is a kinematic representation of a dual 3D four bar mechanism prescribing an isokinetic motion. The parameters used for the bicycle and rider correspond to the above mentioned experimental conditions by Moore et al. (2011), using both bicycle types (hybrid and city bicycle) and with hands on the handlebars and hands free cycling, in order to get an indication for the importance of system characteristics on lateral behaviour due to pedalling.

3.1.1.1 Whipple Bicycle Model The Carvallo-Whipple (Carvallo, 1899; Whipple, 1899) bicycle model, also known as simply the Whipple model, has been benchmarked by Meijaard et al. (2007). They reviewed the bicycle stability literature and produced linearised equations of motion of the Whipple model. This Whipple model has been extensively validated using experimental research (for forward speeds between 3 and 6 m/s) and widely used as basis for bicycle and motorcycle modelling (Sharp, 2008; Popov et al., 2010; Schwab and Meijaard, 2013). It is therefore an obvious choice to use as basis for our own bicycle model.

The model consists of four rigid bodies or segments as shown in Figure 3.1, the rear wheel, the rear frame, the front frame and the front wheel. These four segments are joined by constraints in such a way, that the system has 7 degrees of freedom in configuration (see Figure 3.2); position in horizontal/transverse x, y -plane, the yaw or heading ψ , the lean or roll ϕ , the pitch or angle of the rear wheel θ_R , the steering angle δ and the pitch or angle of the front wheel θ_F . In this figure the pitch of the rear frame θ_B is also shown although this is not a true degree of freedom, since both the wheels are constrained to the ground. Due to non-holonomic non-slipping wheel contact constraints there are less degrees of freedom in velocity, these are parametrized by $\dot{\theta}_R$, $\dot{\phi}$ and $\dot{\delta}$ and (rear wheel, roll or lean and steering angular velocity).

These three degrees of freedom in velocity and thus acceleration mean that the system can be described by three equations of motion. Meijaard et al. (2007) linearised these equations of motion around the neutral reference point, straight ahead ($\delta = 0$) and upright ($\phi = 0$) at constant forward speed ($v = -\dot{\theta}_R r_R$). Due to lateral symmetry in the system there is no coupling between the forward motion and the roll and the steer, meaning that the equation of motion for the rear wheel rotation simply describes the rear wheel acceleration as a function of propulsive force and bicycle parameters (inertia and wheel diameters). The other two equations of motion, regarding roll and steering, are more interesting since they define the lateral movement of the bicycle and thus the stability. They are two coupled linearised second-order, constant coefficient ordinary differential equations where forward velocity v and gravitational acceleration g can be defined explicitly.

$$M\ddot{\mathbf{q}} + v\mathbf{C}_1\dot{\mathbf{q}} + [g\mathbf{K}_0 + (v)^2\mathbf{K}_2]\mathbf{q} = \mathbf{f} \quad (3.1)$$

where \mathbf{M} is the generalized mass matrix, $\mathbf{q} = [\phi(t), \delta(t)]^T$ is the generalized coordinate (roll and steering) vector, $v\mathbf{C}_1$ is the generalized damping matrix which is linear in forward velocity, $g\mathbf{K}_0$ is the velocity independent and gravitational acceleration linear part of the generalized stiffness matrix, $(v)^2\mathbf{K}_2$ is quadratic in forward speed part of the generalized stiffness matrix and $\mathbf{f} = [T_\phi(t), T_\delta(t)]^T$ is the generalized external force vector containing roll torque and steering torque. Here the vectors are time varying and the matrices are constant which are defined in 25 bicycle design parameters in Meijaard et al. (2007). They give values for the constant matrices together with a parameter set for the benchmark bicycle. (Meijaard et al., 2007)

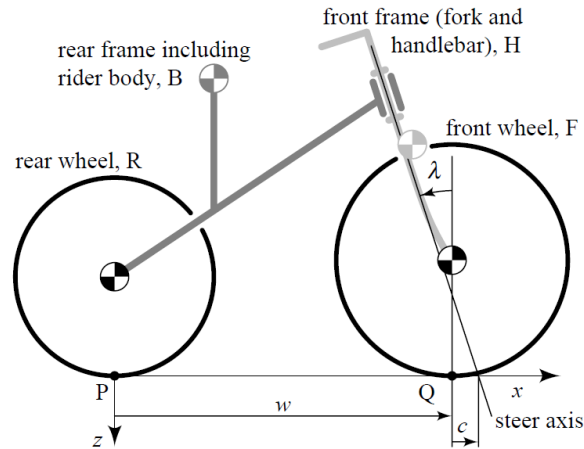


Figure 3.1: Wipple bicycle model parameters by Meijaard et al. (2007), the bicycle consists of four parts: the rear wheel, the rear frame including a rigid rider body, the front frame and the front wheel. The model is defined by the centre of mass locations of the four parts expressed in the x and z coordinate reference frame and some other displayed parameters, where P is the origin of the coordinate frame, w is the wheel base, c is the trail, λ is the tilt in the steer axis.

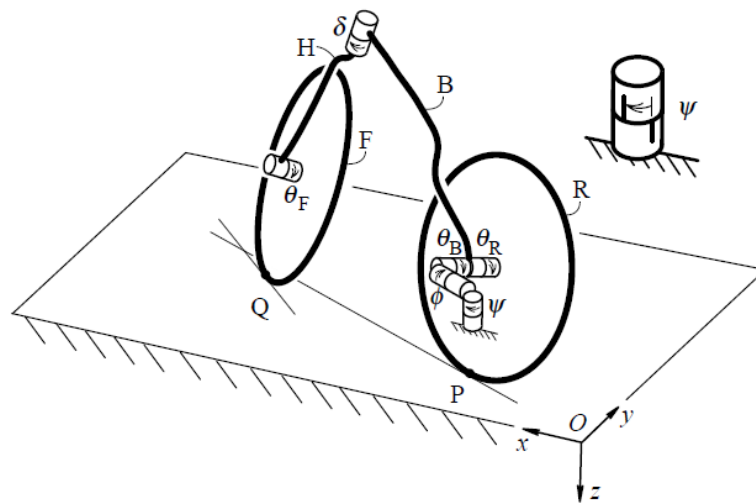


Figure 3.2: Wipple bicycle model configuration by Meijaard et al. (2007), depicting the degrees of freedom of the bicycle; position in horizontal/transverse x, y -plane, the yaw ψ , the roll ϕ , the pitch of the rear frame θ_B , the pitch of the rear wheel θ_R , the steering angle δ and the pitch of the front wheel θ_F .

3.1.1.2 Passive Upper Body Rider Model In the Whipple bicycle model, the rider is modelled as rigid attached inertia added to the rear frame of the bicycle. Schwab et al. (2012) has shown that a more realistic passive rider, modelled as 9 rigid segments where the arms are attached to the handlebars, can drastically change the stability behaviour. Therefore it would be interesting to investigate if the behaviour due to the pedalling disturbance also changes depending on rider posture.

Schwab et al. (2012) has extended the original Whipple model with a passive upper body rider model without adding any degrees of freedom to the system. This last fact is very useful for comparing behaviour since the equation of motion can then be transformed to the same formulation as the linearised equation of motion of the original model (Equation 3.1) and the same simple methods for determining stability can be used. Two passive rider-bicycle models are developed for two distinct upper body rider postures corresponding to two different types of bicycle. The first type corresponds to a hybrid bicycle (namely the Batavus Stratos bicycle), where the handlebars are straight, the arms are stretched and the trunk is leaned forward (Figure 3.3(a)). The second type corresponds to a city bicycle (namely the Batavus Browser bicycle), where the handlebars have a U-shape, the arms are flexed and the trunk is upright (Figure 3.3(b)). This posture and bicycle type, is what we in Dutch call a grandmother bicycle (literal translation), where the hybrid bicycle has a more 'sportive' posture.

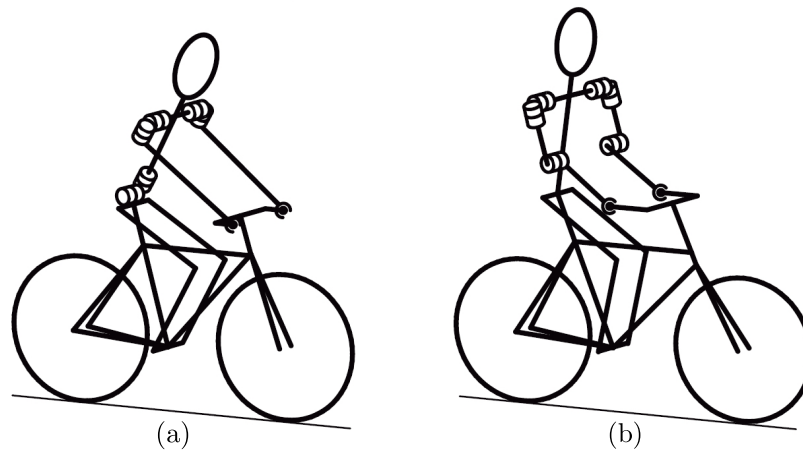


Figure 3.3: Passive upper body rider models from Schwab et al. (2012), depicting two rider postures: (a) a rider with forward leaned trunk and stretched arms corresponding to a hybrid bicycle and (b) a rider with an upright trunk and flexed arms corresponding to a city bicycle. In these models by Schwab et al. (2012), the legs are modelled as inertia added rigidly to the rear frame of the bicycle.

3.1.1.3 Implementation of a new Multibody Dynamics Bicycle-Rider Model New bicycle-rider models have been developed in a multibody dynamics software package in order to be able to investigate the influence of the full leg movement disturbance. The models are based on the Whipple bicycle model (Section 3.1.1.1) in combination with rigid and passive upper body rider models by Schwab et al. (2012) (Section 3.1.1.2), with an extension of cranks and moving leg segments as described in Section 2.1.1. These four new models correspond to two bicycles with both a hands free and a hands on the handlebar posture based on real world bicycle-rider parameters used in the motion capture experiments Moore et al. (2011). These models have been carefully designed to have the same number of degrees of freedom as the original Whipple model (see Figure 3.4 for segment connectivity).

The models are used in both full non-linear and linearised form, since the linearised approach has computational benefits especially for unstable solutions as is discussed in Section 3.1.2.2. However in order to be able to validate the linearity assumption and the simplification of the pedalling disturbance as sinusoidal roll and steering torques a full multibody dynamics model is also desired.

The models have been implemented in the multibody dynamics software package SPACAR (Jonker and

Meijaard, 1990; van Soest et al., 1992), since it can easily be used to calculate linearised second order differential equations and is also available as a toolbox for Matlab, which enhances usability and flexibility.

The new models are built up in three main stages. First the benchmark bicycle model is implemented. As a verification step, the model is linearised and verified using the linearised matrices \mathbf{M} , \mathbf{C}_1 , \mathbf{K}_0 and \mathbf{K}_2 (Equation 3.1) provided in Meijaard et al. (2007) with double numerical precision.

In the second stage an upper body is added to the bicycle models as described in Schwab et al. (2012) as well as the rider's legs and the cranks. Where Schwab et al. (2012) added the leg inertia to the bicycle frame inertia, since the legs are fixed to the frame segment, here the legs defined as separate segments in such a way, that they could be easily adjusted to describe the pedalling motion in Section 2.1.1 (Figure 2.1). Applying fixed legs and the bicycles and anthropomorphic parameters as in Schwab et al. (2012) (corresponding to experimental set-up of Moore et al. (2011)), another verification step was made by linearising the system again and comparing to the linearised matrices provided by A. L. Schwab (relative discrepancy of 1E-13).

Finally the leg motion was coupled to the cadence such that the leg motion corresponds to Section 2.1.1. The leg segments motion was constrained as depicted in Figure 3.4 using hinge elements, carefully designed not to under or over-constrain the system. The bicycle and anthropomorphic parameters as in Schwab et al. (2012) needed to be adjusted slightly to accommodate for the leg motion. The given saddle height for the city bicycle does not allow for a full circle motion of the pedal, since the leg is not long enough to reach the pedal in the down position. The saddle height is positioned according to 0.96 trochanteric height and the crank dimensions and mass have been added (following Section 2.1.1; van Soest and Casius (2000); Wilson (2004)). The general motion was verified by visualising the nodal points by implementing a Matlab animation. Details for the SPACAR model, such as element types and node numbers, can be found in Appendix B.

In order to be able to solve the system analytically, the models are also linearised. The system is linearised around the equilibrium position ($\phi = 0$, $\delta = 0$, $\dot{\phi} = 0$ & $\dot{\delta} = 0$) and crank angle θ_A is zero, meaning that the right foot is in the most forward position. The choice of putting the left or right foot forward is arbitrary, however the horizontal crank position is marginally preferred as a linearisation configuration over for instance the vertical crank position. This preference is based on left-right symmetry in vertical leg centre of mass position. The configuration also corresponds to a low roll torque during the crank cycle (see Section 2), making it a preferred initial condition for the system. Linearised matrices for these four models are created corresponding to the second order differential equation (Equation 3.1) and can be found in Appendix B.

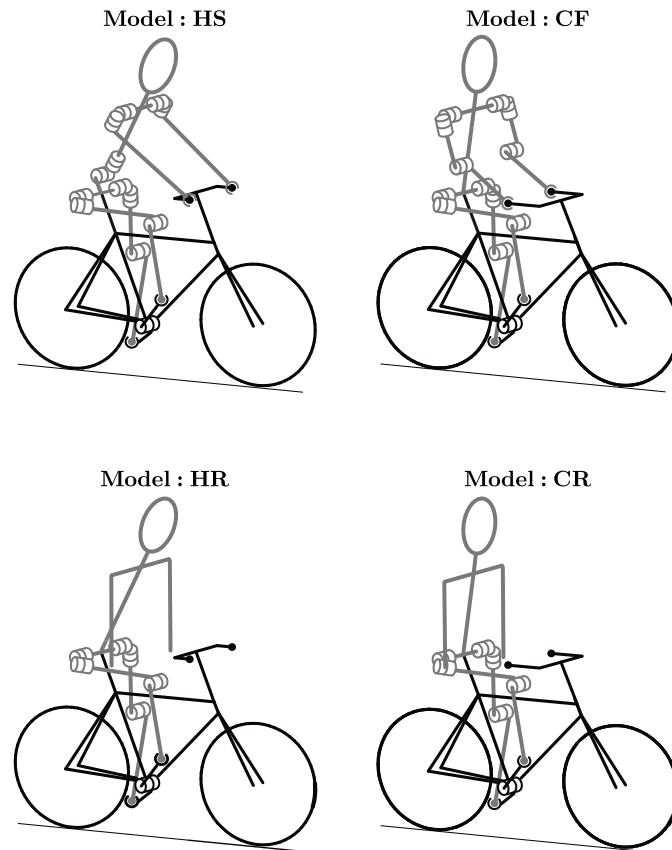


Figure 3.4: Four full body passive rider models modified to include leg motion, showing segment connectivity of the rider model. Cans depict hinge elements allowing rotation about can axis and constraining other rotations. Ball and socket joints depicted at hand-handle bar contact and foot-pedal contact indicate free rotations about all axes. The left two schematics show models corresponding to a hybrid bicycle (H: left, the Batavus Stratos) and the right two schematics show models corresponding to a city bicycle (C: right, the Batavus Browser). The upper body is either rigid (R: bottom), which has a rigid and free arms or attached to the handlebars with straight attached arms (S: top left) or flexed attached arms (F: top right). The bottom two models (HR & CR) look very similar due to the rigid upper body, however correspond to different bicycles, recognisable by the different handle bar geometry.

3.1.2 Solution Methods

The influence of the disturbance defined in Section 2 is investigated by applying inertial steering and roll torques to the dynamical models or by actually prescribing leg segment motion coupled to cadence (pedalling frequency). The system is solved for a wide range of forward speeds and cadences using three main different approaches, with increasing model and solution method simplifications. These simplifications are applied in order to investigate the possibility of developing a simplified method of determining the response of a specific bicycle-rider system to the pedalling disturbance. The evaluation corresponding to this investigation is discussed in Section 3.1.3.

The solution method that is covered first is mainly applied to the most comprehensive bicycle-rider and disturbance model combination. This is the method of generating time series through numerically integrating the equations of motion corresponding to the full non-linear multibody dynamics model including prescribed leg kinematics. This time signal is transformed to frequency domain using a discrete Fourier transform in order to distil the periodic response corresponding to the periodic pedalling disturbance. This solution method is also applied to a simpler bicycle-rider and disturbance model combinations; the non-linear and the linear bicycle-rider model with applied roll and steering torques as pedalling disturbance (defined in Section 2).

The second solution method that is covered is an analytic method of solving an approximate linearised system with applied sinusoidal generalised inertial torques. This entails solving the linearised equations of motion of the bicycle-rider system which consists of two coupled second order differential equations in an analytic manner. The corresponding solution consists of a particular solution part, which corresponds to the periodic response to the periodic applied roll and steering torques, and a homogeneous solution part, which corresponds to the transient response to the initial conditions. Here the particular part is used directly as a measure for the influence due to the disturbance. Also the full time signal including transient solution is transformed to frequency domain using a discrete Fourier transform so that we can compare this to the numerical solutions discussed above.

Finally the solution method corresponding to the conservation of angular momentum principle is covered. This is a further approximation which is based on the idea that the angular momentum associated with the leg motion is in equilibrium with the bicycle angular momentum, the generalised momentum around the bicycle roll and steering angles. This method neglects behaviour due to forward speed and gravity. For the application of this solution method we use the mass matrix of the linearised bicycle-rider model and for the disturbance we use the angular momentum associated with the leg COM forward and vertical velocity. Here we use the velocity of the COM mass trajectory corresponding to the leg kinematic model as discussed in Section 2 and the simplified skew-elliptical path only consisting of the cadence frequency.

3.1.2.1 Numerical Method: Solving a non-linear Multibody Dynamics Model Time series solutions of the non-linear (and the linear) bicycle-rider models with applied pedalling disturbance are solved using numerical time integration methods (also called ODE solvers). The non-linear multibody dynamics model is solved using the built-in default integration algorithm in the SPACAR toolbox. This is a Shampine-Gordon integration algorithm (Shampine and Gordon, 1975), which is a variable-step variable-order multi-step integration algorithm. This means that the predictor and corrector steps are of variable order and size, to ensure given local tolerance specifications in an efficient manner. The local error tolerances are also set to default ($\text{abstol} = 1\text{E-}5$, $\text{reltol} = 1\text{E-}4$).

The linear bicycle-rider models are also solved using numerical integration, however this primarily applied as a verification step for the general application of the analytic solution method covered in Section 3.1.2.2. This analytic solution method gives an exact solution of a linear model, without the introducing any numerical integration error, however it is not applicable to non-linear models. For the numerical time integration of the linear bicycle-rider models the standard built-in solver in Matlab is used in combination with the default error tolerances (ode45 , $\text{abstol} = 1\text{E-}6$, $\text{reltol} = 1\text{E-}3$). This algorithm is a variable step size, 4th-5th order single step integration algorithm based on an explicit Runge-Kutta (Dormand and Prince, 1980).

These local error tolerances are very high if we would be interested in the specific configuration for an unstable or chaotic system at a specific time corresponding to a long integration time duration, since the local errors build up every step and can have a large impact on the configuration after a long period of time

integration. However in this study we are interested in the periodic response to a periodic disturbance, where the error on the amplitude determination is much lower than the error on determining a specific state at a specific time. This means that numerical integration error is expected to have only a minor contribution on the total errors of the solution method and simplifications combined, since error contributions due to simplifications in model linearity or disturbance type are of a larger order of magnitude. Therefore a choice was made not to lower the error tolerance, since this would greatly increase computational time per simulation, and therefore limit the amount of cycling conditions that could be practically solved for.

Time solutions are generated for a wide range of cadences and forward speeds ($\omega = 0:0.5:4\pi$ rad/s, $v = 0:0.4:10$ m/s, in total 676 runs), in order to capture the response of system dependent on cycling conditions (see Section 3.1.3.2 for variable range choice). A time period of up to 180 seconds was chosen, such that the periodic solution component is clearly visible. For the unstable forward speed region the program (SPACAR toolbox) gave an error message, if the bicycle 'fell down', stopping the simulation. This error was caught and the simulation was run iteratively using a smaller or larger time period until it could complete the simulation for a maximal time domain. This means that for each of the 676 found solutions, the simulation had to be repeated up to 12 times to find an appropriate integration time.

The time solutions are compared directly to each other. Also the periodic solution parts of the time solutions are obtained, using a discrete Fourier transformation, which is covered next. The amplitudes corresponding to the cadence is compared to each other and compared to the particular solution amplitude for the linear system discussed in Section 3.1.2.2.1.

3.1.2.1.1 Periodic Solution: Fourier Analysis In the stable forward speed region, the time solution will converge to a periodic solution. In general terms this periodic solution has the same frequency as the forcing frequency, which in our case means the cadence. The periodic solution can therefore easily be distilled from the time solution by transforming the signal to the frequency domain by a Fourier transform (fft function in Matlab) and subsequently picking out the amplitude and phase information at the cadence peak.

However due to a phenomenon called leakage the found amplitude can be up to 36% lower than the real value (Brandt, 2011). To understand when this phenomenon occurs and how to minimize it, we need to understand how the Fourier transform works. Beginning with the basis for discrete Fourier transform is (Brandt, 2011):

$$X(k) = \sum_{n=0}^{N-1} x(n)e^{-j2\pi kn/N}, \quad \text{for } k = 0, 1, \dots, N-1 \quad (3.2)$$

$$= \sum_{n=0}^{N-1} x(n) \cos(2\pi kn/N) - j \sum_{n=0}^{N-1} x(n) \sin(2\pi kn/N), \quad \text{for } k = 0, 1, \dots, N-1 \quad (3.3)$$

This comprises of a real and imaginary part, which gives the information about the amplitude and phase of the corresponding frequency. How this resulting amplitude and phase relates to the time signal can be found by rewriting the inverse discrete Fourier transform:

$$x(n) = \frac{1}{N} \sum_{k=0}^{N-1} X(k)e^{j2\pi nk/N}, \quad \text{for } n = 0, 1, \dots, N-1 \quad (3.4)$$

$$x(t) = X(0) + \sum_{k=1}^{N-1} |X(k)| \cos(2\pi f(k)t + \angle(X(k))), \quad \text{for } t = 0, \Delta t, \dots, T \quad (3.5)$$

Where,

$$f(k) = k\Delta f \quad (3.6)$$

$$= k \frac{1}{T} = \frac{k}{N\Delta t} = \frac{k}{N} f_s \quad (3.7)$$

This basically means that the resolution of the frequency domain is dependent on the sampling frequency f_s and length of the time domain N . If the cadence frequency ω is not part of the discrete frequency domain, the amplitude of the cadence frequency is smeared over nearby frequencies, where the amplitude of the closest frequency is up to 36% lower than the true amplitude of the ω . The cause of this error can also be seen as the incorrect truncation of a continuous periodic signal (Brandt, 2011). For the stable forward speed region, this problem is solved by tuning the sampling frequency and precise time domain over which the Fourier transformation is taken, such that the periodic signal is truncated to contain an integer number of whole periods. However for the unstable forward speed region this simple solution cannot be applied. The underestimation due to leakage is therefore especially a problem for the unstable forward speed region, since the length of the time domain is limited, because the bicycle will fall down and the simulation is forced to stop.

Another effect which is especially a problem in the unstable region is influence on the frequency amplitudes due to the transients. As mentioned in Section 3.1.2.2 the time solution can be seen as a summation of the transients and the periodic forcing part. In the unstable region the transients will dominate the periodic forcing part corresponding to the cadence, meaning the amplitude of the ω could be greatly overestimated by simply picking out the amplitude the frequency (closest to) the ω . An underestimation is also possible if the transient and the periodic forcing part have a phase difference which can lead to destructive interference. This effect can also be seen as an addition of two imaginary numbers, where the result can have a smaller amplitude than either of the original numbers due to the angles in the complex plane.

In order to reduce the under and overestimation of the amplitude corresponding to the cadence frequency, a window function is used to reduce the transients in the signal. Several window designs were tested on performance (flat top, Blackman, Hanning (or Hann), Hamming), giving very similar results. Therefore the choice of window design was made by referencing Brandt (2011), which recommends the Hanning window as a broad purpose window. An added effect of Hanning-type windowing is that it also reduces the effect due to leakage (See Figure 3.5) (Brandt, 2011). This Hanning window $H(t)$ is applied to the time signal, before transforming it to the frequency domain. The amplitudes in the frequency domain are multiplied by a correction factor of $A_H = \frac{N}{\sum_{n=0}^{N-1} H(n)}$ in order to compensate for the signal loss by the multiplication of the window in time domain.

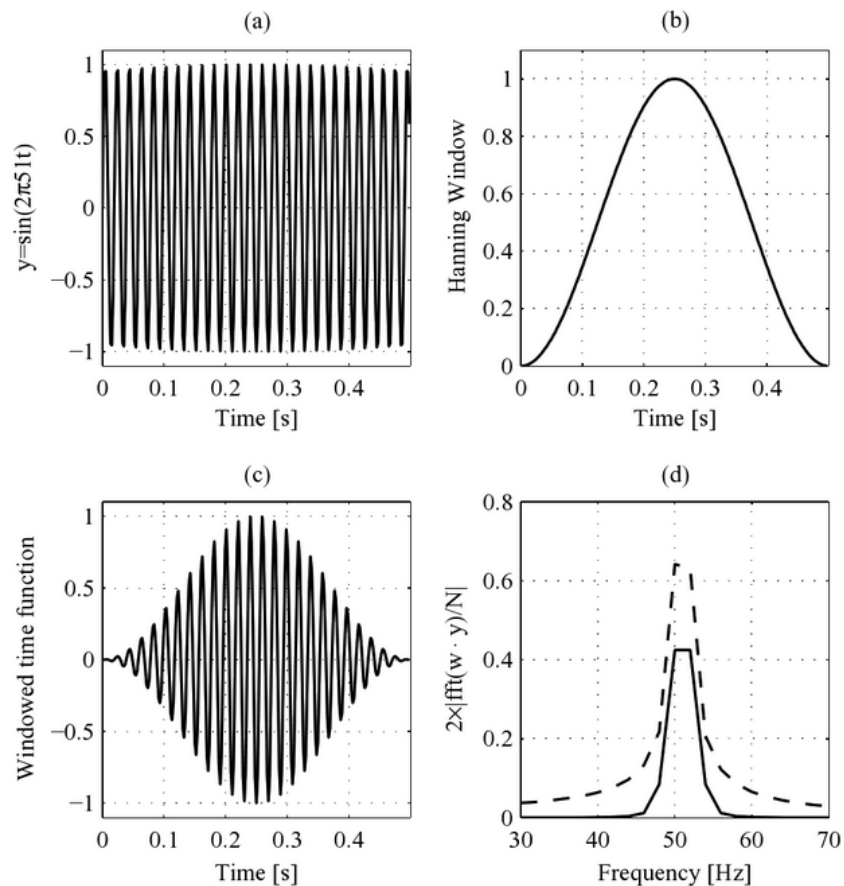


Figure 3.5: Illustration of the method of Hanning windowing by Brandt (2011): *Illustration of time-windowing with a Hanning window. The window reduces the jumps at the ends of the repeated signal. In (a) the signal is shown. In (b) is shown the Hanning window, in (c) the result of the multiplication of the two. In (d) the result of calculating the spectrum with the Hanning window (solid) and without (dashed) is shown.* The amplitude can be corrected by multiplying the acquired frequency domain by a correction factor, giving an amplitude signal with a maximum of 15% error due to leakage phenomenon instead of 36% error.

3.1.2.2 Analytic Method: Solving a System of Linearised Differential Equations A broadly applied approximation of non-linear dynamical systems such as our bicycle-rider model, is linearisation. A wide range of solution and system identification methods can only be applied to linear time-invariant systems. It would therefore be valuable to identify the possibility of and the error associated with this simplification. Linear systems can be solved analytically without introducing time integration errors. The periodic solution corresponding to a harmonic disturbance can be easily and accurately obtained analytically without any problems associated with the transient dominating the solution or leakage (Section 3.1.2.1.1).

The linearised bicycle-rider system is defined by a system of 2 coupled linearised second order differential equations (Equation 3.1) and the pedalling disturbance is defined as the generalised inertial torques defined in Section 2 by interpreting the acceleration of the leg masses as an external inertial roll and steering torque:

$$\mathbf{M}\ddot{\mathbf{q}} + v\mathbf{C}_1\dot{\mathbf{q}} + [g\mathbf{K}_0 + (v)^2\mathbf{K}_2]\mathbf{q} = \mathbf{f}_L \quad (3.8)$$

Where \mathbf{f}_L are the generalised inertial forces due to the leg acceleration disturbance defined in Equation 2.15, 2.22 and 2.24. These generalised inertial forces \mathbf{f}_L represent the d'Alembert inertial forces associated with the disturbance caused by the relative motion of the legs to the bicycle frame. The acceleration of the leg inertia in the global inertial reference frame is in fact an addition of terms caused by the acceleration and angular velocity of the local reference frame and the acceleration of the leg with respect to the local frame (Greenwood, 2006). In order to keep the effects of the leg's global acceleration corresponding to the acceleration and angular velocity of the bicycle (the local reference frame), the leg inertia should still be added to the bicycle-rider model as inertia with a constant location in the local reference frame.

The response of a linear system to disturbance is determined by the eigenfrequencies and eigenmodes of the system and the frequency content of the disturbance. The behaviour corresponding to the eigenfrequencies of the system is called the homogeneous solution (\mathbf{q}_h) and the behaviour corresponding to the forcing frequency is called the particular solution (\mathbf{q}_p). According to the superposition principle these solution parts can be simply added to each other. (Stewart, 2003; Boyce and DiPrima, 2005)

$$\mathbf{q}(t) = \mathbf{q}_p(t) + \mathbf{q}_h(t) \quad (3.9)$$

Where $\mathbf{q}_p(t)$ and $\mathbf{q}_h(t)$ are a function of constant multipliers, which is specified in Sections 3.1.2.2.1 and 3.1.2.2.2 respectively. These constant multipliers can be solved by filling in the solution with it's time derivatives ($\mathbf{q}(t)$, $\dot{\mathbf{q}}(t)$ and $\ddot{\mathbf{q}}(t)$) in the linear second order differential equations and solving them for boundary conditions (a.k.a initial conditions). For our case we assume that the roll and steering angles and angular velocities are zero at zero time. (Stewart, 2003; Boyce and DiPrima, 2005). The implementation of the analytic method was verified by using a build-in numerical integration solver of Matlab (`ode45`, `abstol = 1E-6`, `reltol = 1E-3`).

The benefit of this analytic method is that the periodic solution corresponding to the pedalling disturbance and the transients corresponding to the homogeneous solution can be solved separately, meaning that the influence of the disturbance is easily obtainable by solving the particular solution. This is especially valuable in the so called unstable forward speed region. This is a region of forward speed where there are eigenvalues of the system which have a positive real part, which effectively means that the bicycle will fall down if it is perturbed from it's equilibrium point, due to the divergent transient. In Figure 3.6 the eigenvalues are shown for the benchmark model as an example for typical eigenvalue behaviour as a function of forward speed. In the self-stable region the real part of the eigenvalues are negative, which means that the transient solution will converge.

3.1.2.2.1 Periodic Solution: the Particular Solution The particular solution corresponding to a periodic disturbance is a periodic function of the forcing frequency, which in our case is the cadence ω . (Stewart, 2003; Boyce and DiPrima, 2005)

$$\mathbf{q}_p(t) = \mathbf{a}_p \sin(\omega t) + \mathbf{b}_p \cos(\omega t) \quad (3.10)$$

$$\dot{\mathbf{q}}_p(t) = \mathbf{a}_p \omega \cos(\omega t) - \mathbf{b}_p \omega \sin(\omega t) \quad (3.11)$$

$$\ddot{\mathbf{q}}_p(t) = -\mathbf{a}_p \omega^2 \sin(\omega t) - \mathbf{b}_p \omega^2 \cos(\omega t) \quad (3.12)$$

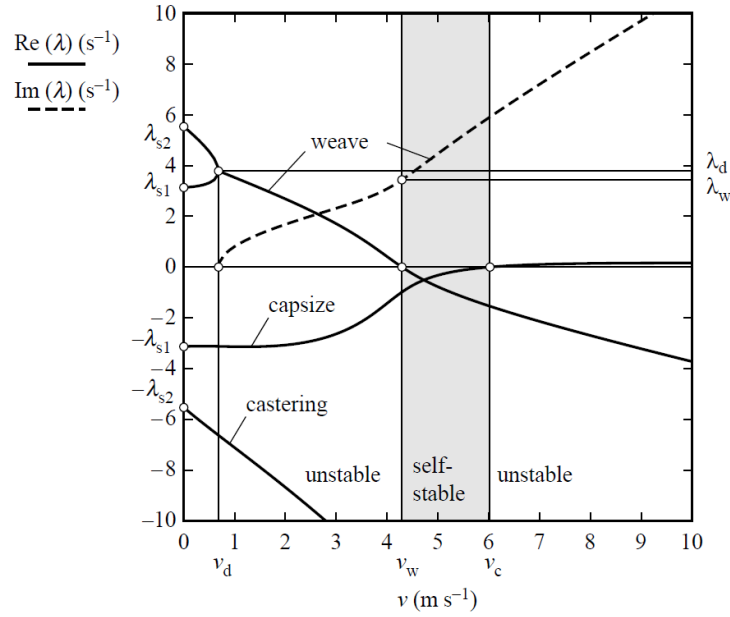


Figure 3.6: Eigenvalues λ as a function of forward speed v of the linearised equation of motion for the benchmark bicycle model from Meijaard et al. (2007). The real part of the eigenvalues are represented by a solid line and the dashed line is the imaginary part of the eigenfrequency corresponding to the weave eigenmode. This eigenmode is dominated by steering which is lagged with respect to a small lean component. The eigenvalue corresponding to the capsize eigenmode has a small positive part for very high forward speed. This eigenmode is dominated by the roll of the bicycle. The eigenvalue corresponding to the castering mode is negative for the full speed range. This eigenmode has to do with front ground contact pursuit following, which can be seen as the straightening of a swivel wheel. For medium to high forward speeds there is a self-stable region, where all real parts of the eigenvalues are negative.

The initial conditions are used to solve for the constant multipliers $\mathbf{a}_p (= \begin{bmatrix} a_\phi \\ a_\delta \end{bmatrix})$ and $\mathbf{b}_p (= \begin{bmatrix} b_\phi \\ b_\delta \end{bmatrix})$. The roll and steering amplitude can be easily calculated from these constants, since sines and cosines are perpendicular by definition.

$$|\mathbf{q}(t)| = \begin{bmatrix} |\phi(t)| \\ |\delta(t)| \end{bmatrix} = \begin{bmatrix} \sqrt{a_\phi^2 + b_\phi^2} \\ \sqrt{a_\delta^2 + b_\delta^2} \end{bmatrix} \quad (3.13)$$

The superposition principle can also be applied here if the forcing term is a function of multiple frequencies, for instance if we would like to add the higher multiples of the cadence frequency (ω & 3ω & ...).

$$\mathbf{f}_L = \sum_{n=1,3,\dots}^{\infty} m_L l_{hh} (n\omega)^2 \begin{bmatrix} |Z_L(n\omega)| \cos(n\omega t + \angle Z(n\omega)) \\ -\frac{1}{w} c \cos(\lambda) (|X_L(n\omega)| \cos(n\omega t + \angle X(n\omega))) \end{bmatrix} \quad (3.14)$$

$$\mathbf{q}_p(t) = \sum_{n=1,3,\dots}^{\infty} \mathbf{a}_n \sin(n\omega t) + \mathbf{b}_n \cos(n\omega t) \quad (3.15)$$

The solution parts corresponding to a single frequency $\mathbf{q}_n(n\omega t)$ can be evaluated using only a part of the forcing term $\mathbf{f}_L(n\omega)$ to solve the constants \mathbf{a}_n & \mathbf{b}_n separately and then adding the solution parts together to get the total particular solution. This means that the amplitude of the disturbance corresponding to the cadence frequency fully determines the amplitude of the dominant frequency of the total particular solution.

The particular solutions are solved for a wide range of cadences and forward speeds with a higher resolution compared to the full time solutions (numerical integration method and homogeneous solutions), since the computational time was relatively low ($\omega = 0:0.124:4\pi$ rad/s, $v = 0:0.1:10$ m/s, in total 10302 combinations).

3.1.2.2.2 Transient Solution: the Homogeneous Solution The homogeneous solution is dependent on the eigenmodes $\boldsymbol{\xi}$ and eigenfrequencies $\boldsymbol{\lambda}$ of the system. (Boyce and DiPrima, 2005)

$$\mathbf{q}_i(t) = c_i e^{\Re(\lambda_i)t} (\Re(\boldsymbol{\xi}_i) \cos(\Im(\lambda_i)t) + \Im(\boldsymbol{\xi}_i) \sin(-\Im(\lambda_i)t)) \quad \text{for } \Im(\lambda_i) \geq 0 \quad (3.16)$$

$$\mathbf{q}_i(t) = c_i e^{\Re(\lambda_i)t} (\Re(\boldsymbol{\xi}_i) \sin(-\Im(\lambda_i)t) - \Im(\boldsymbol{\xi}_i) \cos(-\Im(\lambda_i)t)) \quad \text{for } \Im(\lambda_i) < 0 \quad (3.17)$$

$$\mathbf{q}_h(t) = \sum_{i=1}^4 \mathbf{q}_i(t) \quad (3.18)$$

Where the constant multipliers c_1 , c_2 , c_3 and c_4 can be solved by filling in the entire solution (Equation 3.9) into the second order differential equation and solving it again for initial conditions. Here it is clearly seen that an eigenvalue with an imaginary part $\Im(\lambda_i)$ has an oscillatory component and the real part of the eigenvalue $\Re(\lambda_i)$ determines the convergence or divergence of the transient solution part. Time solutions are generated for a wide range of cadences and forward speeds ($\omega = 0:0.5:4\pi$ rad/s, $v = 0:0.4:10$ m/s, in total 676 runs), for periods of time such that the periodic solution component is clearly visible (180 s).

3.1.2.3 Simple Method: Conservation of Angular Momentum The simplest solution method used to approximate the system response to the pedalling disturbance is the conservation of angular momentum method. The principle of conservation of angular momentum states that when a system is not subjected to an external torque or angular impulse, the sum of the angular momentum of the bodies in the system remains constant. This can be formulated for a general system of rigid bodies as follows:

$$\mathbf{L} = \sum_n \mathbf{r}_n \times m_n \mathbf{v}_n + \mathbf{I}_n \boldsymbol{\omega}_n = \text{constant} \quad (3.19)$$

Where \mathbf{L} is the angular momentum, \mathbf{r}_n is the position vector of the centre of mass of body n relative to the pivot point, m_n is the mass of body n , \mathbf{v}_n is the velocity vector of the centre of mass of body n , \mathbf{I}_n is the moment of inertia tensor of body n around the centre of mass and $\boldsymbol{\omega}_n$ is the rotational velocity vector of body n . (Fowles and Cassiday, 1999)

In the case of our bicycle-rider model with pedalling motion, we assume that the generalised angular momentum associated with the leg velocity \mathbf{L}_L is in equilibrium with the generalised momentum $\mathbf{M}\dot{\mathbf{q}}$ associated with the velocity of the generalised coordinates ($\dot{\phi}$ and $\dot{\delta}$).

$$\mathbf{M}\dot{\mathbf{q}} + \mathbf{L}_L = \text{constant} \quad (3.20)$$

Where \mathbf{M} is the linearised mass matrix and $\mathbf{q} = [\phi(t), \delta(t)]^T$ is the generalised coordinate (roll and steering) vector both the same as in the second order differential equation (Equation 3.1). By comparing these equations to the linearised second order differential equations (Equation 3.8 and realising that $\mathbf{L}_L = -\int \mathbf{f}_L dt$) it can be seen that the approaches are very similar. The main simplification is that this method does not include the bicycle behaviour corresponding to gravity and forward speed. The constant is solved by assuming that the roll and steering angles deviate about the neutral angle. In order to derive the generalised leg momentum \mathbf{L}_L , we first derive the Cartesian angular momentum $\mathbf{L}_{\mathbf{x}_L}$ and then transform it to generalised coordinates. This method is similar to the method of deriving the Cartesian torques $\mathbf{T}_{\mathbf{x}_L}$ (Section 2.1.2) and then transforming it to the generalised torques \mathbf{f}_L (Section 2.1.3).

$$\mathbf{L}_{\mathbf{x}_L}(t) = \begin{bmatrix} \mathbf{x}_{riL}(t) \times [\mathbf{M}_L \dot{\mathbf{x}}_{riL}(t)] + \mathbf{x}_{leL}(t) \times [\mathbf{M}_L \dot{\mathbf{x}}_{leL}(t)] + \dots \\ \mathbf{I}_{ul} \boldsymbol{\omega}_{riul}(t) + \mathbf{I}_{ul} \boldsymbol{\omega}_{leul}(t) + \mathbf{I}_{ll} \boldsymbol{\omega}_{riil}(t) + \mathbf{I}_{ll} \boldsymbol{\omega}_{leil}(t) + \mathbf{I}_{cr} \boldsymbol{\omega}_{ricr}(t) + \mathbf{I}_{cr} \boldsymbol{\omega}_{lecr}(t) \end{bmatrix} \quad (3.21)$$

$$= \begin{bmatrix} \frac{1}{2} l_{hh} m_L (\dot{z}_{ril}(t) - \dot{z}_{lel}(t)) \\ L_{y_L} \\ \frac{1}{2} l_{hh} m_L (-\dot{x}_{ril}(t) + \dot{x}_{lel}(t)) \end{bmatrix} \quad (3.22)$$

Since the moment of inertia tensors \mathbf{I}_i are diagonal matrices and the angular velocity vectors $\boldsymbol{\omega}_i$ only have a second entry corresponding to the pitch velocities $\dot{\theta}_i$, these terms only contribute to the pitch angular momentum L_{y_L} . The details of the pitch angular momentum L_{y_L} are not specified here, however in Appendix B.2 the inertial pitch torque T_{y_L} is derived which can be used to gain insight in the terms since $L_{y_L} = -\int T_{y_L} dt$. In order to transform the Cartesian angular momentum to generalised angular momentum we first express the Cartesian angular momentum in terms of the bicycle parameters roll ϕ , pitch θ and yaw ψ .

$$\mathbf{L}_{\mathbf{x}_L} = \begin{bmatrix} L_{x_L} \\ L_{y_L} \\ L_{z_L} \end{bmatrix} = \begin{bmatrix} L_{\phi_L} \\ L_{\theta_L} \\ L_{\psi_L} \end{bmatrix} \quad (3.23)$$

then we can apply the transformation using the kinematic relations specified in Section 2.1.3 ($\dot{\theta} = 0$ and $\frac{\partial \psi}{\partial \delta} = \frac{1}{w} c \cos(\lambda_s)$):

$$\mathbf{L}_L = \begin{bmatrix} L_{\phi_L} \\ L_{\delta_L} \end{bmatrix} = \begin{bmatrix} L_{\phi_L} \\ \frac{1}{w} c \cos(\lambda_s) L_{\psi_L} \end{bmatrix} \quad (3.24)$$

$$= \begin{bmatrix} \frac{1}{2} l_{hh} m_L (\dot{z}_{ril}(t) - \dot{z}_{lel}(t)) \\ \frac{1}{w} c \cos(\lambda) \frac{1}{2} l_{hh} m_L (-\dot{x}_{ril}(t) + \dot{x}_{lel}(t)) \end{bmatrix} \quad (3.25)$$

Where l_{hh} is the hip to hip length which is also a reasonable measure for pedal to pedal distance (Moore et al., 2009), m_L is the leg mass (Moore et al., 2009), $\dot{z}_{ril}(t)$ and $\dot{z}_{lel}(t)$ is the vertical velocity (positive down) and $\dot{x}_{ril}(t)$ and $\dot{x}_{lel}(t)$ is the forward velocity of the right and left leg COM respectively. Where the same kinematic relation used for transforming the inertial yaw torques to steering torques (Equation 2.13) are used to transform the yaw momentum to a steering momentum.

This method is the simplest form of approximating the influence of the pedalling disturbance on the behaviour of the bicycle. However when the generalized coordinates deviate from their equilibrium position ($\mathbf{q} \neq [0, 0]^T$ or $\dot{\mathbf{q}} \neq [0, 0]^T$) which is inevitable due to the disturbance, the principle of conservation of angular momentum does not hold any more. When there is a slight roll, the gravity force in fact causes a small external torque around the pivot point. Also a slight deviation from either position or velocity of the generalized coordinates together with a forward speed ($v \neq 0$) effectively also brings about a generalized roll and steering torque (see Equation 3.1), which have to do with the lateral ground contact forces and gyroscopic effects. This means that this approach will likely only give reasonable results for small deviations around the equilibrium point. The error of these simplifications, is illustrated by making an estimation of the contribution of these neglected influences (see Section 3.2.3.1 for details).

3.1.3 Data analysis: Parameter Dependence and Method Evaluation

The evaluation of the results are six fold, described in the evaluation points stated below. The first three evaluation points correspond to the method evaluation, this is also schematically represented by Figure 3.7. The last three evaluation points are focussed on ascertaining if the lateral bicycle behaviour due to pedalling is dependent on parameters associated with bicycle design, posture and cycling conditions. With this analysis we want to investigate the possibility of developing a simple method of applying a pedalling disturbance to a bicycle-rider model, without losing the response behaviour associated with these parameters and variables.

We want to identify errors/differences associated with and possibly validate:

1. Simplifications made to the full non-linear multibody dynamics model

- a) Fixing leg inertia to rear frame of the bicycle
→ Compare non-linear model torques ($\mathbf{T}(\omega, 3\omega, 5\omega)$) to non-linear model pedalling
- b) Linearisation around roll and steering angle (ϕ, δ)
→ Compare linear model torques ($\mathbf{T}(\omega, 3\omega, 5\omega)$) to non-linear model torques ($\mathbf{T}(\omega, 3\omega, 5\omega)$)
- c) Neglecting behaviour corresponding to forward speed ($v = 0$) and gravity ($g = 0$)
→ Compare conservation of angular momentum solution to particular solution

2. Simplifications made to the pedalling disturbance
 - a) Multiple harmonic inertial torques on steering and roll ($\mathbf{T}(\omega, 3\omega, 5\omega)$)
→ Compare non-linear model torques ($\mathbf{T}(\omega, 3\omega, 5\omega)$) to non-linear model pedalling
 - b) Neglecting higher cadence harmonics ($\mathbf{T}(\omega)$)
→ Compare linear model torques ($\mathbf{T}(\omega)$) to linear model torques ($\mathbf{T}(\omega, 3\omega, 5\omega)$)
3. Differences in solution approaches
 - a) Numerical time integration vs. analytical time solution approaches
→ Compare linear model numerical to analytic
 - b) Discrete Fourier transform vs analytical amplitude determination approach
→ Compare analytic to particular solution
4. Differences in cycling conditions
 - a) Forward speed and cadence combinations (v & ω)
→ Compare combinations of v & ω in grid to a reference value
5. Differences in rider posture
 - a) Hands free rigid upper body vs. hands on the handle bars passive upper body
→ Compare model HR to HS
→ Compare model CR to CF
6. Differences in bicycle design parameters
 - a) City bicycle vs. hybrid bicycle
→ Compare model CR to HR

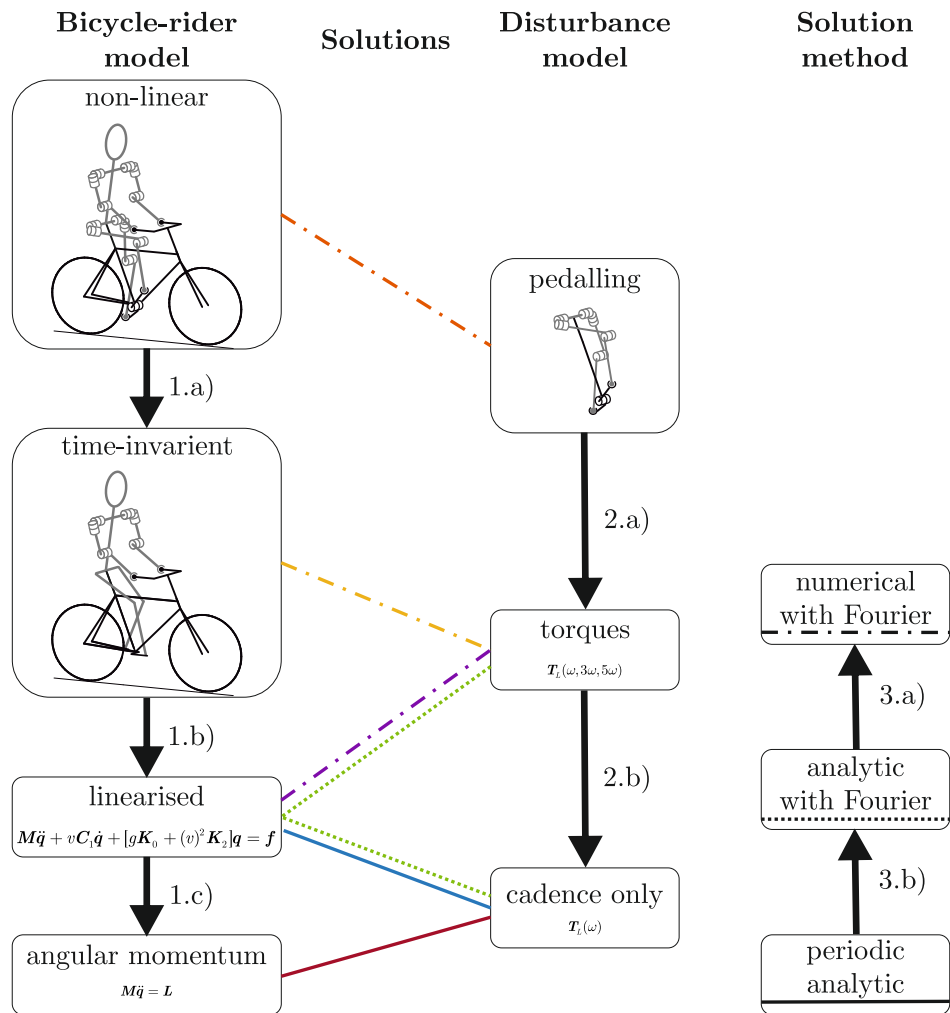


Figure 3.7: Model and solution method evaluation schematic. Arrows indicate model simplifications or solution method introduced errors that are evaluated corresponding to the evaluation points defined. The coloured lines indicate solution model combinations that are available for this evaluation, where the line style indicates the solution method corresponding to this model combination.

3.1.3.1 Model and Solution Method Evaluation For the first part of the evaluation we start by analysing the general time, frequency and forcing response amplitude results corresponding to the different solution approaches (for the four bicycle-rider models and for a range of forward speed & cadence combinations). Then we ascertain the relative differences or errors associated with the methods and simplifications by comparing the corresponding solution/model combinations proposed above in evaluation points 1-3. If we include the sub-points, we find 7 method differences we want to evaluate for points 1-3. For these 7 sub-points we can see that 1(a) and 2(a) have the same proposed model-method combination to compare, leaving 6 model-method combinations. This is because the simplification of the disturbance has a dual effect, it simplifies the disturbance itself and it simplifies the model's mass distribution. This simplification of the mass distribution can also be seen as part the linearisation of the bicycle-rider model, since it does not only entail linearisation around a specific coordination of the generalised coordinates, but also around a specific leg configuration corresponding to a crank angle. Because this last effect is not a trivial part of the simplification, this aspect is briefly explained by explaining it in terms of linearising the bicycle-rider system.

The analytic solution method discussed in Section 3.1.2.2 uses linearised equation of motion of the bicycle-rider system. These linearised equations of motion represent the system well for small deviations around the equilibrium point (upright and straight ahead). Although it is expected that the particular solution would only have small periodic deviations around this configuration ($\phi < 0.1$ rad & $\delta < 0.1$ rad), the pedal motion cannot be easily seen as a small motion around an equilibrium point. This would effectively mean that the linearised matrices (\mathbf{M} , \mathbf{C}_1 , \mathbf{K}_0 and \mathbf{K}_2 in Equation 3.1) cannot be considered constant, but have harmonic components. In order to investigate this effect we can compare the non-linear multibody dynamics models with pedalling legs with the non-linear model with applied torques.

In order to quantitatively compare the 6 model-method combinations, we define a measure for disturbance response and relative difference of this response. We use the amplitudes of the roll and steering angles corresponding to the cadence ($|\phi(\omega)|$ & $|\delta(\omega)|$ respectively) as a measure of disturbance response. The relative difference between the amplitudes corresponding to two model-method combinations is used as a measure of difference or error:

$$RD_{1 \rightarrow 2} = \left| \frac{|\phi_1(\omega)| - |\phi_2(\omega)|}{|\phi_1(\omega)|} \right| 100\% \quad (3.26)$$

This represents the relative difference RD or error percentage associated with the simplification or method case 2 compared to the reference case 1. This error calculation is also done for the steering angle in the same manner. On the basis of this evaluation we choose a suitable solution method and proceed with the second part of the evaluation.

3.1.3.2 Cycling Condition and Parameter Dependent Response For the second part we explore the parameters and cycling conditions impacting the pedalling response results. Here we are interested in ascertaining the general lateral bicycle behaviour due to pedalling for 'normal cycling' and if it is dependent on parameters associated with bicycle design, posture and cycling conditions. We do not expect to give a concrete answer on what the effect is of the concerning parameters, more give an impression in what range the response lies and if the bicycle design parameters, posture parameters and cycling conditions should be taken into account for specific cases in future research.

For this evaluation we first ascertain the working range of civil cycling. In Figure 3.8 the total grid corresponding to the forward speed and cadence combinations we use as simulation variables ($\omega = 0$ to 4π rad/s, $v = 0$ to 10 m/s) is depicted. The working range and the area of combinations corresponding to 'normal cycling' conditions are also visualised in Figure 3.8. During cycling the cadence is coupled to the forward speed by a gear ratio, defined by the ratio between the number of teeth on the front and rear sprockets. A gear ratio of 1 means there are as many front teeth as rear teeth and a gear ratio of 2 means there are twice as many front teeth as rear teeth on the sprockets. Gear ratios of single gear bicycles usually have a gear ratio somewhere between 2 and 2.5. Bicycles with multiple gears have a larger working range dependent on the numbers of gears and their ratio, common gears range from a ratio of 1 till 4.

Commuters have an average cycling speed of 14 km/h depending on gender and age (CBS: Molnar (2002)). However for favourable cycling conditions (flat straight cycling, good tyre pressure), higher speeds are possible with a medium effort. This speed is dependent on bicycle type, where the average forward speed for a city

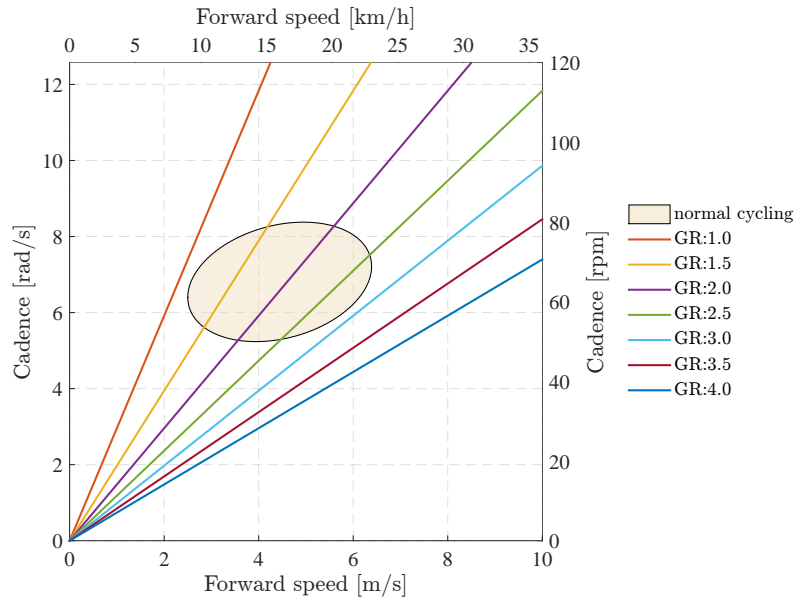


Figure 3.8: Gear ratios (GR: 1 till GR:4) shown as a function of forward speed and cadence and inside the ellipse a rough indication is given of speed-cadence combinations corresponding to 'normal cycling' conditions.

bicycle lies lower (100 Watt: 18.8 km/h) than for a hybrid bicycle type (100 Watt: 21.9 km/h; Fietsersbond: Bakker (2011)). Normal cadences range from 50 rpm to 80 rpm for recreational and utility cycling. Both these numbers can be much higher for recreational cycling on a racing bike, where sprint cycling (250 Watt) could correspond to speeds up to 36 km/h and 120 rpm. We are interested in the differences in response corresponding to normal cycling conditions, however to illustrate how the general behaviour changes outside this region, a larger range of cycling conditions is chosen: a full grid from 0 to 120 rpm and 0 to 36 km/h ($\omega = 0$ to 4π rad/s, $v = 0$ to 10 m/s). A reference value of $\omega = 2\pi$ rad/s (60 rpm) and $v = 5$ m/s (18 km/h) is arbitrarily chosen as a mid-value of the grid lying inside the 'normal cycling' range.

For our evaluation we illustrate the pedalling disturbance response corresponding to the 4 different bicycle-rider models. This will give an impression of the influence on response corresponding to bicycle design parameters (a Hybrid and a City bicycle) and different postures. These postures are either rigid or passive postures, where we are not (yet) interested in the active or posture control motion, but rather in the influence of the mass distribution and connectivity. The rigid upper body rider model represents a no hands cycling posture (HR and CR), and the two passive upper body rider models (HS and CF) represent two different hands on the handle bars postures corresponding to the two bicycle types. The hybrid bicycle has a straight arm posture and the city bicycle has flexed arms posture. Note that model HS and model CF correspond to different postures and bicycle design parameters.

3.2 Results and Discussion

The results and discussion of this chapter are split in two general topics: Evaluation of the model and solution methods and evaluation of the parameters and variables effecting the response corresponding to 'normal' cycling.

The model and solution method evaluation has the largest contribution to the volume of this section. First the results of the particular solution in combination with the time domain are shown and discussed in Section 3.2.1. Section 3.2.2 focusses on the periodic and frequency domain results and discussion. Then the results for the conservation of angular momentum is discussed in a separate section (3.2.3) and the neglected momenta associated with this simplification is discussed in Section 3.2.3.1. Then we proceed with the model and solution method evaluation by quantifying and discussing the relative differences corresponding

to simplification steps or method differences in Section 3.2.4.

Finally in Section 3.2.5 the implications of the solutions corresponding to the different cycling conditions and variety between the bicycle-rider models are illustrated and discussed.

3.2.1 Particular Solutions and Time Domain

The eigenvalues as a function of forward speed corresponding to the linearised bicycle-rider models are shown in Figure 3.9. The models corresponding to the figures can be easily recognised by the little bicycle-rider model schematic depicted below the figure. These eigenvalue figures give a good indication of how the transient part of the time solution behaves as a function of forward speed. The homogeneous part of the analytic solution corresponding to the linearised model, is determined by the eigenvalues, eigenmodes and initial conditions of the system, where the rise and decay of the transient are determined by the real part of the eigenvalue and the oscillatory component is determined by the imaginary part of the eigenvalue. This means that these eigenvalue figures can directly give insight in the behaviour of the bicycle-rider system which is added to the periodic response corresponding to the particular solution corresponding to the disturbance.

Here we can see that three out of the four models (HS, HR and CR) show very similar general behaviour to the benchmark bicycle behaviour shown in Figure 3.6. In this figure also generally accepted names can be found for the eigenmodes (weave, capsizes and caster). For low speeds these three models have a positive real part eigenvalue corresponding to the weave mode. The weave mode also exhibits an oscillatory component, for the largest part of the forward speed range, which can be seen due the imaginary part of the eigenvalue. These three models have a self-stable region for the medium to high speed range, where all the eigenvalues have a negative real part. This self-stable speed range is very interesting to emphasize, since this forward speed range represent cycling conditions where the periodic solution represents the steady state solution. For the high speeds, the capsizes eigenmode becomes unstable, with a low positive real part eigenvalue. The eigenvalue plots closely correspond to the eigenvalue plots in Schwab et al. (2012), since the only physical difference for the linearised system is the slight change in leg configuration.

The exception is the top right eigenvalue plot, which corresponds to the model CF. This model does not have a self-stable speed range, meaning that the bicycle will fall down for all speeds. The main difference lies in the eigenvalue behaviour corresponding to the capsizes eigenmode. This eigenvalue has a positive real part for low forward speeds. The other eigenvalues are only marginally different in behaviour. This eigenvalue figure is not the same as the corresponding figure in Schwab et al. (2012). This is due to the fact that we had to change the seat post length parameter (lower the saddle), in order to accommodate a full crank rotation for the pedalling motion. If we keep the seat post length parameter the same as in Schwab et al. (2012), we do find a very similar eigenvalue behaviour (shown in Appendix, Figure E.1)

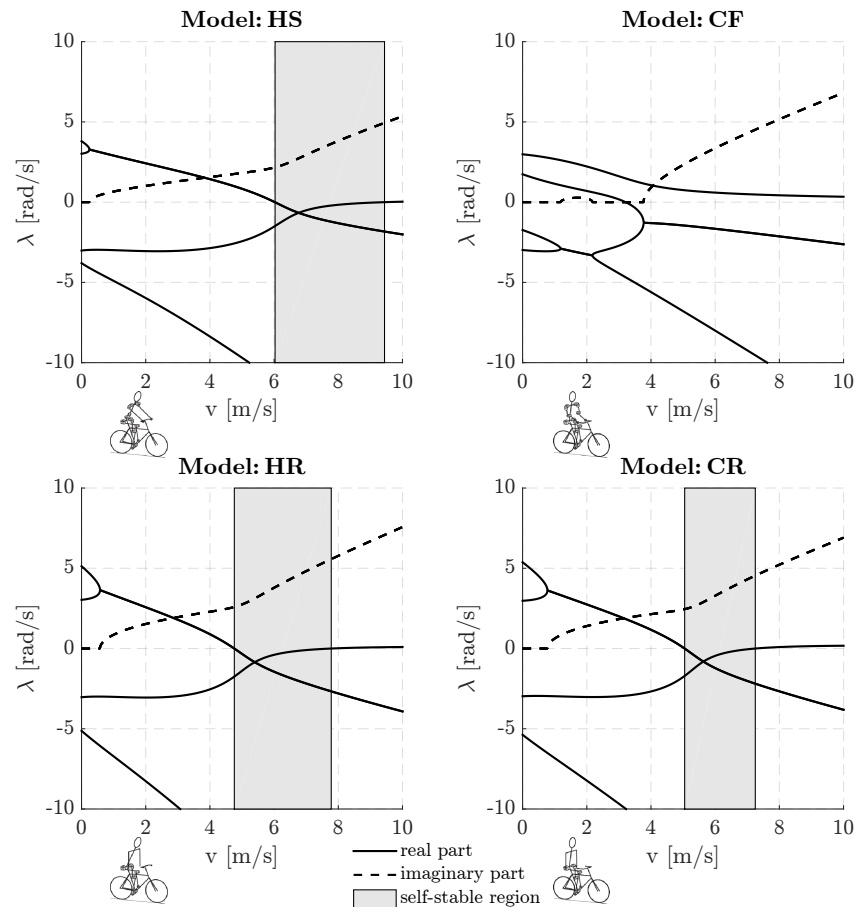


Figure 3.9: Eigenvalues λ as a function of forward speed v of the linearised equation of motion for all four bicycle-rider models. The models are identified by the caption above and the little bicycle-rider schematic below the figure. The real part of the eigenvalues are represented by a solid line and the dashed line is the imaginary part of the eigenfrequency corresponding to the weave eigenmode, which has a positive part for low to medium forward speeds. The eigenvalue corresponding to the capsize eigenmode has a small positive part for very high forward speed. Medium to high forward speeds there is a self-stable region in three of the four models, where all real parts of the eigenvalues are negative.

The particular solution for the 4 bicycle-rider models are shown in contour plots in Figure 3.10 till 3.17 on the left side. Here the roll or steering amplitudes are shown as a function of forward speed and cadence.

The isoline corresponding to the conservation of angular momentum solution is shown in the contour plots. This is an isoline of the particular solution corresponding to the value of the conservation of angular momentum solution. The contour plot of the angular momentum solution itself would be the same value for all cadences and forward speed combinations. More on the behaviour and discussion corresponding to the conservation of angular momentum solution can be found in Section 3.2.3

In general the roll and steering amplitudes are low for very low cadences. For normal forward cycling speeds and cadences, the roll amplitude is around the 0.01 rad and the steering amplitude around the 0.02 rad. Except for model HS (hybrid bicycle straight arms) where the steering amplitude also is lower; around 0.01 rad. The models with a stable region, show a peak of the amplitudes at the forward speed where the real part of the eigenvalue is zero and the cadence matches the imaginary part of the eigenvalue. This means that the oscillatory weave mode is undamped and an excitation of this frequency will result in resonance. The imaginary part of the weave eigenvalue and the stable region (where all the real parts of the eigenvalues are negative) are shown in the figures for reference. The shape of the isolines seem to be effected by the

oscillatory part of the weave eigenvalue, generally raising the amplitudes near this frequency.

On the right hand side some example time solutions are shown for different forward speeds corresponding to the same gearing ratio (≈ 2.3 medium gearing ratio), generated using the various different methods. As we expected from discussing the eigenvalue figures, in the stable region, the particular solution is representative for the steady state solution, whereas in the unstable region the transient solution will diverge and the bicycle will fall down, because there is no control present in the model. For high forward speeds, the time the bicycle will take to fall down can be very long, since the real part of the capsize eigenvalue is very small positive, meaning that there is a relatively small divergent transient present in the roll angle. For low forward speeds, the bicycle will fall down quickly, since the real part of the weave eigenvalue is relatively large. For very low speeds, the periodic component of the time solution is not even identifiable by eye, because the bicycle falls down so quickly.

The model CF does not have a self-stable forward speed region, however the weave mode becomes stable at 3.2 m/s. In Figures 3.12 and 3.13 we can see that after the weave mode becomes stable, there is only a small positive capsize eigenvalue left and the bicycle stays up long enough for the periodic solution to be visible in the time solution.

Speed-cadence combination number 3 of Figure 3.11 (model HS) seems to have a periodic part in the time solution with a frequency other than the cadence frequency with a higher amplitude. Figure 3.18 shows time solutions corresponding to the same forward speed and different cadences for model HS. Here a dominant periodic frequency can be seen in all 6 time solution with a time period of around 3 seconds. This corresponds to around the $1/3$ Hz or $2/3 \pi$ rad/s ≈ 2.1 rad/s, which is the same frequency as the imaginary part of the weave eigenvalue. It is visible that the time solutions oscillates about this weave signal with the cadence frequency, where the amplitude is largest for number 5, as expected from the particular solution plot on the left, since it is closest to the undamped weave frequency peak. Similar behaviour is seen for the hands free models (see Figure 3.19 for model CR).

Overall the time solutions for the different methods are very similar, with some minor exceptions such as speed-cadence combination number 4 for Figure 3.12. These usually small differences seem to be in the transient, since the amplitude of the periodic signal looks the same, however in some cases this is maybe better identified in frequency domain (Section 3.2.2). In Section 3.2.4 these relative differences between the model and solution methods are identified and discussed. In Section 3.2.5 the implications of the solutions corresponding to the different cycling conditions and variety between the model's bicycle design parameters and rider posture are discussed.

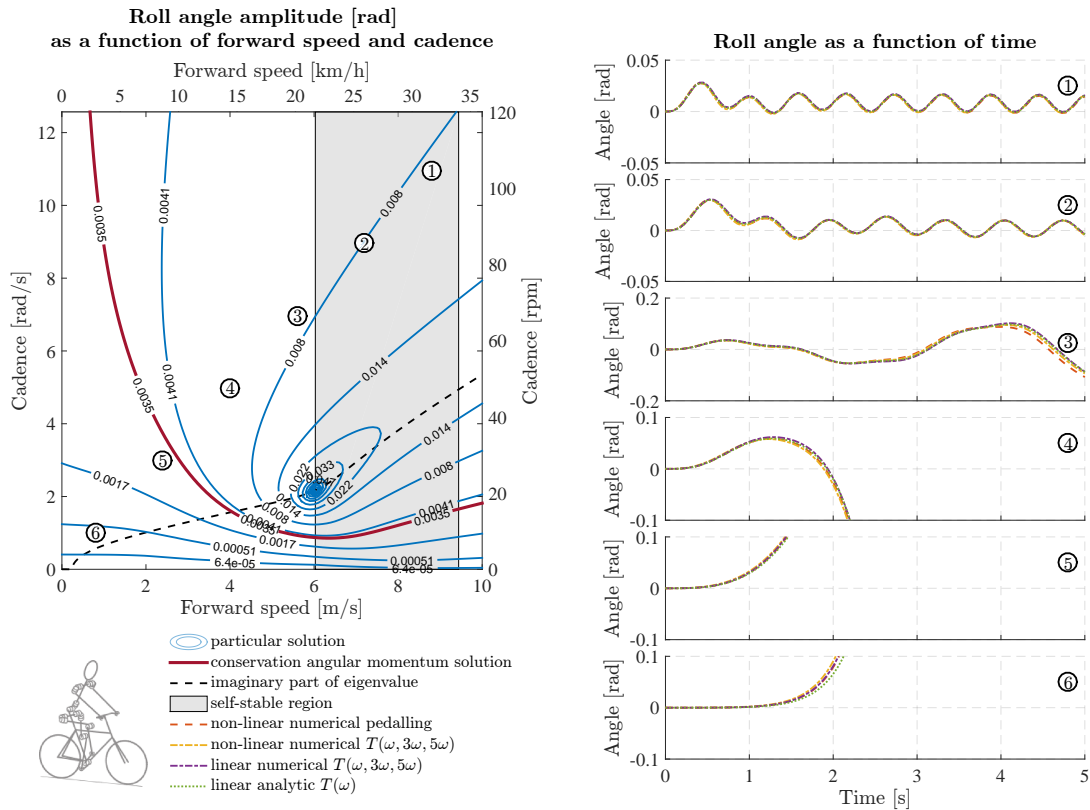


Figure 3.10: Roll amplitude of the particular solution (left) and time solutions corresponding to other solution methods (right), for model HS shown bottom left in figure. The six numbers corresponding to the six plots on the right are indicated on the roll angle amplitude plot on the left, to indicate the speed-cadence combination belonging the time solution. The isoline corresponding to the amplitude of the conservation of angular momentum solution is shown in the particular solution contour plot on the left for comparison; the conservation of angular momentum solution itself is independent on forward speed and cadence. The imaginary part of the weave eigenvalue and the self-stable region are shown for reference. The particular solution left is the periodic cadence frequency component of the linear analytic time solution shown right, by definition. The non-linear model is solved using prescribed leg motion as disturbance. The linear and non-linear models are also solved using a multiple frequency torque disturbance.

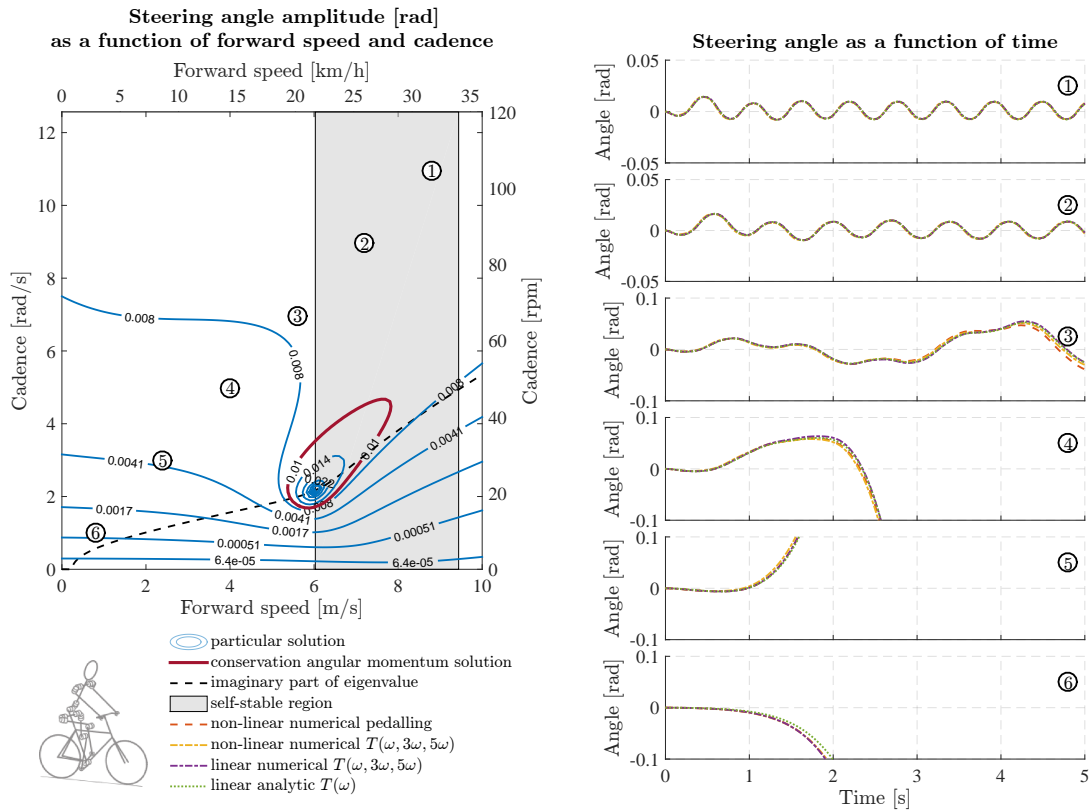


Figure 3.11: Steering amplitude of the particular solution (left) and time solutions of other methods (right), for model HS shown bottom left in figure. The six numbers corresponding to the six plots on the right are indicated on the roll angle amplitude plot on the left, to indicate the speed-cadence combination belonging the time solution. The isoline corresponding to the amplitude of the conservation of angular momentum solution is shown in the particular solution contour plot on the left for comparison; the conservation of angular momentum solution itself is independent on forward speed and cadence. The imaginary part of the weave eigenvalue and the self-stable region are shown for reference. The particular solution left is the periodic cadence frequency component of the linear analytic time solution shown right, by definition. The non-linear model is solved using prescribed leg motion as disturbance. The linear and non-linear models are also solved using a multiple frequency torque disturbance.

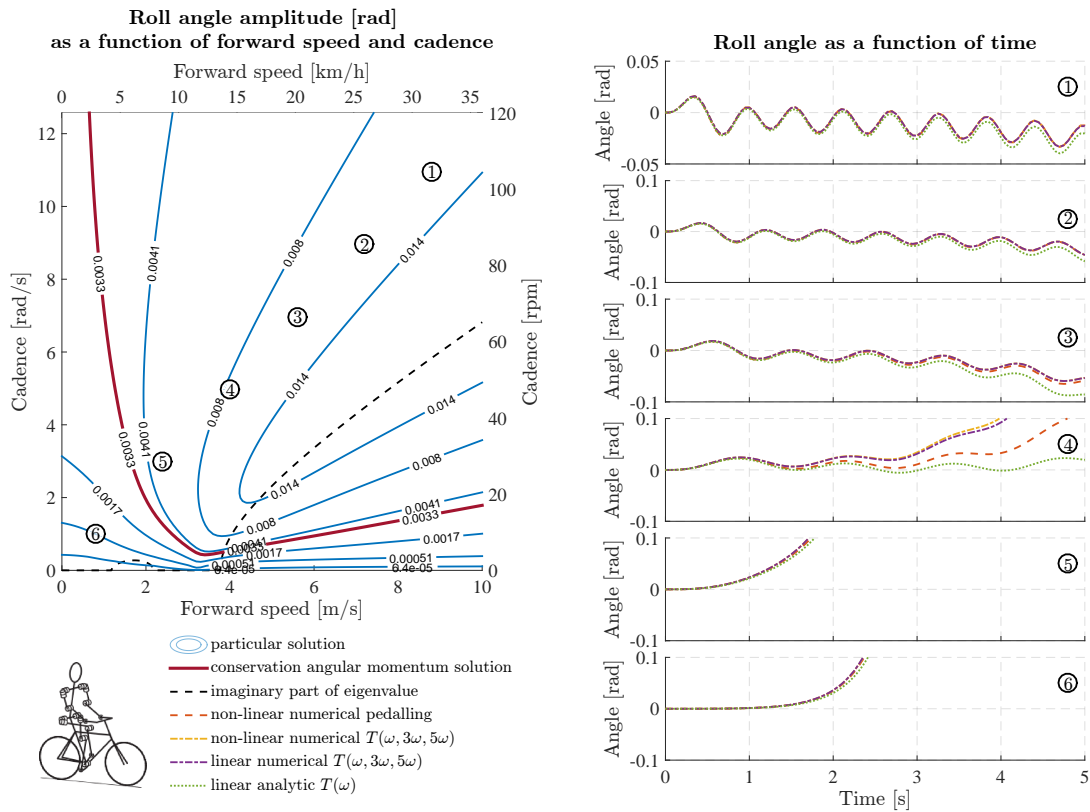


Figure 3.12: Roll amplitude of the particular solution (left) and time solutions of other methods (right), for model CF shown bottom left in figure. There is no stable region, however the weave mode is stable from 3.2 m/s (real part of eigenvalue of weave mode is negative from 3.2 m/s). The imaginary part of the weave eigenvalue and is shown for reference. The six numbers corresponding to the six plots on the right are indicated on the roll angle amplitude plot on the left, to indicate the speed-cadence combination belonging the time solution. The isoline corresponding to the amplitude of the conservation of angular momentum solution is shown in the particular solution contour plot on the left for comparison; the conservation of angular momentum solution itself is independent on forward speed and cadence. The particular solution left is the periodic cadence frequency component of the linear analytic time solution shown right, by definition. The non-linear model is solved using prescribed leg motion as disturbance. The linear and non-linear models are also solved using a multiple frequency torque disturbance.

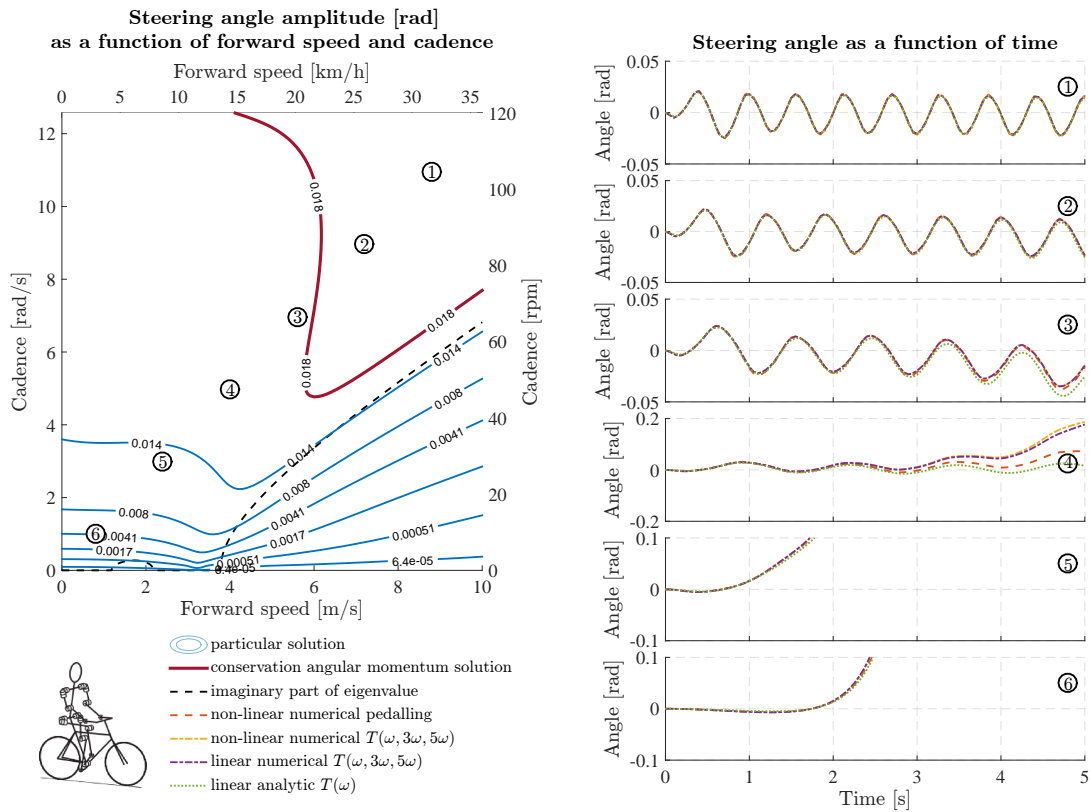


Figure 3.13: Steering amplitude of the particular solution (left) and time solutions of other methods (right), for model CF shown bottom left in figure. There is no stable region, however the weave mode is stable from 3.2 m/s (real part of eigenvalue of weave mode is negative from 3.2 m/s). The imaginary part of the weave eigenvalue and is shown for reference. The six numbers corresponding to the six plots on the right are indicated on the roll angle amplitude plot on the left, to indicate the speed-cadence combination belonging the time solution. The isoline corresponding to the amplitude of the conservation of angular momentum solution is shown in the particular solution contour plot on the left for comparison; the conservation of angular momentum solution itself is independent on forward speed and cadence. The particular solution left is the periodic cadence frequency component of the linear analytic time solution shown right, by definition. The non-linear model is solved using prescribed leg motion as disturbance. The linear and non-linear models are also solved using a multiple frequency torque disturbance.

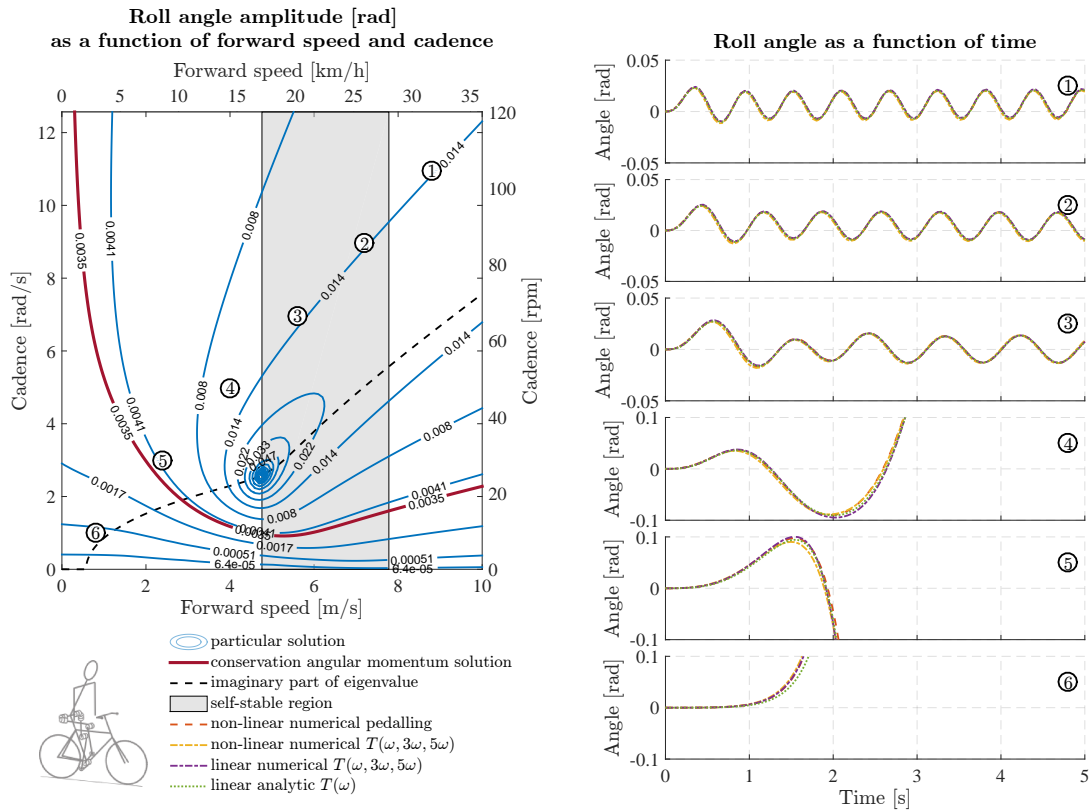


Figure 3.14: Roll amplitude of the particular solution (left) and time solutions of other methods (right), for model HR shown bottom left in figure. The six numbers corresponding to the six plots on the right are indicated on the roll angle amplitude plot on the left, to indicate the speed-cadence combination belonging the time solution. The isoline corresponding to the amplitude of the conservation of angular momentum solution is shown in the particular solution contour plot on the left for comparison; the conservation of angular momentum solution itself is independent on forward speed and cadence. The imaginary part of the weave eigenvalue and the self-stable region are shown for reference. The particular solution left is the periodic cadence frequency component of the linear analytic time solution shown right, by definition. The non-linear model is solved using prescribed leg motion as disturbance. The linear and non-linear models are also solved using a multiple frequency torque disturbance.

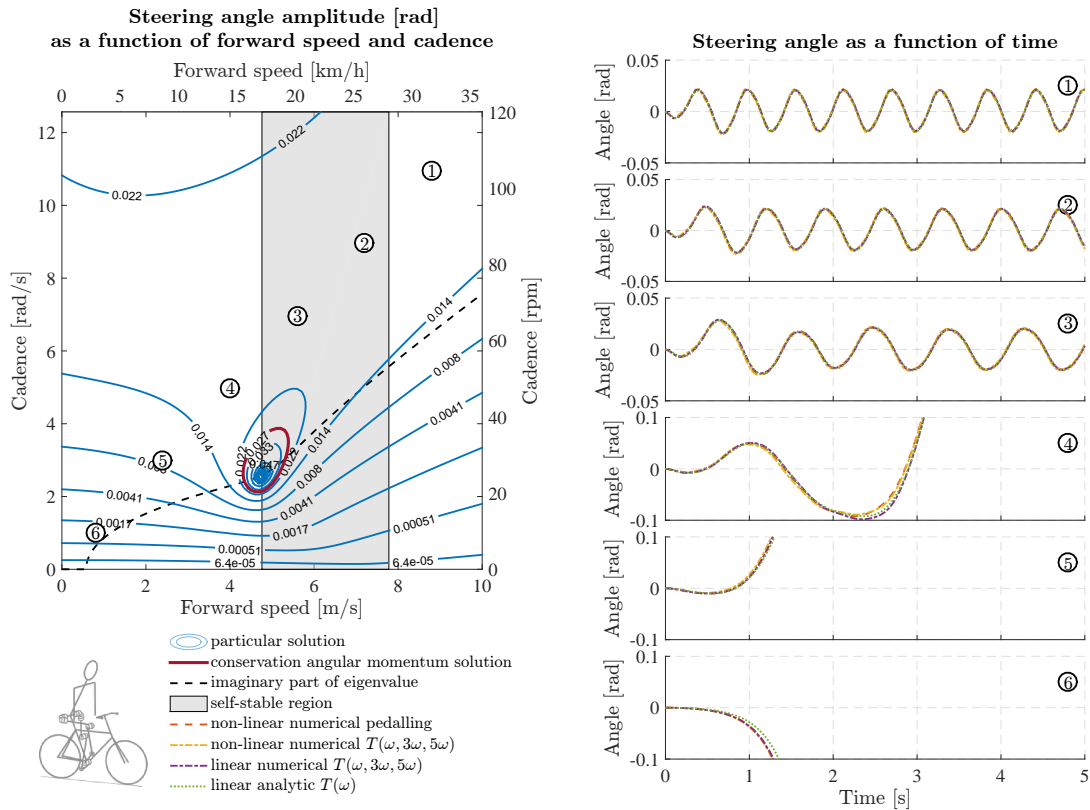


Figure 3.15: Steering amplitude of the particular solution (left) and time solutions of other methods (right), for model HR shown bottom left in figure. The six numbers corresponding to the six plots on the right are indicated on the roll angle amplitude plot on the left, to indicate the speed-cadence combination belonging the time solution. The isoline corresponding to the amplitude of the conservation of angular momentum solution is shown in the particular solution contour plot on the left for comparison; the conservation of angular momentum solution itself is independent on forward speed and cadence. The imaginary part of the weave eigenvalue and the self-stable region are shown for reference. The particular solution left is the periodic cadence frequency component of the linear analytic time solution shown right, by definition. The non-linear model is solved using prescribed leg motion as disturbance. The linear and non-linear models are also solved using a multiple frequency torque disturbance.

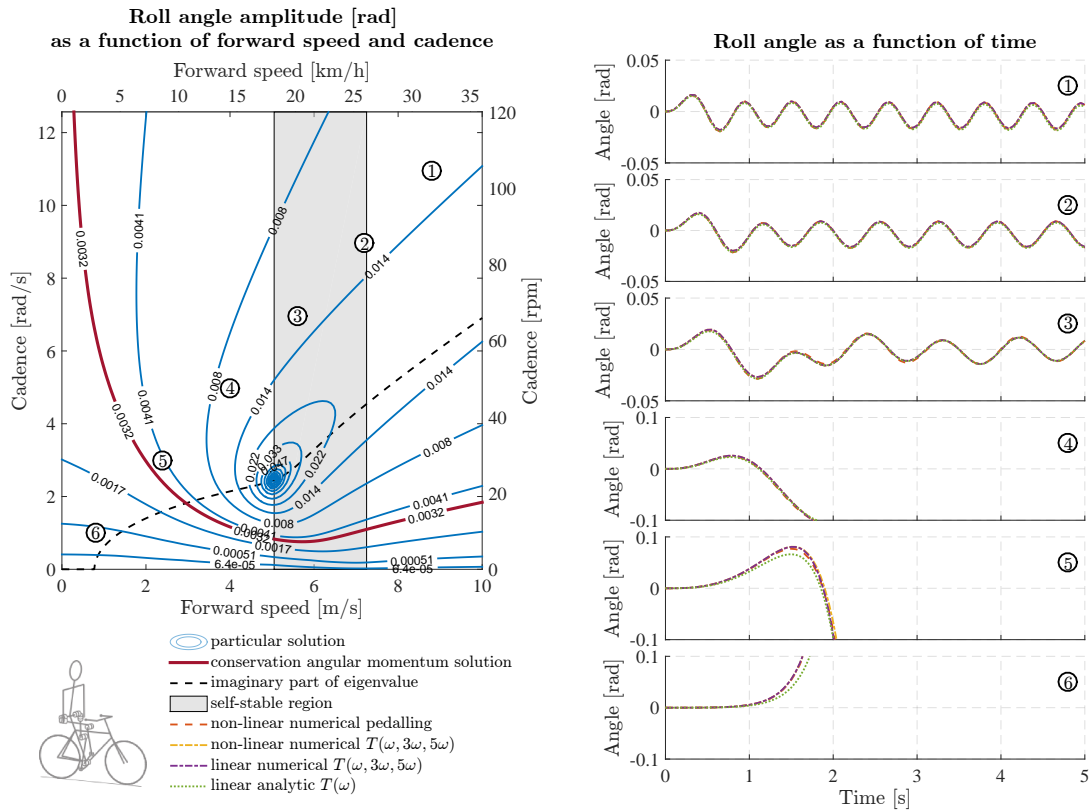


Figure 3.16: Roll amplitude of the particular solution (left) and time solutions of other methods (right), for model CR shown bottom left in figure. The six numbers corresponding to the six plots on the right are indicated on the roll angle amplitude plot on the left, to indicate the speed-cadence combination belonging the time solution. The isoline corresponding to the amplitude of the conservation of angular momentum solution is shown in the particular solution contour plot on the left for comparison; the conservation of angular momentum solution itself is independent on forward speed and cadence. The imaginary part of the weave eigenvalue and the self-stable region are shown for reference. The particular solution left is the periodic cadence frequency component of the linear analytic time solution shown right, by definition. The non-linear model is solved using prescribed leg motion as disturbance. The linear and non-linear models are also solved using a multiple frequency torque disturbance.

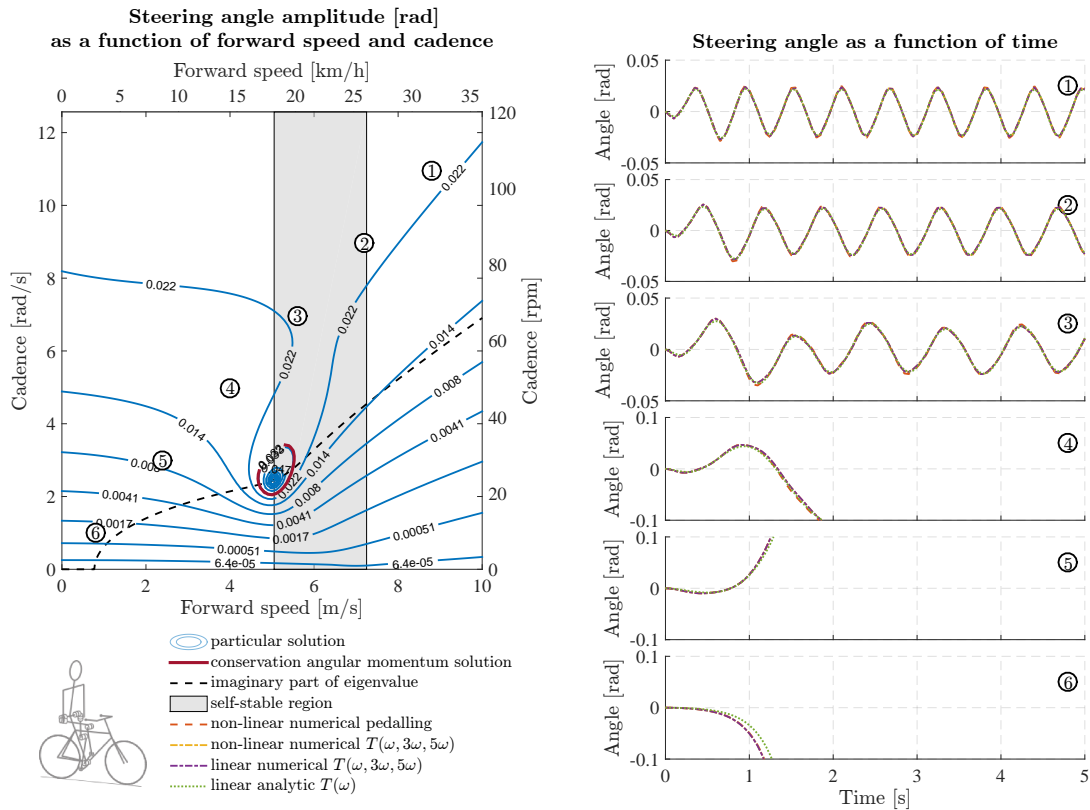


Figure 3.17: Steering amplitude of the particular solution (left) and time solutions of other methods (right), for model CR shown bottom left in figure. The six numbers corresponding to the six plots on the right are indicated on the roll angle amplitude plot on the left, to indicate the speed-cadence combination belonging the time solution. The isoline corresponding to the amplitude of the conservation of angular momentum solution is shown in the particular solution contour plot on the left for comparison; the conservation of angular momentum solution itself is independent on forward speed and cadence. The imaginary part of the weave eigenvalue and the self-stable region are shown for reference. The particular solution left is the periodic cadence frequency component of the linear analytic time solution shown right, by definition. The non-linear model is solved using prescribed leg motion as disturbance. The linear and non-linear models are also solved using a multiple frequency torque disturbance.

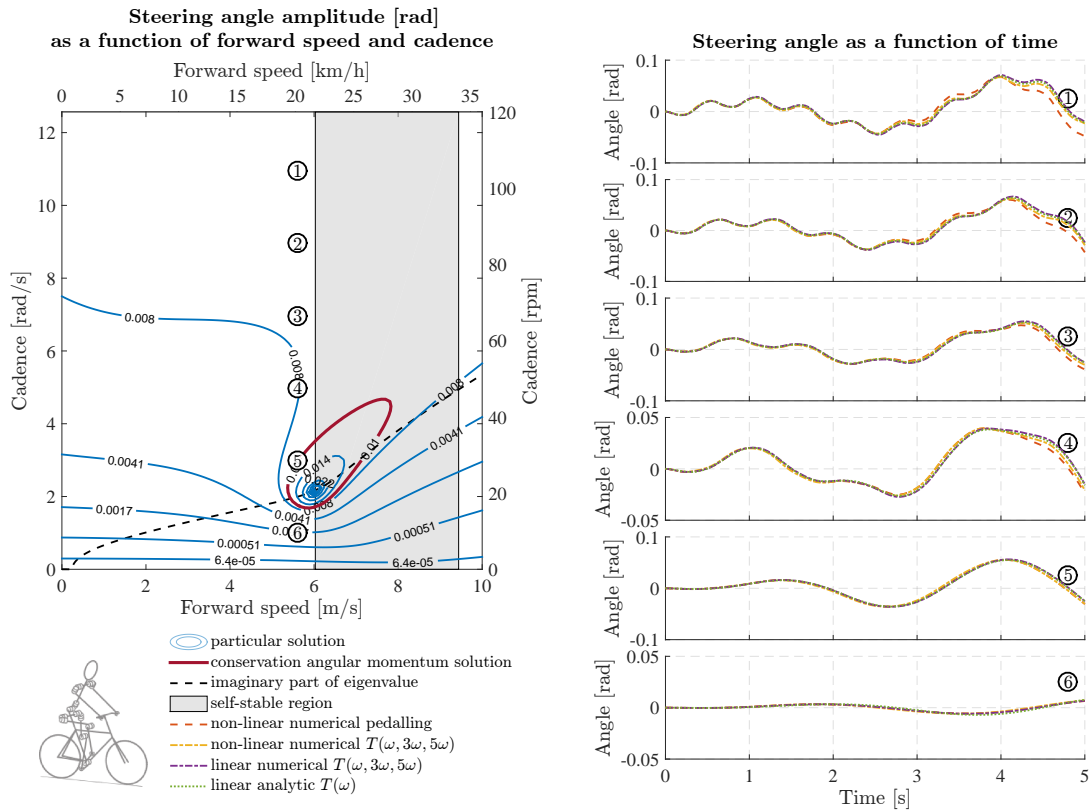


Figure 3.18: Steering amplitude of the particular solution (left) and time solutions of other methods (right), for model HS shown bottom left in figure. The six numbers corresponding to the six plots on the right are indicated on the roll angle amplitude plot on the left, to indicate the speed-cadence combination belonging the time solution. The isoline corresponding to the amplitude of the conservation of angular momentum solution is shown in the particular solution contour plot on the left for comparison; the conservation of angular momentum solution itself is independent on forward speed and cadence. The imaginary part of the weave eigenvalue and the self-stable region are shown for reference. The particular solution left is the periodic cadence frequency component of the linear analytic time solution shown right, by definition. The non-linear model is solved using prescribed leg motion as disturbance. The linear and non-linear models are also solved using a multiple frequency torque disturbance.

3.2.2 Periodic Solutions and Frequency Domain

In Figure 3.20 till 3.27 periodic solutions are shown obtained from the Fourier transform of the time signal. On the left the amplitudes corresponding to the cadence frequency are shown together with the particular solution, on the right several examples are shown of the frequency domain, where also the particular solution is indicated (same data and speed-cadence combinations as Figures 3.10 till 3.19).

In general the frequency domain of the linear models are dominated nearly completely by the transient signal outside of the stable region (except for very low capsized eigenvalue condition). The non-linear models still show some nice congruity with the particular solution for high forward speeds. Inside the stable region all the methods show very similar results for the amplitude corresponding to the cadence, as expected from the time signals. For low speeds, where the weave eigenmode is unstable, the frequency domain for the non-linear models show high transient signal-noise and a low frequency domain resolution. This last problem is due very small time domain, because the bicycle fell down quickly and the simulation ended.

The effect of the Hanning window can be seen nicely in for instance speed-cadence combination number 3 of Figure 3.20. Without the Hanning window, the frequency domain has a wide range of frequency content and the amplitude of the cadence frequency lies lower than the neighbouring frequencies. This is due to a phase difference between the transient and the periodic signal, exacting destructive interference. In the frequency domain with the Hanning window two peaks are seen; the oscillatory weave frequency of around 1/3 Hz together with the cadence frequency, which now has a similar amplitude to the particular solution.

Figure 3.28, shows that the oscillatory weave frequency can be seen at the same frequency for combinations of the same forward speed and that the cadence frequency peak shifts to lower frequencies, as expected from the time domain solutions. The high amplitude corresponding to the oscillatory weave frequency is precisely what we predicted by looking at the time signal. However, more peculiar frequency results are seen in Figure 3.29 in similar speed-cadence combinations for model CR (city bicycle hands free). Here the weave frequency is easily recognised again by a constant frequency peak at the place where we would expect it from the imaginary part of the eigenvalue. There is also a peak at the cadence frequency, where we would expect it. However there are also other smaller peaks present, which seem to be multiples of the cadence and weave frequency. The behaviour corresponding to the weave mode is seen for slightly different frequencies, when comparing the non-linear model with pedalling and torques disturbance types. This behaviour in the non-linear models is probably due to the non-linearity of the model, where it could be that the weave frequency is not a constant, but can be seen as a summation of frequencies. This would mean that it is easier to create a sort of resonance with periodic forcing. This phenomenon is seen for both the hands free bicycle-rider models, for a small forward speed range, just below the self-stable range. This area corresponds to a low positive real part of the oscillatory weave frequency.

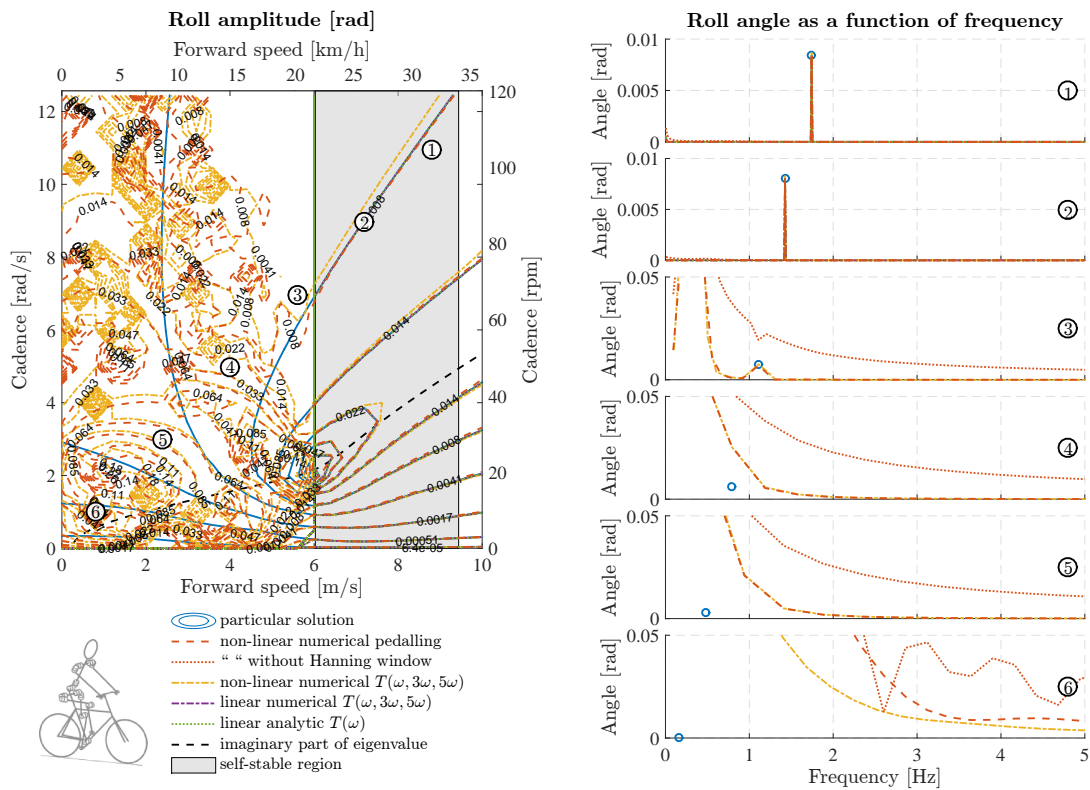


Figure 3.20: Roll amplitude of the particular solution and corresponding periodic solutions of other methods (left) and angle as a function of frequency of other methods (right), for model HS shown bottom left in figure. The six numbers corresponding to the six plots on the right are indicated on the roll angle amplitude plot on the left, to indicate the speed-cadence combination belonging the frequency solution. The imaginary part of the weave eigenvalue and the self-stable region are shown for reference. The particular solution left is the periodic cadence frequency component of the linear analytic time solution shown right, by definition. The non-linear model is solved using prescribed leg motion as disturbance, shown with and without the transformation using a Hanning window. The linear and non-linear models are also solved using a multiple frequency torque disturbance.

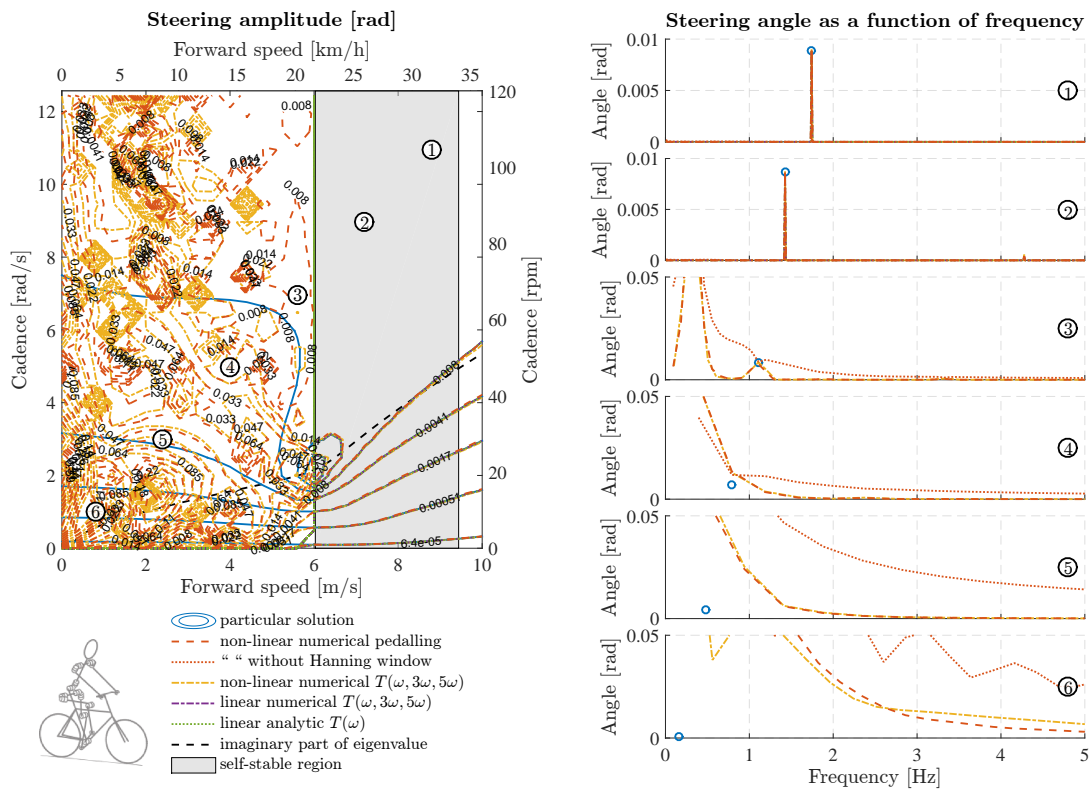


Figure 3.21: Steering amplitude of the particular solution and corresponding periodic solutions of other methods (left) and angle as a function of frequency of other methods (right), for model HS shown bottom left in figure. The six numbers corresponding to the six plots on the right are indicated on the steering angle amplitude plot on the left, to indicate the speed-cadence combination belonging to the frequency solution. The imaginary part of the weave eigenvalue and the self-stable region are shown for reference. The particular solution left is the periodic cadence frequency component of the linear analytic time solution shown right, by definition. The non-linear model is solved using prescribed leg motion as disturbance, shown with and without the transformation using a Hanning window. The linear and non-linear models are also solved using a multiple frequency torque disturbance.

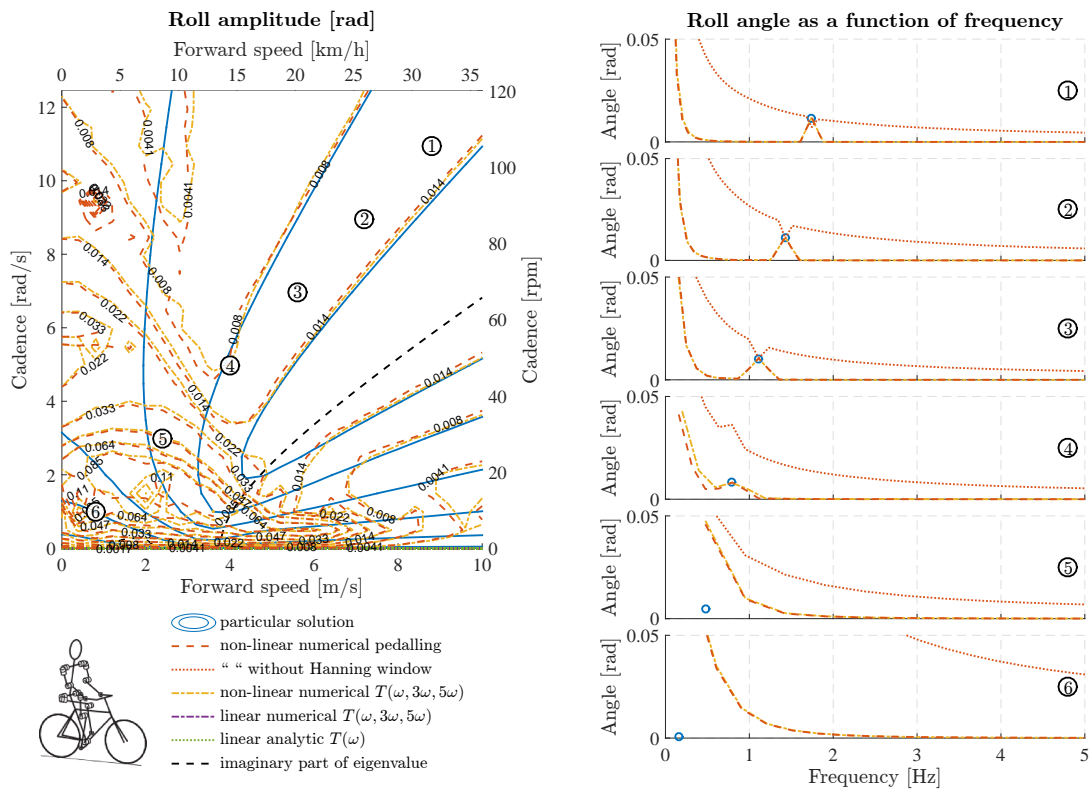


Figure 3.22: Roll amplitude of the particular solution and corresponding periodic solutions of other methods (left) and angle as a function of frequency of other methods (right), for model CF shown bottom left in figure. The six numbers corresponding to the six plots on the right are indicated on the roll angle amplitude plot on the left, to indicate the speed-cadence combination belonging to the frequency solution. The imaginary part of the weave eigenvalue is shown for reference. No stable region, however capsizes mode is stable from 3.2 m/s (real part of eigenvalue of capsizes mode is negative from 3.2 m/s). The particular solution left is the periodic cadence frequency component of the linear analytic time solution shown right, by definition. The non-linear model is solved using prescribed leg motion as disturbance, shown with and without the transformation using a Hanning window. The linear and non-linear models are also solved using a multiple frequency torque disturbance.

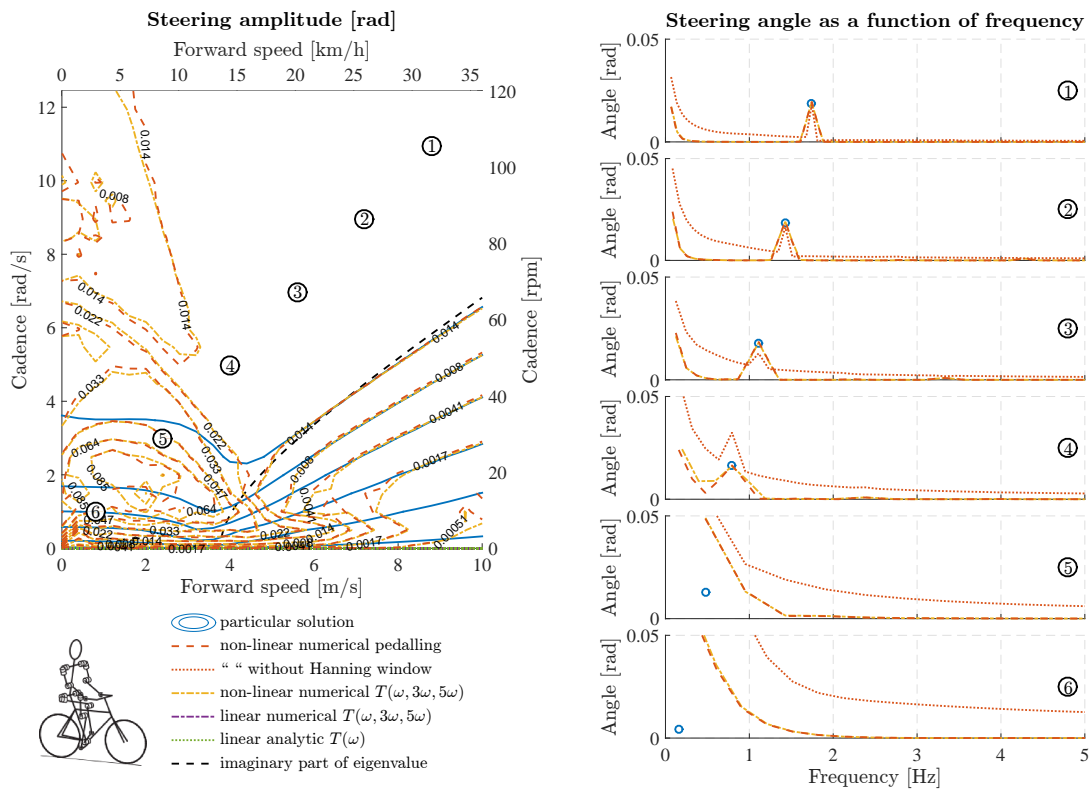


Figure 3.23: Steering amplitude of the particular solution and corresponding periodic solutions of other methods (left) and angle as a function of frequency of other methods (right), for model CF shown bottom left in figure. The six numbers corresponding to the six plots on the right are indicated on the steering angle amplitude plot on the left, to indicate the speed-cadence combination belonging to the frequency solution. The imaginary part of the weave eigenvalue is shown for reference. No stable region, however capsized mode is stable from 3.2 m/s (real part of eigenvalue of capsized mode is negative from 3.2 m/s). The particular solution left is the periodic cadence frequency component of the linear analytic time solution shown right, by definition. The non-linear model is solved using prescribed leg motion as disturbance, shown with and without the transformation using a Hanning window. The linear and non-linear models are also solved using a multiple frequency torque disturbance.

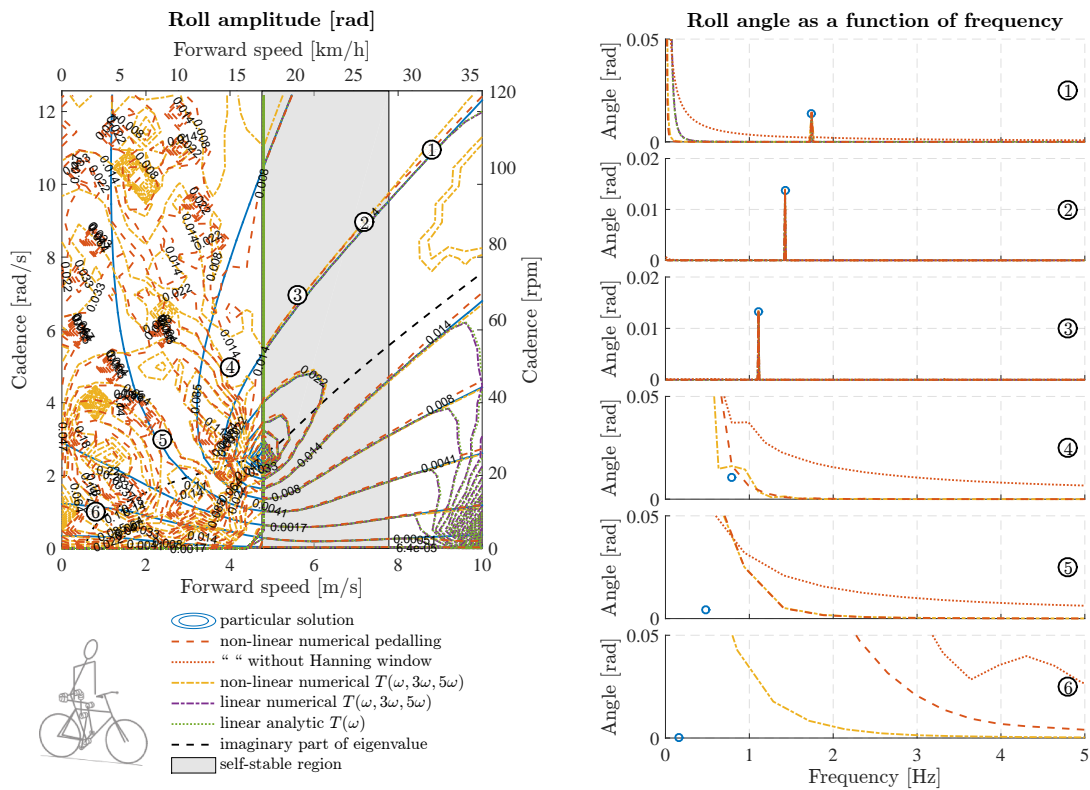


Figure 3.24: Roll amplitude of the particular solution and corresponding periodic solutions of other methods (left) and angle as a function of frequency of other methods (right), for model HR shown bottom left in figure. The six numbers corresponding to the six plots on the right are indicated on the roll angle amplitude plot on the left, to indicate the speed-cadence combination belonging the frequency solution. The imaginary part of the weave eigenvalue and the self-stable region are shown for reference. The particular solution left is the periodic cadence frequency component of the linear analytic time solution shown right, by definition. The non-linear model is solved using prescribed leg motion as disturbance, shown with and without the transformation using a Hanning window. The linear and non-linear models are also solved using a multiple frequency torque disturbance.

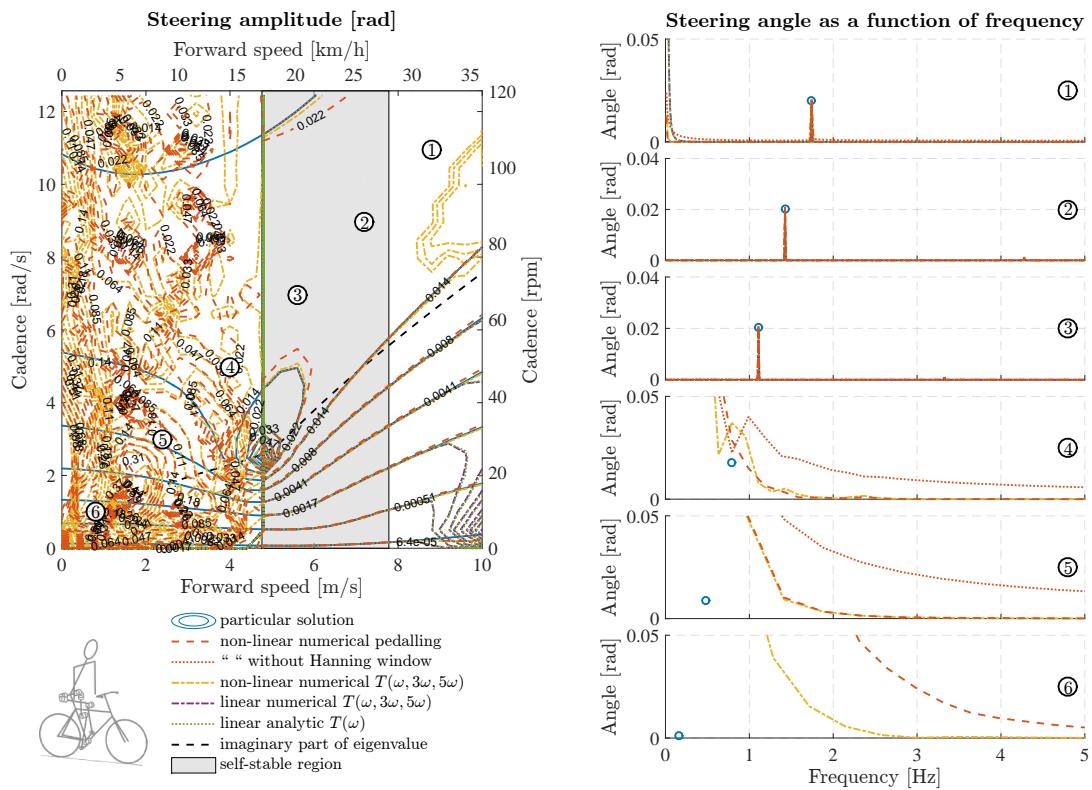


Figure 3.25: Steering amplitude of the particular solution and corresponding periodic solutions of other methods (left) and angle as a function of frequency of other methods (right), for model HR shown bottom left in figure. The six numbers corresponding to the six plots on the right are indicated on the steering angle amplitude plot on the left, to indicate the speed-cadence combination belonging the frequency solution. The imaginary part of the weave eigenvalue and the self-stable region are shown for reference. The particular solution left is the periodic cadence frequency component of the linear analytic time solution shown right, by definition. The non-linear model is solved using prescribed leg motion as disturbance, shown with and without the transformation using a Hanning window. The linear and non-linear models are also solved using a multiple frequency torque disturbance.

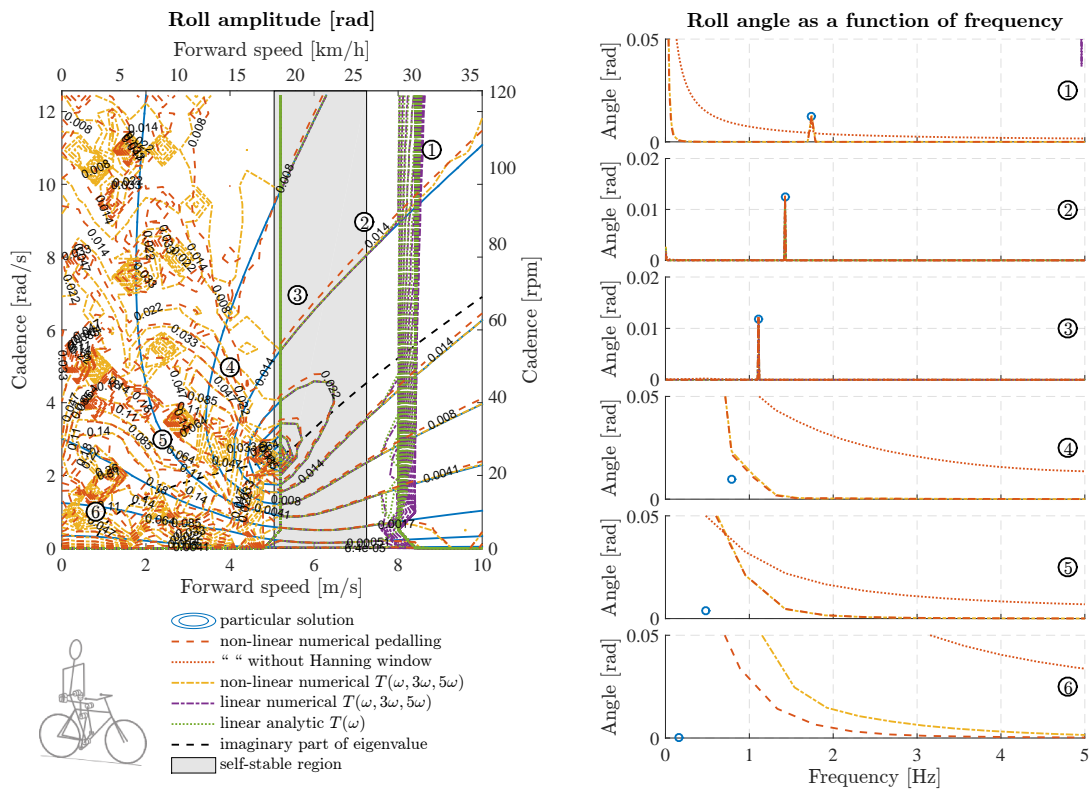


Figure 3.26: Roll amplitude of the particular solution and corresponding periodic solutions of other methods (left) and angle as a function of frequency of other methods (right), for model CR shown bottom left in figure. The six numbers corresponding to the six plots on the right are indicated on the roll angle amplitude plot on the left, to indicate the speed-cadence combination belonging the frequency solution. The imaginary part of the weave eigenvalue and the self-stable region are shown for reference. The particular solution left is the periodic cadence frequency component of the linear analytic time solution shown right, by definition. The non-linear model is solved using prescribed leg motion as disturbance, shown with and without the transformation using a Hanning window. The linear and non-linear models are also solved using a multiple frequency torque disturbance.

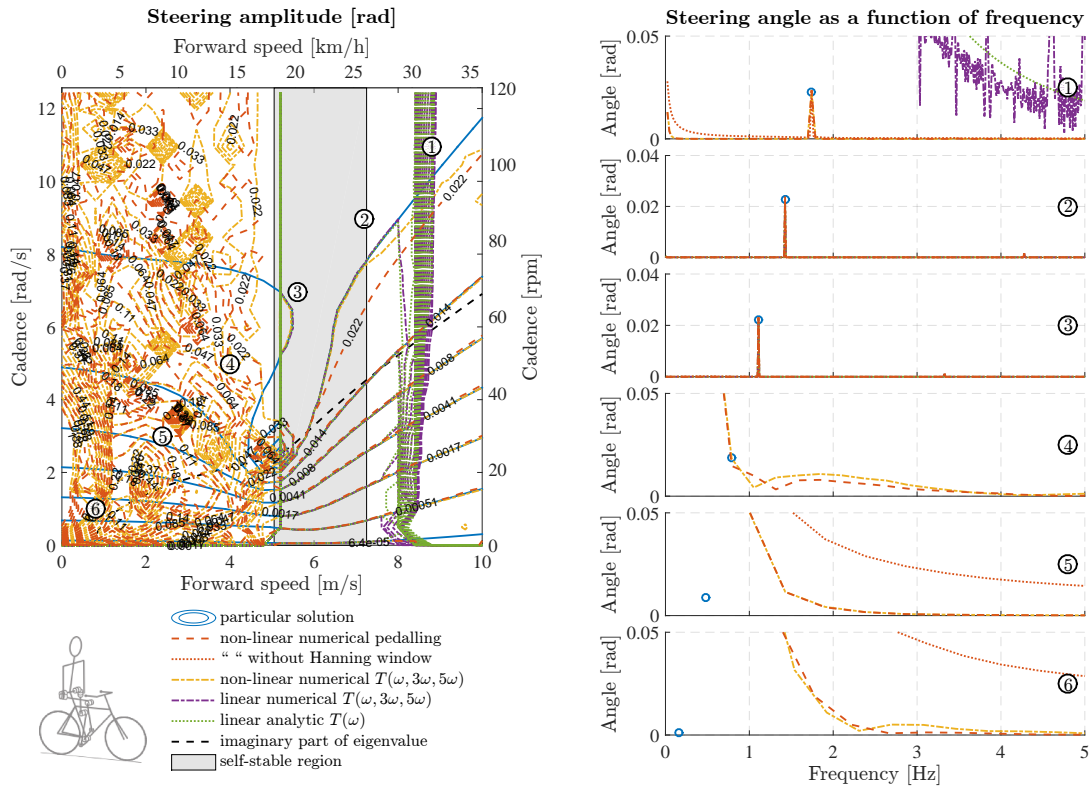


Figure 3.27: Steering amplitude of the particular solution and corresponding periodic solutions of other methods (left) and angle as a function of frequency of other methods (right), for model CR shown bottom left in figure. The six numbers corresponding to the six plots on the right are indicated on the steering angle amplitude plot on the left, to indicate the speed-cadence combination belonging the frequency solution. The imaginary part of the weave eigenvalue and the self-stable region are shown for reference. The particular solution left is the periodic cadence frequency component of the linear analytic time solution shown right, by definition. The non-linear model is solved using prescribed leg motion as disturbance, shown with and without the transformation using a Hanning window. The linear and non-linear models are also solved using a multiple frequency torque disturbance.

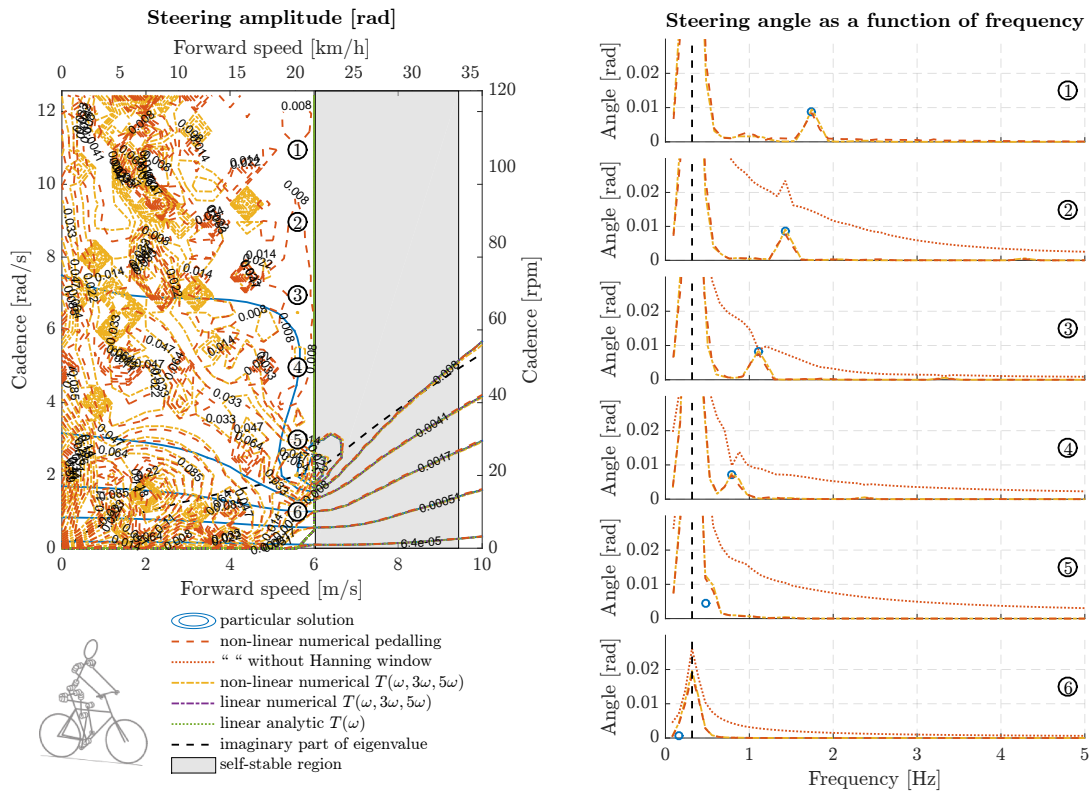


Figure 3.28: Steering amplitude of the particular solution and corresponding periodic solutions of other methods (left) and angle as a function of frequency of other methods (right), for model HS shown bottom left in figure. The six numbers corresponding to the six plots on the right are indicated on the steering angle amplitude plot on the left, to indicate the speed-cadence combination belonging the frequency solution. The imaginary part of the weave eigenvalue and the self-stable region are shown for reference. The particular solution left is the periodic cadence frequency component of the linear analytic time solution shown right, by definition. The non-linear model is solved using prescribed leg motion as disturbance, shown with and without the transformation using a Hanning window. The linear and non-linear models are also solved using a multiple frequency torque disturbance.

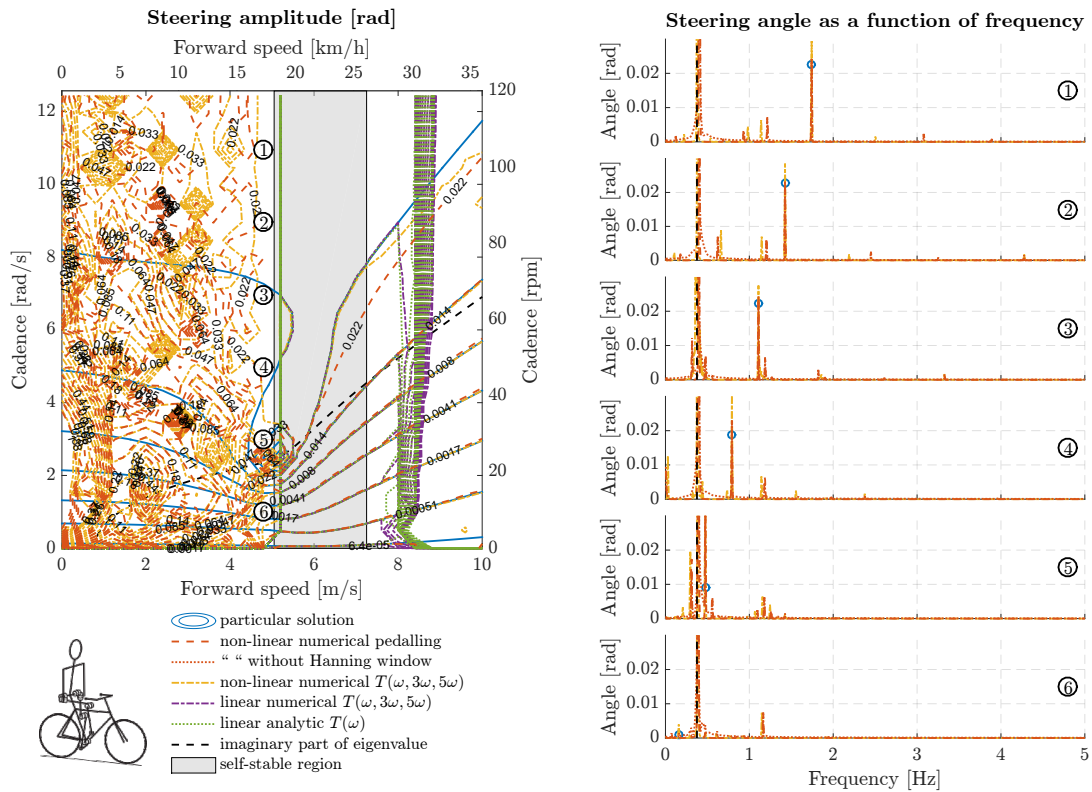


Figure 3.29: Steering amplitude of the particular solution and corresponding periodic solutions of other methods (left) and angle as a function of frequency of other methods (right), for model CR shown bottom left in figure. The six numbers corresponding to the six plots on the right are indicated on the steering angle amplitude plot on the left, to indicate the speed-cadence combination belonging the frequency solution. The imaginary part of the weave eigenvalue and the self-stable region are shown for reference. The particular solution left is the periodic cadence frequency component of the linear analytic time solution shown right, by definition. The non-linear model is solved using prescribed leg motion as disturbance, shown with and without the transformation using a Hanning window. The linear and non-linear models are also solved using a multiple frequency torque disturbance.

3.2.3 Conservation of Angular Momentum

The general behaviour of the bicycle over time is estimated using the conservation of angular momentum principle as described in Section 3.1.2.3. This is done for the four bicycle-rider models, for different cadences and for the two pedal disturbance types (modelled in Section 2.1.1).

The general bicycle behaviour corresponding to the two disturbance types is shown in Figure 3.30 (for model HS). A result shown for a disturbance consisting only of a roll torque is also shown for comparison. This last result does not follow the behaviour of the leg model very well, especially looking at the steering angle results. However if the steering torque is added, the disturbance using only the cadence frequency does follow the leg model result well, especially looking at the angle results. This means that the yaw momentum component of the pedal disturbance has a substantial effect on the amplitude and the phase of the steering angle.

When comparing the results corresponding to the different cadences it can be seen that although the amplitude of the momentum itself will increase due to an increase in cadence, the amplitude of the roll and steering will stay the same. This means that the amplitude results of the conservation of angular momentum equations do not depend on forward speed or cadence, only on amplitude of the leg motion and the generalised mass matrix of the model. This does seem very unlikely as the bicycle behaviour is known to be very forward speed dependent, therefore we have a look at the validity of the simplifications of this model, before we go on to the results of the other methods.

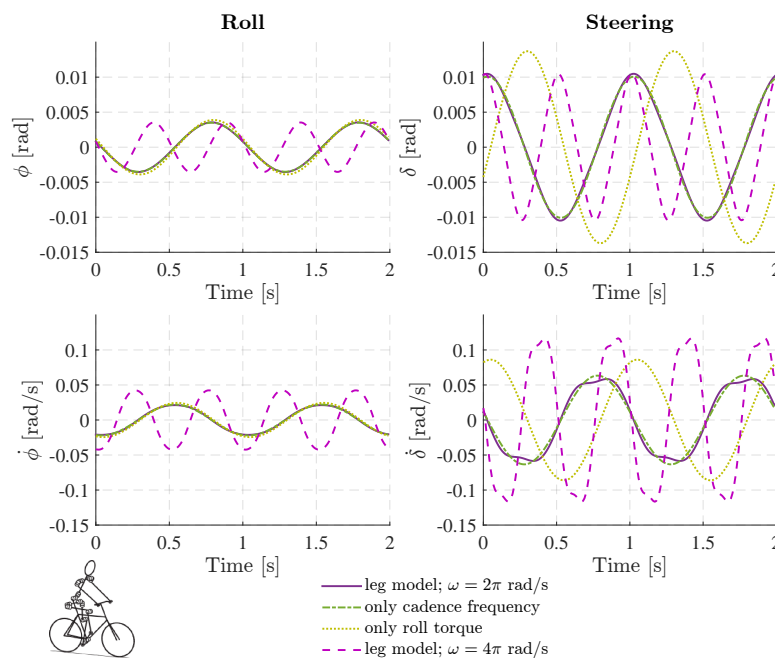


Figure 3.30: Roll (left) and steering (right) angle (top) and angular velocity (bottom) estimated using conservation of angular momentum principle using the mass parameters for model HS. The pedal disturbance is modelled using a motion prescribed by a dual 3D four bar linkage ('leg model; $\omega = 2\pi$ & 4π rad/s'), a simplified leg COM motion and a very simplified vertical leg COM motion (only roll torque) both prescribed using only the cadence frequency of 60 rpm ($= 2\pi$ rad/s)

3.2.3.1 Neglected Momenta In order to make an estimation of the validity of neglecting the external forces due to gravity, ground contact and such, we investigate which of these terms are small compared to the angular momentum terms used to estimate the roll and steering angular velocities and angles here. In general the sum of all the generalized d'Alembert forces is equal to the time derivative of the momentum. For our system this means that we can use the system of linearised second order differential equations to

include all the momenta:

$$\mathbf{L} = \int (\mathbf{M} \ddot{\mathbf{q}} + v\mathbf{C}_1 \dot{\mathbf{q}} + [g\mathbf{K}_0 + (v)^2\mathbf{K}_2] \mathbf{q} - \mathbf{f}_L) dt \quad (3.27)$$

The generalized d'Alembert forces corresponding to the pedal disturbance \mathbf{f}_L can be easily related to the previously defined generalized momentum corresponding to the leg moment \mathbf{L}_L :

$$\mathbf{L}_L = - \int \mathbf{f}_L dt \quad (3.28)$$

This leads to an expression very close to the one used (Equation 3.20), however with some extra terms which were neglected in our simplified conservation of angular momentum assumption:

$$\mathbf{L} = \mathbf{M} \dot{\mathbf{q}} + \underbrace{v\mathbf{C}_1 \mathbf{q} + g\mathbf{K}_0 \int \mathbf{q} dt + (v)^2\mathbf{K}_2 \int \mathbf{q} dt}_{\text{Neglected momenta}} + \mathbf{L}_L \quad (3.29)$$

In order for these conservation of angular momentum results generated here to be a reasonable representation of the true behaviour the neglected terms should be much smaller than the angular momentum associated with the moving legs ($(v\mathbf{C}_1 \mathbf{q} + \int g\mathbf{K}_0 \mathbf{q} dt + \int (v)^2\mathbf{K}_2 \mathbf{q} dt) / \mathbf{L}_L \ll 1$). If we temporally go with this assumption and use the results we obtained here, we can check this assumption using the results we obtained.

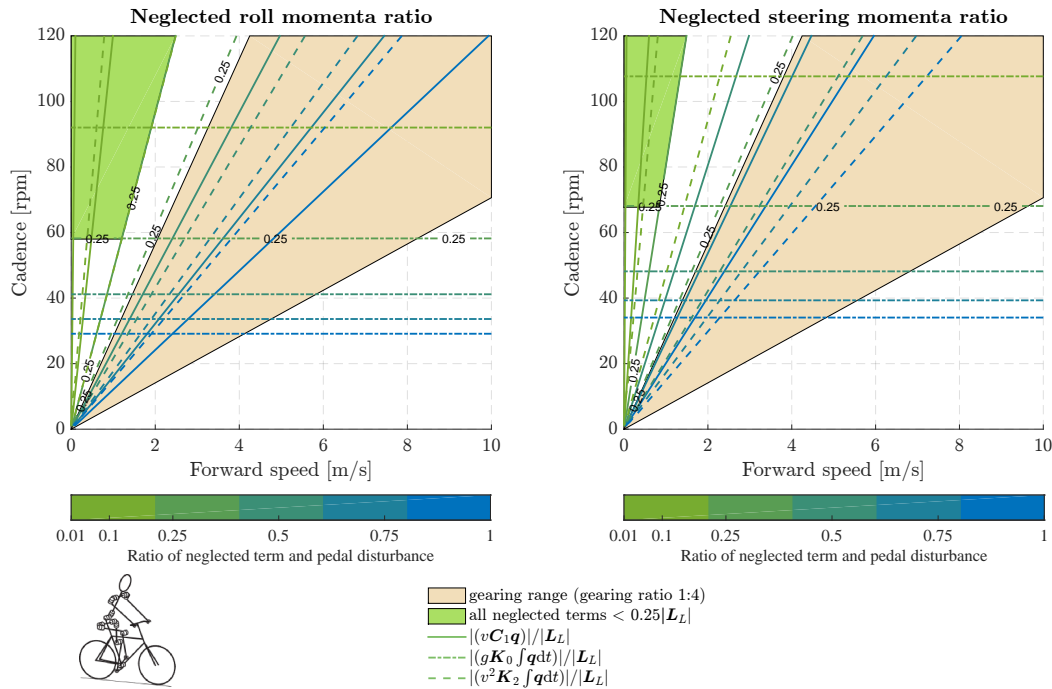


Figure 3.31: Neglected momenta as a ratio of the pedalling disturbance momentum for model HS corresponding to roll (left) and steering (right). The area where all the neglected momenta terms are less than a quarter of the pedalling disturbance momentum is filled in (top left corner). Also the gearing range is depicted indicating the possible cadence and forward speed combinations in the normal operating range of the bicycle. This corresponds to a range from gearing ratio 1 to 4, equivalent to 1 to 4 times as many front sprocket teeth as rear sprocket teeth.

Figure 3.31 shows that the neglected momenta terms could only be regarded as negligible for very low speeds in combination with reasonably high cadences. These forward speed-cadence combinations, do not lie

in the normal operating range of the bicycle due to the set gearing of a bicycle. This is true for all the models, where the figures can be found in Appendix F for the other models. Therefore the simplistic conservation of angular momentum approach applied here does not provide a useful representation of the bicycle behaviour due to the pedalling disturbance. It is not expected to give realistic amplitude results for 'normal cycling' and cannot capture behaviour due to cycling conditions.

3.2.4 Evaluation of Model Simplifications and Solution Methods

In Figure 3.32 and 3.33 the relative difference (RD) is shown corresponding to the different evaluation points presented in Section 3.1.3, corresponding the roll amplitude solutions of model HR and CF respectively. The steering amplitude results and the results for the other two bicycle-rider models are not shown here, since they show similar behaviour (see Appendix H). Here we discuss the errors associated with the solution methods and model simplifications according to the same evaluation points. Most of the issues and behaviour have all ready been discussed qualitatively in either the method section or in the previous result sections. In this section we provide an overview according to the evaluation points (also indicated in the figures), where after we give recommendations for future use based on error contribution.

1. Simplifications made to the full non-linear multibody dynamics model

a) Fixing leg inertia to rear frame of the bicycle

→ Compare non-linear model torques ($\mathbf{T}(\omega, 3\omega, 5\omega)$) to non-linear model pedalling

The simplification step corresponding to changing the disturbance type from moving leg segments to two multiple harmonic torques as applied inertial forcing disturbance is dual; fixing the leg inertia and simplifying the disturbance. Here we discuss the fixing of the leg inertia, which is thought to represent the major determinant of the error contribution due to model simplifications.

The leg inertia is fixed to the rear frame, effectively changing time variant harmonic system properties to be time invariant. In a linearised system this same effect would be analogous to representing a summation of a constant mass matrix and harmonic terms by only the constant mass matrix: $\mathbf{M} + \sum_{n=1}^{\infty} \mathbf{M}_n(n\omega t) \approx \mathbf{M}$

In our bicycle-rider models, this fixing of the leg inertia might not only effect the generalised mass characteristics, but also the generalised damping and the generalised stiffness (forward speed and gravitational acceleration effects on the generalised coordinates and their velocity). The change in system characteristics from harmonic to constant has a typical contribution on the error of 0.1% up to 5% for the self-stable region and low positive real part eigenvalues range. This simplification seems to mainly change the behaviour corresponding to the oscillatory part of the weave eigenmode (also seen in frequency domain). For the forward speed region, where the bicycle is highly unstable, the time result is dominated by the transient. Here we see that the transient is impacted more by this simplification, seen by the large erratic error behaviour typically ranging from 0.5% to 300%, making determination of the error on the periodic forcing response difficult.

b) Linearisation around roll and steering angle (ϕ, δ)

→ Compare linear model torques ($\mathbf{T}(\omega, 3\omega, 5\omega)$) to non-linear model torques ($\mathbf{T}(\omega, 3\omega, 5\omega)$)

Linearisation of the bicycle-rider model has a very low impact on the periodic forcing response, with an associated error typically around 0.1% to 2.5%. The simplification of linearisation is reliable only for small deviations around the equilibrium position, which means that in the self-stable region the linearised and non-linear models show the same behaviour. Outside the self-stable region, the transient diverges from small deviations around the equilibrium position, making the time signal very inaccurate (error of $\gg 1E100$ %). However the particular part, corresponding to the response to the periodic forcing of the system, is solved separately from the transient part (the homogeneous solution) and does stay within the small deviations range, making it much more reliable than the transient part of the time solution even outside the self-stable range.

c) Neglecting behaviour corresponding to forward speed ($v = 0$) and gravity ($g = 0$)

→ Compare conservation of angular momentum solution to particular solution

The conservation of angular momentum solution introduces a very large simplification to the model

corresponding to an error ranging up to infinity. The error corresponding to this simplification is typically only small (2.5% to 10%) for very low forward speeds and very high cadences, a cycling condition which is not feasible on a normal bicycle. In some cases a larger or different part of the error graph shows good congruity between the particular solution and the angular momentum solution, than the analysis of the neglected momenta in Section 3.2.3.1 would suggest. This should not be attributed to the idea that the simplistic conservation of angular momentum approach is valid in a greater forward speed-cadence region. It is more reasonable to assume that the neglected momenta cancel each other out in such a way, that cannot be easily predicted without taking their effect into account. This method does not capture any disturbance response behaviour due to cycling conditions and only very limited behaviour due to bicycle design and posture parameters.

2. Simplifications made to the kinematic pedalling disturbance

a) Multiple harmonic inertial torques on steering and roll ($\mathbf{T}(\omega, 3\omega, 5\omega)$)

→ Compare non-linear model torques ($\mathbf{T}(\omega, 3\omega, 5\omega)$) to non-linear model pedalling

We are interested in the lateral movement amplitude response of pedalling as disturbance. From this standpoint the simplification of the disturbance from pedalling kinematics to steering & roll torques is negligible. We basically only throw away higher cadence harmonics ($\geq 7\omega$) of the torques, which theoretically does not have any error contribution on the amplitude response corresponding to the cadence frequency.

However if the interest and/or model design may change in the future, it is important to re-evaluate this point, therefore it is important to note the following considerations. With this simplification we throw away the effect on vertical wheel contact forces, which could be important if the wheel-ground contact condition is made dependent on ground reaction forces. We also throw away the effect on forward speed, since the harmonic forward inertial forces will add a slight variation on forward speed. This could also introduce a very small error on the lateral behaviour, because this is forward speed dependent.

b) Neglecting higher cadence harmonics ($\mathbf{T}(\omega)$)

→ Compare linear model torques ($\mathbf{T}(\omega)$) to linear model torques ($\mathbf{T}(\omega, 3\omega, 5\omega)$)

Throwing away the frequency content of the disturbance corresponding to the uneven multiples of the cadence theoretically does not impact the response corresponding to the cadence frequency. This is reflected very low error values in the self-stable region (typically 1E-5 to 1E-3%). The total forcing response amplitude is dominated by the cadence frequency, so only the higher frequency content in the response is lost due to this simplification.

3. Differences in solution approaches

a) Numerical time integration vs. analytical time solution approaches

→ Compare linear model numerical and analytic

Solving the linear system for time using a numerical integration algorithm introduces a relatively low error contribution, showing a value of typically around 1E-4% in the stable forward speed region. This error value is lower than the set relative local error tolerance and in the same order of magnitude as the set absolute local error tolerance. This supports the idea that the accumulated integration error over time has a smaller impact on amplitude determination compared to a specific configuration at a specific time.

b) Discrete Fourier transform vs analytical amplitude determination approach

→ Compare particular solution and analytic

The error in self-stable region is typically around 1E-5% to 1E-8%. This was expected to be low, since theoretically the steady state solution should only consist of the cadence frequency. This means that the discrete Fourier transform is a very reliable method for the identification of the amplitude, as long as the signal is not incorrectly truncated. However in the unstable forward speed range the signal is dominated by the transient. For solutions corresponding to high positive value eigenvalues and

low cadences, the bicycle even fell down before a single period corresponding to the periodic forcing response could be completed. This unstable forward speed region typically shows error ranging up to 1E200%.

The behaviour of the non-linear bicycle-rider model is dominated by the transient signal for low forward speed, due to the instability of the system, resulting in a high error when picking out the periodic forcing part solution. Solving the non-linear system response takes a lot of computational time and effort, making it an impractical modelling approach to use for a parameter/variable evaluation with a high dimension or resolution.

The analytic particular solution method can be implemented easily and efficiently. This is especially true for bicycle-rider models consisting of a rigid rider, since the bicycle design parameters (25 in total) can be used to directly obtain the linearised matrices needed to define the system (Meijaard et al., 2007).

In Figure 3.34 the relative difference of the particular solution compared to the full non-linear pedalling model solution is shown for all the four models, for the roll and the steering amplitudes. This shows that an error of up to 5% is generally seen, in identification of pedalling disturbance amplitude response, corresponding to the simplifications of linearising the system and assuming the system is time-invariant. A wide range of system-identification and solution approaches are available for linear time-invariant (LTI) systems, making this assumption a powerful one.

In our case this assumption is reasonable, since we are interested in ascertaining the general lateral behaviour response for normal cycling conditions and normal bicycle and rider parameters. A quick peak at the variation in amplitude response corresponding to the different bicycles, postures and cycling conditions discussed in the next section (Figure 3.35) shows us that an error of 5% is small compared to the variation of the behaviour we are interested in. Therefore we conclude that the particular solution of the linearised bicycle-rider model perturbed using the simple inertial steering and roll torques defined in Section 2 is a useful and simple tool to investigate the pedalling disturbance response corresponding to specific bicycle-rider systems and/or cycling conditions.

For some cases however, the errors introduced by the simplification of the model and the disturbance are too large. This could be for instance the case if only a very small area of the design parameter and/or variable space is of interest. It could also for instance be the case if the exact frequency dependent behaviour of the weave mode is of interest. This behaviour is seen to be influenced slightly (corresponding to $\pm 5\%$ error) by the harmonic time variant properties of the system due the movement of the leg inertia as a function of crank angle.

In the case that these model simplifications are not acceptable for the specific research line, careful consideration should be taken into account to increase the reliability of the solution method. The solution method used here is not suitable for a bicycle-rider system that falls down quickly (large instability behaviour), because the transient dominates the periodic forcing response behaviour. Two possible relatively easy solutions is to only solve for the stable region or to add control to the system. However the stable region can be limited and control changes the system properties. Another possibility that does not change system properties is to use the theory of numerical continuation. This can be applied to non-linear unstable systems to find periodic solutions (Doedel et al., 2003).

Doedel (1981) developed an open-source software package, based on numerical continuation and bifurcation theory, called AUTO. This software is implemented in Fortran, where it is could possibly be used to interface with SPACAR (also Fortran based). AUTO is also used as the foundation of a Matlab toolbox called MATCONT. This package offers a very similar usage as the built-in Matlab ode-solvers, which also could offer the possibility of easy integration with the Matlab SPACAR toolbox.

It is important to realise that the errors quantified here are solely the errors associated with the simplifications and solutions methods evaluated here. This means that we take behaviour defined by the non-linear dynamic Whipple bicycle model as a golden standard, as it is the benchmarked model accepted widely by the bicycle research community. However it is off course still only a model, with it's own assumptions and simplifications.

On of the main simplifications in the bicycle model is the rigid body assumption. In the model the rider is rigidly attached to the rear frame, however the observed rider motions (Kooijman et al., 2009; Moore et al.,

2011) are expected to greatly influence bicycle behaviour. Not only the rider is assumed to be rigid but also the bicycle frame. This means that the model does not allow for the bicycle frame to bend and twist under the applied disturbance. If the frame bends with the lateral motions, it would likely mean that the extreme points of the bicycle will have a larger lateral displacement, than now attributed to the disturbance. Another possibility is that there will be energy storage in the deformation of the frame. This will likely have an elastic and a damping component. This damping component could possibly attenuate the lateral motions.

Another simplification in the Whipple bicycle model are the simplified contact conditions of the wheels with the ground. In the basic benchmarked Whipple bicycle model, the contact condition is modelled as a non slip purely rolling contact condition, without the presence of any tyre dynamics. This would mean for instance in a simple case that, if the bicycle would stand still and the steering angle is changed, there would not be any ground reaction torques due to the tyre friction on the road. In real life this friction torque would obviously be present. Moore (2012) found a discrepancy of a factor of 2-3 in measured steering angle and the amount of steering torque needed to drive the Whipple model in the same trajectory (Schwab et al., 2013). For the Whipple model with added arm inertia similar to the passive rider model of Schwab et al. (2012), the congruity with the model inputs (steering and roll torque) are even worse. This could be attributed to measurement errors or model limitations. The magnitude of the steering torque necessary to steer a bicycle is very low relative to the other forces on the front frame. This makes it very difficult to measure accurately. But if the error is caused due to model limitations, this would mean that the steering angle results due to the steering torque could be widely overestimated. It is proposed by Moore (2012) that a simple scrub torque would likely improve the fidelity of the model, however they did not specify what the precise parameters would be of this suggested scrub torque. An option to improve model accuracy would be to include tyre dynamics (Pacejka, 2012).

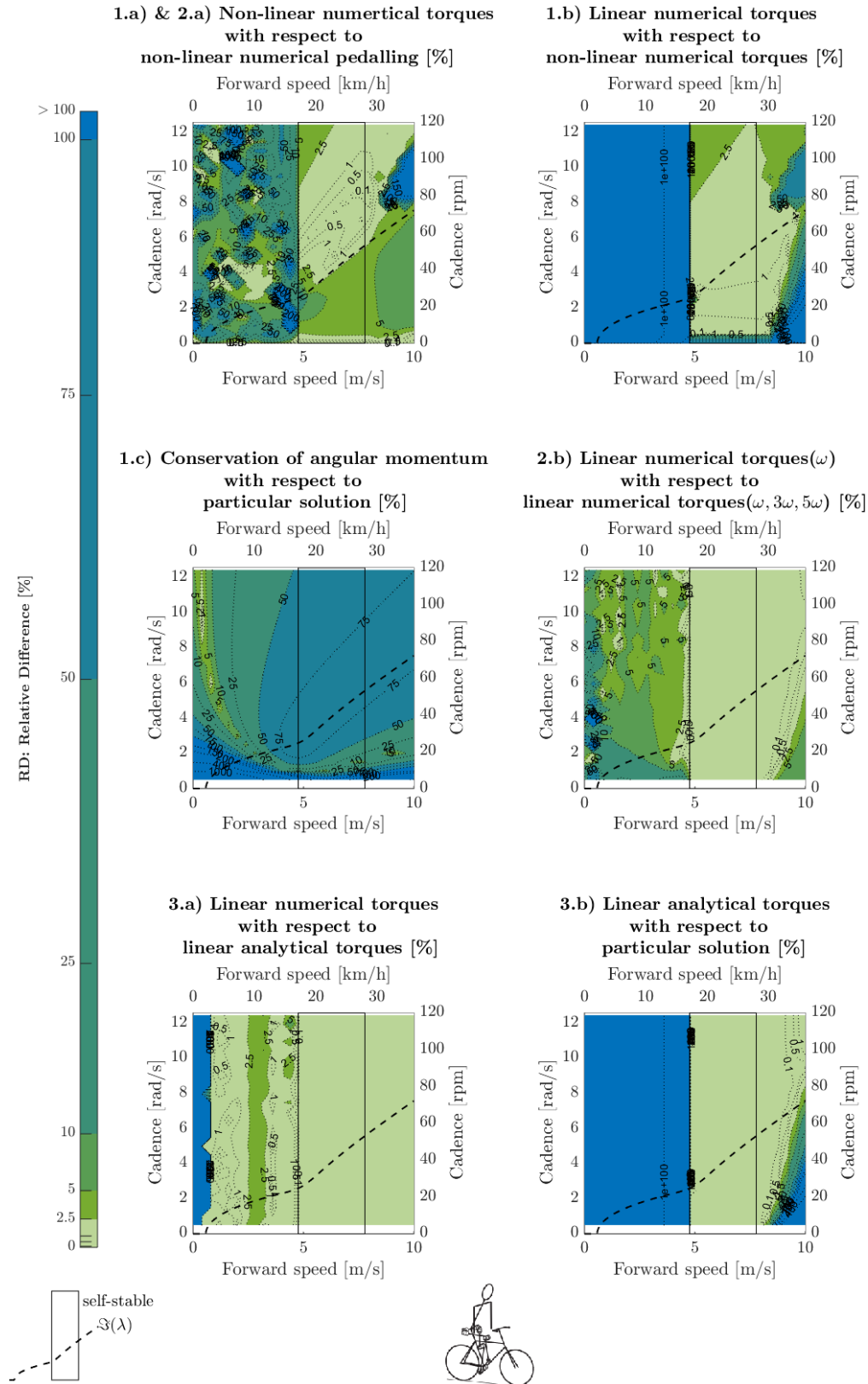


Figure 3.32: Model simplifications and solution method evaluation corresponding to points defined in Section 3.1.3. The relative difference of roll amplitude solutions is depicted as a function of forward speed and cadence, corresponding to model HR. The self-stable speed region is indicated by a box and the imaginary part of the eigenvalue of the weave eigenmode is indicated with a dashed line.

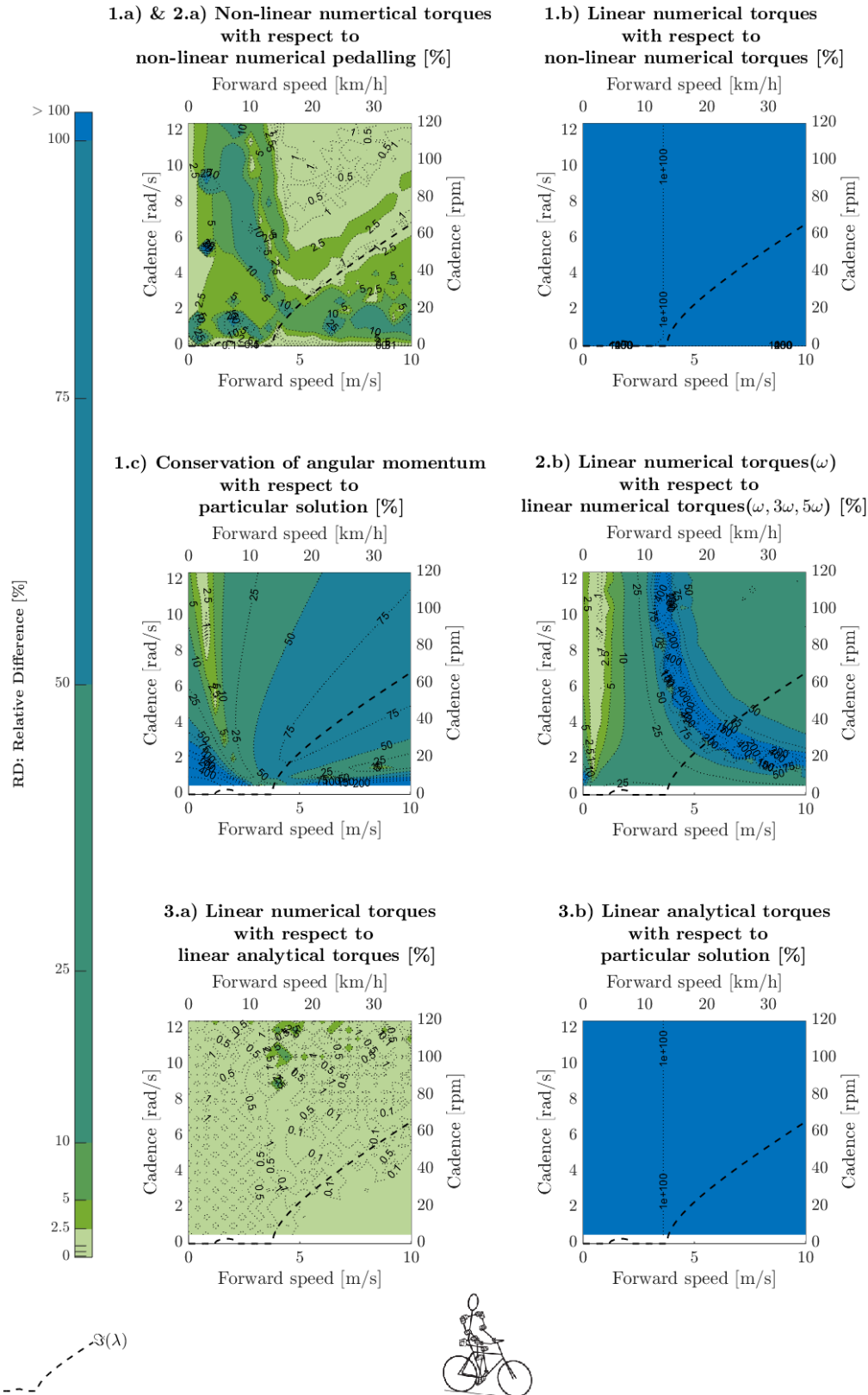


Figure 3.33: Model simplifications and solution method evaluation corresponding to points defined in Section 3.1.3. The relative difference of roll amplitude solutions is depicted as a function of forward speed and cadence, corresponding to model CF. This bicycle-rider model is not self-stable and the imaginary part of the eigenvalue of the weave eigenmode is indicated with a dashed line.

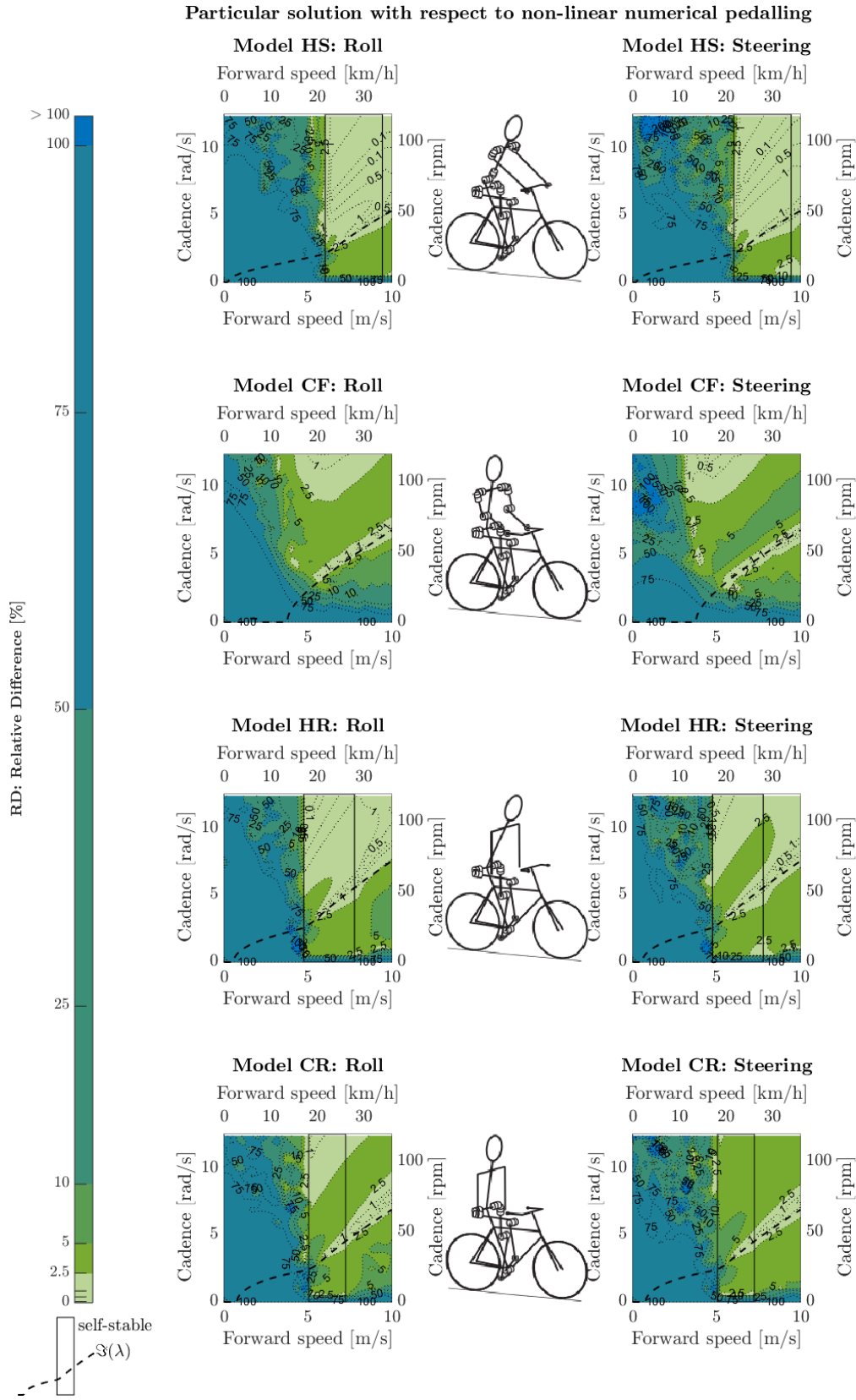


Figure 3.34: The relative differences, of the particular solution method compared to the non-linear pedalling model, of roll and steering amplitude solutions, are depicted as a function of forward speed and cadence, corresponding to all four bicycle-rider models. The self-stable speed region is indicated by a box and the imaginary part of the eigenvalue of the weave eigenmode is indicated with a dashed line.

3.2.5 Normal Cycling: Variation due to Parameters and Conditions

Figure 3.35 gives an overview of the roll and steering amplitude response to the pedalling disturbance for all the cycling conditions and the four models. The working range and the area corresponding to normal cycling is depicted. In general there are large variations in response seen for the variation of forward speed, cadence and posture.

As a rule the roll amplitude is low for low frequencies and low speeds. The weave mode properties seems to determine a large part of the roll response variation in forward speed and cadence. In general the steering amplitude response is low for low cadences. There are some smaller variations seen in steering amplitude response for the variation forward speed that can also be attributed to weave mode properties.

Model HS shows a lower roll response in the working range compared to the other models. The oscillatory part of the weave frequency is lower for this model compared to the other models. Also the amplitude peak corresponding to the resonance of the undamped oscillatory weave mode is further away (higher speed & lower frequency) from the working range than for models HR and CR. The steering amplitude response is higher for rigid upper body models (HR & CR) compared to the passive upper body rider models (HS & CF), this probably due to the added inertia and generalised stiffness to the steering assembly. Smaller differences in response are seen between the two bicycles (HR and CR).

Here we can see that the location of the undamped weave mode and the frequency of the imaginary part of the weave eigenvalue in general will have a great influence on pedalling response. If there is a desire to lower the pedalling response, due to undesired handling properties for instance, this knowledge could be implemented in design choices. It would be advisable to adjust bicycle parameters, such that the bicycle-rider system has an undamped weave frequency and an oscillatory weave frequency in general, further away from the working range. This in general would mean a higher weave speed and a lower imaginary part eigenvalue.

In order to better visualize what these solutions and insights mean for the working range of the bicycle, the behaviour for several common gear ratios (GR) are investigated (Figure 3.36). These gearing specific plots can be seen as cross sections of the contour plots in Figure 3.35, where the location of GR 1 and GR 4 are shown. In general we can see low roll amplitude behaviour for low GRs, which increase with increasing GR. The steering amplitude response does not show this general trend. Model HS does show a consistently lower steering amplitude response as expected from seen behaviour in Figure 3.35. Both roll and steering amplitude show a peak in GR 4 for the rigid upper body rider models, corresponding to proximity of the undamped weave frequency. For some bicycle-rider cases this small peak could be much larger and true resonance could occur in the normal working range of the bicycle (see for instance benchmark results in Figure G.8). This could possibly be solved by tuning bicycle parameters, or might even be solved post fabrication a careful choice of gear ratios. The amplitudes for the four bicycle-rider models, amplitudes stay below 0.03 rad

In order to the ascertain the introduced error by neglecting cycling condition variables, rider posture and bicycle design parameters, Figures 3.37 and 3.38 show the relative difference (RD) corresponding to the evaluation points defined in Section 3.1.3.

We start by looking into the cycling condition variation (Figure 3.37). This error has some similarities to the error associated with the conservation of angular momentum solution simplification, since this solution neglected behaviour due to gravity and forward speed giving the same amplitude result for all cadences. However here we illustrate what is the result of simplifying a single response value corresponding to a normal speed and cadence, for the entire range of forward speeds and cadences. If we compare an arbitrarily chosen reference value of $v = 5$ m/s (=18 km/h) and $\omega = 2\pi$ rad/s (= 60 rpm) to the rest of the normal cycling speed range, we typically see that the error on the roll amplitude is much larger than the error on the steering amplitude ($RD_\phi \approx 25\%$, $RD_\delta < 10\%$). For some other areas of the working range, such as low cadence & low forward speed, this error goes up to 100% for both roll and steering angle response.

Figure 3.38 illustrates the error introduced by using a rigid rider to ascertain the pedalling response of a hands on the handlebars posture. For the hybrid bicycle the introduced error is very large (HR with respect to HS; $RD_\phi \approx 75\%$, $RD_\delta > 100\%$), especially for the steering angle amplitude. The flexed arms posture corresponding to the city bicycle also has significant influence (CR with respect to CF; $RD \approx 20\%$). The error introduced by using different bicycle design parameter can also be significant for relatively small differences in bicycle design (CR with respect to HR; $RD_\phi > 10\%$, $RD_\delta > 5\%$). These errors due to posture

and bicycles design parameters are the error values introduced by these specific cases as an illustration of which parameters and variables should be taken into account. The exact error values would depend highly on the specific cases that are compared. From this evaluation we can conclude that the pedalling disturbance response differs with the variation of cycling conditions, posture and bicycle design parameters.

Here we only investigated the influence of forward speed and cadence, however other cycling conditions would probably also affect the response. These could for instance be ground surface conditions, - inclination, tyre pressure, bicycle maintenance, rider properties, windy weather, acceleration-deceleration, heading tasks etc. The passive upper body rider models also capture only part of the passive influence on the bicycle. Here the upper body models only represent the inertia added in a more realistic manner compared to the rigid rider model in the Whipple model. However a real rider would have a much larger passive influence to the system. Humans can for instance add passive stiffness and damping to the steering assembly (Doria and Tognazzo, 2014) and the upper body lean and yaw as passive posture control. The reflexive gains corresponding to arm posture control can also vary significantly with disturbance frequency van der Helm et al. (2002). In this study these passive effects and other effects such as lateral dynamics control and upper body movements are not investigated. In Section 5.1 we will first explore these effects by comparing our model results to the results of previous experimental research. After this we will discuss what steps could be taken in the future to better understand a wider range of rider behaviour and their influence to the total system behaviour. Here we will also clarify how this study can be used in future work.

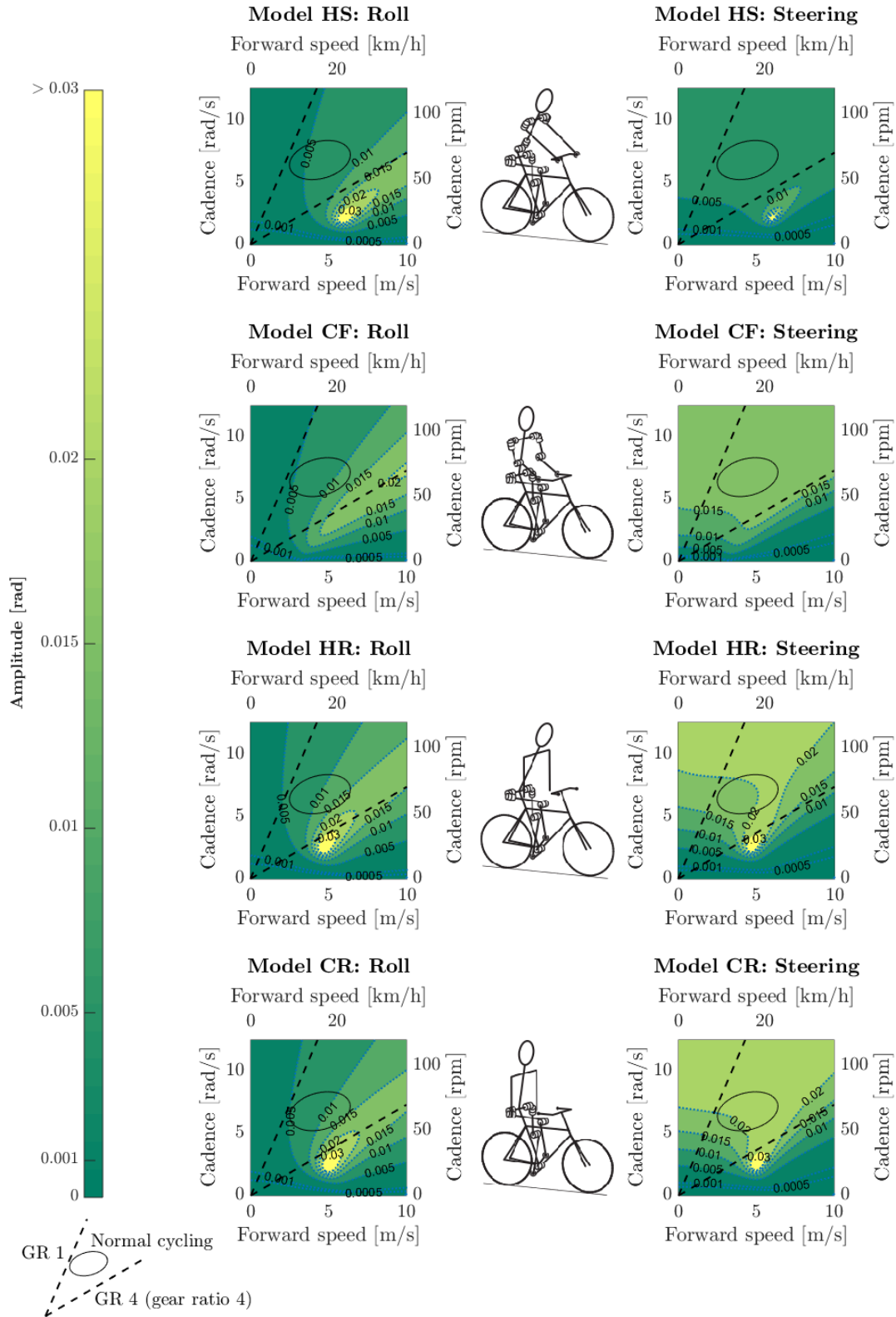


Figure 3.35: Roll and steering amplitudes [rad] as a function of forward speed and cadence corresponding to all four linearised bicycle-rider models. The analytic particular solution method is used to generate the results. The working range of cycling is indicated by two dashed gearing ratio lines and the normal cycling region is indicated by an ellipse.

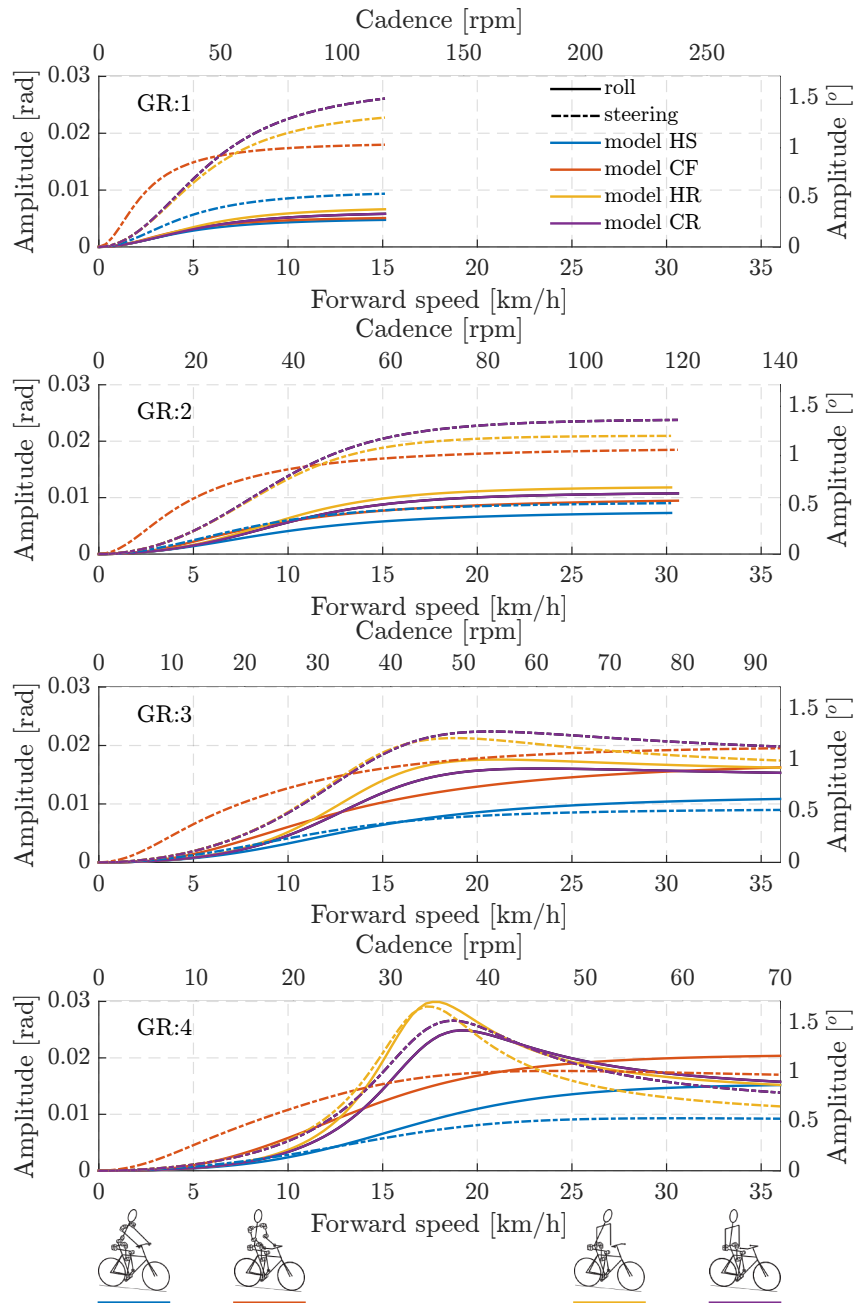


Figure 3.36: Roll (solid lines) and steering amplitudes (dashed lines) function of forward speed and cadence for a gear ratio of 1, 2, 3 and 4, for the four linearised bicycle-rider models (colours).

4.a) Cycling condition variation with respect to 60 rpm 5 m/s combination

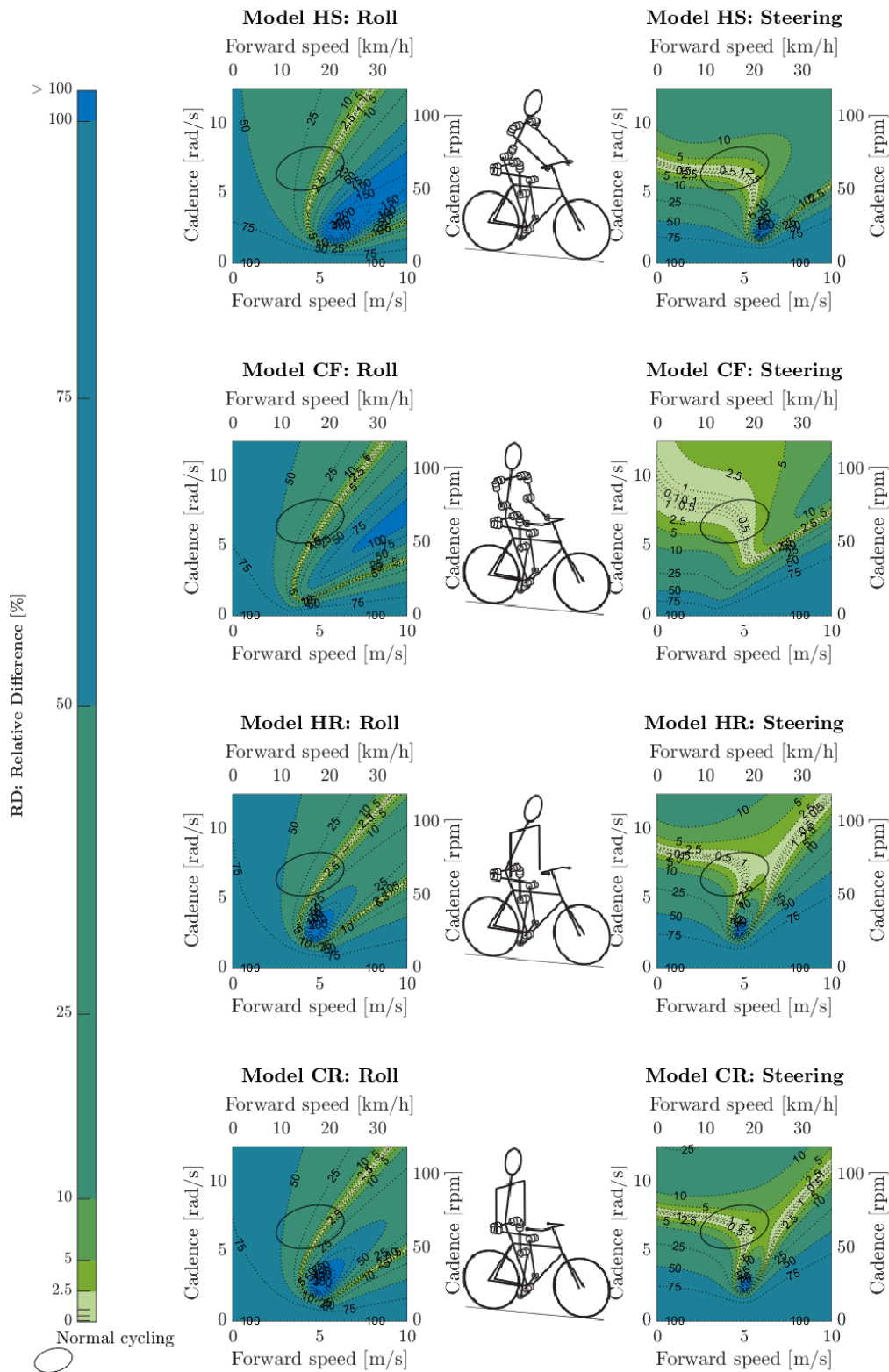


Figure 3.37: The relative difference corresponding to evaluation point 4 (defined in Section 3.1.3) of roll and steering amplitude solutions as a function of forward speed and cadence, corresponding to all four bicycle-rider models. The cycling conditions are compared to a reference value, corresponding to 60 rpm and 5 m/s (centre grid)

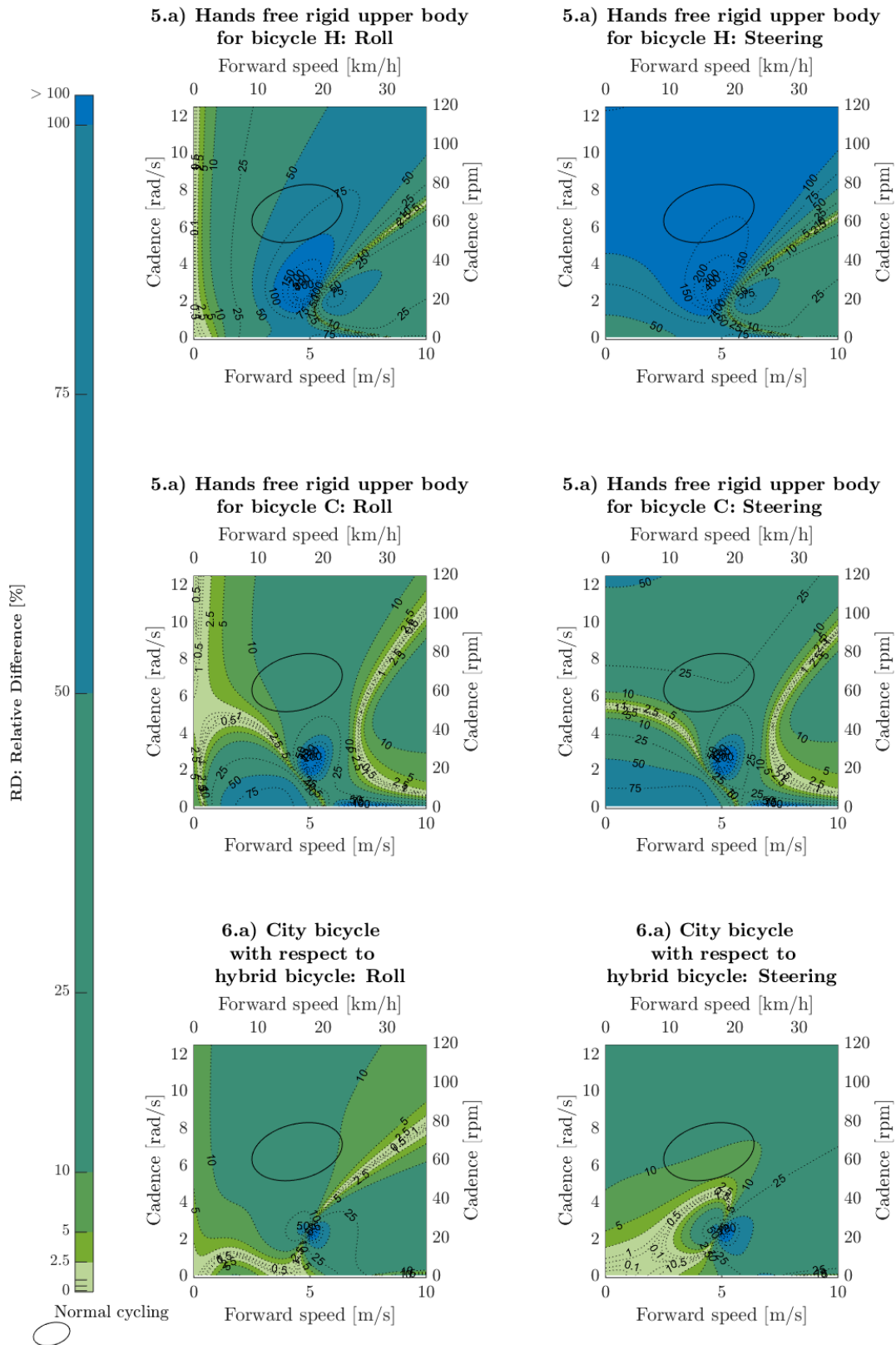


Figure 3.38: The relative difference corresponding to evaluation points 5 & 6 (defined in Section 3.1.3) of roll and steering amplitude solutions as a function of forward speed and cadence. The passive upper body rider models are compared to the rigid upper body rider models in order to illustrate posture influence. The city bicycle is compared to the hybrid bicycle to illustrate bicycle design parameters influence.

3.3 Conclusion

In Section 2 two modelling approaches of the pedalling disturbance are developed. One is applicable to a non linear multibody dynamics model which includes leg segments and its close approximation is applicable on practically any dynamical bicycle-rider model, including a linearised model. In this section we developed and evaluated methods for applying the developed pedalling disturbances to bicycle-rider systems and solving the disturbance response.

Using the particular solution method, the periodic response can be easily found, independent of stability characteristics of the bicycle-rider system. This method is found to be reliable and computationally efficient. The particular solution method proposed here assumes a linearised time-invariant (LTI) system where the pedalling disturbance is modelled as harmonic steering and roll torques (as defined in Section 2). This modelling approach opens up a wide range system identification and solution tools which are only suitable for LTI systems. The LTI assumption brings with it a relative error of up to 5%, mainly attributed to fact that the position of the leg inertia is a function of time, introducing harmonic system properties.

The models and methods have been extensively cross verified. Also the basis of the bicycle-rider model has a benchmarked bicycle model at its basis, of which the lateral dynamics have been validated using experimental approaches. However validation of the specific results for the lateral bicycle behaviour due to the pedalling disturbance is not a simple matter, since cycling on a bicycle without controlling the system brings with it large challenges in safety and experimental design. In Section 4 a comparison of the results of open loop model developed here is compared to experimental results.

The bicycle roll and steering angles show motions which are directly coupled to the disturbance. For the open loop model, the amplitudes of these motions are typically around 0.5° to 1° (≈ 0.01 to 0.02 rad) for normal cycling speed and cadences. The amplitude response is found to be dependent on forward speed, cadence, posture and bicycle design parameters.

We developed a simple method of applying a pedalling disturbance to an easily obtained linearised bicycle model. The pedalling response is shown to exhibit dangerous resonance behaviour for some bicycle-rider combinations within the normal cycling range. This method could be used directly by bicycle designers to investigate the behaviour due to pedalling disturbance before the bicycle is fabricated and avoid such dangerous behaviour. It is also very useful in future research (see Section 5.1).

4 Closed Loop Response and Model Validation

This study so far has developed a method of identifying the lateral dynamic response of an uncontrolled bicycle-rider system to a pedalling disturbance. This is part of a larger effort in the bicycle dynamics field to better understand the bicycle-rider interaction in order to be able to improve safety and handling properties of cycling. (Kooijman et al. (2009); Moore et al. (2011); Schwab et al. (2012, 2013); Vlakveld et al. (2015); Kalsbeek (2016))

One of the motives, of starting this study's specific line of research, was understanding experimental results of Moore et al. (2011). They performed an extensive experimental study by cycling on a large treadmill and capturing bicycle and rider motion. Multiple riders, postures, bicycles and cycling conditions were tested often giving rise to as many questions as answers. They found and quantified a range of rider and bicycle motions that were somehow coupled to pedalling. However what the function of these movements are or how they exactly are coupled is not clear. It could be that they are a direct response to the pedalling disturbance, they are a result of passive or active control methods, they somehow contribute to the pedalling performance, they are somehow biomechanically coupled (through muscle-tendon attachments etc) or a combination of all of some of these aspects.

Since it is not possible to simply switch off all but one of these aspects to identify it's contribution in an experimental set-up, we chose a modelling approach to identify the direct response to the pedalling disturbance. This is a first step in understanding the coupling of the found bicycle and rider movements and pedalling. In this section we will take a second step to by identifying the lateral motion bicycle motions for the full motioned closed loop system. We will compare the behaviour of specific cycling conditions to the open loop system as general validation of the developed model and investigate the influence of control and upper body motions. In Section 5.1 we will explore possible next steps that could be taken to get a full picture of the rider behaviour due to pedalling.

In this section we will use experimental results of previous research to identify the response of pedalling on the steering and roll (lateral motions) of the bicycle. It is important to note that it is not reasonable to expect that the developed modelling results directly agree with experimental results. This is because the modelling results correspond to an uncontrolled system and normal cycling without controlling the bicycle is not feasible. Here we will however compare the modelled uncontrolled system results with the measured controlled system in order to ascertain the contribution of the direct pedalling disturbance to the total lateral motion response. With this comparison we address the following research question: *'What is the nature of the coupling between steering and pedalling?'*

We will compare our direct response results to the experimental results of Moore et al. (2011). This data is available for open use and has a wealth of partly undiscovered and unpublished experimental results. Moore et al. (2011) characterised the higher steering angle amplitude found at the pedalling frequency as a 'steering action'. This implies that the rider had to take 'action' for the steering angle change to occur, however in Section 3 we found a significant response in the steering angle as a direct result of the disturbance. It would therefore be interesting to investigate the contribution of the direct pedalling response to the overall response of the lateral bicycle motions we see in real cycling.

This means that the investigation in this section is twofold. For some cycling conditions, such as hands free cycling in the self-stable forward speed region, we expect the influence of the control actions to be very small. This would mean that we also expect a better agreement with the open loop system for these cycling conditions. These conditions where we expect a reasonable model agreement are ascertained and used for model validation. If this validation step generates reasonable results, we can use the other cycling conditions to get an impression what the contribution is of the direct response to the overall response. With this line of questioning we could also possibly identify the behaviour that can and cannot be predicted by our simple uncontrolled model, opening a path for recommendations and future work.

4.1 Method

The parameters and upper body postures we use in our four models correspond to the parameters and upper body postures of a specific rider and two bicycles used in the experiments by Moore et al. (2011).

The data corresponding to the model CF, city bicycle with flexed arms posture, was the only data published in the original article (Moore et al., 2011), however all the experimental data is obtainable (at <https://github.com/moorepants>). Two different bicycles were used, a hybrid bicycle (Batavus Stratos) and a city bicycle (Batavus Browser), which have different associated rider postures (Figure 4.1). The cyclist rode the bicycles with his hands on the handlebars and hands free. These postures correspond to the models HS and HR for the hybrid bicycle and CF and CR for the city bicycle respectively (Figure 3.4). Also several different forward speeds and gear ratio's (with associated cadences) were tested. For some tests the bicycle was towed (instead of a pedalling, the rider kept the legs still) to see the influence of pedalling on rider behaviour. The motion of the rider and the bicycle was captured using 20 active markers on the rider and 11 markers on the bicycle (for location see Appendix C).

From these markers the front and rear frame orientations of the bicycle and the corresponding roll and the steering angles are obtained following method defined in Moore et al. (2011). Methods defined in Section 3.1 are used to generate model results. Marker data from the right foot is used to synchronise the experimental with model time results. This data is also transformed to the frequency domain (Section 3.1.2.1.1) in order to obtain the cadence. The cadence is used together with the forward speed to generate specific matching results using the non-linear pedalling model (Section 3.1.2.1) and the linearised torques model (analytic time series and particular solution Section 3.1.2.2).

These experimental and modelling results are compared in time domain and frequency domain. The roll and steering amplitudes corresponding to the cadence frequency are used as a measure for disturbance response and the RD (relative difference, Section 3.1.3) is calculated of the model results compared to the measurement results

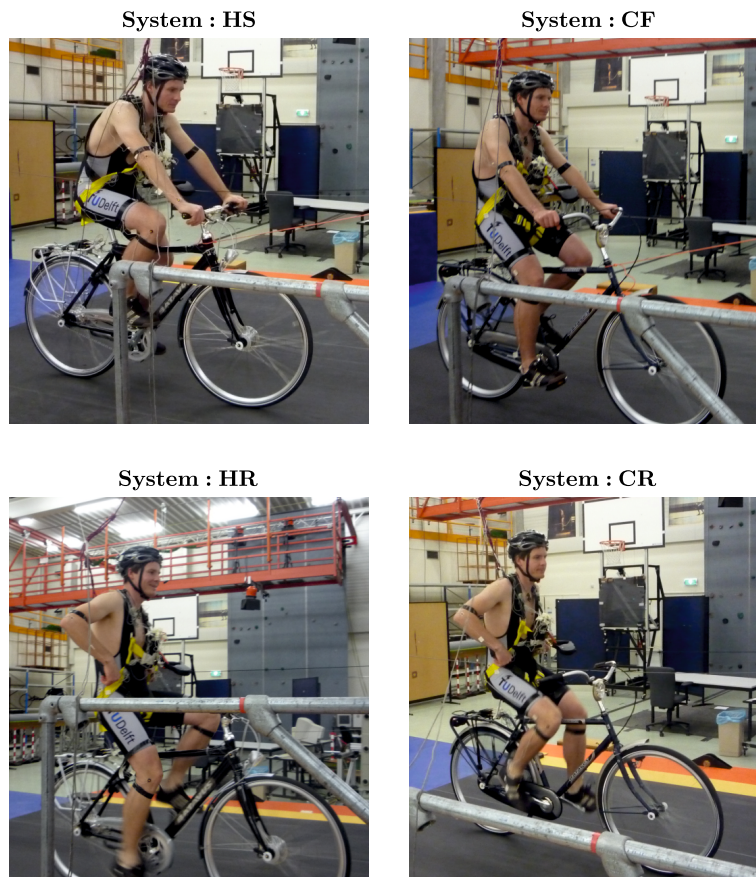


Figure 4.1: Postures corresponding to the hybrid bicycle (left), the city bicycle (right), hands on the handlebars (top) and hands free cycling (bottom) corresponding to experimental data (Moore et al., 2011; Schwab et al., 2012). These are represented by models HS, CF, HR and CR shown in Figure 3.4.

4.1.1 Model Validation

The model we developed in Sections 2 and 3 is an open loop model (a model without control). We would expect the open loop system to have the best agreement with the closed loop system for forward speeds in general the self-stable forward speed range and above.

Our model is used to ascertain the direct response of pedalling on the lateral bicycle movements, it therefore does not include upper body movements associated with pedalling. The upper body is added to system either as rigid attachment to the bicycle frame or as a mechanism attached to the handlebars effectively attaching inertia to the front frame assembly. However the attached arms would also add passive stiffness and damping properties to the handle bars. These properties are connected to biomechanical systems such as connective tissue, passive elements of the muscle-tendon system, active elements through co-contraction and muscle reflexes. Also the rider is thought to add more control to the system when the rider holds the handlebars, this is seen in the measurements, as the rider was not able to ride the bicycle below 12 km/h. Therefore the models corresponding to the hands free cycling condition (model HR and CR), would be best suited to validate the direct pedalling response.

If we use these criteria, we can use 7 tests to compare the model results to the experimental results. These tests correspond to the following cycling conditions:

4 tests for the system HR: $v = \{18.1, 20, 25, 30\}$ km/h; $\omega = \{84, 82, 88, 78\}$ rpm

3 tests for the system CR: $v = \{20, 25, 30\}$ km/h; $\omega = \{77, 64, 70\}$ rpm

4.1.2 Open Loop Compared to Closed Loop Response

When we have identified the model error for the direct open loop response, we can use the other models and cycling conditions to estimate the contribution of the direct response to the overall response. This means that the difference between the open loop modelled results and the full rider closed loop measurements that cannot be attributed to a model error, can be seen as a measure for the overall behaviour that is not captured by the contribution of direct response.

4.2 Results and Discussion

Table 4.1 shows the measurement and model roll and steering amplitudes for the cycling conditions proposed for model validation. We see that the modelled amplitudes are in the same order of magnitude as the measured amplitudes and are in some cases higher and in some cases lower. The relative difference varies a lot with a median value of $< 20\%$ and range of around $30\% \& 80\%$. This relatively high variation around the median error value could be in part by the low number of test used for comparison combined with the high variability in the experiments due to other disturbances and human factors. With this in mind, the model does capture the overall trend of the measurement data very well, where a larger scale experimental study could possibly shed light on the contribution of variability in the experiments to the relative difference.

In Figure 4.2 through 4.5 we can see 6 example measured and modelled roll and steering angle results as a function of time, for the systems HS through CR respectively. In general we see that our modelled result can give good predictions of the measured signals. If we first look at the high speeds for the hands free systems, we can recognise the cadence frequency as the dominant frequency in the measurement result. They seem to be not only of a similar amplitude, but also phase compared to the modelled signal. We would expect the model and the measurement to have the best agreement for these conditions, since the effect of control should be small. This is because the system is stable, thus there is not a lot to control. Also the bicycle rider cannot control the system very effectively without using steering as a direct input (Schwab et al., 2012). This was also seen during the measurement, as low forward speeds were not obtainable for the hands free cycling postures.

For low forward speeds tests, the experimental results for all the four systems show very erratic behaviour. The amplitudes are large and the cadence frequency is not easily recognisable any more by eye.

Figures 4.6 to 4.9 show for the same 6 examples results of the roll and steering frequency domain for the four systems. In general we can see large low frequency content for low forward speeds, which could indicate

Table 4.1: Model validation. Roll ϕ and steering δ amplitudes at cadence frequency, corresponding to cycling conditions used for open loop model validation. These are high forward speed cycling conditions, corresponding to a stable weave mode, for the hands free cycling models and measurements. The difference and the relative difference are also shown together with their mean and standard deviation value.

	system HR				system CR			median (range)
Forward speed v [km/h]	18.1	20	25	30	20	25	30	
Cadence ω [rpm]	84	82	88	78	70	64	77	
Measurement $ \phi(\omega) $ [rad]	0.011	0.011	0.014	0.014	0.017	0.019	0.019	
Model $ \phi(\omega) $ [rad]	0.009	0.011	0.013	0.017	0.011	0.016	0.016	
Difference [rad]	1.8E-3	1E-4	7E-4	-2.8E-3	5.4E-3	3.0E-3	3.5E-3	1.8E-3 (8.1E-3)
RD [%]	16.1	1.2	5.3	20.0	32.6	15.7	18.0	16 (31)
Measurement $ \delta(\omega) $ [rad]	0.025	0.020	0.017	0.010	0.031	0.022	0.020	
Model $ \delta(\omega) $ [rad]	0.021	0.021	0.021	0.018	0.022	0.022	0.021	
Difference [rad]	4.8E-3	-7E-4	-3.7E-3	-8.3E-3	8.2E-3	4E-4	-5E-4	-5E-4 (1.7E-2)
RD [%]	18.8	3.3	21.8	83.0	26.8	1.8	2.5	19 (81)

the presence of low frequency noise and control actions. For higher forward speed, the frequency content is much calmer and a clear peak is visible at the cadence frequency.

System HS and CF show peaks at the second multiple of the cadence that are not seen in the model results, especially in the steering angle frequency content. This second multiple would appear in the response if the pedalling motion is not completely symmetrical or if the upper body motions are disturbing the system at that frequency. Moore et al. (2011) performed a principle component analysis on the measurement data of system CF, showing 'longitudinal' upper body movement with a 'small lateral component' at the second multiple of the cadence. This description sounds similar to an upper body twist motion, which would be expected to result in a steering disturbance. With careful inspection all four systems show small peaks at the third multiple of the cadence, which were predicted from the model results as part of the pedalling disturbance (see Section 2).

The hands free posture systems and system HS seem to show the best agreement with the modelled open loop response in the self-stable forward speed range. For low forward speeds the closed loop systems show very large amplitudes at the cadence frequency and also surrounding low frequencies. For the other cycling conditions the hands on the handlebars systems seem to have a smaller closed loop compared open loop response, where the hands free postures show smaller differences which are both higher and lower response.

The typical value of the cadence response varies from 0.005-0.05 rad for both the roll as the steering angle. Which is in the same general order of magnitude as the found open loop responses. However, the general trend seen as function of forward speed is not the same. The direct pedalling response to the roll angle generally decreases with decreasing forward speed, however in the overall response, this behaviour is not seen. The direct pedalling response on the steering angle does not exhibit any general difference for low forward speeds, however the overall behaviour show a large increase in steering response. This differences in response is probably due to the large effect only a minor disturbance can have on an unstable system. The time series open loop solutions also showed large exponentially increasing behaviour for low forward speeds in steering and roll angles, supporting this idea.

The different system responses are difficult to compare to each other, since the experimental conditions (forward speed and cadence) are not consistent. This is due to the different gear ratios in the two bicycles and the inability to control certain speeds for the hands free cycling conditions. This means that it not reasonable to quantify the differences in overall system response based on this available data. We can however explore general trends.

In order to get a more complete overview, the angle amplitudes at the cadence frequency corresponding to the 4 systems are shown in Figure 4.10 and the relative difference of the model results compared to the measurement results are shown in Figure 4.11. We can see that the relative distance results for the hands free systems is lower than the hands on handlebars systems. System CF, without self-stable region shows

Table 4.2: Median and range of the relative difference of the modelled open loop results compared to the measured closed loop results.

	System HS	System CF	System HR	System CR
median RD $ \phi(\omega) $ [%]	59	134	40	47
range RD $ \phi(\omega) $ [%]	254	710	80	56
median RD $ \delta(\omega) $ [%]	53	86	40	42
range RD $ \delta(\omega) $ [%]	208	925	80	58

the least agreement (see Table 4.2). This supports the general notion that the arms add not only inertia to the steering assembly, but also stiffness, damping and/or control which can be either active or passive.

Another possibility is that the model parameters are not accurate enough to capture the system response to the disturbance correctly. For model CF the seat post length that was given in Schwab et al. (2012) was inconsistent with the given rider parameters and or other bicycle dimensions, since the saddle height was too high to allow for a full crank rotation. Here a choice was made to adjust the set post height to 0.96 trochanteric (hip) height, however this small change drastically changed the eigenvalue plot (Figure 3.9 and E.1). It could be equally possible that the given leg length was actually incorrect, or any other number of parameters. The possible effect of an error in different bicycle and rider parameters is difficult to predict.

Another possible problem with the CF model is that the Batavus Browser bicycle, has reasonably low and wide handlebars. Some films are also available of the experiments, where the upper body posture is not always consistent with the traditional city bicycle posture. Instead of always cycling with flexed arms, riders sometimes seem to switch between a straight arm and flexed arm posture. Also the handle bar width is modelled to be the same as the shoulder to shoulder width, however the arms seem to be directed a bit outwards. Both the lateral positioning of the hands and the straight versus flexed arm posture can have a significant effect on model behaviour Schwab et al. (2012).

Another thing that should be noted is that the measurements themselves can have errors. The experimental design was based on ascertaining general cycling behaviour and rider motion. This experimental design would probably change if open loop model validation would be the aim of the study. For instance, the marker placement would be adjusted or another measurement system all together would be adopted or combined to get accurate angle measurements, the number of repetitions per cycling condition would increase, in order to obtain measurement variability, the rider's upper body movements would be restricted or discouraged etc.

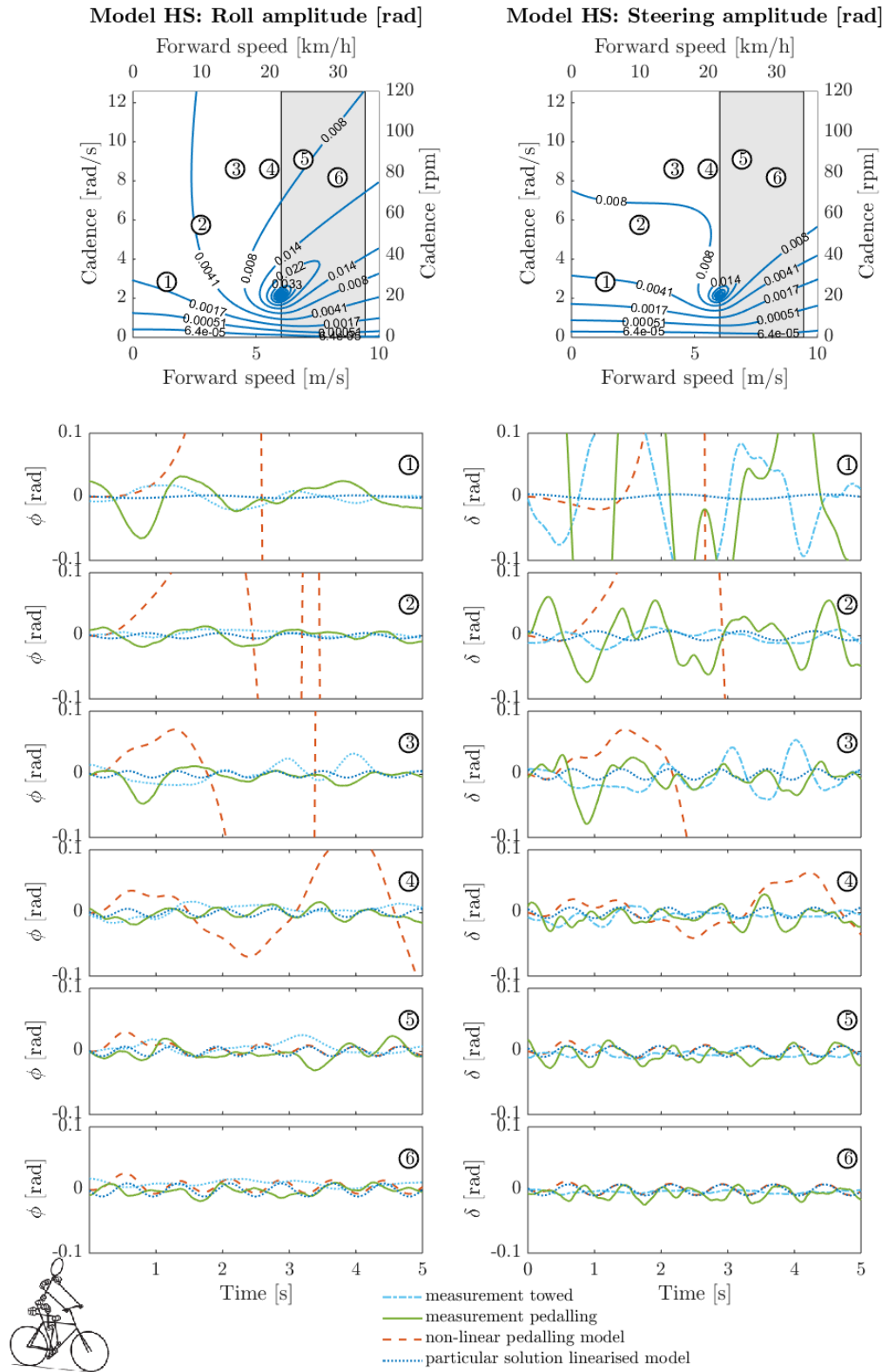


Figure 4.2: Modelled open loop response compared to measured closed loop response for 6 example experimental conditions. The roll (left) and the steering angle (right) is shown as a function of time. The experimental condition combinations are numbered and indicated in the particular solution contour plot (top). The results correspond to system/model HS.

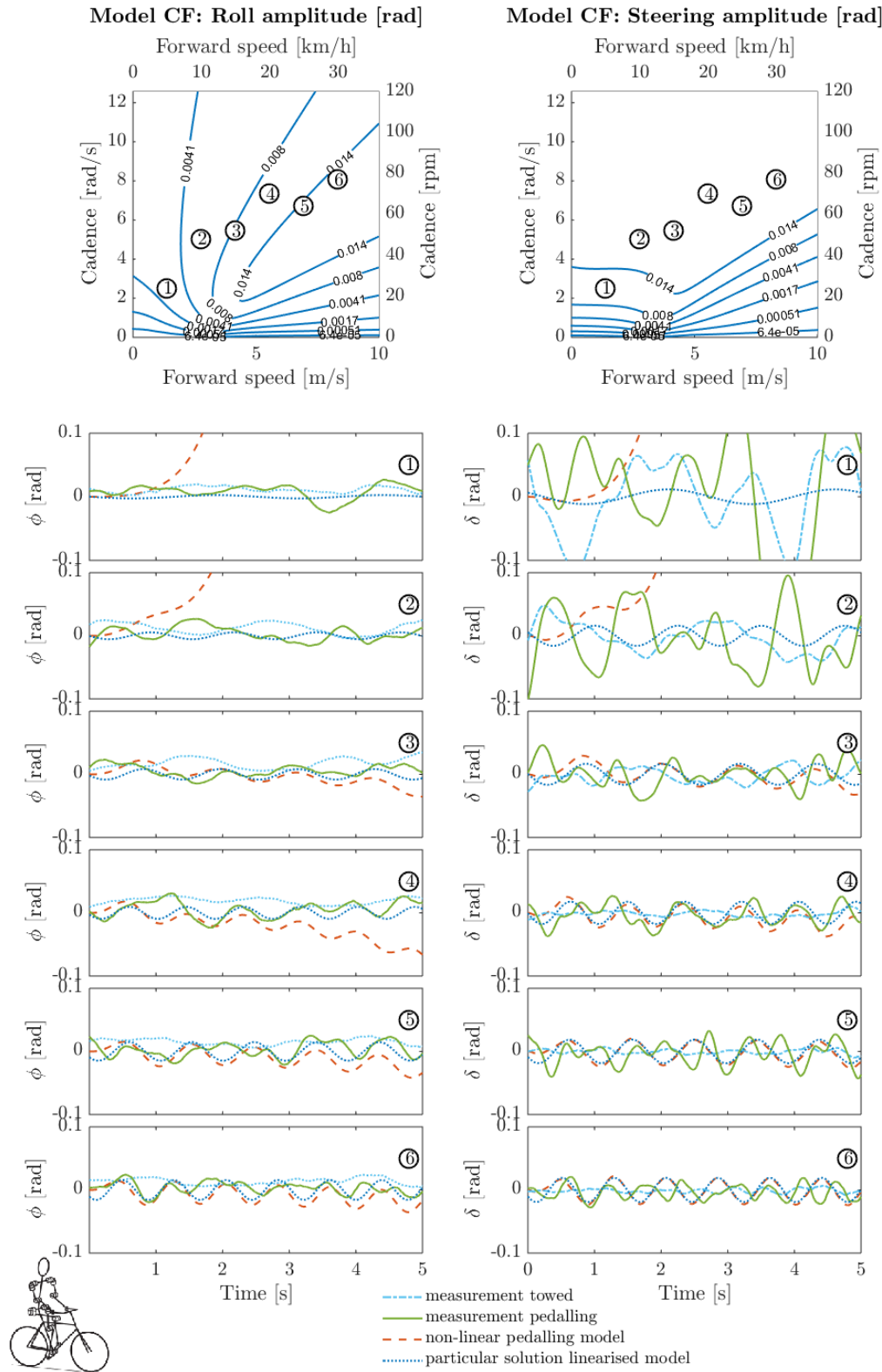


Figure 4.3: Modelled open loop response compared to measured closed loop response for 6 example experimental conditions. The roll (left) and the steering angle (right) is shown as a function of time. The experimental condition combinations are numbered and indicated in the particular solution contour plot (top). The results correspond to system/model CF.

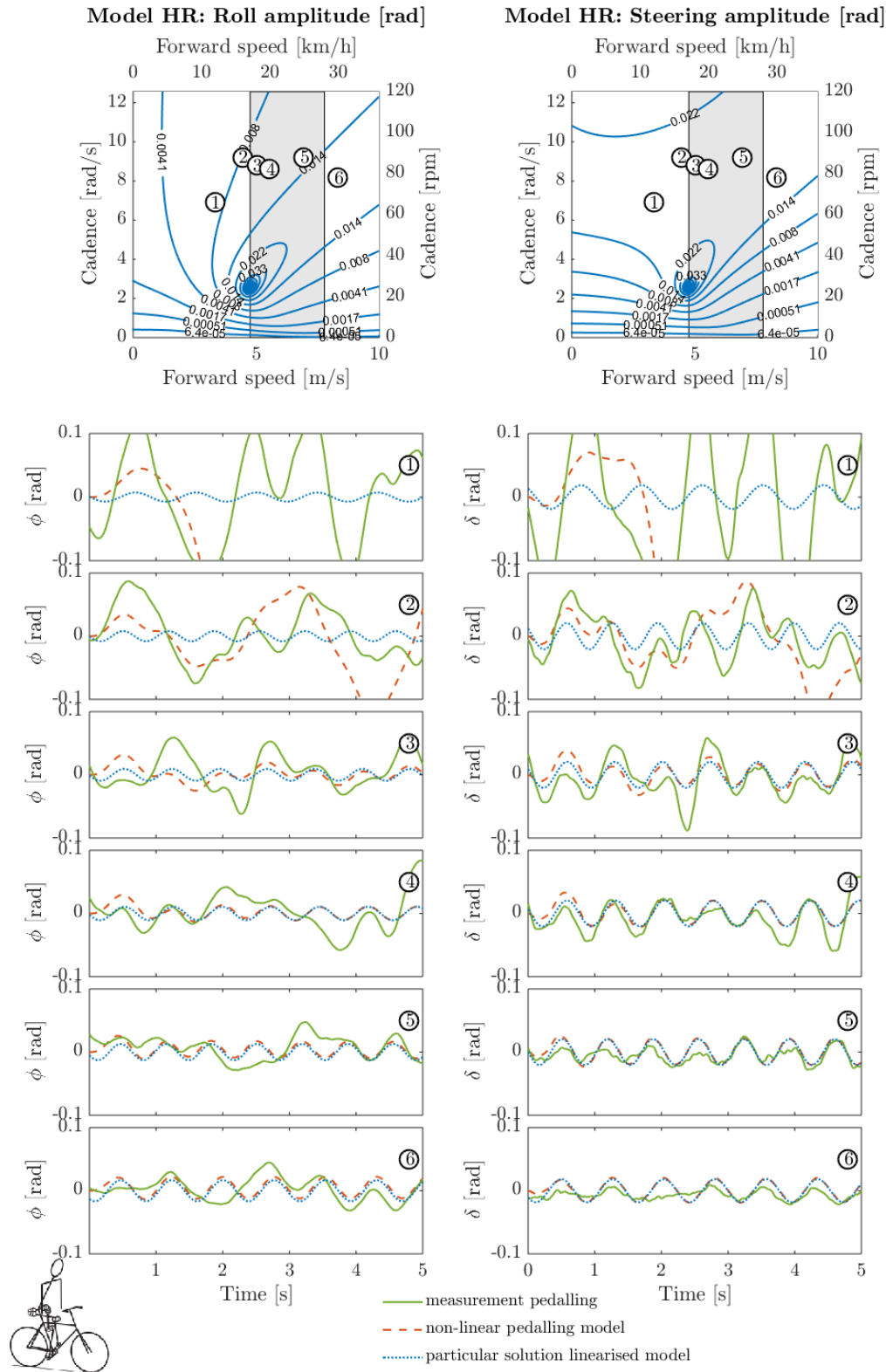


Figure 4.4: Modelled open loop response compared to measured closed loop response for 6 example experimental conditions. The roll (left) and the steering angle (right) is shown as a function of time. The experimental condition combinations are numbered and indicated in the particular solution contour plot (top). The results correspond to system/model HR.

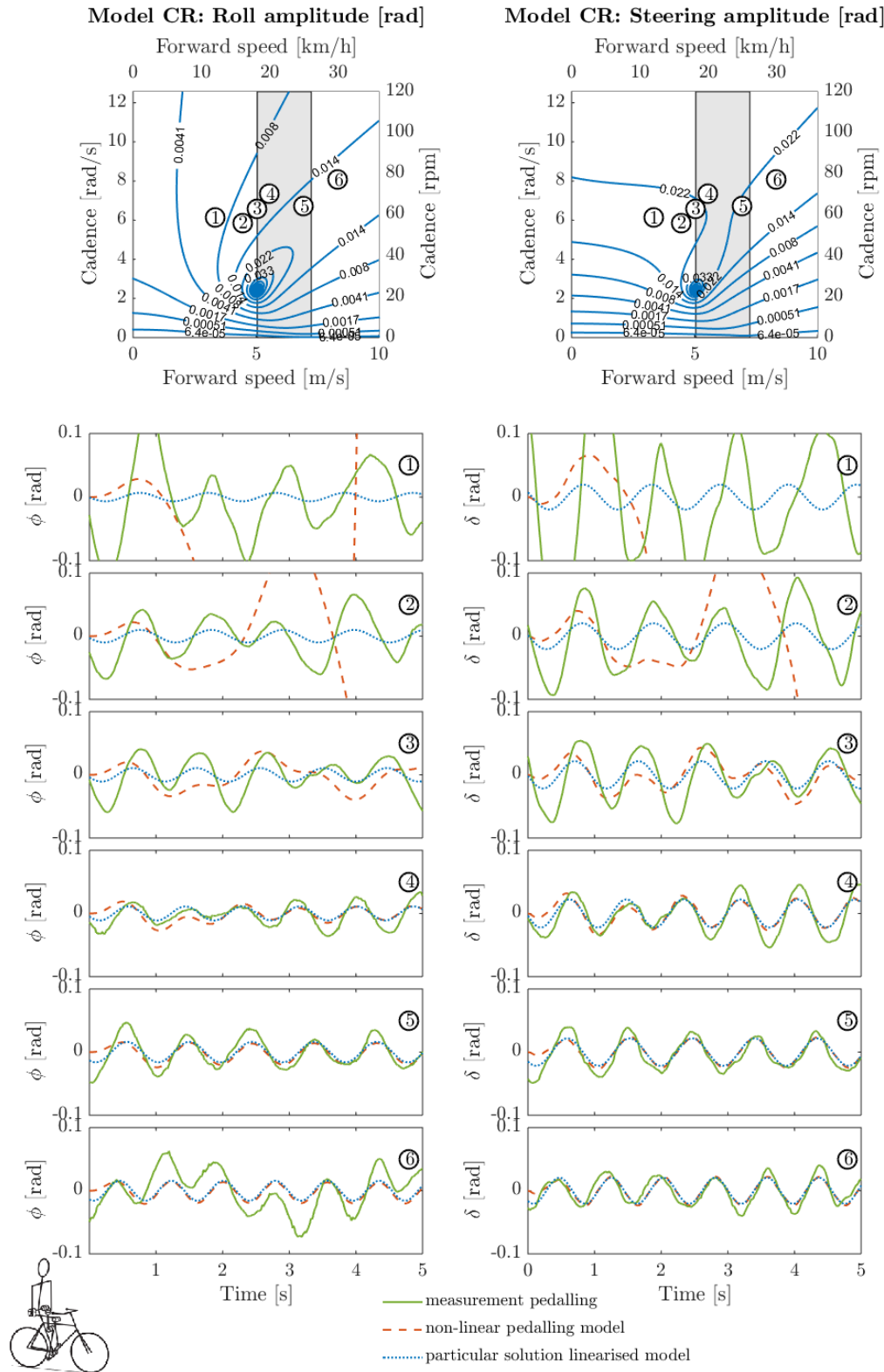


Figure 4.5: Modelled open loop response compared to measured closed loop response for 6 example experimental conditions. The roll (left) and the steering angle (right) is shown as a function of time. The experimental condition combinations are numbered and indicated in the particular solution contour plot (top). The results correspond to system/model CR.

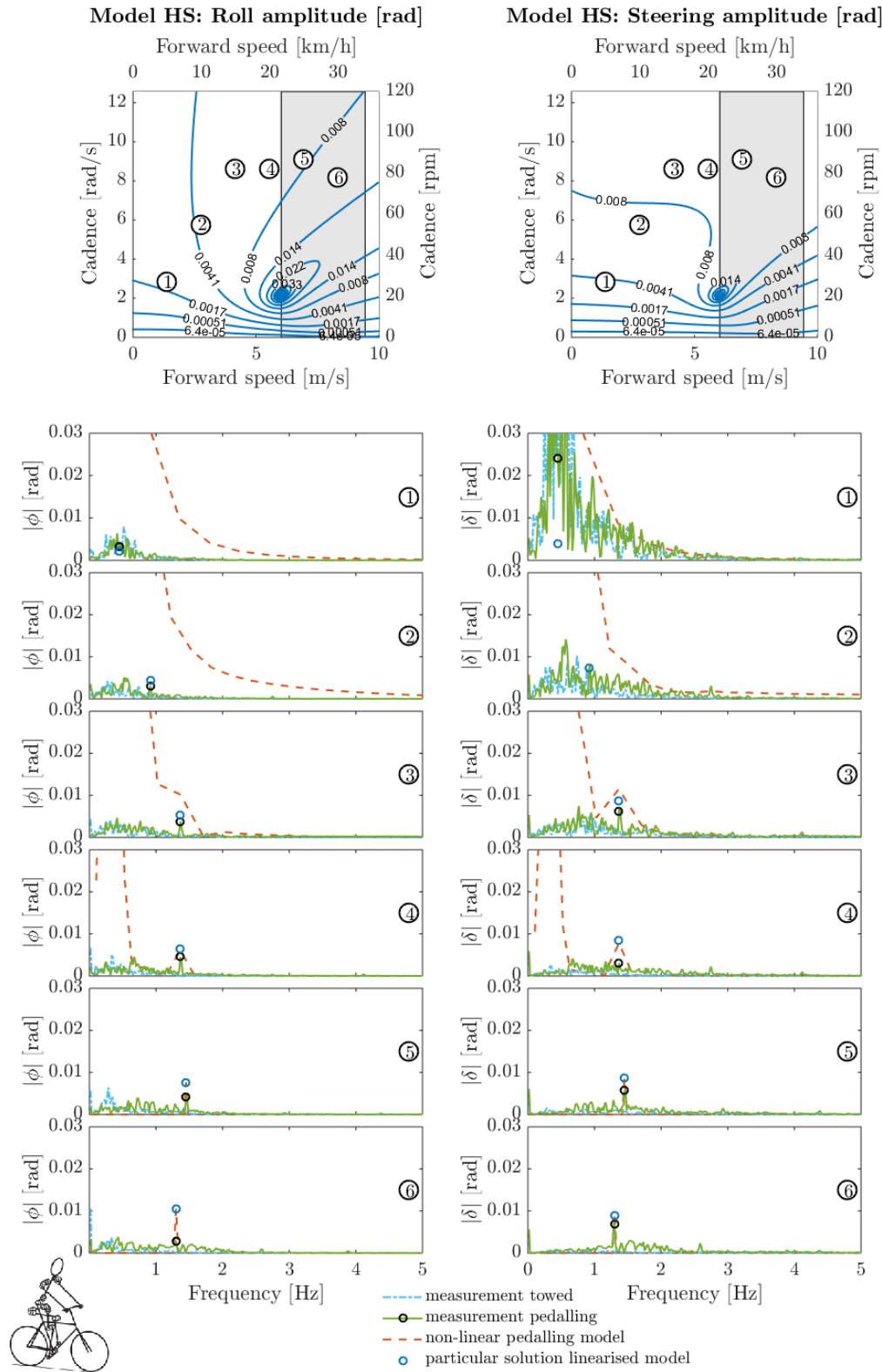


Figure 4.6: Modelled open loop response compared to measured closed loop response for the same 6 example experimental conditions as the time series solution in Figure 4.2. The amplitudes of roll (left) and the steering angle (right) is shown as a function of frequency. The experimental condition combinations are numbered and indicated in the particular solution contour plot (top). The results correspond to system/model HS.

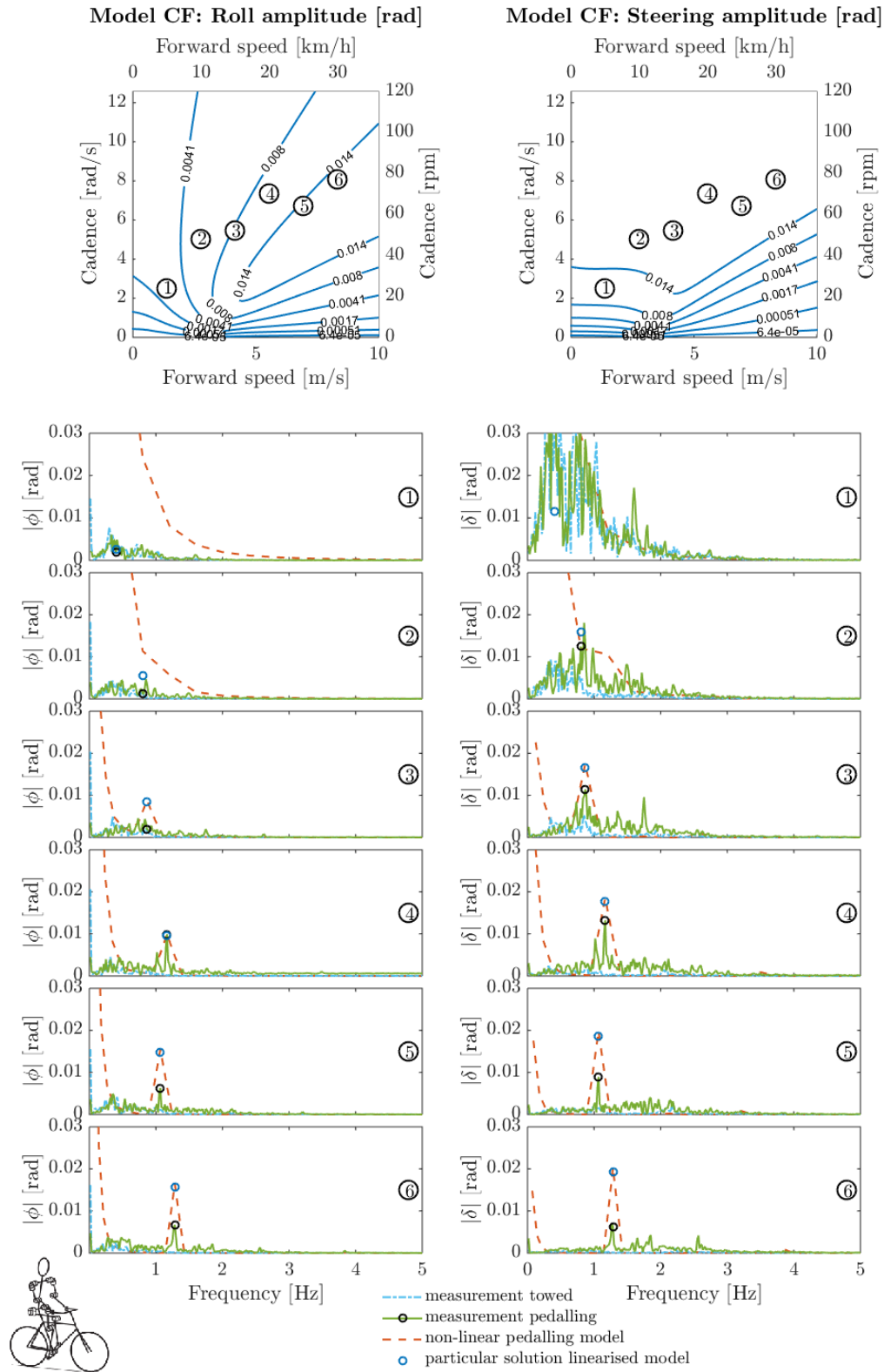


Figure 4.7: Modelled open loop response compared to measured closed loop response for the same 6 example experimental conditions as the time series solution in Figure 4.3. The amplitudes of roll (left) and the steering angle (right) is shown as a function of frequency. The experimental condition combinations are numbered and indicated in the particular solution contour plot (top). The results correspond to system/model CF.

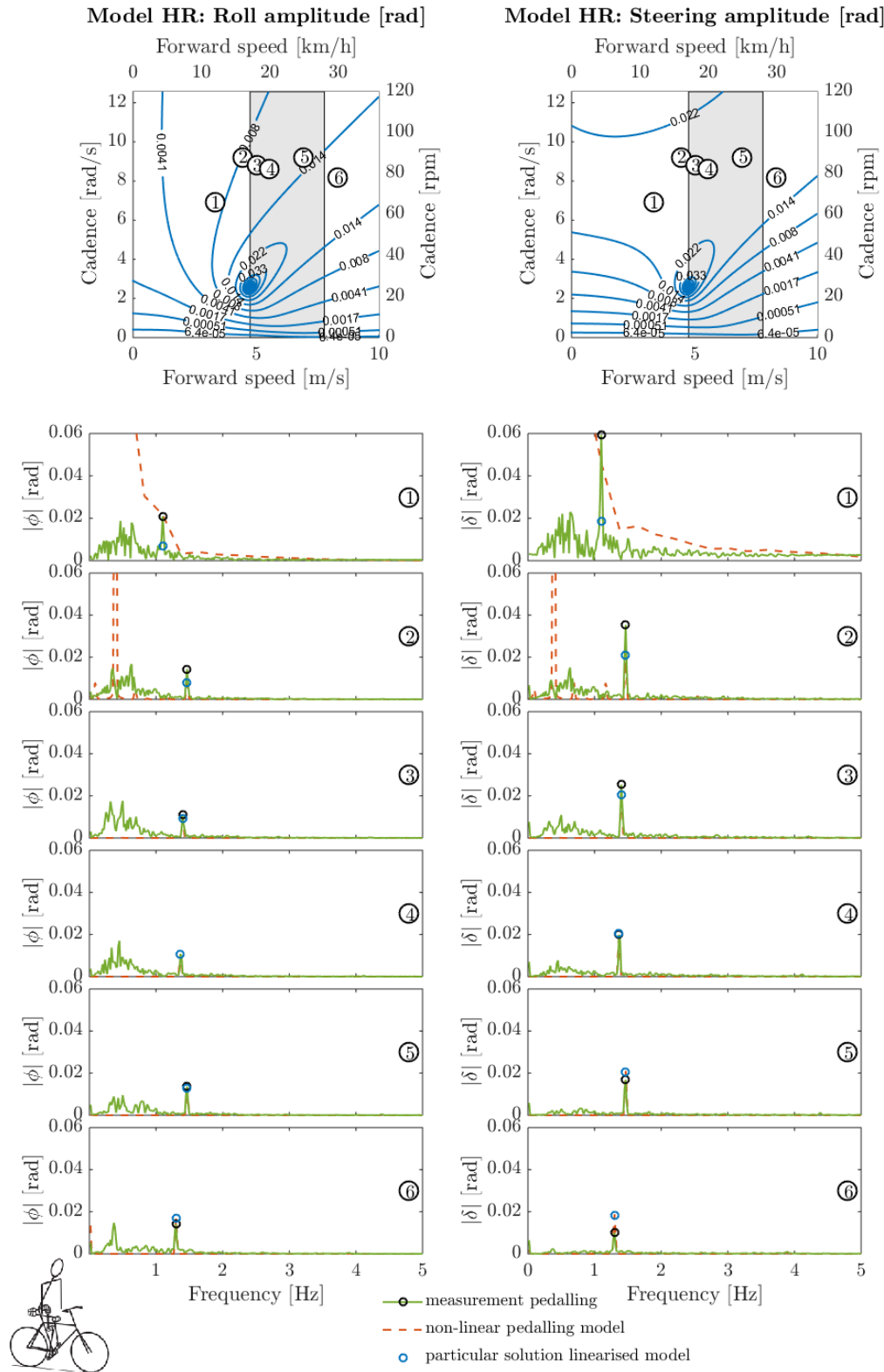


Figure 4.8: Modelled open loop response compared to measured closed loop response for the same 6 example experimental conditions as the time series solution in Figure 4.4. The amplitudes of roll (left) and the steering angle (right) is shown as a function of frequency. The experimental condition combinations are numbered and indicated in the particular solution contour plot (top). The results correspond to system/model HR.

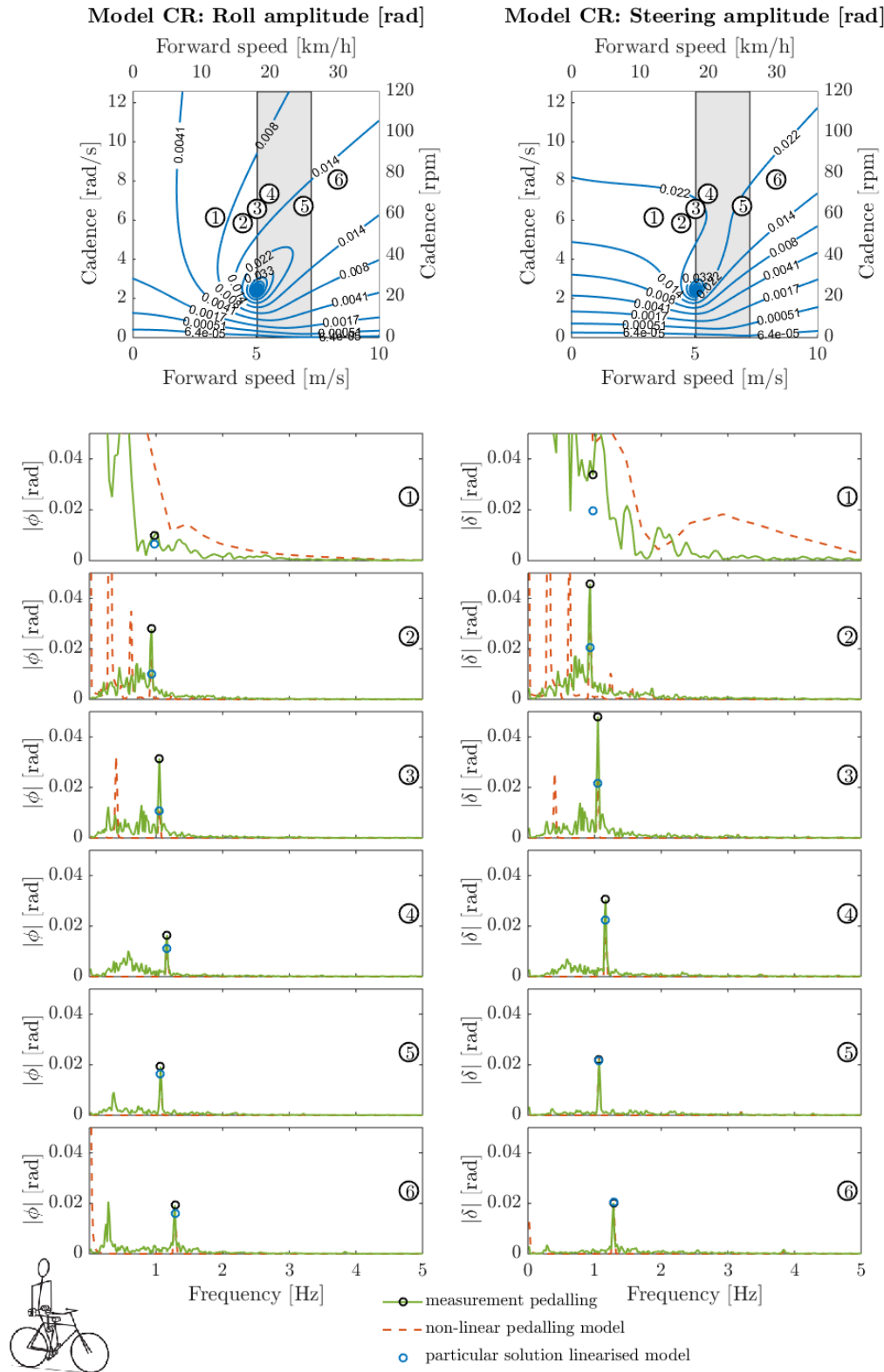


Figure 4.9: Modelled open loop response compared to measured closed loop response for the same 6 example experimental conditions as the time series solution in Figure 4.5. The amplitudes of roll (left) and the steering angle (right) is shown as a function of frequency. The experimental condition combinations are numbered and indicated in the particular solution contour plot (top). The results correspond to system/model CR.

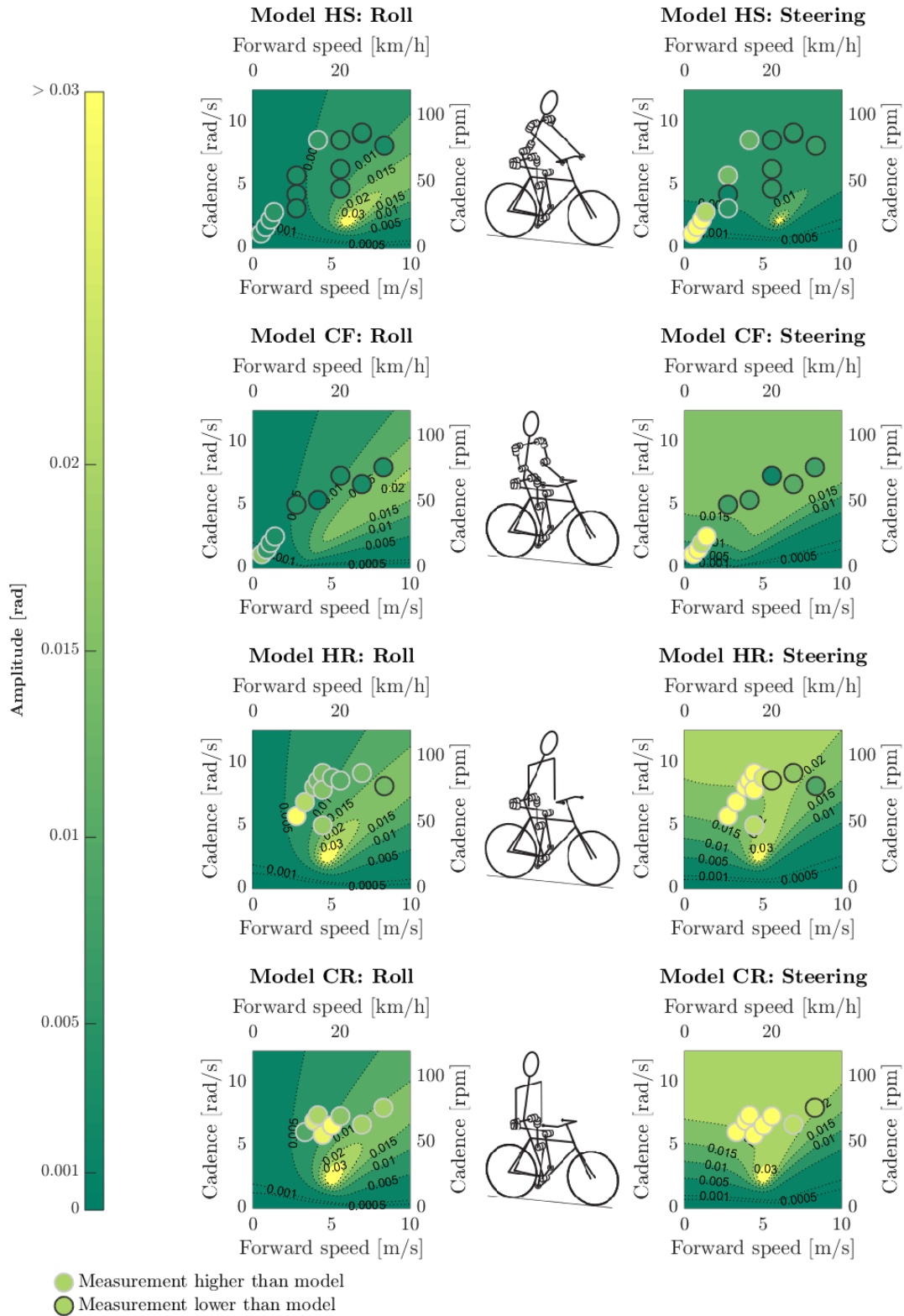


Figure 4.10: Experimental closed loop pedalling response shown as a single circle corresponding to each experimental condition, in relation with the closed loop modelled response. The colour of the inside of the circle corresponds to the value of the amplitude of the closed loop response and the border colour of the circle corresponds to the relation between the modelled open loop amplitude and the measured closed loop amplitude.

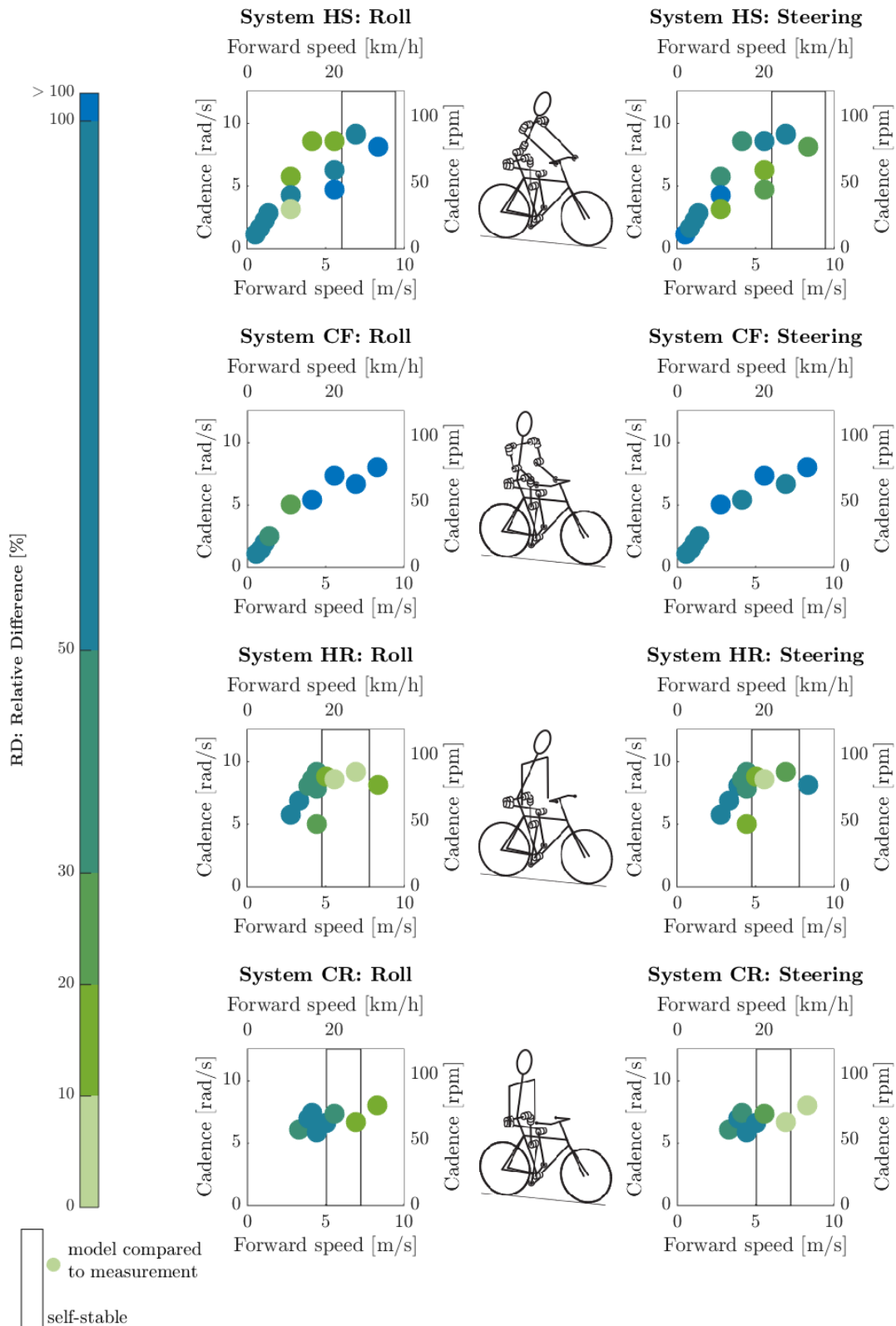


Figure 4.11: An overview of the relative difference is shown for the modelled open loop response compared to the measured closed loop response.

4.3 Conclusion

In Sections 2 and 3 we developed a linearised dynamics model for a pedalling disturbance and the lateral bicycle response respectively. In this section this open loop model has been validated using experimental motion capture data corresponding to hands free cycling on a large treadmill. This is done by comparing the open loop model to the closed loop measurement results, corresponding to experimental conditions closest to open loop, where the open loop bicycle-rider system is self-stable. For these cycling conditions there is a good qualitative and quantitative agreement between model and measurement, with relative difference of 16% for the roll angle and 19% difference for the steering angle.

For other conditions and normal cycling with hands attached to the handle bars the congruity is still reasonable. However the relative differences between the modelled open loop responses and the closed loop measured responses are for some cases much higher depending on system and cycling condition. For normal cycling on a city bicycle this median relative difference is the highest (up to 130%) mainly attributed large effects of upper body movements, passive stiffness and control, but could also be in part by model(parameter) inaccuracies.

In normal cycling we see broad low frequency behaviour attributed to control. We see a response in the second multiple of the cadence frequency attributed to upper body motions. We also see a lower cadence response for medium to high speeds compared to the modelled closed loop response. This is attributed to passive and active stiffness, damping and/or control by the arms on the handle bars. Overall the amplitude is higher for low forward speeds and for hands free cycling, attributed to the high instability of the system. The cadence frequency response in normal cycling varies from 0.25° to 3° (≈ 0.005 to 0.05 rad) for the roll and steering angle depending on cycling conditions and posture.

5 Conclusions and Recommendations

The nature of the pedalling disturbance is now understood and we are able to predict size and frequency by an simplified model. The direct lateral response and the overall lateral bicycle-rider behaviour due to pedalling are explored. This uncovered parameter dependencies and differences due to rider properties and behaviour.

We developed and validated a simple method of applying a pedalling disturbance to an easily obtained linearised bicycle model. Some bicycle-rider combinations exhibit resonance behaviour due to pedalling within the normal cycling range, this model could be used to slightly change bicycle design parameters such that this dangerous behaviour is avoided. It could also be very useful in future research (see Section 5.1).

 We ascertained the nature of the pedalling disturbance and identified parameters influencing it.

The disturbance on the lateral dynamics due to pedalling is caused by the vertical and the forward acceleration of the left and right leg centre of mass. The vertical acceleration promotes an inertial torque disturbance about the bicycle roll and the forward acceleration promotes an inertial torque disturbance about the steering of the bicycle. These generalised inertial torques only contain odd multiples of the cadence frequency. Both torques are proportional to the leg mass, the hip width and cadence squared. The steering torque is also proportional to the mechanical trail ($c \cos(\lambda_s)$) and inverse proportional to the wheelbase ($\frac{1}{w}$), which are the parameters associated with yaw-steering coupling. The rest of the amplitude and phase behaviour is dependent on the geometry of the lower limbs and the saddle to crank axis distance and orientation defining the forward and vertical motion of the leg centre of masses.

 We developed a pedalling disturbance model which can be easily applied on bicycle rider systems.

The modelled forward and vertical motion of the leg centre of masses is based on a leg kinematic model represented by the motion of a dual 4-bar mechanism, consisting the saddle to crank axis frame part as the base, the cranks, upper and lower legs. The motion of the leg centre of mass can be represented by sinusoidal motions containing the cadence frequency and its multiples. This can be approximated by using only the cadence frequency, with an error in the times series of 2% in forward direction and 3.4% in vertical direction. These simplified motions result in a simple representation of the disturbance as sinusoidal torques containing only the cadence frequency, which can be easily applied on the steering and roll of a bicycle model.

 We developed an easy method for determining the direct lateral response of pedalling.

We developed a model to ascertain direct lateral response to the pedalling disturbance. This open loop model, with direct disturbance applied, represents the system that needs to be controlled by the rider. We evaluated a range of model and solution methods to estimate the direct response corresponding to the pedalling disturbance.

A full non-linear dynamics model of the bicycle-rider system can be combined with the full leg kinematic model developed in this study. However, generating solutions for a non-linear model can be consuming in both implementation as computational time. Accurately ascertaining periodic direct responses for a non-linear unstable system presents difficulties due to dominant transient response.

The developed sinusoidal roll and steering torques, the close approximation the pedalling disturbance, can be easily applied to a linearised bicycle-rider model. Using the particular solution method, the periodic response can be easily found, independent of stability characteristics of the bicycle-rider system. This method is found to be reliable and computationally efficient. The easy method proposed here assumes a linearised time-invariant (LTI) system where the pedalling disturbance is modelled as harmonic steering and roll torques (as defined in Section 2). This modelling approach opens up a wide range system identification and solution tools which are only suitable for LTI systems. The LTI assumption brings with it a relative error of up to 5%, mainly attributed to fact that the position of the leg inertia is a function of time, introducing harmonic system properties.

 We validated the model using experimental data.

The models and methods have been extensively cross verified. Also the basis of the bicycle-rider model has a benchmarked bicycle model at its basis, of which the lateral dynamics have been validated using experimental approaches. However validation of the specific results for the lateral bicycle behaviour due to the pedalling disturbance is not a simple matter, since cycling on a bicycle without controlling the system brings with it large challenges in safety and experimental design. Here it is done by comparing the open loop model to the closed loop measurement results, corresponding to experimental conditions closest to open loop, which is hands free cycling at a self-stable forward speed on a large treadmill. This comparison gives a median relative difference of 16% for the roll angle and 19% difference for the steering angle.

 We explored the relation between direct response and overall response in normal cycling.

The bicycle roll and steering angle shows motion which is directly coupled to the disturbance. The amplitudes of these motions directly coupled to the disturbance are typically around 0.5° to 1° (≈ 0.01 to 0.02 rad) for normal cycling speed and cadences. Where the overall response for normal forward speed ranges from around 0.25° to 3° (≈ 0.005 to 0.05 rad) for both roll and steering angle.

The measured overall cycling frequency response shows signs of control and upper body movements. We also see a lower cadence response for medium to high forward speeds compared to modelled direct response for normal hands-on cycling. However for both hands on and hands free we see a higher cadence response for low speeds for the closed loop response compared to the open loop response. The differences between the open loop direct response and the normal closed loop response is mainly attributed to instability and control, but also to model inaccuracies, upper body movements, passive joint properties and posture control.

 We identified variables influencing the direct and overall lateral response for normal cycling conditions.

Both the direct and the overall pedalling disturbance response is found to be dependent on forward speed, cadence, posture and bicycle design parameters. However the dependency seen in the direct response is in some cases different than the dependency seen in the overall response.

The direct roll response generally decreases with decreasing forward speed, however in the overall roll response, this behaviour is not seen. The direct steering response does not exhibit any general difference for low forward speeds, however the overall steering response shows a large increase in steering response for low speeds. This difference is attributed to instability associated with low forward speed.

5.1 Future Work

This study has uncovered differences in direct modelled open loop response and overall measured responses. In order to better understand the nature of these differences we could combine the pedalling bicycle-rider model presented in this study and extend it with upper body motions, passive elements and control. This line of research would not only clarify differences found here, but also could be used to answer research questions previously formulated in Appendix A which are mainly based on observations by Moore et al. (2011).

First we will look at the possible steps in understanding the nature and effect of the upper body movements. A wide range of possible functions could possibly be linked with the seen upper body motions. The upper body movements are somehow connected to pedalling, since these movements are much less dominant for cycling conditions without pedalling (Moore et al., 2011). These upper body movements could for instance be linked with lateral balance control, aiding the pedalling performance, posture control and biomechanical coupling with pedalling motion.

As a part of this line of research we supervised a bachelor project group, which did some promising first findings in upper body movement aided pedalling performance (Dijkink et al., 2015). They found indications that forward backward motions, called bounce by Moore et al. (2011), could be adopted by cyclists to aid pedalling performance. A 3D musculoskeletal modelling approach could possibly be used to identify the

physiological grounds on which this observation is based. This same line of investigation could also identify if there is a biomechanical coupling between the upper and lower segments which could explain (part of) the upper body motions.

First we would like to explore functions associated with posture control and lateral dynamics control. The reason for the added upper body motions could possibly be due to the lateral perturbations associated with pedalling. For instance the upper body motions could be adopted to keep the head level (posture control) or compensate for the pedalling disturbance as a kind of feed forward control. In order to investigate this it would be interesting to first ascertain the frequency information of the various upper body motions (the bend, twist and lean) in relation to the pedalling motion. With the amplitude and the phase known, a simple first estimation could be made to see if the phase of the upper motions would relate to an added disturbance or a compensation of the pedalling disturbance. A similar approach to the one applied in this study to investigate the effect of the pedalling motion, could be applied to investigate the effect of an upper body motion.

Another possible line of research could lead us to better understanding the bicycle control. We would like to better understand the choice that is made between different control actions. Why does the lateral knee movement action only appear in low speeds and only when pedalling? How do the physiological capabilities of the human neuromusculoskeletal and sensory system effect controllability and control effort? How does the choice between different control actions change, based on disturbance type? It would be reasonable to expect that a disturbance that is predictable, such as a pedalling disturbance, could be controlled by feed forward control. Disturbances that are not predictable could possibly be controlled using different strategies depending on frequency content. Aside from providing some intrinsic or passive stiffness Doria and Tognazzo (2014), humans controllers can also for instance adapt their reflex gains according to frequency content of a disturbance if it is in the low to medium frequency range (van der Helm et al., 2002) or apply co-contraction to increase joint stiffness in the case of high frequency disturbance types. How do the control strategies change with different tasks and cycling conditions? Schwab et al. (2013) found that control strategies change with forward speed, which was attributed to the change in task.

For the identification of control, a standard approach is to measure the systems response to a disturbance. This measurement can be used to fit parameters of a modelled controller in order to identify the control strategy and control gains. During cycling, pedalling is a naturally occurring disturbance which could possibly be used in a system identification approach. If an impulse type disturbance is desired, it could still be important to take the pedalling disturbance into account.

References

- Bakker, K. (2011). Snelheid van 5 verschillende fietsen vergeleken. "<http://www.fietsersbond.nl/de-fiets/snelheid-5-verschillende-type-fietsen-vergeleken#.U0PNKrRbXik>" accessed on 08-04-2014.
- Bini, R. R., Hume, P. A., and Kilding, A. E. (2014). Saddle height effects on pedal forces, joint mechanical work and kinematics of cyclists and triathletes. *European journal of sport science*, 14(1):44–52.
- Boyce, W. E. and DiPrima, R. C. (2005). *Elementary differential equations and boundary value problems*. John Wiley & Sons, 8 edition.
- Brandt, A. (2011). *Noise and vibration analysis signal analysis and experimental procedures*. Wiley.
- Brown, D. A., Kautz, S. A., and Dairaghi, C. A. (1996). Muscle activity patterns altered during pedaling at different body orientations. *Journal of Biomechanics*, 29(10):1349–1356.
- Carvallo, E. (1899). *Théorie du Mouvement du Monocycle et de la Bicyclette*. Gauthier-Villars, Paris, France.
- Connors, B. (2009). Modeling and stability analysis of a recumbent bicycle with oscillating leg masses. Master's thesis, University of California, Davis.
- Connors, B. and Hubbard, M. (2008). *Modelling and Stability Analysis of a Recumbent Bicycle with Oscillating Leg Masses (P131)*. Springer.
- Dijkink, L., Duin, L. B. G. R., Otten, G. J. M., and Wijburg, E. R. (2015). The effect of upper body movement during urban cycling.
- Doedel, E. J. (1981). Auto: A program for the automatic bifurcation analysis of autonomous systems. *Congr. Numer*, 30:265–284.
- Doedel, E. J., Govaerts, W., and Kuznetsov, Y. A. (2003). Computation of periodic solution bifurcations in odes using bordered systems. *SIAM Journal on Numerical Analysis*, 41(2):401–435.
- Doria, A. and Tognazzo, M. (2014). The influence of the dynamic response of the riders body on the open-loop stability of a bicycle. *Proceedings of the Institution of Mechanical Engineers, Part C: Journal of Mechanical Engineering Science*, 228(17):3116–3132.
- Dormand, J. R. and Prince, P. J. (1980). A family of embedded runge-kutta formulae. *Journal of Computational and Applied Mathematics*, 6(1):19–26.
- Fowles, G. R. and Cassiday, G. L. (1999). *Analytical mechanics*. Brooks/Cole Thomson Learning, sixth edition edition.
- Greenwood, D. T. (2006). *Advanced dynamics*. Cambridge University Press.
- Jonker, J. B. and Meijaard, J. P. (1990). Spacar computer program for dynamic analysis of flexible spatial mechanisms and manipulators. In Schiehlen, W., editor, *Multibody Systems Handbook*, pages 123–143. Springer Berlin Heidelberg.
- Kalsbeek, I. (2016). Experimental investigation into the shimmy motion of the bicycle for improving model-based shimmy estimations.
- Kingma, J., Duursma, N., and Duis, H. J. A. N. t. (1997). The aetiology and long-term effects of injuries due to bicycle accidents in persons aged fifty years and older. *Perceptual and Motor Skills*, 85(3):1035–1041.
- Kooijman, J. D. G. and Schwab, A. L. (2009). Experimental validation of the lateral dynamics of a bicycle on a treadmill. *Proceedings of Asme International Design Engineering Technical Conferences and Computers and Information in Engineering Conference, Vol 4, Pts a-C*, pages 2029–2034.

- Kooijman, J. D. G., Schwab, A. L., and Moore, J. K. (2009). Some observations on human control of a bicycle. *Proceedings of Asme International Design Engineering Technical Conferences and Computers and Information in Engineering Conference, Vol 4, Pts a-C*, pages 2021–2028.
- Meijaard, J. P., Papadopoulos, J. M., Ruina, A., and Schwab, A. L. (2007). Linearized dynamics equations for the balance and steer of a bicycle: a benchmark and review. *Proceedings of the Royal Society a-Mathematical Physical and Engineering Sciences*, 463(2084):1955–1982.
- Molnar, H. (2002). Fietsend achterop. In *INDEX Centraal Bureau voor de Statistiek*, volume 7, pages 28–29.
- Moore, J., Kooijman, J., Schwab, A., and Hubbard, M. (2011). Rider motion identification during normal bicycling by means of principal component analysis. *Multibody System Dynamics*, 25(2):225–244.
- Moore, J. K. (2012). *Human Control of a Bicycle*. PhD thesis, University of California Davies.
- Moore, J. K., Hubbard, M., Kooijman, J. D. G., and Schwab, A. L. (2009). A method for estimating physical properties of a combined bicycle and rider. *Proceedings of Asme International Design Engineering Technical Conferences and Computers and Information in Engineering Conference, Vol 4, Pts a-C*, pages 2011–2020.
- Neptune, R. and Hull, M. (1998). Evaluation of performance criteria for simulation of submaximal steady-state cycling using a forward dynamic model. *TRANSACTIONS-AMERICAN SOCIETY OF MECHANICAL ENGINEERS JOURNAL OF BIOMECHANICAL ENGINEERING*, 120:334–341.
- Neptune, R., Kautz, S., and Hull, M. (1997). The effect of pedaling rate on coordination in cycling. *Journal of Biomechanics*, 30(10):1051–1058.
- Neptune, R. R., Kautz, S. A., and Zajac, F. E. (2000). Muscle contributions to specific biomechanical functions do not change in forward versus backward pedaling. *Journal of Biomechanics*, 33(2):155–164.
- Pacejka, H. (2012). *Tire and Vehicle Dynamics*. Elsevier Science.
- Popov, A., Rowell, S., and Meijaard, J. (2010). A review on motorcycle and rider modelling for steering control. *Vehicle System Dynamics*, 48(6):775–792.
- Raasch, C. C. and Zajac, F. E. (1999). Locomotor strategy for pedaling: Muscle groups and biomechanical functions. *J Neurophysiol*, 82(2):515–525.
- Raasch, C. C., Zajac, F. E., Ma, B., and Levine, W. S. (1997). Muscle coordination of maximum-speed pedaling. *Journal of Biomechanics*, 30(6):595–602.
- Ruby, P., Hull, M. L., and Hawkins, D. (1992). Three-dimensional knee joint loading during seated cycling. *Journal of Biomechanics*, 25(1):41–53.
- Scaramuzza, G., Uhr, A., and Niemann, S. (2015). *E-Bikes im Strassenverkehr: Sicherheitsanalyse*. bfu - Beratungsstelle für Unfallverhütung.
- Schepers, J. P., Fishman, E., den Hertog, P., Wolt, K. K., and Schwab, A. L. (2014). The safety of electrically assisted bicycles compared to classic bicycles. *Accident Analysis Prevention*, 73:174–180.
- Schwab, A., de Lange, P., Happee, R., and Moore, J. K. (2013). Rider control identification in bicycling using lateral force perturbation tests. *Proceedings of the Institution of Mechanical Engineers, Part K: Journal of Multi-body Dynamics*, 227(4):390–406.
- Schwab, A. and Meijaard, J. (2013). A review on bicycle dynamics and rider control. *Vehicle System Dynamics*, 51(7):1059–1090.
- Schwab, A. L., Meijaard, J. P., and Kooijman, J. D. G. (2012). Lateral dynamics of a bicycle with a passive rider model: stability and controllability. *Vehicle System Dynamics*, 50(8):1209–1224.

- Shampine, L. F. and Gordon, M. K. (1975). *Computer solution of ordinary differential equations: the initial value problem*, volume 85. WH Freeman San Francisco.
- Sharp, R. and Limebeer, D. (2004). On steering wobble oscillations of motorcycles. *Proceedings of the Institution of Mechanical Engineers, Part C: Journal of Mechanical Engineering Science*, 218(12):1449–1456.
- Sharp, R. S. (2008). On the stability and control of the bicycle. *Applied Mechanics Reviews*, 61(6):060803.
- Stewart, J. (2003). *Calculus: Early Transcendentals*. Thomson Learning, 5e edition.
- Ting, L. H., Kautz, S. A., Brown, D. A., and Zajac, F. E. (1999). *Phase Reversal of Biomechanical Functions and Muscle Activity in Backward Pedaling*, volume 81.
- van der Helm, F. C. T., Schouten, A. C., de Vlugt, E., and Brouwn, G. G. (2002). Identification of intrinsic and reflexive components of human arm dynamics during postural control. *Journal of Neuroscience Methods*, 119(1):1–14.
- van Soest, A. J. and Casius, L. J. (2000). Which factors determine the optimal pedaling rate in sprint cycling? *Medicine and Science in Sports and Exercise*, 32(11):1927–1934.
- van Soest, A. J., Schwab, A. L., Bobbert, M. F., and van Ingen Schenau, G. J. (1992). Spacar: A software subroutine package for simulation of the behavior of biomechanical systems. *Journal of Biomechanics*, 25(10):1219–1226.
- VeiligheidNL (2014). Fietsongevallen - ongevals cijfers. Technical report, VeiligheidNL.
- Vlakveld, W. P., Twisk, D., Christoph, M., Boele, M., Sikkema, R., Remy, R., and Schwab, A. L. (2015). Speed choice and mental workload of elderly cyclists on e-bikes in simple and complex traffic situations: A field experiment. *Accident Analysis & Prevention*, 74:97–106.
- Whipple, F. J. (1899). The stability of the motion of a bicycle. *Quarterly Journal of Pure and Applied Mathematics*, 30(120):312–321.
- Wilson, D. G. (2004). *Bicycling science*. MIT press.
- Winter, D. (1990). *Biomechanics and motor control of human movement*. Wiley, New York.

List of Symbols

Roman symbols - lower case

f	generalised external force vector
q	generalised coordinates
q_h	homogeneous solution
q_p	particular solution
c	trail
f	frequency
f_s	sampling frequency
g	gravitational acceleration
l	length
m	mass
n	number of
r	radius
t	time
v	forward speed
w	wheel base
x	forward direction
y	lateral direction, right
z	vertical direction, down

Roman symbols - upper case

C	damping matrix
F	Cartesian external force vector
I	inertia tensor
K	stiffness matrix
M	mass matrix
R	rotation matrix
H	Hanning window
L	angular momentum
N	number of samples
O	origin
P	power
T	length time series

T	torque
W	work
CF	city bicycle flexed arms
CR	city bicycle rigid upper body
HR	hybrid bicycle rigid upper body
HS	hybrid bicycle straight arms
C	saddle point
P	rear wheel contact point
Q	front wheel contact point

Greek symbols

δ	steering angle
λ	eigenvalue
λ_s	tilt steering axis
ω	cadence
ϕ	roll
ψ	yaw
θ	pitch
δ	virtual/variation
φ	angle in complex plane
ξ	eigenmode

Subscripts

l_{hh}	hip to hip length
x_{\max}	maximum
x_{\tan}	tangential
x_A	crank axis
x_{cr}	crank
x_{le}	left
x_{ll}	lower leg
x_L	leg
x_{ri}	right
x_{ul}	upper leg

A Research questions

What is the influence of the riders propulsive pedalling action on the dynamic behaviour and control of the total bicycle-rider system? This main research question can be divided into smaller subquestions in order to be able to further define the focus of this research. The subquestions are briefly discussed with attention to what kind of approach would suit the question best. Here there are three main subdivisions for the approaches of interest, namely **experimental**, **dynamical modelling** and **biomechanical modelling**, which also takes the human physiology (e.g. musculoskeletal geometry, muscle characteristics and properties) into account. The focus of this research lies with the first subquestion: 'What is the effect of pedalling on the lateral dynamic bicycle behaviour assuming an uncontrolled system?'. Finally this research will touch upon the third subquestion: 'What is the function of the rider's upper body movements during cycling?'

1. 'What is the effect of pedalling on the lateral dynamic bicycle behaviour assuming an uncontrolled system?'

In order to better understand what system the human has to control, the dynamic behaviour of the bicycle including a pedal disturbance (moving leg masses) needs to be investigated. Herein we are interested in what the influence is of this disturbance when there is no control present. Since the exclusion of control would pose a great challenge in implementation and safety for an experimental approach, a **dynamic modelling** approach is better suited to the answer this question. The dynamic behaviour of a bicycle, for instance the benchmarked Whipple bicycle (Meijaard et al., 2007) with rigid rider or even a passive rider (Schwab et al., 2012), could be investigated when applying a suitable disturbance.

- (a) 'What is the disturbance associated with pedalling?'

This subquestion is discussed in detail in Section 2

- (b) 'What is the direct effect of the pedalling disturbance on the lateral dynamics of a bicycle-rider system?'

This subquestion is discussed in detail in Section 3

- (c) 'What is the nature of the coupling between steering and pedalling?'

Moore et al. (2011) shows a high steering angle amplitude at the pedal frequency. Is this high steering angle amplitude at pedal cadence a direct result of the disturbance, a result of control action or a combination of both? Moore et al. (2011) characterises this high steering amplitude as a steering action, however this could be only part of the answer. If the steering amplitude is a direct result of the disturbance and coupling between roll and steering angle of the bicycle could be investigated using either a **experimental**, **dynamical modelling** or **biomechanical modelling** approach. It would be interesting to investigate if this steering amplitude is higher due to the extra control needed to compensate for the disturbance or if the steering angle amplitude would actually be higher due to the disturbance and it is lower due to the damping effect of the control action of the rider.

2. 'What is the function of the rider's upper body movements during cycling?'

Experimental research shows that upper body movements are more prominent when the bicycle rider pedals compared to when the bicycle is towed Moore et al. (2011). The trunk of the rider twists, bends forward and sideways and leans laterally with a frequency coupled to the pedalling cadence. The function of these movements are not fully understood. An insight to the possible function could be made by investigating different aspects and possibilities associated with the upper body movements.

- (a) 'Do the upper body movements add to or compensate for the leg disturbance?'

Using a **dynamic model** it could be investigated what upper body movements would in fact compensate for the disturbance, possibly through some kind of optimization method. The feasibility of these resulting upper body movements could be tested either by the use of a biomechanical model or compared to **experimental** measurements.

Alternatively the upper body movements during pedalling could be recorded primarily using **experimental** approach. A **dynamic model** could be used to investigate the behaviour of the

bicycle (similar to subquestion 1) with and without the addition of upper body movements in order to compare the behaviour with and without the seen upper body movements.

- (b) *'How does the task of balancing the bicycle influence the upper body movements associated with pedalling?'*

In order to better understand the function of the upper body movements it would be interesting to see if the upper body movements are connected to the balancing task. For instance using an **experimental** approach the upper body movements could be observed by comparing normal cycling to cycling on a stationary bicycle.

- (c) *'Are the upper body movements directly coupled to the leg movements?'*

In order to better understand the upper body movements it would be interesting to investigate the **biomechanical** coupling between the pedalling leg movements and upper body movements. Possibly the functioning and structure of the musculoskeletal system contributes to this coupling. It is plausible that the pelvis (or maybe even the spine) also moves or rotates as a direct result of the active muscle contractions and inertial forces associated with pedalling. A three dimensional musculoskeletal model including the legs and the trunk could be used to investigate the passive effect of the pedalling action on the trunk movements.

- (d) *'Could the upper body movements be aiding the pedalling performance?'*

Besides passive upper body movements as discussed in subquestion 2c it could also be that the rider actively moves their upper body in order to aid the pedalling performance. It could be that the rider changes its upper body posture or moves their upper body forwards and backwards in order to optimize the muscle length of a muscle spanning the hip joint according to its force-length or force-velocity relationship. The rider could also possibly rotate their pelvis in order to assist in lifting their leg. These possibilities of active upper body movements in order to increase cycling performance could be investigated using a **biomechanical modelling** approach as in subquestion 2c, or an **experimental** approach could also be applied. A rider's performance could be measured and compared where for instance some upper body movements are restricted or in fact encouraged.

3. *'What is the function of the lateral knee movements and why are they typically seen in very low speeds?'*

Lateral knee movements are observed in low speeds of 5 km/h and below and Moore et al. (2011) proposed that it could possibly be used as a low speed bicycle stabilization action. An interesting observation is that if the bicycle rider does not pedal, but the bicycle is towed, the increasing lateral knee movements for lower forward speeds is not observed. It is not clear however what conclusions can be drawn from these observations due to the low number of subjects and observations in this study. It would be interesting to investigate the functionality of this lateral knee movement for low speed stabilization and cornering.

- (a) *'Is there a coupling between lateral knee movements and pedalling?'*

In a larger scale **experimental** study it could be investigated if there is a true difference in lateral knee movements when the bicycle rider does or does not pedal. Also the general behaviour with respect to forward speed or disturbances could possibly be identified in more detail.

- (b) *'How are lateral knee movements used in cornering?'*

It has been observed, in a casual setting, that the knees sometimes move lateral during cornering, especially if the speed is high or the corner is tight. It would be interesting to determine the prevalence of these lateral knee movements during cornering in an **experimental** study. Here it would be interesting to investigate what aspects such as speed and cornering angle and duration influence the behaviour.

Using a **dynamical modelling** approach functionality of lateral knee movements during cornering could be investigated. Here the forces during a steady turn could be investigated, where the influence of the lateral knee or upper body movement (both shift the center of gravity) are of interest.

- (c) *'What is the controllability for lateral knee movement and how does this change with forward speed?'*

It would be interesting to see if the bicycle could theoretical be controlled using only lateral knee movements using a **dynamical modelling** approach. It would also be interesting how the controllability changes with forward speed. Possibly the modal controllability could be used to give a measure of the effectiveness or difficulty of the control action as done for the steering action and body lean action in combination of a passive rider in Schwab et al. (2012).

4. *'How does pedalling influence the bicycle rider's choice between different control actions?'*

Research has shown that the bicycle is controllable using different (combination of) control actions. It is not fully understood how the bicycle rider chooses between the different possibilities. Investigating the characteristics and capabilities of the different possible actions, could possibly shed some light on how the rider chooses to control the bicycle. Subsequently the influence of the pedalling disturbance could be investigated.

(a) *'How does dynamical controllability compare for the lateral knee movement, the body lean action and/or the steering action?'*

The controllability of the control actions as for the lateral knee movement discussed in subquestion 3c could be investigated using a **dynamical modelling** approach. Where the modal controllability could be investigated as function of forward speed in order to give an indication if the choice between control actions would likely depend on forward speed or not.

(b) *'In what way do the physiological capabilities effect controllability for the lateral knee movement, the body lean action and/or the steering action?'*

It is likely that physiological capabilities such as delay in reaction time due to neuromuscular properties is different for the various control actions. Therefore it would be interesting to use a **biomechanical modelling** approach in order to define the limitations and capabilities of the control actions and investigate the influence on the controllability.

(c) *'How does the control effort compare for the lateral knee movement, the body lean action and/or the steering action?'*

It is thought that human are inherently lazy and that humans in some way try to optimize their control effort when there are multiple control methods possible. What this control effort is, could be defined in several ways. It would be interesting to apply different definitions of control effort and investigate the differences between control actions. Depending on the definitions of control effort used, a **biomechanical** and/or **dynamical modelling** approach would be applicable.

(d) *'How does the pedalling disturbance influence the control effort compared for the lateral knee movement, the body lean action and/or the steering action?'*

It would be interesting to in some way quantify the control effort needed to control the pedalling disturbance. The influence of cadence on the control effort would be an interesting aspect of the pedalling disturbance. Similar to subquestion 4c depending on the definitions of control effort used, a **biomechanical** and/or **dynamical modelling** approach would be applicable.

B Model details

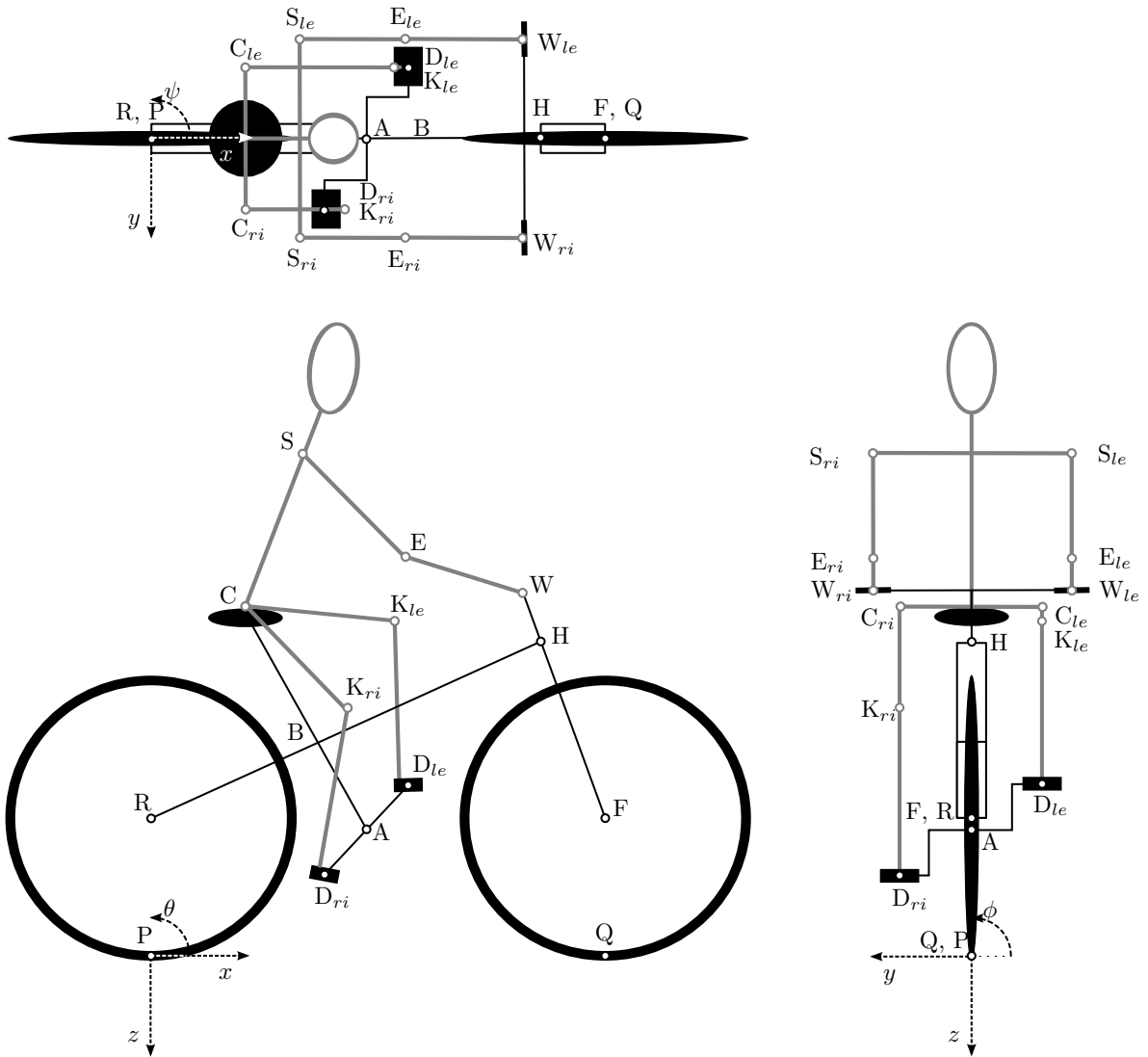


Figure B.1: Pedal disturbance visualized in a top, side and front view bicycle-rider schematic (transverse, sagittal and frontal plane). Showing names of segments and hinges

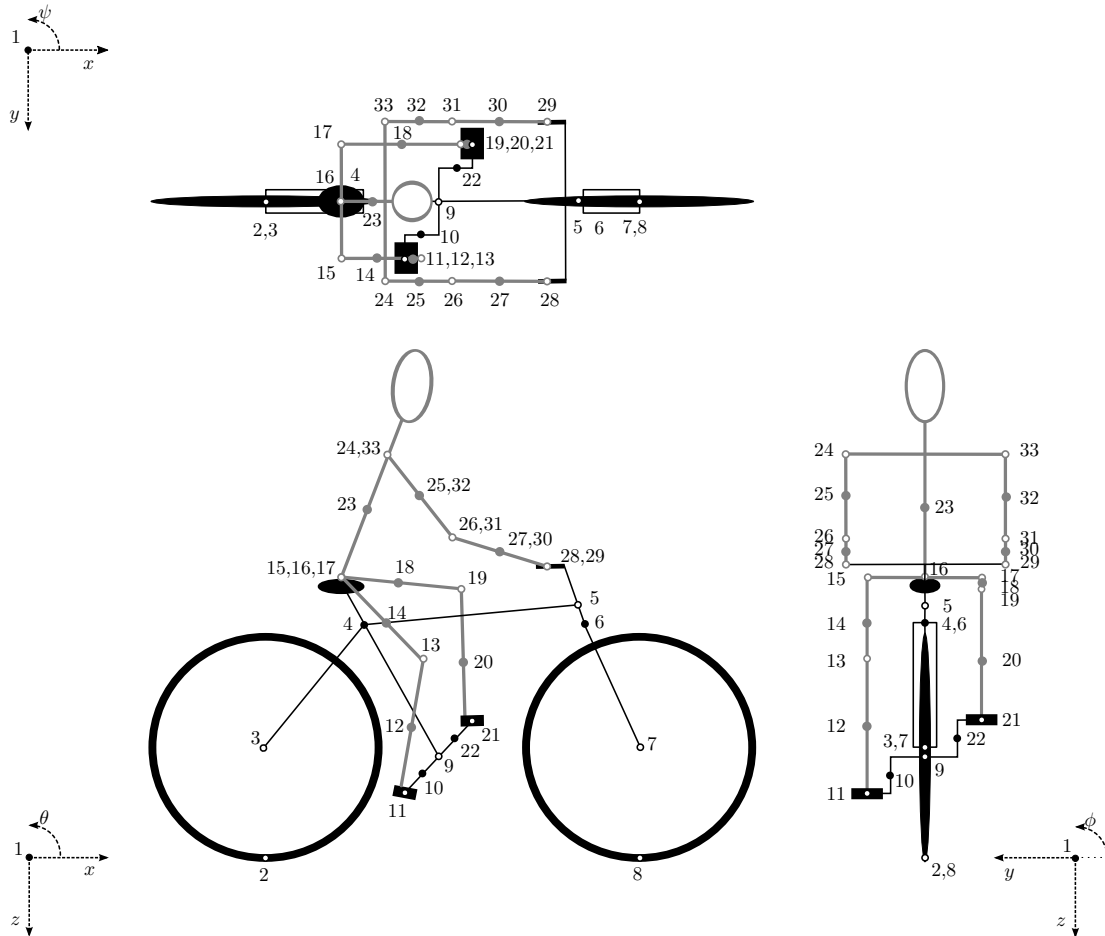


Figure B.2: SPACAR model visualized in a top, side and front view bicycle-rider schematic (transverse, sagittal and frontal plane). Showing position node numbers.

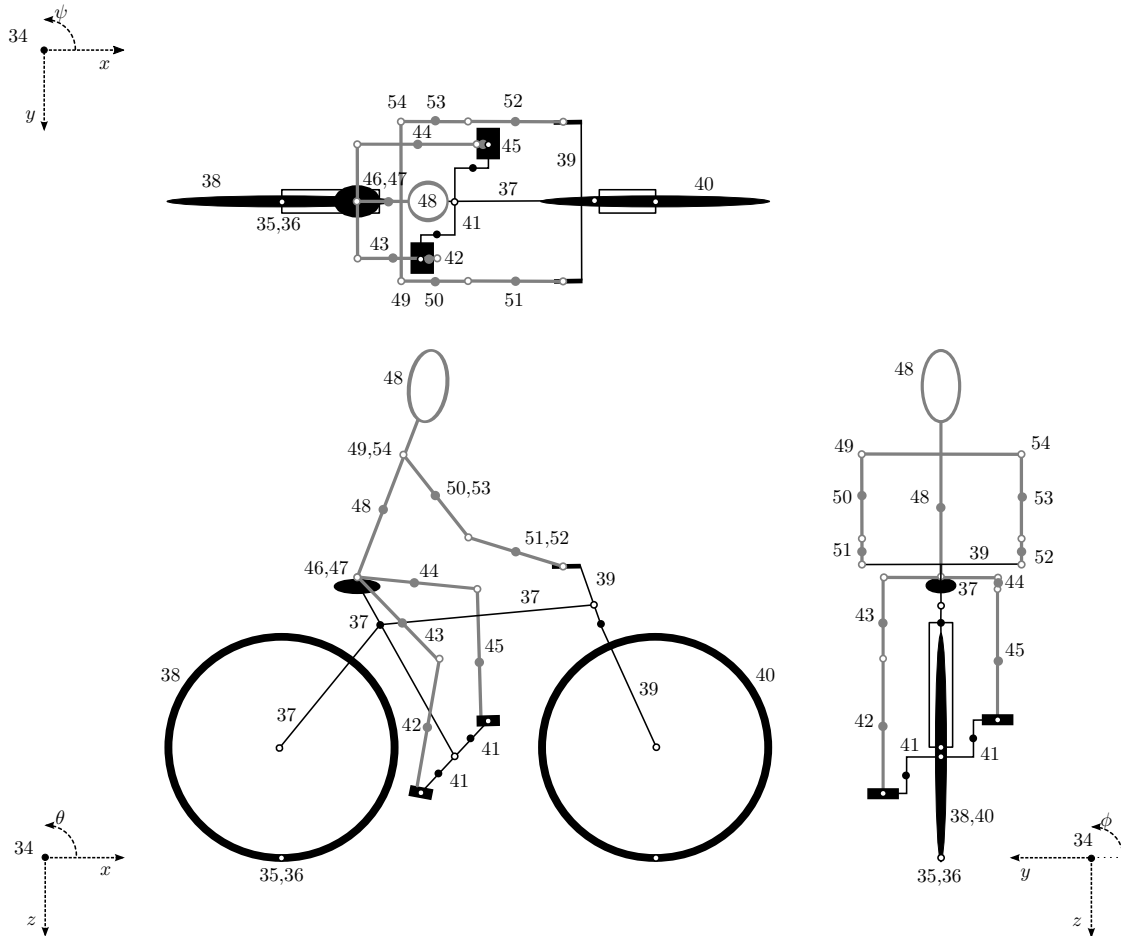


Figure B.3: SPACAR model visualized in a top, side and front view bicycle-rider schematic (transverse, sagittal and frontal plane). Showing rotation node numbers.

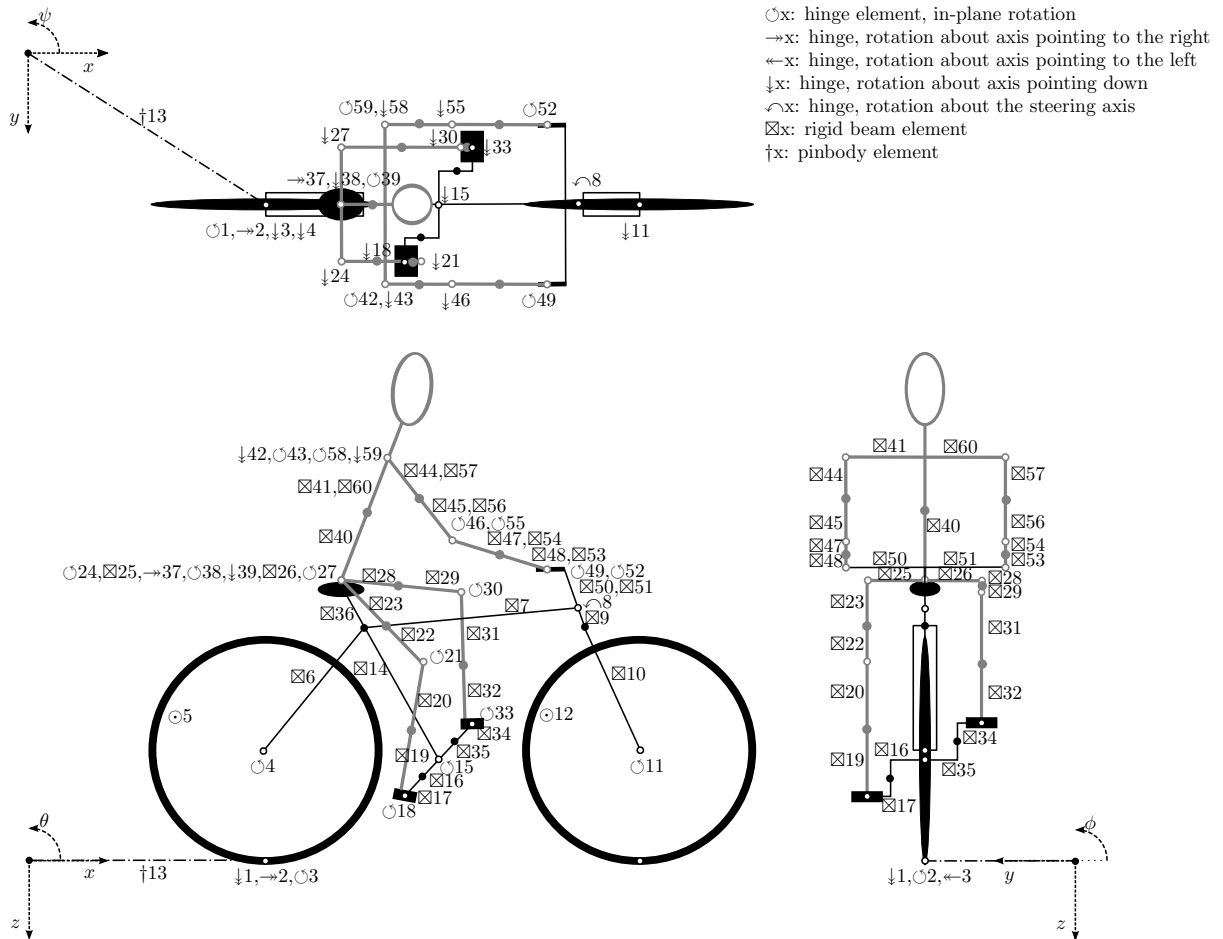


Figure B.4: SPACAR model visualized in a top, side and front view bicycle-rider schematic (transverse, sagittal and frontal plane). Showing element types and numbers.

The linearised matrices for the models corresponding to Figure 3.4.

$$\mathbf{M} \ddot{\mathbf{q}} + v\mathbf{C}_1 \dot{\mathbf{q}} + [g\mathbf{K}_0 + (v)^2\mathbf{K}_2] \mathbf{q} = \mathbf{f} \quad (\text{B.1})$$

HS:

$$\mathbf{M} = \begin{bmatrix} 87.931877425895138 & 2.339616241384371 \\ 2.339616241384371 & 0.664093946360865 \end{bmatrix} \quad (\text{B.2})$$

$$\mathbf{C}_1 = \begin{bmatrix} -0.000000000000018 & 39.121565684630056 \\ -0.489133134732113 & 2.287316991742449 \end{bmatrix} \quad (\text{B.3})$$

$$\mathbf{K}_0 = \begin{bmatrix} -82.272183512820732 & -2.650322167629509 \\ -2.650322167629510 & -0.963344735400068 \end{bmatrix} \quad (\text{B.4})$$

$$\mathbf{K}_2 = \begin{bmatrix} 0.000000000000038 & 76.757780481550242 \\ 0.000000000000002 & 2.569130724497826 \end{bmatrix} \quad (\text{B.5})$$

CF:

$$\mathbf{M} = \begin{bmatrix} 95.989132934397517 & 1.310942631998618 \\ 1.310942631998618 & 0.445163608549845 \end{bmatrix} \quad (\text{B.6})$$

$$\mathbf{C}_1 = \begin{bmatrix} 0.000000000000003 & 26.747934019121921 \\ -0.449732670994970 & 1.123255142283839 \end{bmatrix} \quad (\text{B.7})$$

$$\mathbf{K}_0 = \begin{bmatrix} -86.484757626024262 & -1.533471132193380 \\ -1.533471132193379 & -0.159421991189502 \end{bmatrix} \quad (\text{B.8})$$

$$\mathbf{K}_2 = \begin{bmatrix} -0.000000000000038 & 71.793424399431728 \\ -0.000000000000001 & 1.398999802577024 \end{bmatrix} \quad (\text{B.9})$$

HR:

$$\mathbf{M} = \begin{bmatrix} 86.372365648886202 & 2.090336681637755 \\ 2.090336681637755 & 0.280347822207299 \end{bmatrix} \quad (\text{B.10})$$

$$\mathbf{C}_1 = \begin{bmatrix} -0.000000000000010 & 37.598475969351171 \\ -0.489133134732113 & 1.607271698865928 \end{bmatrix} \quad (\text{B.11})$$

$$\mathbf{K}_0 = \begin{bmatrix} -81.445637690855648 & -2.341783931373640 \\ -2.341783931373640 & -0.680761725783457 \end{bmatrix} \quad (\text{B.12})$$

$$\mathbf{K}_2 = \begin{bmatrix} -0.000000000000076 & 75.995147626871145 \\ 0 & 2.284450323677391 \end{bmatrix} \quad (\text{B.13})$$

CR

$$\mathbf{M} = \begin{bmatrix} 94.775551048722065 & 1.544632245453181 \\ 1.544632245453181 & 0.251156295922915 \end{bmatrix} \quad (\text{B.14})$$

$$\mathbf{C}_1 = \begin{bmatrix} -0.000000000000017 & 26.322539639992179 \\ -0.449732670994970 & 1.072143825122140 \end{bmatrix} \quad (\text{B.15})$$

$$\mathbf{K}_0 = \begin{bmatrix} -85.851035901776569 & -1.801203353821006 \\ -1.801203353821006 & -0.700891364044618 \end{bmatrix} \quad (\text{B.16})$$

$$\mathbf{K}_2 = \begin{bmatrix} -0.000000000000038 & 71.272661505973232 \\ 0 & 1.619009628770652 \end{bmatrix} \quad (\text{B.17})$$

B.1 Extra derivations: Leg Kinematics

Section 2.1.1 describes the kinematic model for the legs associated with the pedal action disturbance. Here the segment COM positions are given as a function of pitch angles corresponding to Figure 2.1.

$$\mathbf{x}_{ricr} = \mathbf{x}_A + \begin{bmatrix} \frac{1}{2}l_{cr} \cos(\dot{\theta}_A t) \\ \frac{1}{4}l_{hh} \\ -\frac{1}{2}l_{cr} \sin(\dot{\theta}_A t) \end{bmatrix} \quad (\text{B.18})$$

$$\mathbf{x}_{rill} = \mathbf{x}_A + \begin{bmatrix} l_{cr} \cos(\dot{\theta}_A t) \\ \frac{1}{2}l_{hh} \\ -l_{cr} \sin(\dot{\theta}_A t) \end{bmatrix} + \begin{bmatrix} \frac{1}{2}l_{ll} \cos(\theta_{rill}) \\ 0 \\ -\frac{1}{2}l_{ll} \sin(\theta_{rill}) \end{bmatrix} \quad (\text{B.19})$$

$$\mathbf{x}_{riul} = \mathbf{x}_A + \begin{bmatrix} l_{cr} \cos(\dot{\theta}_A t) \\ \frac{1}{2}l_{hh} \\ -l_{cr} \sin(\dot{\theta}_A t) \end{bmatrix} + \begin{bmatrix} l_{ll} \cos(\theta_{rill}) \\ 0 \\ -l_{ll} \sin(\theta_{rill}) \end{bmatrix} + \begin{bmatrix} \frac{1}{2}l_{ul} \cos(\theta_{riul}) \\ 0 \\ -\frac{1}{2}l_{ul} \sin(\theta_{riul}) \end{bmatrix} \quad (\text{B.20})$$

$$\mathbf{x}_{lecr} = \mathbf{x}_A + \begin{bmatrix} \frac{1}{2}l_{cr} \cos(\dot{\theta}_A t + \pi) \\ -\frac{1}{4}l_{hh} \\ -\frac{1}{2}l_{cr} \sin(\dot{\theta}_A t + \pi) \end{bmatrix} \quad (\text{B.21})$$

$$\mathbf{x}_{lell} = \mathbf{x}_A + \begin{bmatrix} l_{cr} \cos(\dot{\theta}_A t + \pi) \\ -\frac{1}{2}l_{hh} \\ -l_{cr} \sin(\dot{\theta}_A t + \pi) \end{bmatrix} + \begin{bmatrix} \frac{1}{2}l_{ll} \cos(\theta_{lell}) \\ 0 \\ -\frac{1}{2}l_{ll} \sin(\theta_{lell}) \end{bmatrix} \quad (\text{B.22})$$

$$\mathbf{x}_{leul} = \mathbf{x}_A + \begin{bmatrix} l_{cr} \cos(\dot{\theta}_A t + \pi) \\ -\frac{1}{2}l_{hh} \\ -l_{cr} \sin(\dot{\theta}_A t + \pi) \end{bmatrix} + \begin{bmatrix} l_{ll} \cos(\theta_{lell}) \\ 0 \\ -l_{ll} \sin(\theta_{lell}) \end{bmatrix} + \begin{bmatrix} \frac{1}{2}l_{ul} \cos(\theta_{leul}) \\ 0 \\ -\frac{1}{2}l_{ul} \sin(\theta_{leul}) \end{bmatrix} \quad (\text{B.23})$$

B.2 Extra derivations: 'd Alembert Forces

Here extra derivation are shown in order to understand why the odd multiples of the cadence frequency ($n\omega$) disappear in the 'd Alembert forces associated with the acceleration of both the leg masses.

$$\mathbf{F}_L = \sum_{n=1}^{\infty} m_L |\mathbf{X}_L(n\omega)| (n\omega)^2 (\cos(n\omega t + (\varphi_{\mathbf{X}_L(n\omega)})^T) + \cos(n\omega(t + \pi/\omega) + (\varphi_{\mathbf{X}_L(n\omega)})^T)) \quad (\text{B.24})$$

$$\mathbf{F}_L = \sum_{n=1}^{\infty} m_L |\mathbf{X}_L(n\omega)| (n\omega)^2 (\cos(n\omega t + (\varphi_{\mathbf{X}_L(n\omega)})^T) + \cos(n\omega t + n\pi + (\varphi_{\mathbf{X}_L(n\omega)})^T)) \quad (\text{B.25})$$

$$\begin{aligned} \mathbf{F}_L &= \sum_{n=1,3,5,\dots}^{\infty} m_L |\mathbf{X}_L(n\omega)| (n\omega)^2 (\cos(n\omega t + (\varphi_{\mathbf{X}_L(n\omega)})^T) + \cos(n\omega t + n\pi + (\varphi_{\mathbf{X}_L(n\omega)})^T)) + \dots \\ &\quad \sum_{n=2,4,6,\dots}^{\infty} m_L |\mathbf{X}_L(n\omega)| (n\omega)^2 (\cos(n\omega t + (\varphi_{\mathbf{X}_L(n\omega)})^T) + \cos(n\omega t + n\pi + (\varphi_{\mathbf{X}_L(n\omega)})^T)) \end{aligned} \quad (\text{B.26})$$

$$\begin{aligned} \mathbf{F}_L &= \sum_{n=1,3,5,\dots}^{\infty} m_L |\mathbf{X}_L(n\omega)| (n\omega)^2 (\cos(n\omega t + (\varphi_{\mathbf{X}_L(n\omega)})^T) - \cos(n\omega t + (\varphi_{\mathbf{X}_L(n\omega)})^T)) + \dots \\ &\quad \sum_{n=2,4,6,\dots}^{\infty} m_L |\mathbf{X}_L(n\omega)| (n\omega)^2 (\cos(n\omega t + (\varphi_{\mathbf{X}_L(n\omega)})^T) + \cos(n\omega t + (\varphi_{\mathbf{X}_L(n\omega)})^T)) \end{aligned} \quad (\text{B.27})$$

$$\mathbf{F}_L = \sum_{n=2,4,6,\dots}^{\infty} m_L |\mathbf{X}_L(n\omega)| (n\omega)^2 2 \cos(n\omega t + (\varphi_{\mathbf{X}_L(n\omega)})^T) \quad (\text{B.28})$$

where $|\mathbf{X}_L(n\omega)| = \begin{bmatrix} |X_L(n\omega)| \\ |Y_L(n\omega)| \\ |Z_L(n\omega)| \end{bmatrix}$ and $(\varphi_{\mathbf{X}_L(n\omega)})^T = [\varphi_{X_L(n\omega)} \quad \varphi_{Y_L(n\omega)} \quad \varphi_{Z_L(n\omega)}]$, where $\mathbf{X}_L(n\omega)$ is the frequency domain of the leg centre of mass position as a function of time $\mathbf{x}_L(t)$ at the n multiple of the

cadence ω . Numerical values for the corresponding amplitudes and angles can be found in Table D.1. The same principle is applied to the pitch torque T_{y_L} :

$$T_{y_L} = - \left(-x_L(t)m_L\ddot{z}_L(t) + z_L(t)m_L\ddot{x}(t) - x_L(t + \pi/\omega)m_L\ddot{z}_L(t + \pi/\omega) + z_L(t + \pi/\omega)m_L\ddot{x}(t + \pi/\omega) + \dots \right. \\ \left. I_{ul}\ddot{\theta}_{ul}(t) + I_{ll}\ddot{\theta}_{ll}(t) + I_{cr}\ddot{\theta}_{cr}(t) + I_{ul}\ddot{\theta}_{ul}(t + \pi/\omega) + I_{ll}\ddot{\theta}_{ll}(t + \pi/\omega) \right) \quad (\text{B.29})$$

$$T_{y_L} = \sum_{n=1}^{\infty} m_L \left(Z_L(0) - X_L(0) \right) |X_L(n\omega)| |Z_L(n\omega)| (n\omega)^2 \left(\cos(n\omega t + \varphi_{X_L(n\omega)}) \cos(n\omega t + \varphi_{Z_L(n\omega)}) + \dots \right. \\ \left. \cos(n\omega t + \pi + \varphi_{X_L(n\omega)}) \cos(n\omega t + \pi + \varphi_{Z_L(n\omega)}) \right) + \dots \\ I_{ul} |\Theta_{ul}(n\omega)| (n\omega)^2 (\cos(n\omega t + \varphi_{\Theta_{ul}(n\omega)}) + \cos(n\omega t + \pi + \varphi_{\Theta_{ul}(n\omega)})) + \dots \\ I_{ll} |\Theta_{ll}(n\omega)| (n\omega)^2 (\cos(n\omega t + \varphi_{\Theta_{ll}(n\omega)}) + \cos(n\omega t + \pi + \varphi_{\Theta_{ll}(n\omega)})) \quad (\text{B.30})$$

$$T_{y_L} = \sum_{n=2,4,6,\dots}^{\infty} m_L \left(Z_L(0) - X_L(0) \right) |X_L(n\omega)| |Z_L(n\omega)| (n\omega)^2 2 \cos(n\omega t + \varphi_{X_L(n\omega)}) \cos(n\omega t + \varphi_{Z_L(n\omega)}) + \dots \\ I_{ul} |\Theta_{ul}(n\omega)| (n\omega)^2 2 \cos(n\omega t + \varphi_{\Theta_{ul}(n\omega)}) + I_{ll} |\Theta_{ll}(n\omega)| (n\omega)^2 2 \cos(n\omega t + \varphi_{\Theta_{ll}(n\omega)}) \quad (\text{B.31})$$

where $X_L(0)$ is the same as the average leg position $\overline{x(t)}$.

C Measurement details

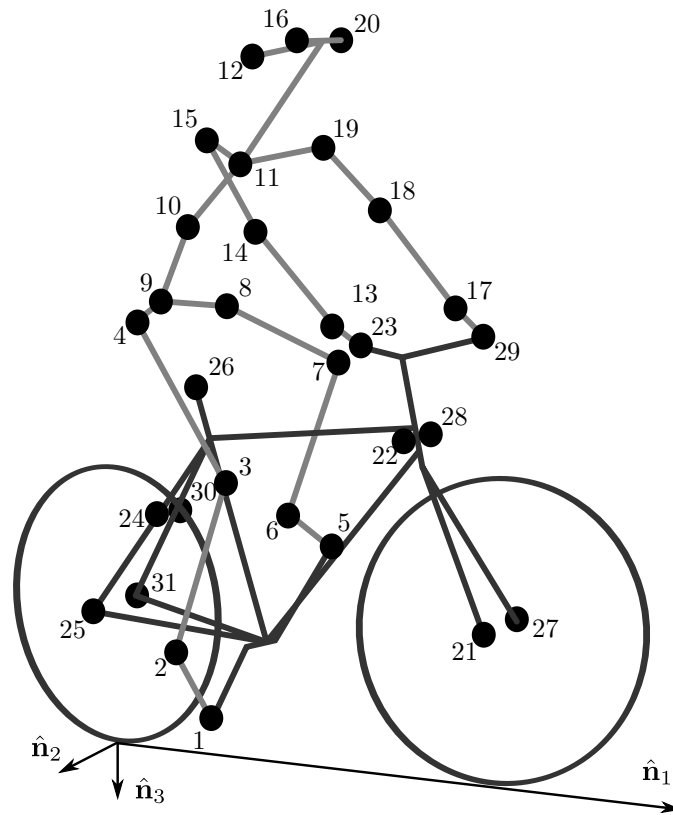


Figure C.1: Markers location corresponding to experimental data used for validation (Moore et al., 2011). The motion of the marker locations were captured using an Optotrak Certus motions capture system, which uses active marker tracking. A wide range of experimental conditions were tested.

D Extra Results: Leg Motion

Table D.1: Amplitude ([m]) and phase φ ([rad]) of the frequency domain of the leg movement \mathbf{X}_L in forward direction X_L and vertical down direction Z_L , for the cadence frequency ω and 5 multiples thereof, corresponding to four parameter sets. Hybrid bicycle corresponds to the Batavus Stratos seat tube angle ($\lambda_{st} = \frac{75^\circ}{180^\circ}\pi$ rad) and length ($l_{sp} + l_{st} = 0.675$ m); City bicycle corresponds to the Batavus Browser seat tube angle ($\lambda_{st} = \frac{68.5^\circ}{180^\circ}\pi$ rad) and length (was $l_{sp} + l_{st} = 0.77$ m however changed to 0.72 m to accommodate a full crank rotation) (Moore et al., 2009; Schwab et al., 2012). Leg and crank length was for all the models the same ($l_{ul} = l_{ll} = 0.46$ m, $l_{cr} = 0.17$ m), as was leg and crank mass ($m_{ul} = 0.1m_{Br} = 7.2$ kg, $m_{ll} = 0.061m_{Br} = 4.392$ kg, $m_{cr} = 0.2$ kg). Mass distribution was homogeneously distributed over the segment in the original model (O), in the (W) models the anthropomorphic (cadaveric study based) distribution was used, where the hip to upper leg COM length is $l_{hul} = 0.433l_{ul}$ and the knee to lower leg COM length is $l_{kll} = 0.606l_{ll}$.

	Hybrid bicycle (O)	Hybrid bicycle (W)	City bicycle (O)	City bicycle (W)
$ X_L(\omega) $	6.8259476656324e-02	6.7036764095302e-02	6.4252452341344e-02	6.2676121374346e-02
$ X_L(2\omega) $	3.4106520950128e-03	2.8528304119950e-03	6.5351118320257e-03	5.4662760260574e-03
$ X_L(3\omega) $	1.6700544798569e-03	1.3969124018222e-03	2.5420187189442e-03	2.1262644524396e-03
$ X_L(4\omega) $	9.4547451035010e-05	7.9083951155161e-05	4.5614432734313e-04	3.8154064766861e-04
$ X_L(5\omega) $	9.1430720645033e-05	7.6476970731822e-05	2.4366885388220e-04	2.0381613176774e-04
$ Z_L(\omega) $	1.0118961617754e-01	9.6237579627533e-02	1.0750314542041e-01	1.0187075009023e-01
$ Z_L(2\omega) $	1.0302033582842e-02	8.6171071958647e-03	9.9362312047217e-03	8.3111328191147e-03
$ Z_L(3\omega) $	1.1680883439239e-03	9.7704423043196e-04	1.1703737957297e-03	9.7895589020704e-04
$ Z_L(4\omega) $	3.3807744093797e-04	2.8278393053560e-04	3.8305693065541e-04	3.2040689899071e-04
$ Z_L(5\omega) $	5.3916956822366e-05	4.5098687834464e-05	9.5985359560070e-05	8.0286685722051e-05
$\varphi_{X_L(\omega)}$	6.6798096398621e-01	5.5571047853977e-01	8.1608359332365e-01	6.7468341457395e-01
$\varphi_{X_L(2\omega)}$	-4.1757205447342e-01	-4.1757205447342e-01	1.2492162245544e-01	1.2492162245544e-01
$\varphi_{X_L(3\omega)}$	-6.1095270756397e-01	-6.1095270756398e-01	-3.4987377096903e-01	-3.4987377096903e-01
$\varphi_{X_L(4\omega)}$	2.3267791778159e+00	2.3267791778160e+00	-1.9408258800042e+00	-1.9408258800042e+00
$\varphi_{X_L(5\omega)}$	3.0213870394282e+00	3.0213870394286e+00	-2.8352403356811e+00	-2.8352403356812e+00
$\varphi_{Z_L(\omega)}$	-1.8870790488577e+00	-1.8478804871292e+00	-1.7520992633349e+00	-1.7306357905351e+00
$\varphi_{Z_L(2\omega)}$	-1.0994568367078e+00	-1.0994568367078e+00	-1.0318955251126e+00	-1.0318955251126e+00
$\varphi_{Z_L(3\omega)}$	1.1722573093763e+00	1.1722573093763e+00	2.1449382600272e+00	2.1449382600272e+00
$\varphi_{Z_L(4\omega)}$	2.6395106431901e+00	2.6395106431900e+00	2.6071534948521e+00	2.6071534948521e+00
$\varphi_{Z_L(5\omega)}$	-1.3660176668061e+00	-1.3660176668067e+00	2.9950547344237e-01	2.9950547344252e-01

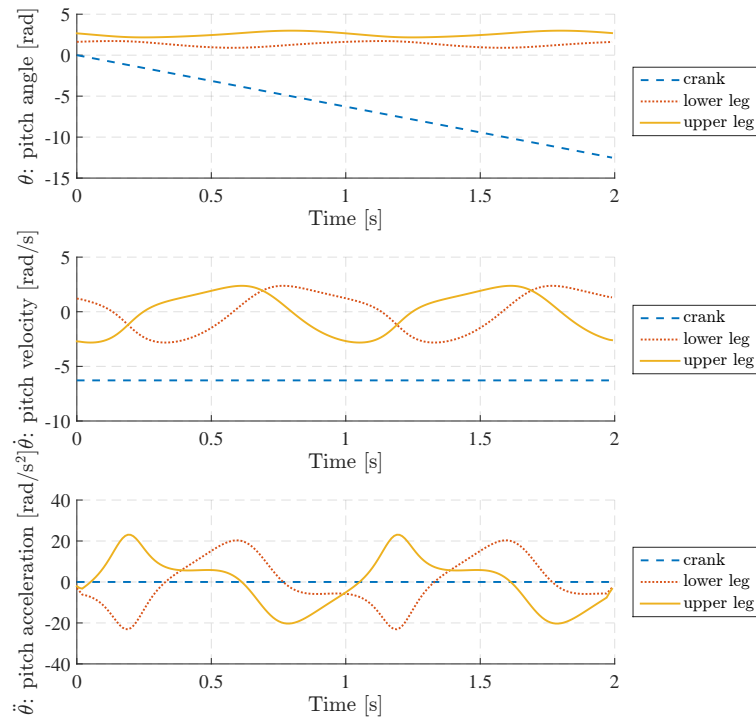


Figure D.1: Pitch angle, angular velocity and angular acceleration for the crank the lower leg and the upper leg, for a cadence of 60 rpm ($= 2\pi$ rad/s)

E Extra Results: Eigenvalues Original Parameters Model CF

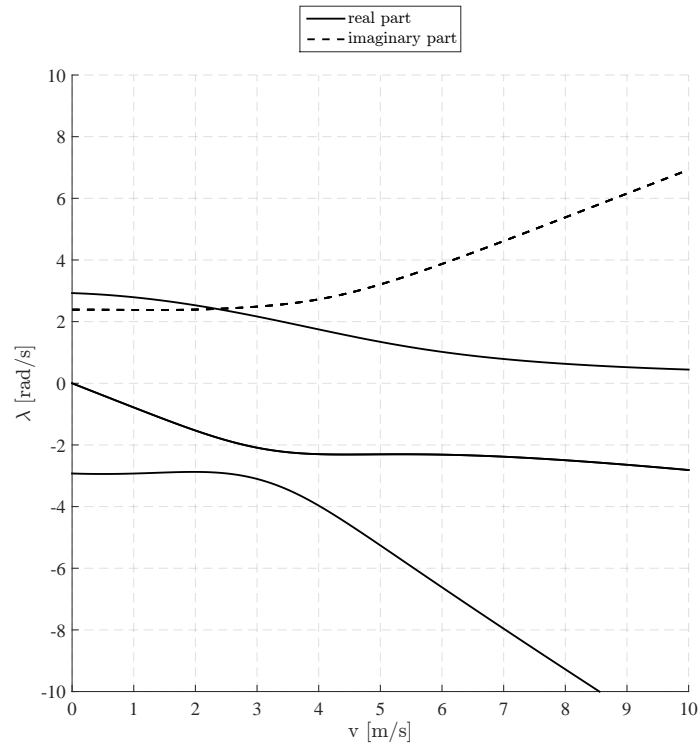


Figure E.1: Eigenvalues λ as a function of forward speed v of the linearised equation of motion for a bicyclist model CF, but then with original seat post length parameter. This change was necessary in our model, because the leg length and seat post length were inconsistent, meaning that the legs could not make a full pedal circle. The plot corresponds to Figure 5(b) in Schwab et al. (2012), since the only physical difference is the slight modification of the leg configuration.

F Extra Results: Neglected Momenta using Conservation of Angular Momentum Method

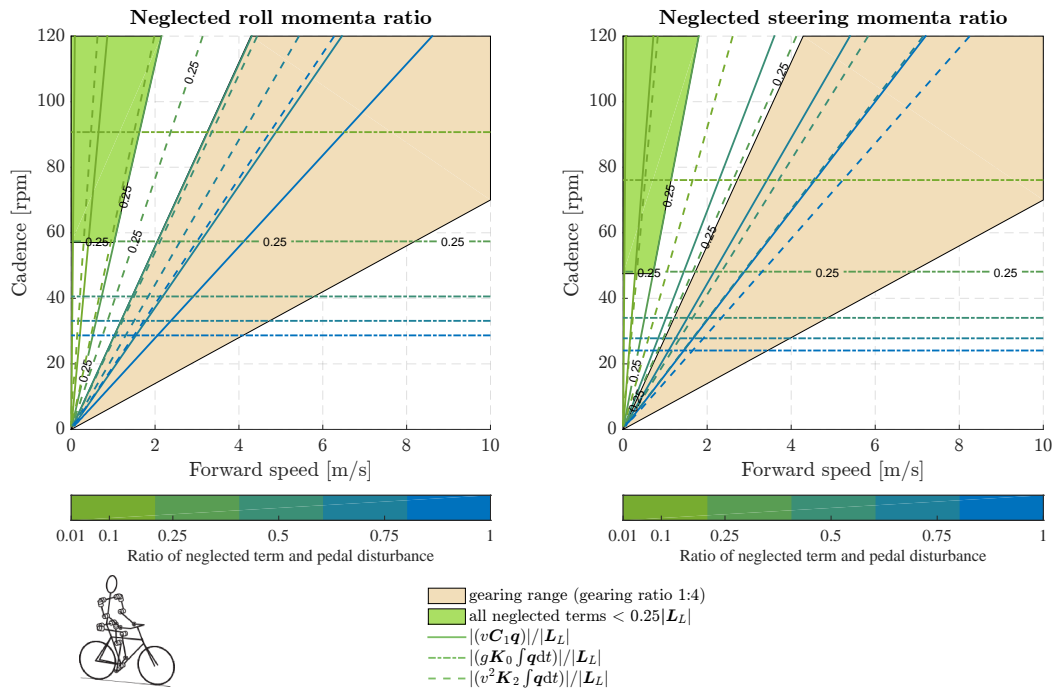


Figure F.1: Neglected momenta as a ratio of the pedalling disturbance momentum for a city bicycle (Batavus Browser) with flexed arms attached to the handlebars. The area where all the neglected momenta terms are less than a quarter of the pedalling disturbance momentum are filled in (top left corner). Also the gearing range is depicted indicating the possible cadence and forward speed combinations. This ranges from gearing ratio 1 till 4, equivalent to 1 till 4 times as many front sprocket teeth as rear sprocket teeth.

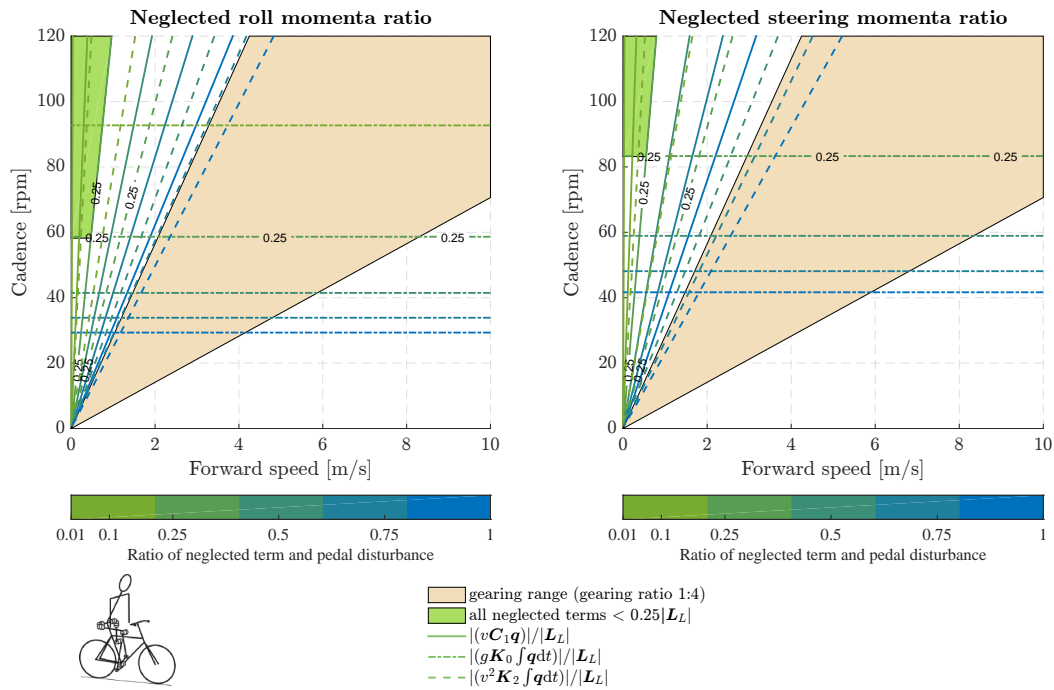


Figure F.2: Neglected momenta as a ratio of the pedalling disturbance momentum for the hybrid (Batavus Stratos) bicycle, with rigid rider. The area were all the neglected momenta terms are less than a quarter of the pedalling disturbance momentum are filled in (top left corner). Also the gearing range is depicted indicating the possible cadence and forward speed combinations. This ranges from gearing ratio 1 till 4, equivalent to 1 till 4 times as many front sprocket teeth as rear sprocket teeth.

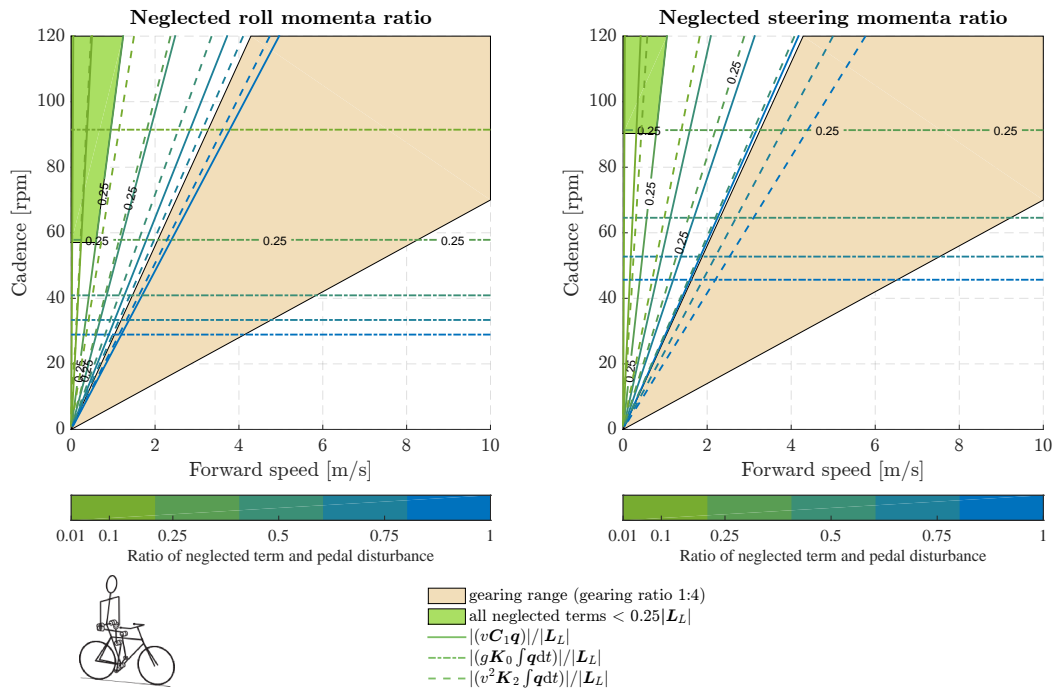


Figure F.3: Neglected momenta as a ratio of the pedalling disturbance momentum for the city (Batavus Browser) bicycle, with rigid rider. The area where all the neglected momenta terms are less than a quarter of the pedalling disturbance momentum are filled in (top left corner). Also the gearing range is depicted indicating the possible cadence and forward speed combinations. This ranges from gearing ratio 1 till 4, equivalent to 1 till 4 times as many front sprocket teeth as rear sprocket teeth.

G Extra Results: Time Solutions

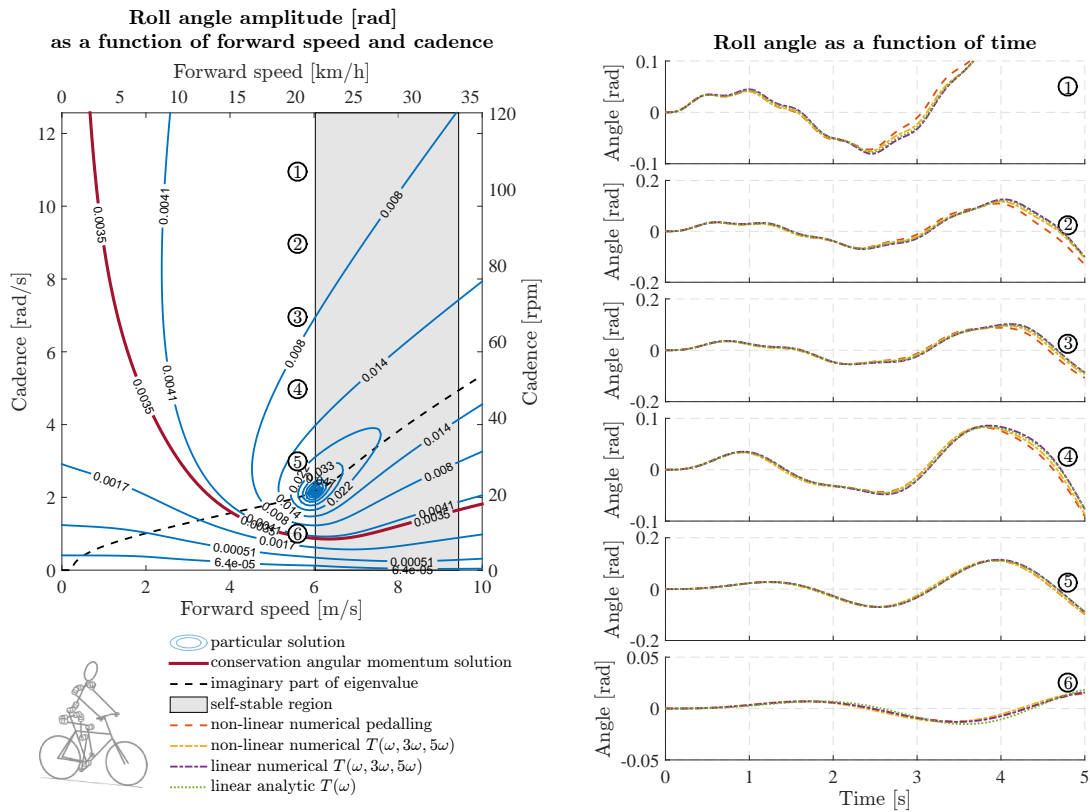


Figure G.1: Roll amplitude of the particular solution (left) and time solutions of other methods (right), for model HS shown bottom left in figure. The six numbers corresponding to the six plots on the right are indicated on the roll angle amplitude plot on the left, to indicate the speed-cadence combination belonging the time solution. The isoline corresponding to the amplitude of the conservation of angular momentum solution is shown in the particular solution contour plot on the left for comparison; the conservation of angular momentum solution itself is independent on forward speed and cadence. The imaginary part of the weave eigenvalue and the self-stable region is shown for reference. The particular solution left is the periodic cadence frequency component of the linear analytic time solution shown right, by definition. The linear and non-linear models are also solved using a multiple frequency torque disturbance. And the non-linear model is solved using prescribed leg motion as disturbance.

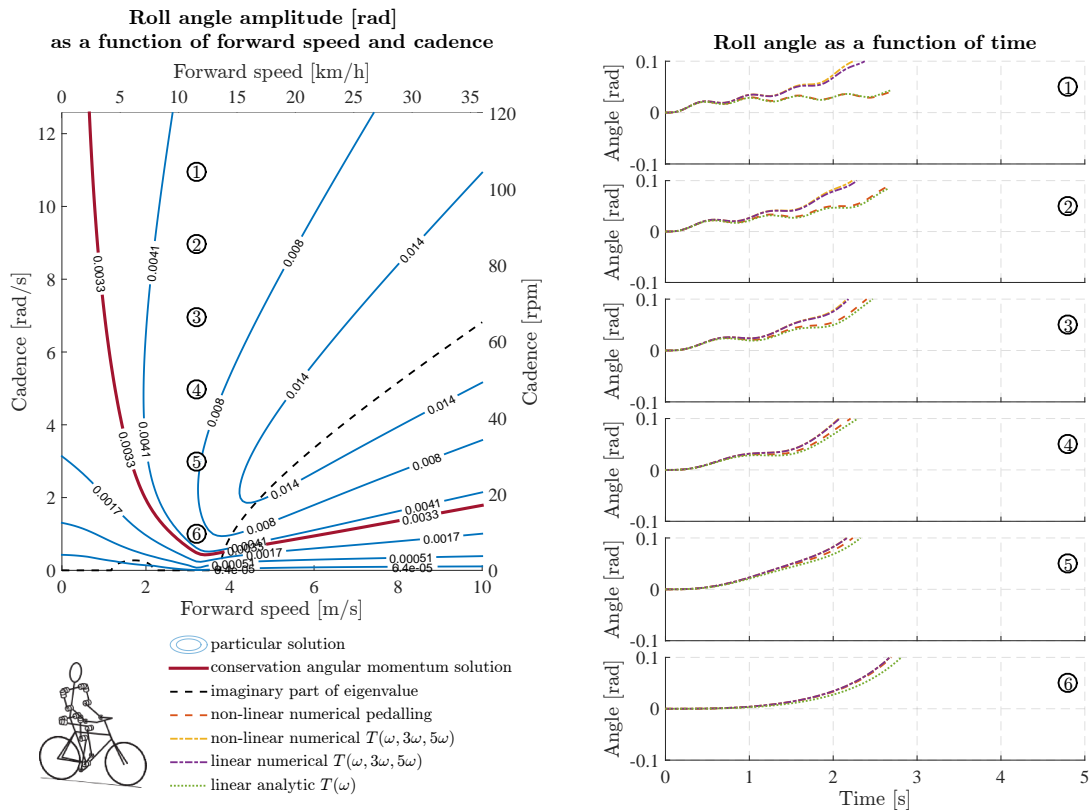


Figure G.2: Roll amplitude of the particular solution (left) and time solutions of other methods (right), for model CF shown bottom left in figure. There is no stable region, however the weave mode is stable from 3.2 m/s (real part of eigenvalue of weave mode is negative from 3.2 m/s). The imaginary part of the weave eigenvalue and is shown for reference. The six numbers corresponding to the six plots on the right are indicated on the roll angle amplitude plot on the left, to indicate the speed-cadence combination belonging the time solution. The isoline corresponding to the amplitude of the conservation of angular momentum solution is shown in the particular solution contour plot on the left for comparison; the conservation of angular momentum solution itself is independent on forward speed and cadence. The particular solution left is the periodic cadence frequency component of the linear analytic time solution shown right, by definition. The linear and non-linear models are also solved using a multiple frequency torque disturbance. And the non-linear model is solved using prescribed leg motion as disturbance.

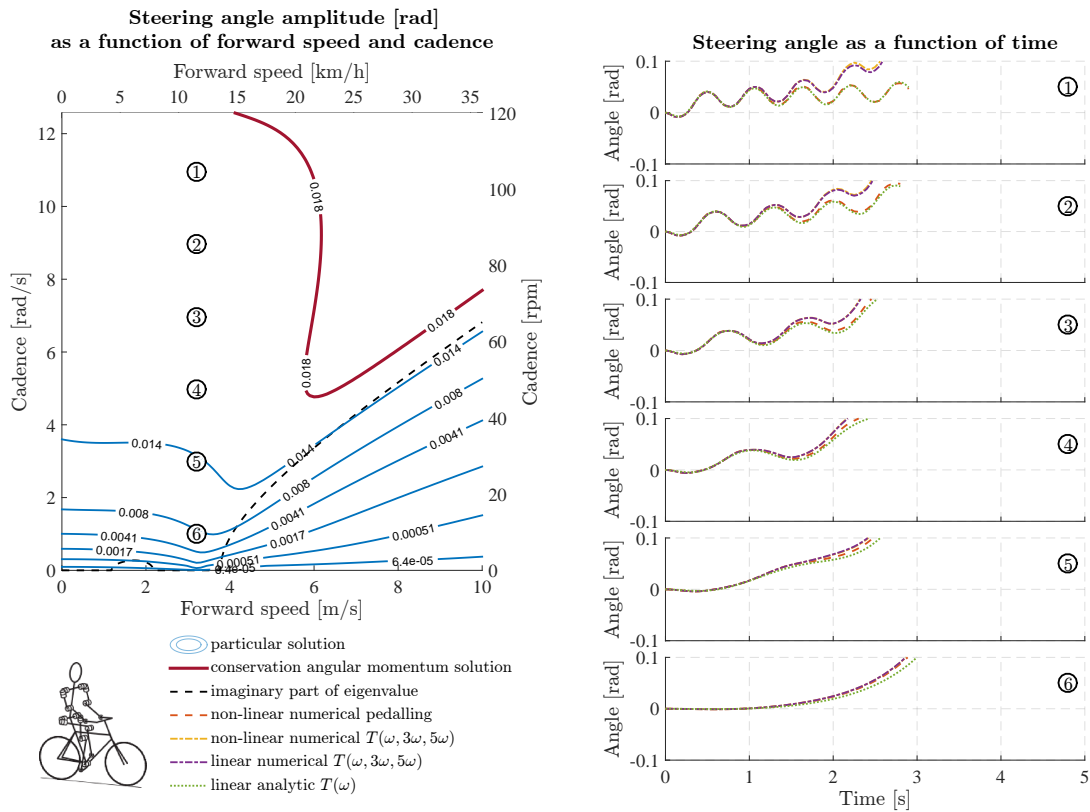


Figure G.3: Steering amplitude of the particular solution (left) and time solutions of other methods (right), for model CF shown bottom left in figure. There is no stable region, however the weave mode is stable from 3.2 m/s (real part of eigenvalue of weave mode is negative from 3.2 m/s). The imaginary part of the weave eigenvalue and is shown for reference. The six numbers corresponding to the six plots on the right are indicated on the roll angle amplitude plot on the left, to indicate the speed-cadence combination belonging the time solution. The isoline corresponding to the amplitude of the conservation of angular momentum solution is shown in the particular solution contour plot on the left for comparison; the conservation of angular momentum solution itself is independent on forward speed and cadence. The particular solution left is the periodic cadence frequency component of the linear analytic time solution shown right, by definition. The linear and non-linear models are also solved using a multiple frequency torque disturbance. And the non-linear model is solved using prescribed leg motion as disturbance.

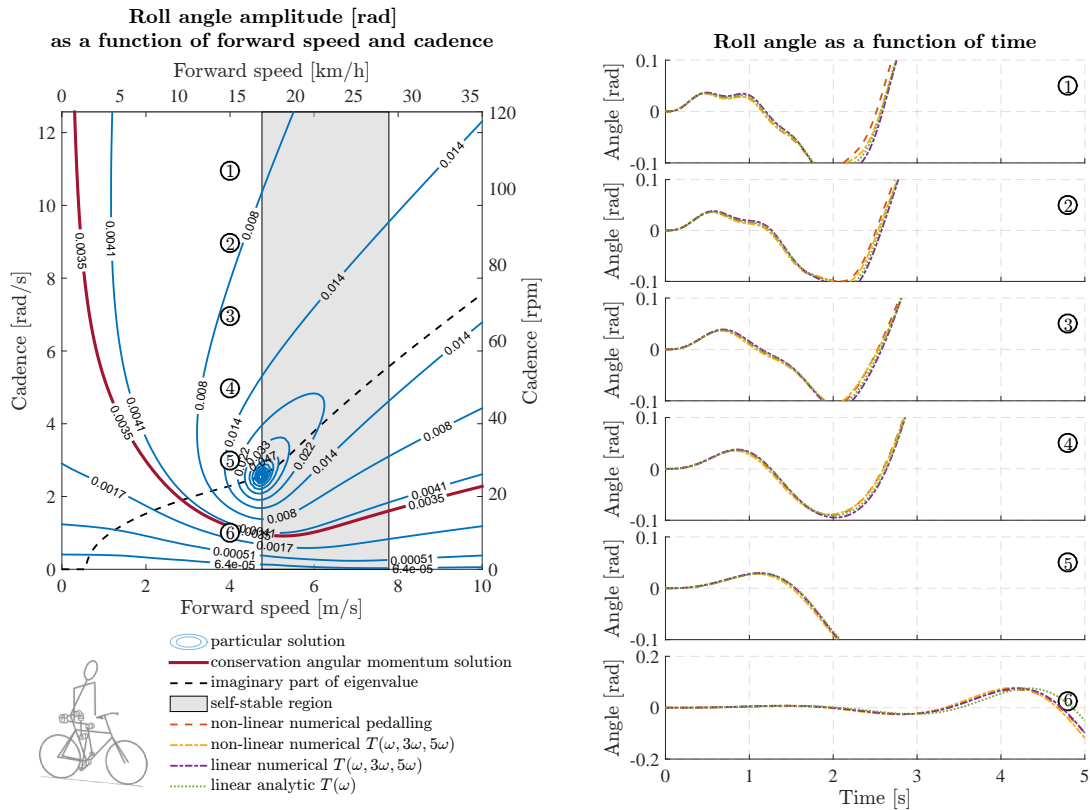


Figure G.4: Roll amplitude of the particular solution (left) and time solutions of other methods (right), for model HR shown bottom left in figure. The six numbers corresponding to the six plots on the right are indicated on the roll angle amplitude plot on the left, to indicate the speed-cadence combination belonging the time solution. The isoline corresponding to the amplitude of the conservation of angular momentum solution is shown in the particular solution contour plot on the left for comparison; the conservation of angular momentum solution itself is independent on forward speed and cadence. The imaginary part of the weave eigenvalue and the self-stable region is shown for reference. The particular solution left is the periodic cadence frequency component of the linear analytic time solution shown right, by definition. The linear and non-linear models are also solved using a multiple frequency torque disturbance. And the non-linear model is solved using prescribed leg motion as disturbance.

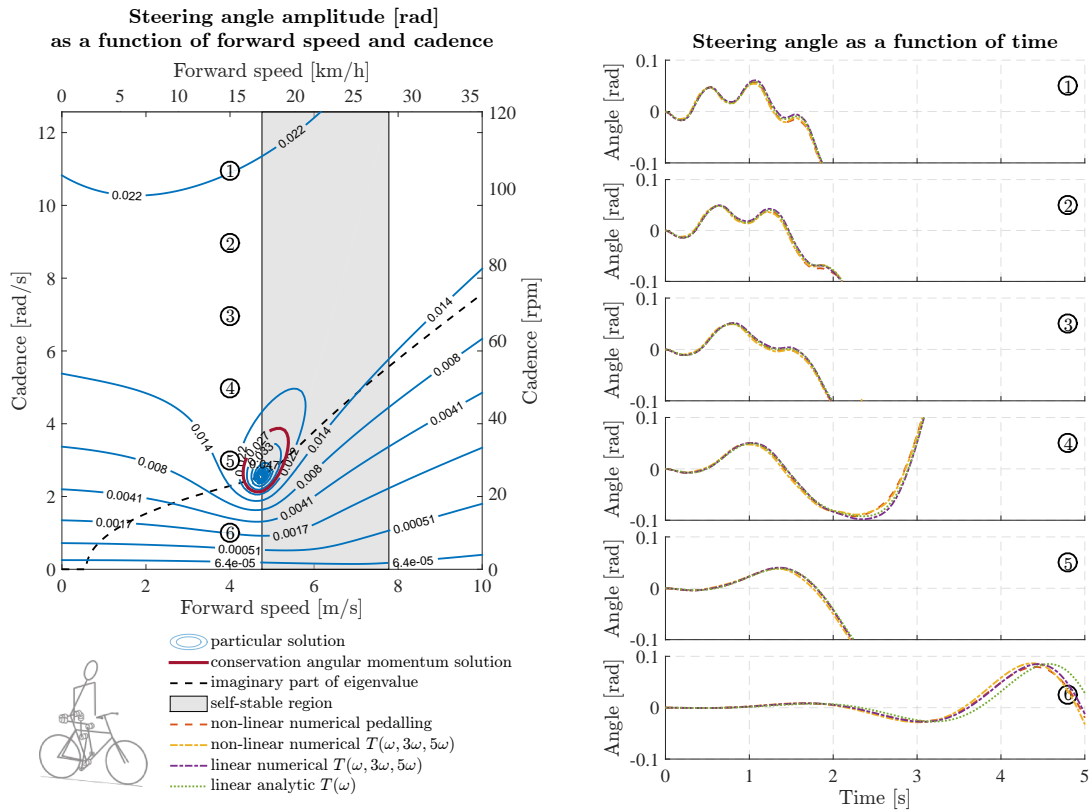


Figure G.5: Steering amplitude of the particular solution (left) and time solutions of other methods (right), for model HR shown bottom left in figure. The six numbers corresponding to the six plots on the right are indicated on the roll angle amplitude plot on the left, to indicate the speed-cadence combination belonging the time solution. The isoline corresponding to the amplitude of the conservation of angular momentum solution is shown in the particular solution contour plot on the left for comparison; the conservation of angular momentum solution itself is independent on forward speed and cadence. The imaginary part of the weave eigenvalue and the self-stable region is shown for reference. The particular solution left is the periodic cadence frequency component of the linear analytic time solution shown right, by definition. The linear and non-linear models are also solved using a multiple frequency torque disturbance. And the non-linear model is solved using prescribed leg motion as disturbance.

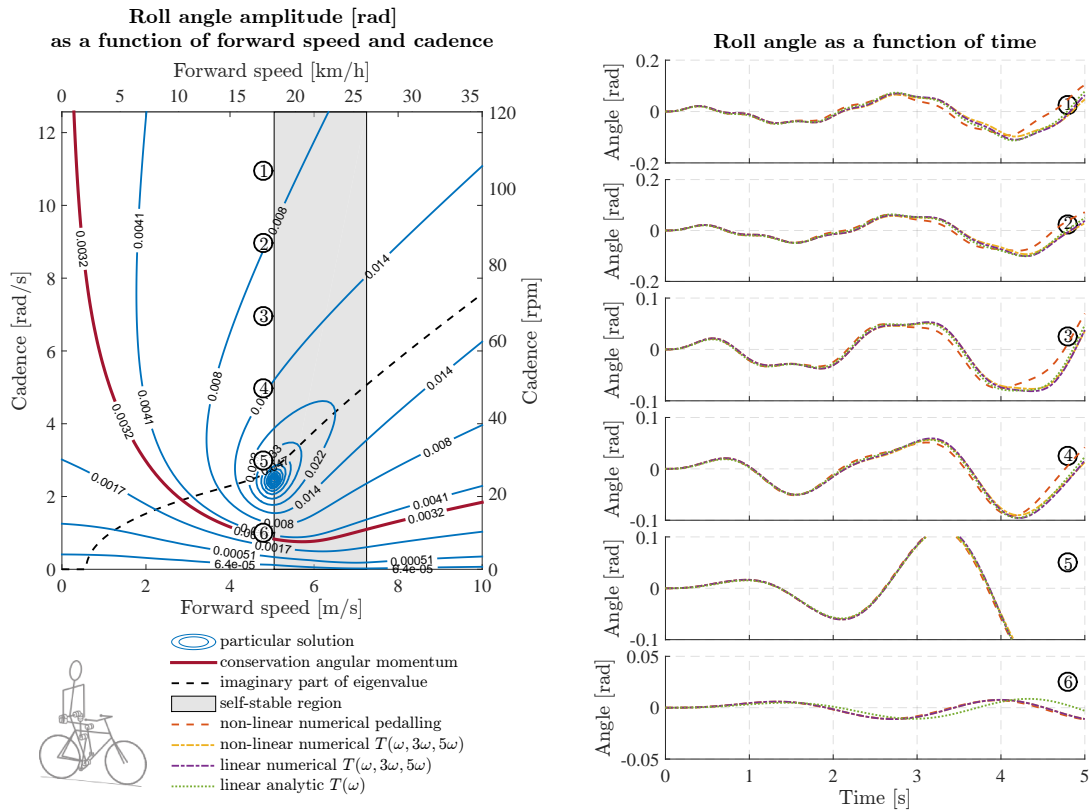


Figure G.6: Roll amplitude of the particular solution (left) and time solutions of other methods (right), for model CR shown bottom left in figure. The six numbers corresponding to the six plots on the right are indicated on the roll angle amplitude plot on the left, to indicate the speed-cadence combination belonging the time solution. The isoline corresponding to the amplitude of the conservation of angular momentum solution is shown in the particular solution contour plot on the left for comparison; the conservation of angular momentum solution itself is independent on forward speed and cadence. The imaginary part of the weave eigenvalue and the self-stable region is shown for reference. The particular solution left is the periodic cadence frequency component of the linear analytic time solution shown right, by definition. The linear and non-linear models are also solved using a multiple frequency torque disturbance. And the non-linear model is solved using prescribed leg motion as disturbance.

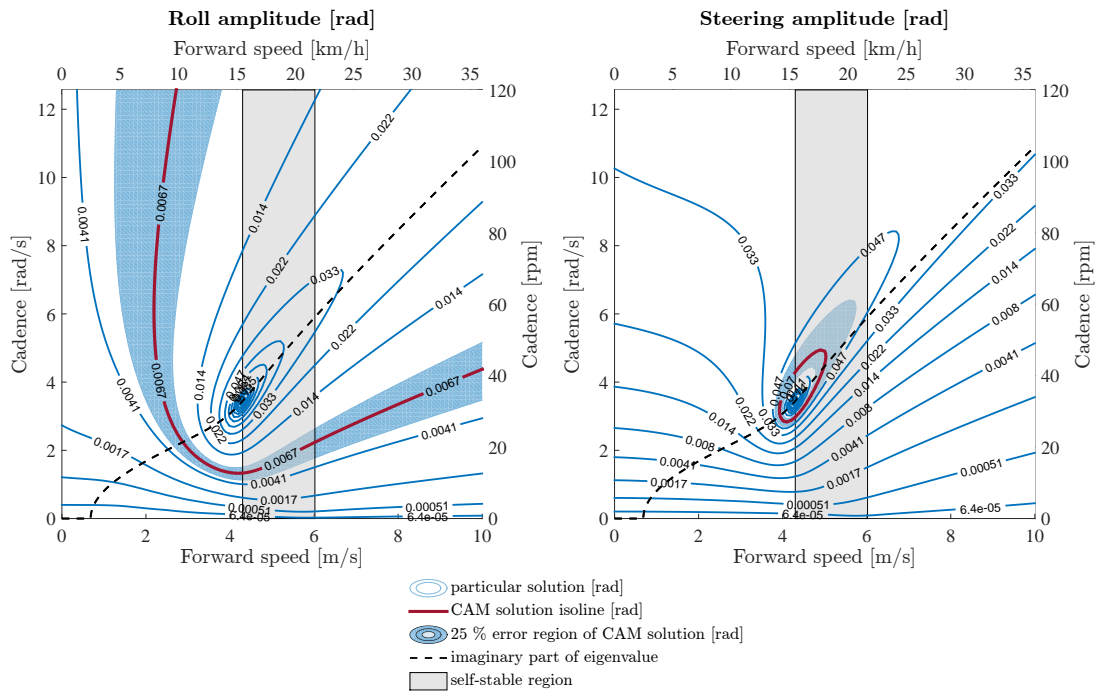


Figure G.7: Roll (left) and steering (right) amplitude of the particular solution of the linear second order differential equation (Eq. 3.1) for the benchmark bicycle model (Meijaard et al., 2007) as a function of forward speed and cadence. The amplitude is in rad, the forward speed is shown in m/s and km/h and the cadence in rad/s and rpm. The result of using the principle of Conservation of Angular Momentum (CAM) is shown using a slightly thicker bourgandy isoline, with a filled 25% error region surrounding it. There is a maximum point seen at the forward speed (4.29 m/s) corresponding to an undamped eigenvalue (see Figure 3.6), where the real part is zero and the imaginary part is the resonance frequency corresponding to the cadence (3.43 rad/s) of the maximum point.

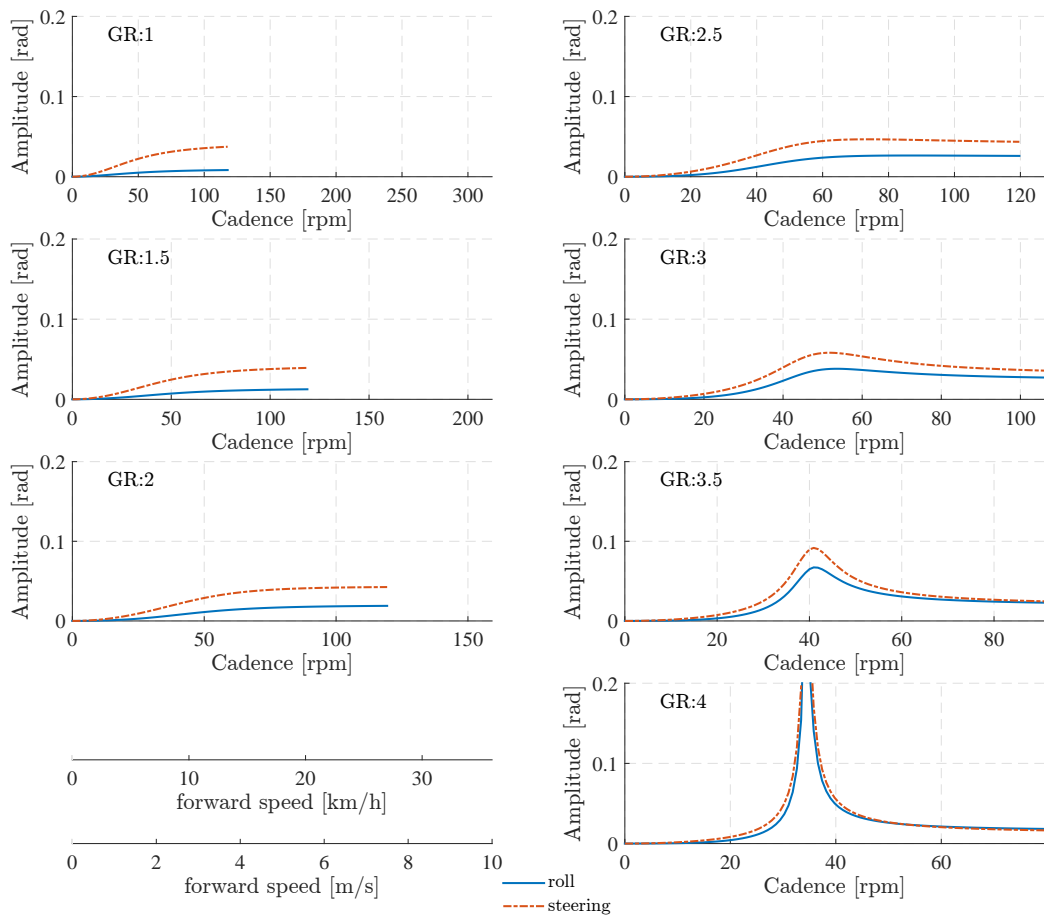


Figure G.8: Amplitude results for roll and steering assuming constant gear ratios, for the hands-free pedalling rider on the benchmark model

H Extra Results: Model Simplifications and Solution Method Evaluation

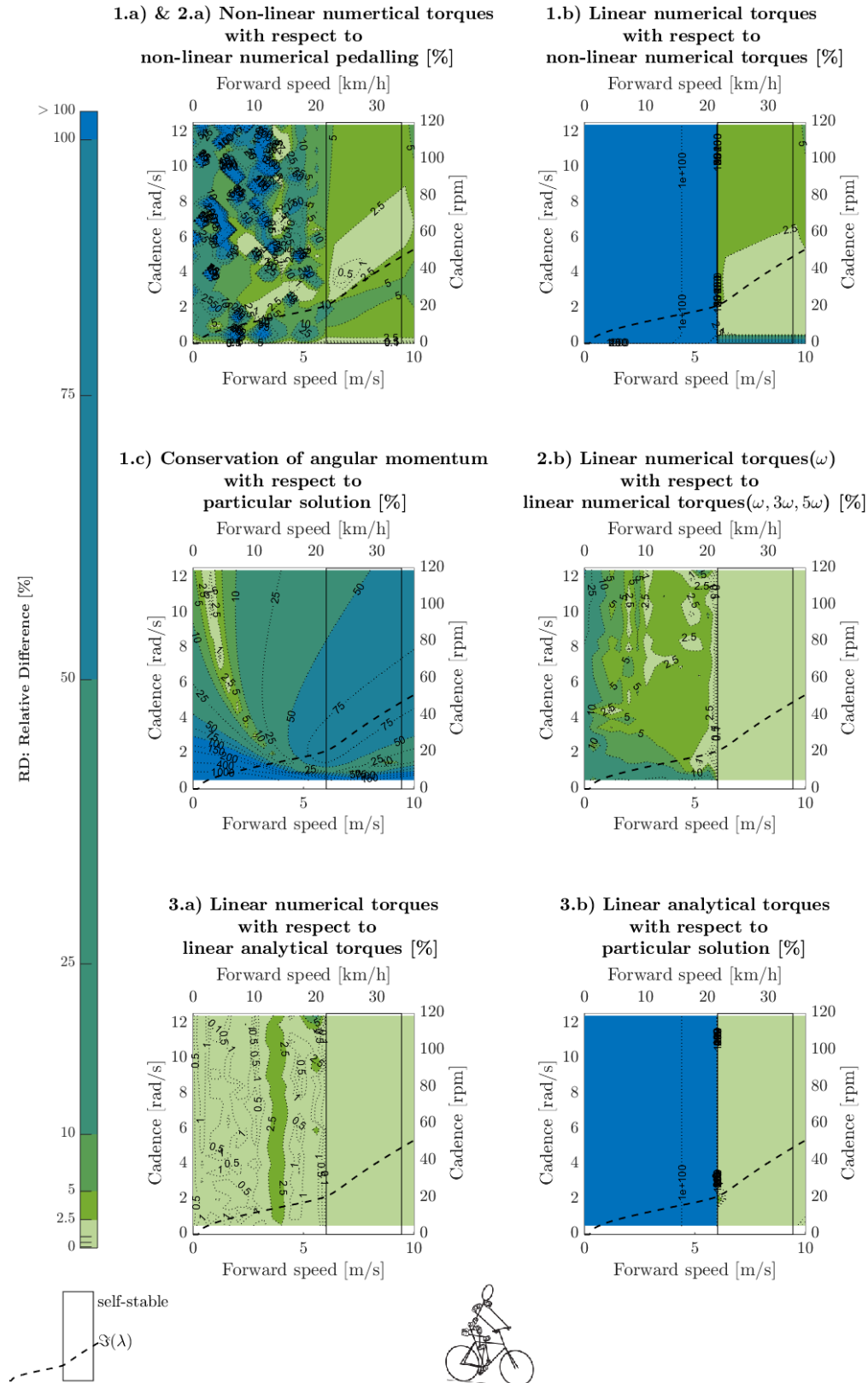


Figure H.1: Model simplifications and solution method evaluation corresponding to points defined in Section 3.1.3. The relative difference of roll amplitude solutions is depicted as a function of forward speed and cadence, corresponding to model HS. The self-stable speed region is indicated by a box and text and the imaginary part of the eigenvalue of the weave eigenmode is indicated with a dashed line.

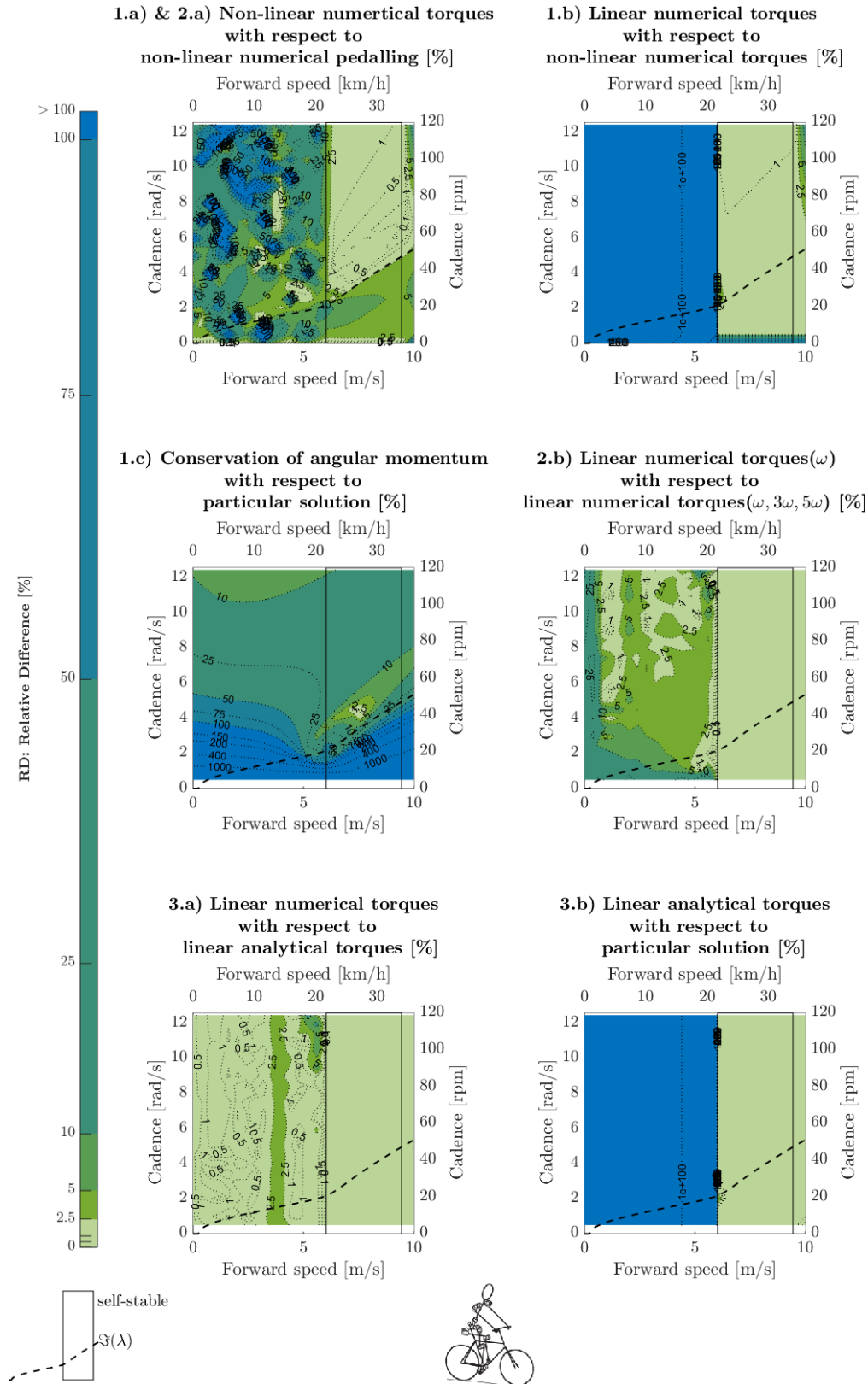


Figure H.2: Model simplifications and solution method evaluation corresponding to points defined in Section 3.1.3. The relative difference of steering amplitude solutions is depicted as a function of forward speed and cadence, corresponding to model HS. The self-stable speed region is indicated by a box and text and the imaginary part of the eigenvalue of the weave eigenmode is indicated with a dashed line.

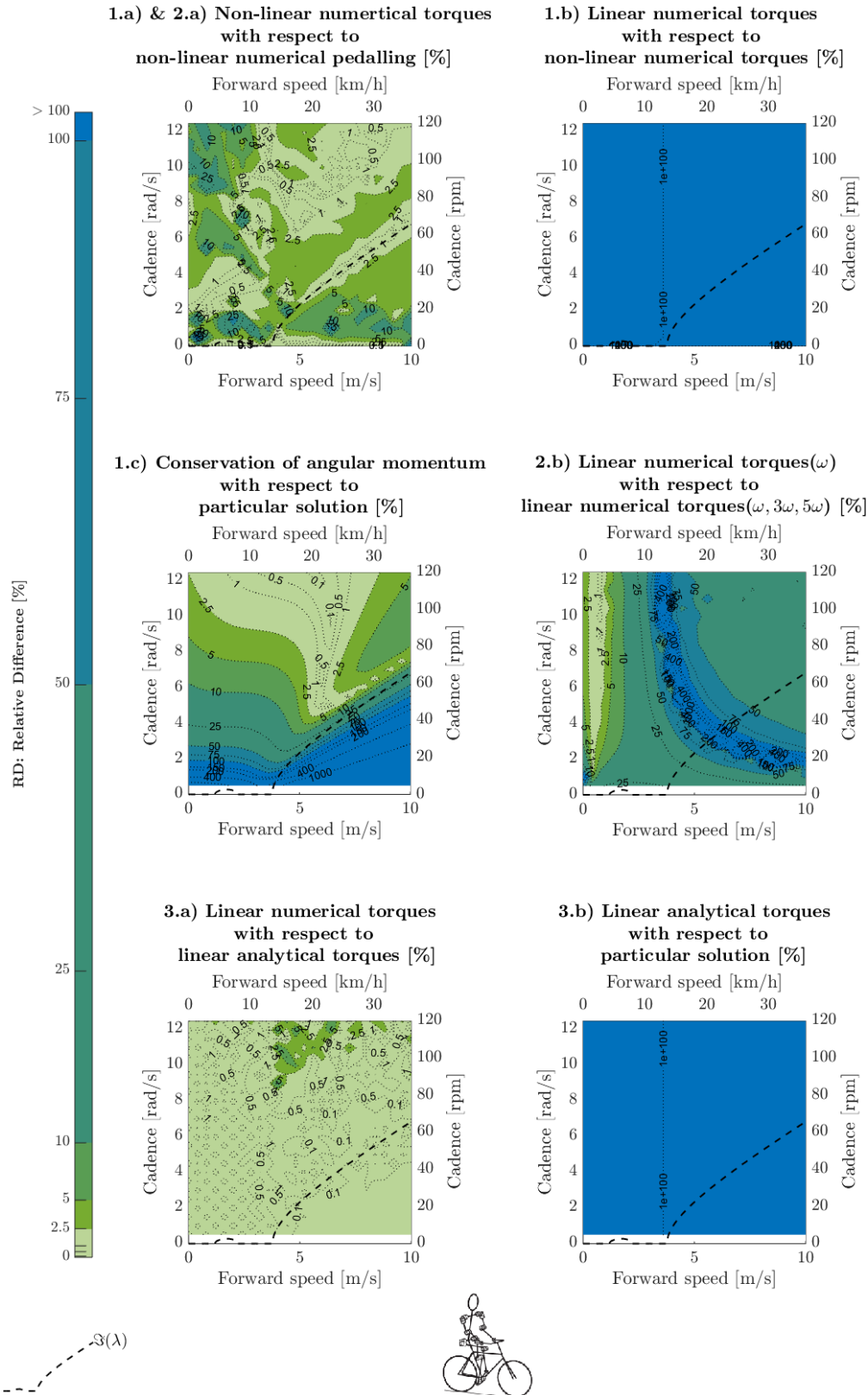


Figure H.3: Model simplifications and solution method evaluation corresponding to points defined in Section 3.1.3. The relative difference of steering amplitude solutions is depicted as a function of forward speed and cadence, corresponding to model CF. This bicycle-rider model is not self-stable and the imaginary part of the eigenvalue of the weave eigenmode is indicated with a dashed line.

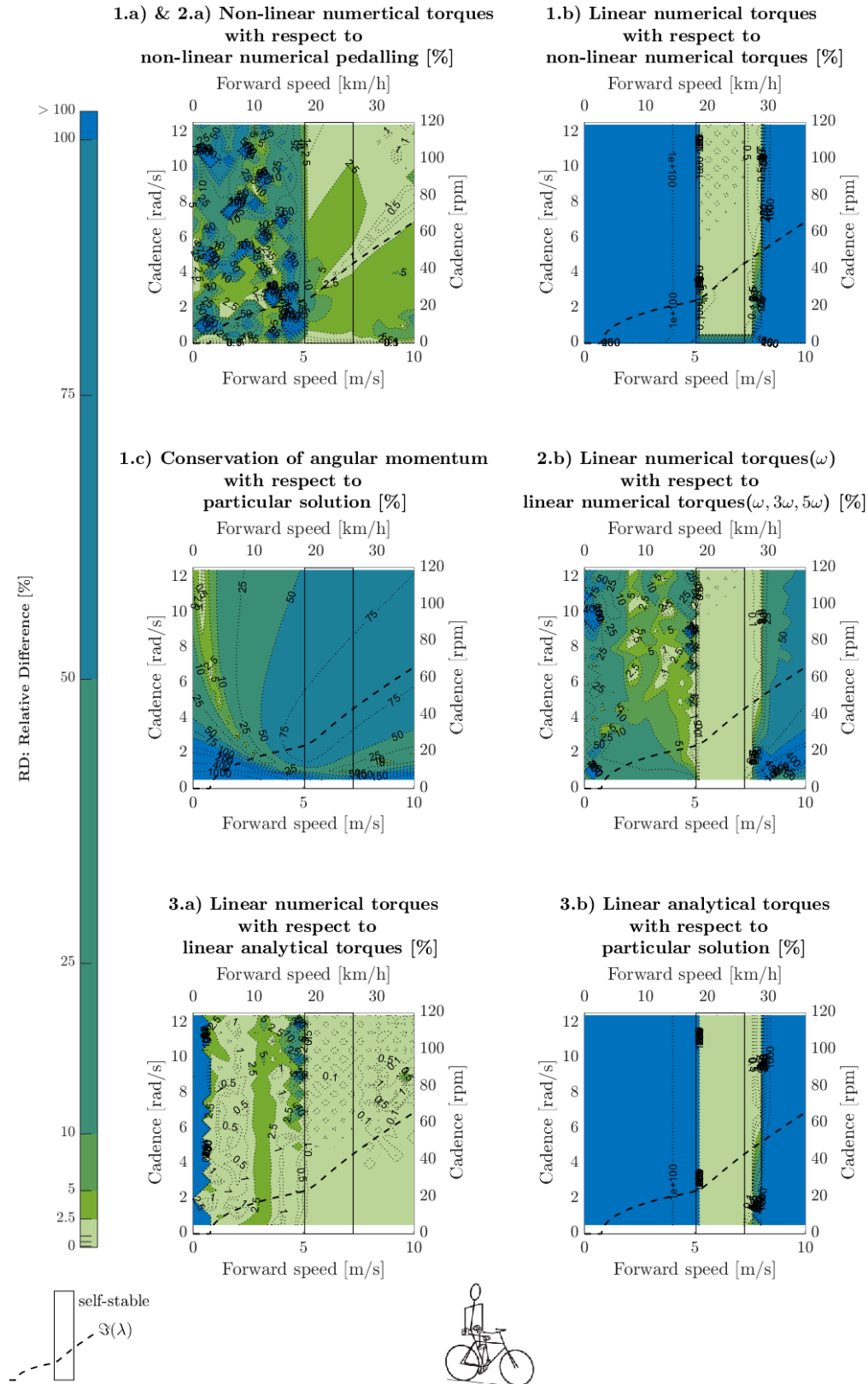


Figure H.4: Model simplifications and solution method evaluation corresponding to points defined in Section 3.1.3. The relative difference of roll amplitude solutions is depicted as a function of forward speed and cadence, corresponding to model CR. The self-stable speed region is indicated by a box and text and the imaginary part of the eigenvalue of the weave eigenmode is indicated with a dashed line.

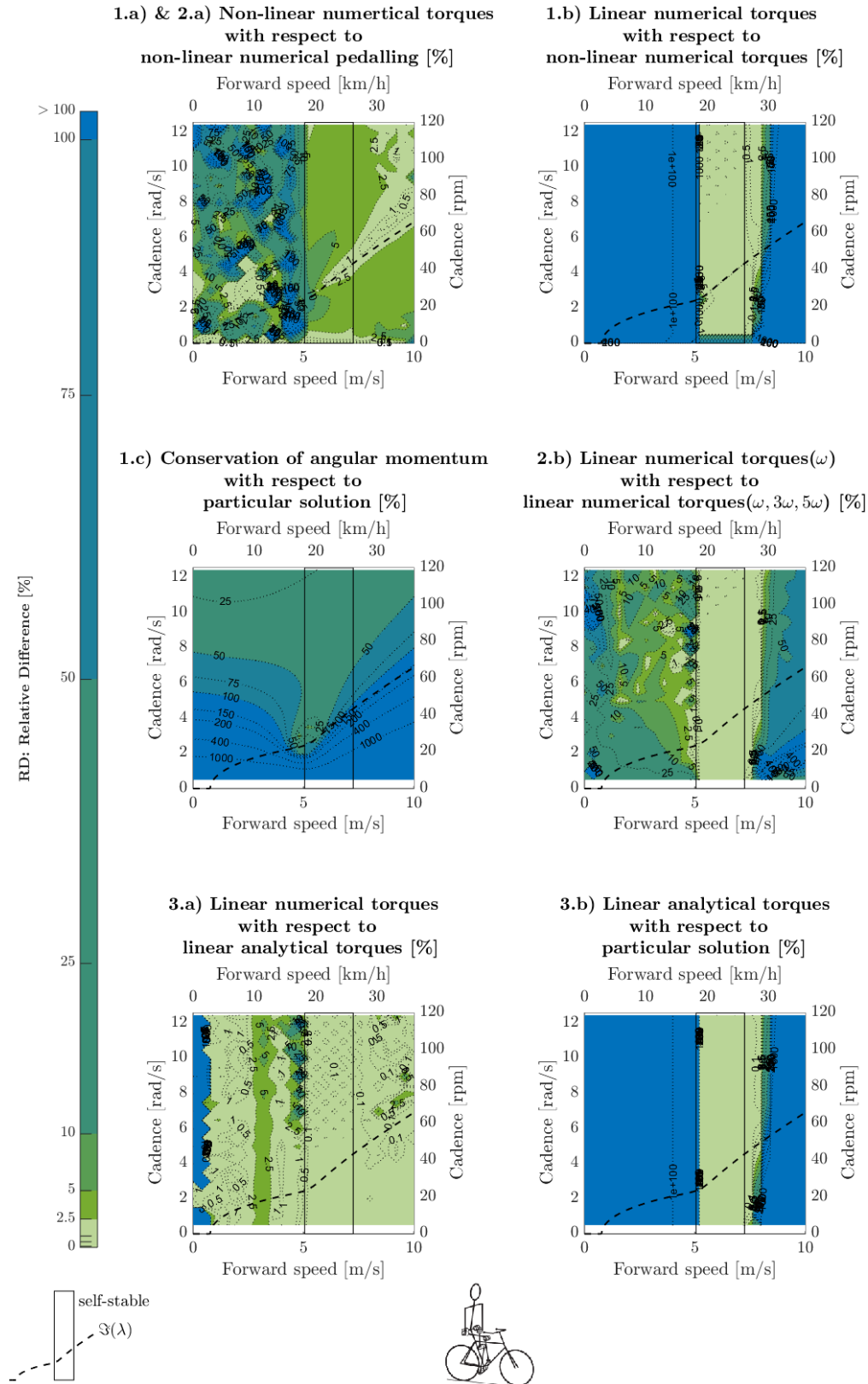


Figure H.5: Model simplifications and solution method evaluation corresponding to points defined in Section 3.1.3. The relative difference of steering amplitude solutions is depicted as a function of forward speed and cadence, corresponding to model CR. The self-stable speed region is indicated by a box and text and the imaginary part of the eigenvalue of the weave eigenmode is indicated with a dashed line.

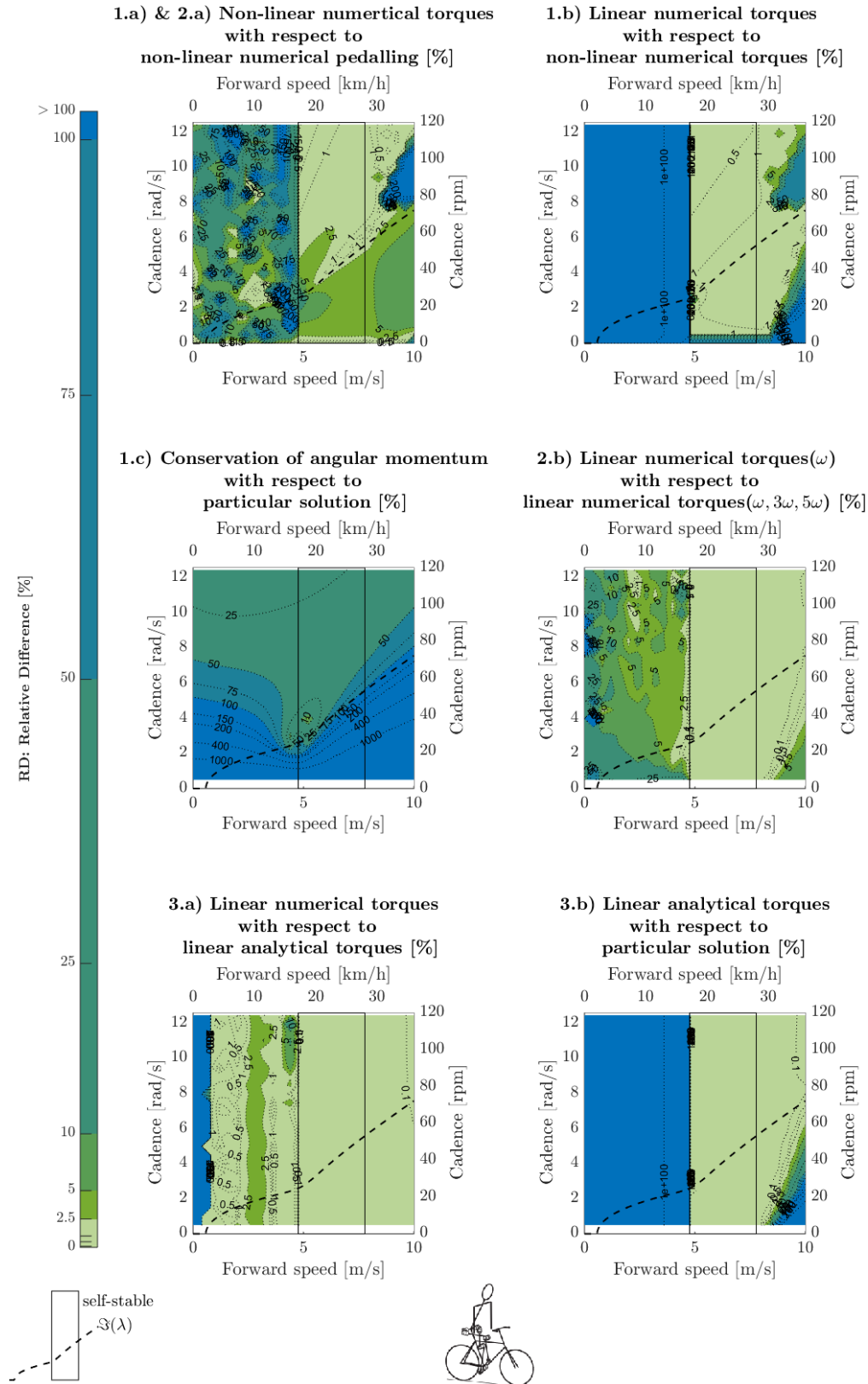


Figure H.6: Model simplifications and solution method evaluation corresponding to points defined in Section 3.1.3. The relative difference of roll amplitude solutions is depicted as a function of forward speed and cadence, corresponding to model HR. The self-stable speed region is indicated by a box and text and the imaginary part of the eigenvalue of the weave eigenmode is indicated with a dashed line.

